Towards the identification of *Verticillium* effector molecules involved in host plant developmental reprogramming

Dissertation zur Erlangung des Doktorgrades
der Mathematisch-Naturwissenschaftlichen Fakultäten
"Doctor rerum naturalium"
der Georg-August-Universität Göttingen
im Promotionsprogramm Biologie
der Georg-August University School of Science (GAUSS)

vorgelegt von

Karin Thole

aus Oldenburg

Göttingen 2016

Betreuungsausschuss

1. Betreuer: Prof. Dr. Volker Lipka
Zellbiologie der Pflanze, Albrecht-von-Haller Institut für Pflanzenwissenschaften

2. Betreuer: PD Dr. Thomas Teichmann
Zellbiologie der Pflanze, Albrecht-von-Haller Institut für Pflanzenwissenschaften

Anleiter: Prof. Dr. Volker Lipka
Zellbiologie der Pflanze, Albrecht-von-Haller Institut für Pflanzenwissenschaften

Mitglieder der Prüfungskommission

Referent: Prof. Dr. Volker Lipka
Zellbiologie der Pflanze
Albrecht-von-Haller Institut für Pflanzenwissenschaften

Korreferent: PD Dr. Thomas Teichmann
Zellbiologie der Pflanze
Albrecht-von-Haller Institut für Pflanzenwissenschaften

Weitere Mitglieder der Prüfungskommission

Prof. Dr. Gerhard Braus
Molekulare Mikrobiologie und Genetik
Institut für Mikrobiologie und Genetik

Prof. Dr. Ivo Feußner
Biochemie der Pflanze
Albrecht-von-Haller Institut für Pflanzenwissenschaften

Prof. Dr. Christiane Gatz
Molekularbiologie und Physiologie der Pflanze
Albrecht-von-Haller Institut für Pflanzenwissenschaften

Prof. Dr. Andrea Polle
Forstbotanik und Baumphysiologie
Fakultät für Forstwissenschaften und Waldökologie

Tag der mündlichen Prüfung: 04.05.2016

Promovierenden-Erklärung

der Georg-August-Universität Göttingen

Die Gelegenheit zum vorliegenden Promotionsvorhaben ist mir nicht kommerziell vermittelt worden. Insbesondere habe ich keine Organisation eingeschaltet, die gegen Entgelt Betreuerinnen und Betreuer für die Anfertigung von Dissertationen sucht oder die mir obliegenden Pflichten hinsichtlich der Prüfungsleistungen für mich ganz oder teilweise erledigt.

Hilfe Dritter wurde bis jetzt und wird auch künftig nur in wissenschaftlich vertretbarem und prüfungsrechtlich zulässigem Ausmaß in Anspruch genommen. Insbesondere werden alle Teile der Dissertation selbst angefertigt; unzulässige fremde Hilfe habe ich dazu weder unentgeltlich noch entgeltlich entgegengenommen und werde dies auch zukünftig so halten.

Die Ordnung zur Sicherung der guten wissenschaftlichen Praxis an der Universität Göttingen wird von mir beachtet.

Eine entsprechende Promotion wurde an keiner anderen Hochschule im In- oder Ausland beantragt; die eingereichte Dissertation oder Teile von ihr wurden nicht für ein anderes Promotionsvorhaben verwendet.

Mir ist bekannt, dass unrichtige Angaben die Zulassung zur Promotion ausschließen bzw. später zum Verfahrensabbruch oder zur Rücknahme des erlangten Grades führen.

Karin Thole Göttingen, den 21.03.2016

Für meine Eltern

List of publications

Michael Reusche, Jekaterina Truskina, Karin Thole, Leonhard Nagel, Sören Rindfleisch, Van Tuan Tran, Susanna A. Braus-Stromeyer, Gerhard H. Braus, Thomas Teichmann, Volker Lipka (2014). Infections with the vascular pathogens *Verticillium longisporum* and *Verticillium dahliae* induce distinct disease symptoms and differentially affect drought stress tolerance of *Arabidopsis thaliana*. Environmental and Experimental Botany, **108**: 23–37.

Michael Reusche, Jana Klásková, Karin Thole, Jekaterina Truskina, Ondřej Novák, Dennis Janz, Miroslav Strnad, Lukáš Spíchal, Volker Lipka, and Thomas Teichmann (2013). Stabilization of cytokinin levels enhances *Arabidopsis* resistance against *Verticillium longisporum*. Molecular Plant-Microbe Interactions **26** (8): 850-860.

Michael Reusche, Karin Thole, Dennis Janz, Jekaterina Truskina, Sören Rindfleisch, Christine Drübert, Andrea Polle, Volker Lipka and Thomas Teichmann (2012). *Verticillium* infection triggers VASCULAR-RELATED NAC DOMAIN7–dependent *de novo* xylem formation and enhances drought tolerance in *Arabidopsis*. The Plant Cell **24** (9): 3823-3837.

Abstract

Infections of *Arabidopsis thaliana* Col-0 plants with the *Verticillium longisporum* isolate VL43 and the *Verticillium dahliae* isolate VdJR2 results in clearly distinguishable disease symptoms, which are characterized by early senescence or plant wilting phenotypes, respectively. To elucidate whether VL43- and VdJR2-like infection symptoms are pathogen species-specific features, a *Verticillium* strain collection, composed of 21 near-diploid *V. longisporum* and 46 haploid *V. dahliae* isolates was systematically analysed in this study and categorized with regard to disease symptom induction on *A. thaliana* wildtype accession Col-0. These analyses allowed the classification of three different interaction classes: "early senescence", "wilting" and "asymptomatic".

For *in-depth* characterization, *Verticillium* isolates which robustly induced disease symptoms in the "early senescence" and the "wilting" interaction class were selected. The strains were compared with respect to *in planta* proliferation and pathogen-induced developmental changes. These analyses showed that strains of the "wilting" interaction class cause enhanced lignification of leaf xylem cell walls. Contrarily, strains of the "early senescence" interaction class trigger developmental reprogramming in the leaf vasculature and induce early senescence. Interestingly, developmental reprogramming in the leaf vasculature represents a common host plant response as this symptom was also induced on *Nicotiana benthamiana*, a *Solanaceae* species. Thus, it was conceivable to postulate that interaction class-specific fungal effector molecule repertoires underlie the early senescence plant response.

In order to identify potential "early senescence" interaction class-specific fungal effector molecules, comparative genome sequence analyses were conducted with haploid *V. dahliae* isolates of the three interaction classes. These data indicated that "early senescence" interaction class-specific sequences exist which are absent in genomes of isolates of the "wilting" and "asymptomatic" interaction class and thus, potentially harbor fungal effector genes involved in "early senescence" interaction class-specific disease symptom induction. Moreover, comparative *in planta* transcriptome studies were performed with *V. dahliae* isolates inducing wilting or early senescence symptoms and identified genes with a higher transcript abundance in the *V. dahliae* isolates of the "early senescence" interaction class compared with the "wilting" interaction class. From this group candidate effector genes were selected. Remarkably, the potential effector molecule repertoire included a ligninase, CEL, which possibly hydrolyzes lignin and influences the differences of xylem cell wall lignification observed between the "wilting" and "early senescence" interaction class. Two candidate effector genes, *CEL* and *CE1,* were selected for comparison of the promoter sequences between *V. dahliae* isolates of the two interaction classes. Noteworthy,

promoter sequence investigations did not indicate interaction class-specific nucleotide differences which may explain the differential expression of *CEL* and *CE1* in the “wilting” and the “early senescence” interaction classes. Hence, the results lead to the hypothesis that expression of these genes is epigenetically controlled.

Zusammenfassung

Die Infektion von *Arabidopsis thaliana* Col-0 Pflanzen mit dem *Verticillium longisporum* Isolat VL43 und dem *Verticillium dahliae* Isolat VdJR2 resultiert in klar zu unterscheidenden Krankheitssymptomen, wie die verfrühte Seneszenz (early senescence) bzw. die Welke (wilting). Um herauszustellen ob VL43- und VdJR2-ähnliche Infektionssymptome Spezies-spezifische Merkmale sind, wurde eine *Verticillium* Stammkollektion, bestehend aus 21 amphihaploiden *V. longisporum* und 46 haploiden *V. dahliae* Isolaten systematisch analysiert und kategorisiert in Bezug auf die Induktion von Krankheitssymptomen auf den *A. thaliana* Ökotyp Col-0. Die Analysen ließen die Klassifizierung von drei unterschiedlichen Interaktionsklassen zu: „early senescence", „wilting" und „asymptomatic".

Für die detaillierte Charakterisierung der Interaktionsklassen „early senescence" und „wilting" wurden *Verticillium* Isolate gewählt, die auf robuste Weise diese Infektionssymptome induzieren. Diese wurden untereinander in Bezug auf ihre Fähigkeit innerhalb der Pflanze zu proliferieren und entwicklungsorientierte Veränderungen innerhalb der Blattvaskulatur der Pflanze zu induzieren verglichen. Die Analysen zeigten, dass Isolate der „wilting" Interaktionsklasse eine erhöhte Lignifizierung der Xylemzellwände in Blättern auslösen. Im Gegensatz dazu induziert die Infektion mit Isolaten der „early senescence" Interaktionsklasse die verfrühte Seneszenz der Pflanze, sowie eine entwicklungsorientierte Umprogrammierung der Blattvaskulatur. Interessanterweise stellen entwicklungsorientierte Veränderungen der Blattvaskulatur eine generelle Antwort von Wirtspflanzen auf diese *Verticillium* Interaktionsklasse dar, da dieses Symptom ebenso in *Nicotiana benthamiana*, eine *Solanaceae* Spezies, induziert wird. Somit wurde postuliert, dass Isolate der Interaktionsklasse „early senescence" spezielle pilzliche Effektormoleküle besitzen, die diese Infektionssymptome auslösen.

Um potentielle pilzliche Effektormoleküle zu identifizieren, die spezifisch für die „early senescence" Interaktionsklasse sind, wurden vergleichende Genomsequenzanalysen mit haploiden *V. dahliae* Isolaten der drei Interaktionsklassen durchgeführt. Die Daten deuteten auf Sequenzen hin, die in der „early senescence" Interaktionsklasse existieren, aber nicht in den Genomen von Isolaten der „wilting" und „asymptomatic" Interaktionsklassen vorkommen und somit möglicherweise Gene für pilzliche Effektoren beherbergen, die in der Symptomentwicklung der verfrühten Seneszenz eine Rolle spielen. Darüberhinaus wurden vergleichende *in planta* Transkriptomanalysen mit *V. dahliae* Isolaten durchgeführt, die Welke oder verfrühte Seneszenz auslösen. Hierbei wurden pilzliche Gene identifiziert, die im Vergleich zur „wilting" Interaktionsklasse eine erhöhte Transkriptmenge in der Interaktionsklasse "early senescence" aufwiesen. Aus dieser Gruppe von Genen wurden Effektorkandidaten ausgewählt.

Bemerkenswerterweise war unter den hochregulierten Effektormolekülen eine Ligninase, CEL, die möglicherweise Lignin hydrolysiert und somit einen Einfluss auf die Unterschiede der Lignifizierungsmenge von Xylemzellwänden hat. Die Gene zweier Kandidateneffektoren, CEL und CE1, wurden bezüglich ihrer Promotersequenzen zwischen den Isolaten der zwei Interaktionsklassen untersucht. Nennenswerterweise wurden keine eindeutigen Sequenzunterschiede in den Promoterregionen der drei Kandidatengene gefunden, die ihre differentielle Expression zwischen der „wilting“ und „early senescence“ Interaktionsklasse erklären würden. Somit wurde angenommen, dass die Expression dieser Gene epigenetisch kontrolliert wird.

Table of abbreviations

°C	degree Celsius
a-	asymptomatic (prefix)
aa	amino acids
Avr	avirulence
bp	base pair(s)
CDB	Czapek Dox Broth
cDNA	complementary DNA
CEB	CTAB extraction buffer
Ct	cycle threshold
d	day(s)
dH_2O	deionised water
DMF	dimethylformamid
DMSO	dimethylsulfoxide
DNA	deoxyribonucleic acid
DNase	deoxyribonuclease
dNTP	deoxynucleosidetriphosphate
dpi	days post infection
EDTA	ethylenediaminetetraacetic acid
EtOH	ethanol
FC	fold change
Fig.	Figure
g	gram
gDNA	genomic DNA
GFP	green fluorescent protein
h	hour(s)
hpi	hours post infection
HR	hypersensitive response
JA	jasmonic acid
kb	kilobase(s)
L	litre
LD	long day
log	decimal logarithm
LRR	leucine-rich repeats
m	milli
M	molar (mol/L)
MAMP	microbe-associated molecular pattern

Mb	megabases
µ	micro
min	minute(s)
mM	millimolar
mRNA	messenger ribonucleic acid
N-	amino-terminal
NB	nucleotide binding
ng	nanogram
nm	nanometer
nt(s)	nucleotide(s)
ORF	open reading frame
PAMP	pathogen-associated molecular pattern
PCR	polymerase chain reaction
PDB	Potato Dextrose Broth
PDF	plant defensin
pH	negative decimal logarithm of the H+ concentration
PR	pathogenesis related
R	resistance
RNA	ribonucleic acid
rpm	rounds per minute
RT	room temperature
RT-PCR	reverse transcription-polymerase chain reaction
s-	early senescence (prefix)
SA	salicylic acid
SD	short day
SD	standard deviation
sec	second(s)
TE	Tris-EDTA
TE	tracheary element
TIR	Drosophila Toll and mammalian interleukin-1 receptor
Tris	Tris-(hydroxymethyl)-aminomethane
U	unit
V	Volt
V.	*Verticillium*
v/v	volume per volume
w-	wilting (prefix)
w/v	weight per volume

Table of content

1 Introduction

1.1 The vascular pathogen *Verticillium spp*

Verticillium spp are soil-borne fungi and severe plant pathogens which colonize the plant's vasculature. They cause *Verticillium* wilt diseases in over 200 host species and economically important crop plants (Eynck *et al.*, 2007). *Verticillium spp* was classified to belong to the phylum Ascomycota and is inable to reproduce sexually. *Verticillium* possesses a hyaline mycelium featuring various characteristics ranging from simple and septate hyphae to a branched, multinucleate mycelium (Fradin and Thomma, Bart P H J, 2006). The conidia are formed on long phialides which are arranged on the conidiophores in a spiral-like, 'verticillate', manner. This conidiophore morphology provided the name for the genus *Verticillium* (Fradin and Thomma, Bart P H J, 2006; Inderbitzin *et al.*, 2011).

Six different plant pathogenic species of the genus *Verticillium* have been identified (Barbara and Clewes, 2003; Klosterman *et al.*, 2009; Inderbitzin *et al.*, 2011). The best analysed of them are *V. dahliae* Klebahn and *V. albo-atrum* Reinke & Berthold (Pegg and Brady, 2002; Barbara and Clewes, 2003; Barbara, 2003). The near-diploid hybrid species *V. longisporum* is the cause of *Verticillium* wilt in oilseed rape, a major disease in Europe (HEALE, 2000). In comparison to the haploid species *V. dahliae* and *V. albo-atrum* the nucleus of *V. longisporum* contains about twice the DNA amount (Karapapa *et al.*, 1997; Karapapa and Typas, 2001; Typas and HEALE, 1980). Phylogenetic analyses of various *Verticillium* isolates indicate that the hybrid species *V. longisporum* developed at least three times by independent different parasexual hybridization events. These gave rise to three different lineages of *V. longisporum*: A1xD1 which occurs in regions of Europe, Japan and North America, A1xD2 occuring solely in Illinois (United States) and A1xD3 which is mainly found in Europe and Japan (Inderbitzin *et al.*, 2011). Species A1, which constitutes a yet unidentified taxon related to *V. albo-atrum*, is a common parent shared among all tested hybrid isolates. Species D1 establishes a so far unknown taxon, whereas lineage D2 and D3 belong to the species *V. dahliae* (Inderbitzin *et al.*, 2011). The hybrid species *V. longisporum* can be discriminated from the haploid species *V. dahliae* and *V. albo-atrum* since its genome carries two isogenes of the conserved *V*erticillium *T*ranscription *A*ctivator gene (*VTA2*) which originated from *V. dahliae* and *V. albo-atrum*, respectively (Dissertation Van Tuan Tran, 2011; van Tran *et al.*, 2013) (Figure 1.1B). In addition, the genome of *V. longisporum* isolates contains rDNA

(including the internal transcribed spacer, ITS) which originated either from *V. dahliae* or from *V. albo-atrum* (Dissertation Van Tuan Tran, 2011; Inderbitzin *et al.*, 2011; van Tran *et al.*, 2013) (Figure 1.1A). With this, phylogenetic distinction between the *V. longisporum* lineages is possible.

According to their pathogenicity on economically important crops, such as potato, tomato, strawberry, linseed, three legumes and *Brassica* species, Zeise and von Tiedemann (2002) assigned various *V. dahliae* and *V. longisporum* isolates to vegetative compatibility groups (VCGs). The *V. longisporum* group lsp* is composed of isolates that are avirulent on oilseed rape (e.g. Vl19 and Vl32). In contrast, infection with isolates from group lsp resulted in disease on *Brassica napus* (Zeise and Tiedemann, 2002). Inderbitzin *et al*. (2011) discovered that the *V. longisporum* groups lsp* and lsp corresponded to the identified *V. longisporum* lineages A1xD3 and A1xD1, respectively.

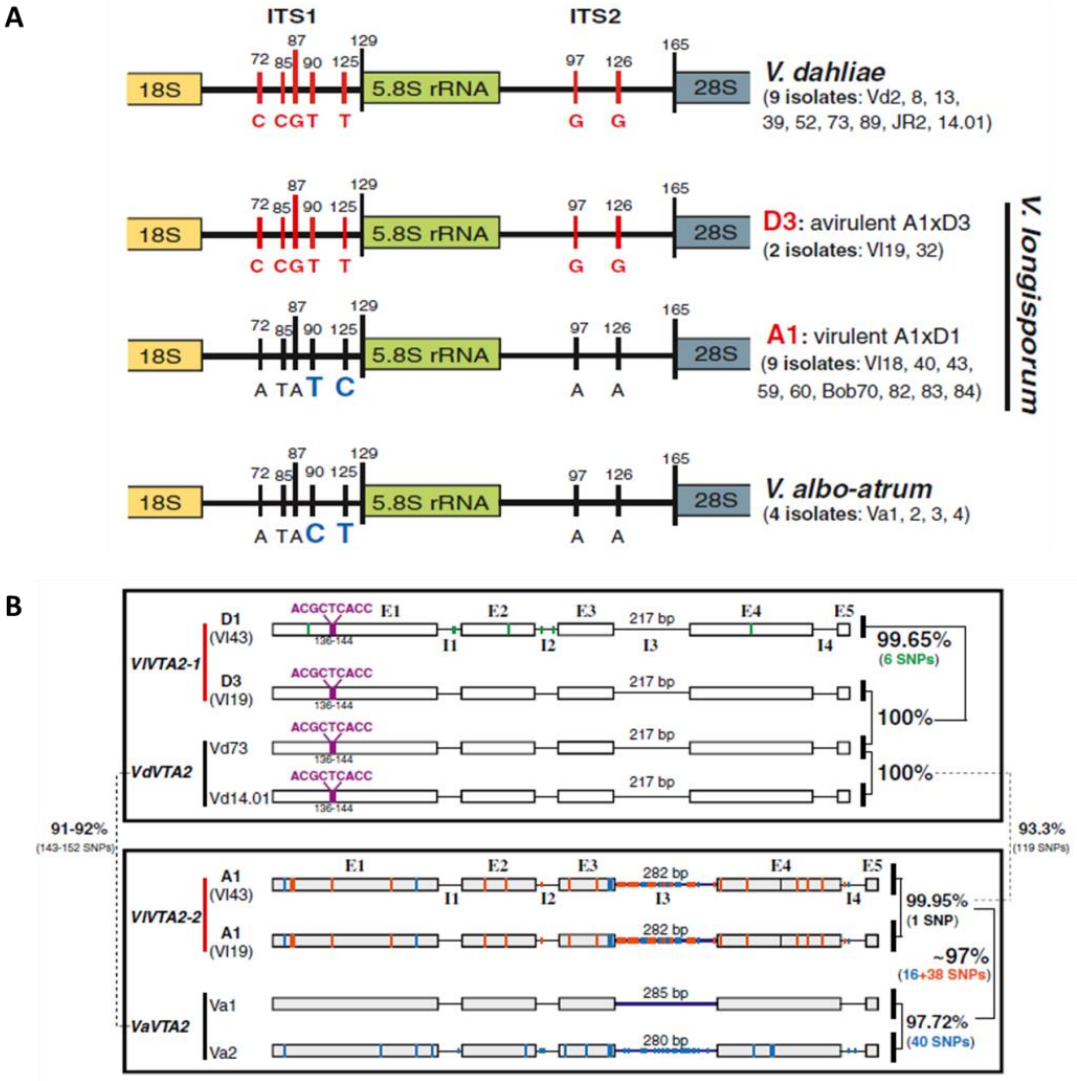

Figure 1.1: Genetic analyses for differentiation between haploid *V. dahliae* and *V. albo-atrum* and diploid *V. longisporum* species as well as between *V. longisporum* A1xD1 and A1xD3 lineages. A: Internal transcribed spacer (ITS) sequence of the ribosomal DNA in the three *Verticillium* species comprising ITS1 (129 nucleotides), 5.8S rRNA and ITS2 (165 nucleotides). *V. longisporum* isolates carry only one type of ITS which is either a derivate of the species *V. dahliae* D3, as it is found in the lineage A1xD3, or of the species A1, which holds true for isolates of the lineage A1xD1. Species A1 corresponds to a yet unknown taxon which is closer related to *V. albo-atrum* than to *V. dahliae*. ITS of A1 differs from the ITS region of *V. albo-atrum* in two pyrimidine exchanges at positions 90 and 125 (**bold**). **B:** Schematic illustration of the *VTA2* gene from the *Verticillium* species *V. dahliae*, *V. albo-atrum* and *V. longisporum*. Both *V. longisporum* lineages A1xD1 and A1xD3 carry two *VTA2* isogenes, *VlVTA2-1* and *VlVTA2-2* deriving from *V. dahliae* and *V. albo-atrum*, respectively. *VlVTA2-1* and the *V. dahliae VdVTA2* possess a nine-nucleotide insertion (ACGCTCACC) in the first exon (E1) and a third intron (I3) of 217 bp length. *VlVTA2-2* and *V. albo-atrum VaVTA2* lack the nucleotide insertion in E1 and carry a longer version of I3 of 280–285 bp. The avirulent A1xD3 isolates Vl19 and Vl32 possess a *VlVTA2-1* isogene which is identical to *V. dahliae VdVTA2* but deviates from *VlVTA2-1* of the virulent A1xD1 lineage in 6 single nucleotide polymorphisms (SNPs). Only one SNP constitutes the difference of *VlVTA2-2* between A1xD1 isolates and A1xD3 isolates. SNPs are indicated in blue and orange; (van Tran *et al.*, 2013).

The hybrid species *V. longisporum* differs from its parental species with regard to morphological characteristics and its host range. In contrast to *V. dahliae* and *V. albo-atrum, Verticillium longisporum* forms elongated spores and it infects primarily the *Brassicaceae* family, i.e. causing wilt of winter oilseed rape (*Brassica napus ssp*. *oleifera*) and other cruciferous plants (Karapapa and Typas, 2001; Zeise and Tiedemann, 2002; Fradin and Thomma, Bart P H J, 2006). This includes the *Brassicaceae* model plant *Arabidopsis thaliana* (Johansson *et al.*, 2006; Floerl *et al.*, 2010; Tischner *et al.*, 2010; Reusche *et al.*, 2012). *V. dahliae* however has a wide range of hosts causing wilt in various plants, including vegetables, flowers (Chrysanthemum), oilseed crops (sunflower) or fibre crops (cotton, flax) and woody perennials (Pegg and Brady, 2002). Previous studies showed that *V. dahliae* is also able to successfully infect the model plant *A. thaliana* (Veronese *et al.*, 2003a; Fradin and Thomma, Bart P H J, 2006; Reusche *et al.*, 2014).

1.2 Plant infection by *Verticillium spp*

1.2.1 The *Verticillium* life cycle

Verticillium fungi are considered hemibiotrophs, and thus, characterized by both a biotrophic and a necrotrophic phase during their infection cycle (Fradin and Thomma, Bart P H J, 2006). *Verticillium* forms microsclerotia or spores which are fungal resting structures remaining viable in the soil or in plant debris (MOL *et al.*, 1995) (Figure 1.2). Host and non-host plants secrete root exudates which stimulate the microsclerotial germination (Fradin and Thomma, Bart P H J, 2006). Germination of microsclerotia results in the development of several hyphae. The hyphal growth is attracted towards the potential host plant possibly by following the gradient of nutrients which are permanently released by the plant. After penetration of cells at the root tip or alternatively

entry at sites of lateral root formation *Verticillium* switches to a parasitic life style (Bishop and Cooper, 1983; Pegg and Brady, 2002; Bachelor thesis, S. Rindfleisch, 2011). *Verticillium* preferentially enters at the root tip or at partially damaged sites of the root surface to circumvent the endodermis which builds a barrier between cortex and vascular cylinder. In contrast to other fungal pathogens *Verticillium* does not produce appressoria, but hyphopodia (Eynck *et al.*, 2007). For successful colonisation of the root xylem conidia formation is crucial, a process referred to as 'budding' (Fradin and Thomma, Bart P H J, 2006). The conidia are furthermore transported with the plant's sap stream and captured at so-called trapping sites i.e. in pit cavities or at vessel end walls (Eynck *et al.*, 2007). At these trapping sites conidia germination takes place which further transit into adjacent vessel elements in order to spread systemically within the vasculature of the plant (Figure 1.2).

The systemic colonization of the plant causes infection symptoms. Disease symptoms comprise brown discolorations of the plants vascular stem tissue, stunted growth and wilting of the leaves, chlorosis and early senescence (Fradin and Thomma, Bart P H J, 2006; Reusche *et al.*, 2014; Klimes *et al.*, 2015). At late stages of the infection *Verticillium* exits the leaf xylem and grows into the leaf mesophyll. During this phase *Verticillium* can enter the necrotrophic stage including massive conidia production which spread via air flow and start another cycle of disease. During the infection cycle huge amounts of microsclerotia are produced in dead plant tissues. The resting structures are released and persist in the soil (Fradin and Thomma, Bart P H J, 2006; Klimes *et al.*, 2015) (Figure 1.2).

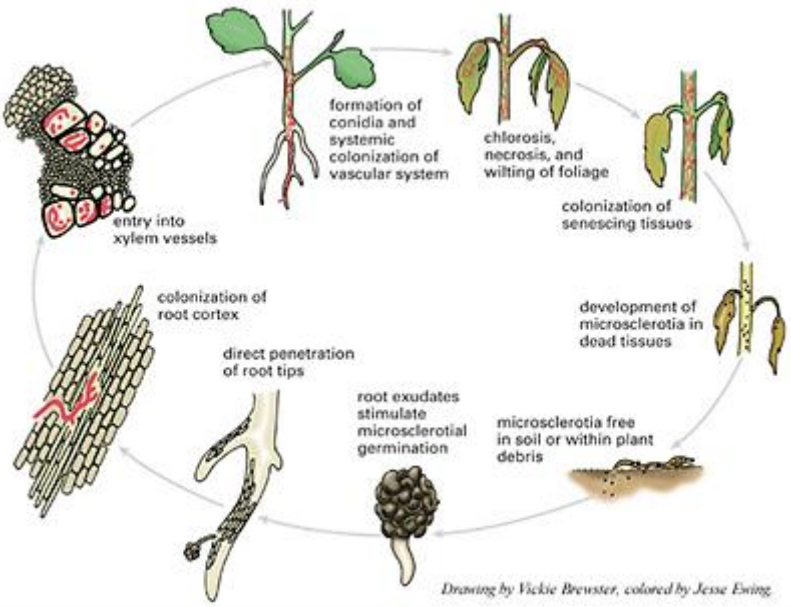

Figure 1.2: Schematic illustration of the *Verticillium* life cycle. The fungus remains viable in the soil via resting structures, the microsclerotia. Via stimulation by root exudates secreted by the plant microsclerotial germination occurs followed by penetration of root tip cell. This results in colonization of the root cortex as well as entry into the xylem vessels. With this *Verticillium* systemically colonizes the vascular system of the plant. Further colonization of the plant vasculature results in disease symptoms like chlorosis, necrosis, wilting of the leaves and subsequent senescence. *Verticillium* spreads within senescing tissues and is further able to develop microsclerotia in the dead tissues. The infection cycle can start again. (http://www.btny.purdue.edu/Extension/Pathology/PHM/BD/vert.htm).

1.2.2 Invasion studies of *V. dahliae* and *V. longisporum* in *A. thaliana* plants

Reusche *et al.* (2014) compared the infection pathway and subsequent *in planta* proliferation of the *V. longisporum* reference isolate VL43 and the *V. dahliae* reference isolate VdJR2 using fluorescently labeled strains. *V. longisporum* as well as *V. dahliae* successfully invaded *Arabidopsis* roots and further colonized the plant's vasculature. However, infestation of the plant's vasculature occurred with different efficiencies (Reusche *et al.*, 2014). The experiments indicated that the reference strains for both *Verticillium* species enter the root tissue of *A. thaliana* Col-0 plants via hyphal penetration of the rhizodermis at the root tips of primary or lateral roots. Moreover, 72 hours post infection (hpi) both species colonized the root's elongation zone inter- and intracellularly and the hyphae further grew towards the vascular cylinder of the differentiation zone. At this point *V. longisporum* as well as *V. dahliae* reaches the proto- and metaxylem of the root resulting in enhanced colonization of the vasculature. Conspiciously, both *Verticillium* species massively proliferate within the roots and on the root surface of *A. thaliana* at early stages of infection (Reusche *et al.*, 2014).

Furthermore, the spatio-temporal proliferation of the *V. longisporum* and *V. dahliae* isolates VL43 and VdJR2, respectively, was analysed in hypocotyl tissues as well as in leaf midribs and the lamina via quantitative real-time polymerase chain reactions (qRT-PCR) and cytological *in situ* studies (Reusche *et al.*, 2014). Already at early time points (14 dpi) an enhanced proliferation of VdJR2 occurs in hypocotyl tissues. VL43 inoculated *A. thaliana* Col-0 plants never showed a comparably high colonization rate like VdJR2 infected plants, neither in hypocotyl structures nor in leaf midribs and lamina tissues. The authours hypothesized that the *V. dahliae* VdJR2 is able to infest *A. thaliana* Col-0 more efficiently than *V. longisporum* VL43 (Reusche *et al.*, 2014).

1.2.3 *Verticillium*-induced disease symptoms and developmental reprogramming in host plants

Verticillium infections typically result in severe wilting symptoms possibly resulting from a reduced cell turgor due to water loss (Tjamos and Beckman, 1989). In contrast, during infections of *Brassicaceae* plants with *V. longisporum* VL43 the water status of *Brassica napus* and *A. thaliana* plants is maintained (Floerl *et al.*, 2008; Floerl *et al.*, 2010). Presumably, maintenance of the water status results from an enhanced water storage capacity of the infected host plants. The enhanced water storage capacity of *A. thaliana* after infection with the strain VL43 was confirmed in an additional study in which a higher drought stress tolerance of these plants was discovered in comparison to uninfected plants (Reusche *et al.*, 2012). In contrast to that, *A. thaliana* plants inoculated with the *V. dahliae* isolate VdJR2 were not able to maintain their water status and showed strong wilting symptoms (Reusche *et al.*, 2014). Both isolates VL43 and VdJR2 induced stunted growth of *A. thaliana* but apart from that triggered clearly distinguishable species-specific disease symptoms (Figure 1.3). Whereas VL43 infection results in chlorosis formation on leaves and subsequent early senescence of the plant, VdJR2 inoculation induces wilting of older rosette leaves and enhanced lateral branch formation (Reusche *et al.*, 2014).

Colonization of the plant's vasculature during fungal infections is often associated with obstruction of the transpiration stream which influences the function of xylem vessels. For example, cell-wall degrading enzymes secreted by *Fusarium oxysporum* f. sp. *cubense* promote in some plants the development of vascular system-obstructing gels resulting in vessel clogging (VanderMolen *et al.*, 1983). Hence, fungal growth in the vascular system would be arrested. Moreover, vessel clogging would limit the access of the fungus to plant-derived nutrients. A similar phenomenon in terms of tyloses formation was observed in hop cultivars after *V. albo-atrum* infection (Talboys, 1958). The volume of xylem parenchyma cells increases upon infection with *V. albo-atrum*. Subsequently, cell-wall material is laid down on the pit membranes between xylem parenchyma cells and vessels forming a balloon-like structure that protrudes into the vessel lumen (Talboys, 1958). The resulting tyloses obstruct the lumen of the xylem vessels and arrest further fungal spread. As a consequence of vessel obstruction, water transport in the xylem cells is compromised. To overcome the dysfunction of obstructed xylem vessels, tyloses formation is often accompanied by the formation of a compensatory secondary xylem. The activity of the vascular cambium increases to build the additional xylem. The newly formed tissue is called hyperplastic tissue and the process hyperplasia (Talboys, 1958; Baayen, 1986). This form of xylem regeneration is crucial to guarantee a successful water transport within the plant by bypassing the flux through adjacent xylem parenchyma cells. Hence, wilting of infected plants is avoided.

Hyperplasia formation in hypocotyl tissues, leaves and roots was also discovered upon infection with *V. longisporum* VL43 (Figure 1.3H; Reusche *et al.*, 2014). The development of a substantially higher number of lignified xylem cells was identified in the vasculature of these tissues (Reusche *et al.,* 2012). Hyperplasia formation is caused by the initial transdifferentiation of xylem parenchyma cells as well as the reactivation of the cambium. The enhanced cambial activity during hyperplasia development can be monitored by expression analysis of *AtHB8*. This gene, encoding a class III homeodomain-leucine zipper (HD-ZIP) of *Arabidopsis* is a marker gene for cambial activity (Scarpella *et al.*, 2004). Indeed, Reusche *et al.* (2012) showed that VL43-induced hyperplastic tissue formation correlates with an enhanced expression of the cambial marker gene *AtHB8* (Reusche *et al.*, 2012). Moreover, VL43 triggers the transdifferentiation of chloroplast-containing bundle sheath cells, which usually surround the leaf vasculature, into functional tracheary elements (TEs) in *A. thaliana* as well as *B. napus* plants (Figure 1.3B; Reusche *et al.,* 2012). These TEs show features of the protoxylem, like annular structures. Likewise, other TEs possess reticulate cell wall fortifications which are typically found in metaxylem. Since transdifferentiation is independent of cambial activity, another molecular marker is needed to consider also *de novo* xylem formation from bundle sheath cells and xylem parenchyma during quantitative analyses of *de novo* xylem formation. The NAC (NAM, ATAF1/2 and CUC2)–domain transcription factor VASCULAR-RELATED NAC DOMAIN7 (VND7) is a key regulator of plant protoxylem vessel formation (Kubo *et al.*, 2005). VL43 infected plants showing transdifferentiation of bundle sheath cells and hyperplasia also exhibit increased transcript levels of *VND7* (Reusche *et al.*, 2012).

De novo xylem formation, like hyperplasia development and bundle sheath cell transdifferentiation was concluded to be the cause of enhanced drought-stress tolerance after VL43 infection. Contrarily, these developmental reprogrammings were not induced by *V. dahliae* VdJR2 (Figure 1.3C, I). VdJR2 infection does not result in enhanced drought stress tolerance of *A. thaliana*, presumably due to its inability to trigger VL43-like developmental changes in the vasculature (Reusche *et al.*, 2014). Thus, water transport and water storage capacity were not improved after VdJR2 infection. Both organisms, the plant and the pathogen, might profit by the *de novo* xylem formation since the plant resists the combination of abiotic and biotic stresses (Reusche *et al.*, 2012; Reusche *et al.*, 2014). This would also guarantee the nutrition of the fungus. Reusche *et al.* (2012), therefore, hypothesized that the *A. thaliana* - *V. longisporum* VL43 pathosystem has conditionally mutualistic features.

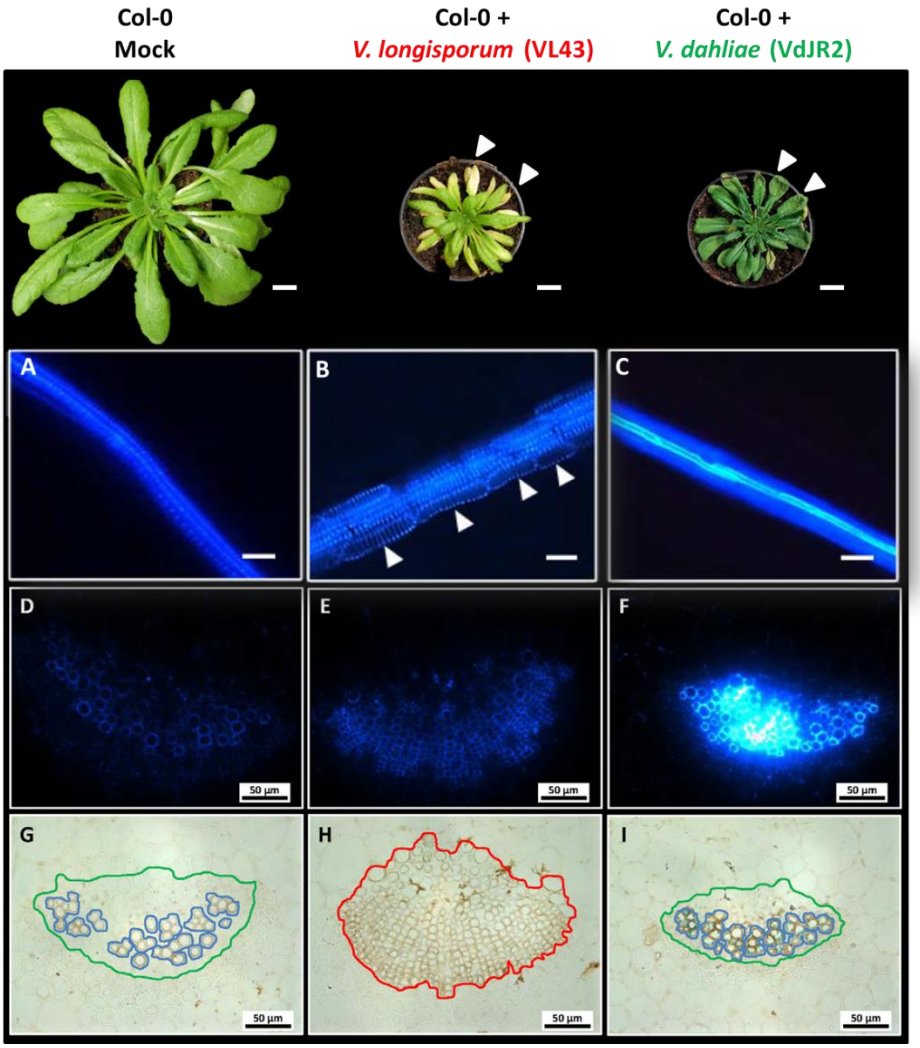

Figure 1.3: Analysis of disease symptom induction and vascular developmental changes during *Verticillium longisporum* VL43 and *Verticillium dahliae* VdJR2 infection. Upper panel: phenotype of mock-treated *A. thaliana* Col-0 plants and macroscopic infection symptoms after inoculation with VL43 and VdJR2 (28 dpi). Chlorosis formation (VL43) and wilting symptoms (VdJR2) are marked by arrowheads. Scale bar: 1 cm. **A-C:** epifluorescence microscopy of leaf veins of mock-treated and infected Col-0 plants. Bundle sheath cell transdifferentiation into tracheary elements (TEs) are marked by arrowheads. Analysis of leaf veins was conducted at 21 dpi. Scale bar: 25 µm. **D-F:** epifluorescence microscopy of leaf midrib cross-sections to study enhanced autofluorescence and lignification levels. **G-I:** bright field microscopy of potassium permanganate stained leaf midrib cross-sections to visualize the extent of lignification (stained in brown). Leaf midrib cross-sections were performed and analysed at 28 dpi. Details of leaf midrib xylem anatomy: xylem cells (blue), xylem parenchyma (green) and hyperplastic xylem (red) are encircled. Figure was adopted from Reusche *et al.*, 2012 and Reusche *et al.*, 2014 and modified.

V. dahliae VdJR2 induced wilting symptoms are accompanied by increased lignification of vascular cells (Figure 1.3F, I; Reusche *et al.*, 2014). The accumulation of lignins or lignin-like phenolic substances was reported before to play a role in various plant-microbe interactions (Vance *et al.*, 1980; Nicholson and Hammerschmidt, 1992). Lignin might act as a barrier against mechanical penetration by plant pathogens or prevent the degradation of plant cell walls via fungal enzymes (Millett *et al.*, 1976; Ride, 1978). Moreover, soluble phenolic compounds

accumulate within vessels to prevent fungal spread. Phenolic compound accumulation was also found in a study comparing VL43 infected *B. napus* cultivars Falcon and SEM 05-500256 (Eynck *et al.*, 2009). There, xylem vessel occlusions via soluble phenolic compounds in the hypocotyl tissues as well as *de novo* formation of lignin and lignin-like polymers at later infection stages occured more intensively in the resistant cultivar SEM 05-500256. Phenol accumulation and lignin deposition may therefore play a role in the defence response of *B. napus* against *V. longisporum*. Likewise, infection studies of *A. thaliana* with *V. longisporum* mutants in the phenylpropanoid pathway suggested that soluble phenylpropanoids are involved in the defence response of *A. thaliana* and inhibit fungal growth (König *et al.*, 2014).

1.3 The function of effector proteins in the plant-pathogen system

1.3.1 The plant innate immune system

Plants are constantly exposed to pathogen attack and have to defend and protect themselves against pathogenic invasion. Plants thereby use constitutive barriers as well as pathogen-induced molecular defence responses. Initially, physical barriers, such as the plant cell wall and cuticle represent a passive defence mechanism to protect the plant against pathogenic invasion (Showalter, 1993). Exo- and endodermis impede soilborne pathogens in entering the plant via the roots. In contrast to the constitutive defence, the inducible reactions against plant pathogens are activated by direct recognition of microbial species. In *A. thaliana* levels of glucosinolates adjust in response to *V. longisporum* infections (Witzel *et al.*, 2015). Glucosinolates are secondary metabolites and are involved in the defence of *Brassicaceae* plants against a variety of biotic stresses (Textor and Gershenzon, 2009; Agerbirk *et al.*, 2009). Global glucosinolate levels were significantly higher upon *V. longisporum* infection in leaf tissues and roots in comparison to non-inoculated plants (Witzel *et al.*, 2015). Specific elicitors, so-called microbial- or pathogen-associated molecular patterns (MAMPs or PAMPs) are recognized by membrane-localised pathogen recognition receptors (PRRs) (Nürnberger and Lipka, 2005). PRRs are receptor-like kinases (RLKs) or receptor-like proteins (RLPs). The perception of PAMPs initiates the PAMP-triggered immunity (PTI) which usually leads to the activation of downstream mitogen-activated protein kinase (MAPK) signalling cascades resulting in the expression of defence genes (Jones and Dangl, 2006). However, pathogens can deliver effector molecules which interfere with PTI to suppress this initial and effective form of plant defence response. Effector molecules can perturb the plant immune response or alter the host cell's structure and function in order to facilitate

infection and enable parasitic colonization of the host (Hogenhout *et al.*, 2009; Win *et al.*, 2012). Pathogenic effector molecules are either secreted into the apoplast or the cytoplasm of the host plant where they target and alter host plant processes and pathways resulting in the so-called effector-triggered susceptibility (ETS). Yet, in resistant genotypes cytoplasmic pathogen-derived effector molecules are recognized by intracellular immunoreceptors of the nucleotide-binding leucine-rich repeat (NB-LRR) class. These immunoreceptors are encoded by *resistance* (*R*) genes and activate the effector-triggered immunity (ETI) (Dangl and Jones, 2001). ETI is established faster and more intensive than PTI and usually results in an hypersensitive response (HR) accompanied by local plant cell death (Greenberg and Yao, 2004).

An evolutionary arms race exists between pathogens and their host plants. If a pathogenic effector protein is successful in stimulating virulence, the frequency of this effector in the pathogen population will be increased. The natural selection pressure would therefore favor this population and maintain the effector function if it escapes host recognition. Via permanently occurring evolutionary processes (e.g. mutations, sexual recombination, chromosomal instability) the host plant would develop *R* genes coding for receptor proteins which are capable of recognizing the pathogenic effector protein. Due to lost effectiveness of the effector, production of this protein would represent fitness costs and the frequency of the effector molecule within the pathogen population would be reduced (Jones and Dangl, 2006). Furthermore, evolutionary mechanisms would promote changes in the virulence profile of pathogens and lead to a variation of individual pathogen lineages or species (Anderson *et al.*, 2010). This evolutionary arms race will continuously proceed between both organisms.

1.3.2 Pathogenic effector molecules and their influence on the plant innate immune system

Effector molecules are found in numerous plant pathogens, including fungi, oomycetes, bacteria and nematodes and are small secreted proteins modifying the cell structure or function of its host (Abramovitch *et al.*, 2006; Birch *et al.*, 2006; Kamoun, 2007; Davis *et al.*, 2008; Klosterman *et al.*, 2011). Effector proteins can have enzymatic functions like cell wall degrading enzymes (CWDEs), but mostly they are defined as small (< 400 amino acids) hypothetical proteins with unknown function (Hogenhout *et al.*, 2009; Klosterman *et al.*, 2011). Typically, the expression of effector molecules is induced upon entry of a pathogen into the plant and subsequent host colonization. Many pathogenic effector molecules carry signal peptides for their secretion from the pathogen and are delivered into the apoplast or the host plant cell (Hogenhout *et al.*, 2009; Raffaele and Kamoun, 2012). In bacteria the type III secretion machinery represents an effective system

injecting effector proteins via needle-like structures into eukaryotic cells (Chatterjee *et al.*, 2013). Likewise, effector proteins can also be secreted unconventionally via the non-classical secretory pathway (Bendtsen *et al.*, 2004a).

During host plant invasion filamentous fungi are often restricted to the extracellular space and they deliver effector proteins mainly to the apoplast (Jonge *et al.*, 2011; Giraldo and Valent, 2013). Yet, fungal effectors can be divided into two classes, since some of them remain in the apoplast and others are translocated into the cytoplasm. Apoplastic effectors include CWDEs, like endoglucanases, ß-1,3-glucanases and chitinases and may play a role in breakdown of the plant cell wall to promote fungal colonization of plant tissues (Carpita and Gibeaut, 1993; Annis and Goodwin, 1997; Jonkers *et al.*, 2009; Tzima *et al.*, 2011). Moreover, the most prominent fungal apoplastic effectors are cysteine-rich secreted proteins which are commonly species-specific or tend to be even isolate-specific (Jonge *et al.*, 2011). Several of these effectors are able to perturb the basal host defence via inhibition of extracellular host proteases. The virulence protein Avr2 of the fungus *Cladosporium fulvum,* for example, interacts with and inhibits apoplastic Cys proteases of tomato which are crucial for basal defence of the plant (van Esse *et al.*, 2008; Shabab *et al.*, 2008). Apoplastic effectors can also protect the fungus from chitin-triggered immune responses of the host plant. The secreted fungal LysM effector Ecp6 of *C. fulvum*, manipulates the chitin-triggered host immunity through competition with host immune receptors for binding of chitin PAMPs (Jonge *et al.*, 2010). Presumably, secretion of Ecp6 is used by *C. fulvum* to avoid its detection.

Apoplastic effector proteins can be subsequently translocated into the cytoplasm of the plant. Thereby, they need to overcome the plant cell wall and the plasma membrane in order to enter the host cytoplasm. In addition, biotrophic and hemibiotrophic fungi are able to enter the plant's cell via the appressoria and deliver effector proteins directly into the cytoplasm (Giraldo and Valent, 2013). With regard to effector molecules of oomycetes the RXLR translocation signal was identified to be essential for delivery into host plant cells (Whisson *et al.*, 2007). Though, also effector proteins without a predicted translocation signal are able to cross the plasma membrane (Kale and Tyler, 2011). So far, detailed information about the mechanism how fungal effectors enter the cytoplasm are missing. How filamentous fungi deliver their effector molecules into host plant cells is a controversial topic in plant-microbe interaction research (Petre and Kamoun, 2014). N-terminal translocation domains, like the oomycete RXLR motif, are under discussion to play a role in host-targeting of fungal effectors. However, a definition for consensus translocation motives for fungal proteins is still missing. Some fungal effectors carry degenerated RXLR-like motifs, though, these motives are highly plastic (Kale *et al.*, 2010). The degenerated RXLR-like

motif was suggested to interact with extracellular phosphatidylinositol-3-phosphate resulting in endocytosis of the fungal effector into host cells (Kale *et al.*, 2010; Plett *et al.*, 2011). Nonetheless, the reproducibility of this finding was challenging, since results of comparable experiments were controversial to the proposed model (Petre and Kamoun, 2014). Since no common motif sequences exist among fungi which may be responsible for cytoplasmic delivery, this suggests that a universal entry mechanism may not exist and that different uptake strategies may have evolved between diverse fungal plant pathogens (Lo Presti *et al.*, 2015).

Cytoplasmic effectors can regulate the transcription of target genes in order to suppress the host defence or alter the structure and function of the cell. For instance, various cytoplasmic pathogenic effector molecules target nuclear components of their host plant to promote virulence. *T*ranscription *A*ctivator-*L*ike (TAL) effectors of the bacterial plant pathogens *Xanthomonas spp* and *Ralstonia solanacearum*, mimic eukaryotic transcription factors (Boch *et al.*, 2009; Scholze and Boch, 2011). With this, TAL effectors have the ability to bind to the promoters of specific host target genes and activate their expression. One example is the effector AvrBs3 of *Xanthomonas campestris* pv. *vesicatoria* which modifies the cell structure of susceptible *Capsicum annuum* varieties via induction of the cell size regulator *upa20* (Kay *et al.*, 2007). Thus, *Xanthomonas* TAL effector AvrBs3 triggers developmental reprogramming of the host cells. Other cytoplasmic TAL effectors, such as PthXo1 of *Xanthomonas oryzae* pv. *oryzae*, affect the expression of genes (e.g. *OsSWEET11*) encoding for sugar transporters (Chen *et al.*, 2010; Deslandes and Rivas, 2012). It was suggested that OsSWEET11 may be involved in the sugar efflux from plants.

1.3.3 Comparative genome studies of plant pathogens identified putative effector molecules

The identification of pathogenic effector molecules is a challenge. Analysis for the presence of signal peptides can be used to predict certain proteins as effector molecules (Spanu *et al.*, 2010; Lo Presti *et al.*, 2015). Often this results in the identification of a catalogue of hundreds of potential effector proteins. Another criterion to identify candidate effector proteins is to detect effector gene expression *in planta* (Spanu *et al.*, 2010; Jonge *et al.*, 2011). Comparative genomics represents a powerful tool to enhance prediction accuracy for most relevant effector proteins involved in disease induction. Genome sequence comparison of the closely related maize pathogens *Ustilago maydis* and *Sporisorium reilianum* discovered conserved effector genes between both species as well as strongly differentiated effector molecule repertoires (Schirawski *et al.*, 2010). Interestingly, the effector genes are often located in clusters within variable genomic

regions which possess low sequence conservation in the otherwise well-conserved syntenic genomes of both species. Schirawski et al. (2010), therefore, concluded that the different sets of effector molecules of the two maize pathogens hint for diverse host molecules targeted during infection. One effector gene cluster in the genome of *U. maydis,* cluster 19A, was studied in detail. Cluster 19A consists of 24 putative effector genes and mutational analyses revealed that this cluster is involved in the virulence of the fungus (Kämper *et al.*, 2006; Brefort *et al.*, 2014). Deletion of cluster 19A resulted in only rare tumor formation and low fungal reproduction in infected tissues of maize plants.

Likewise, conduction of comparative genomics with the three phenotypically diverse species *Fusarium graminearum*, *Fusarium verticillioides* and *Fusarium oxysporum* f. sp. *lycopersici* identified the presence of lineage-specific (LS) genomic regions in *Fusarium oxysporum* (Ma *et al.*, 2010). These LS regions include four entire chromosomes and encode a number of proteins involved in pathogenicity of *Fusarium*. Moreover, one of the LS chromosomes contains all known SIX (secreted-in-xylem) effector proteins (Ma *et al.*, 2010; Schmidt *et al.*, 2013). At least two of the SIX effector proteins contribute to the general virulence of *Fusarium oxysporum* to tomato (Rep *et al.*, 2004; Houterman *et al.*, 2009; Takken and Rep, 2010). Interestingly, transfer of this specific LS chromosome between strains of *F. oxysporum* resulted in the conversion of a non-pathogenic strain into a pathogen.

Also for *V. dahliae* (LS) regions harboring effector genes were discovered via comparative genomics. The cell-surface receptor-like protein Ve1 in tomato governs resistance to race 1 *V. dahliae* strains. In comparison, race 2 strains are not contained by *Ve1* suggesting an effector gene in race 1 strains which is recognized by Ve1 (Jonge *et al.*, 2012). Comparative population genome sequencing of race 1 and race 2 *V. dahliae* isolates identified the corresponding *Ave1* effector gene which is located in a 50 kb sequence region which solely exists in genomes of race 1 isolates, but not in race 2 isolates (Jonge *et al.*, 2012). Functional studies confirmed the role of Ave1 in the establishment of *V. dahliae* virulence since it activates Ve1-mediated resistance. In addition to Ave1, numerous other putative effector molecules which are expressed *in planta* are encoded in the LS regions.

1.4 SA and JA/ET hormone signaling in response to biotrophic and necrotrophic pathogens

Biotrophs are classified as pathogens feeding from living tissues of its host plants, whereas necrotrophic pathogens kill host tissues to obtain their nutrients (Agrios, 1997). Other pathogens, such as *Verticillium* exhibit a hemibiotrophic life style (Fradin and Thomma, Bart P H J, 2006). During the initial biotrophic phase the pathogen is able to suppress the immune system of the host plant which allows the pathogen to spread within plant tissues. In the subsequent necrotrophic phase the pathogen secretes specific lytic enzymes, toxins and other molecules triggering cell death in the host plant.

Usually, *R*-gene mediated resistance is associated with the production of reactive oxygen species (ROS) initiating an hypersensitive response (HR) in form of induced plant cell death (Glazebrook, 2005; Chisholm *et al.*, 2006; Vellosillo *et al.*, 2010). HR, therefore, restricts a biotrophic pathogen in accessing plant-derived nutrients and water. On the other side, pathogen attack triggers the initiation of the salicylic acid (SA)-dependent signaling pathway and further results in the establishment of HR. The SA signaling cascade is established via NON EXPRESSOR OF *PR* GENES1 (NPR1)-dependent and –independent mechanisms (Cao *et al.*, 1994; Fan and Dong, 2002; Tada *et al.*, 2008). In the absence of SA, NPR1 is present in the cytoplasm in an oligomeric form built by disulfide bridges. SA is produced after pathogen infection via the phenylalanine ammonia lyase (PAL) or isochorismate synthase (ICS) biosynthesis pathway (Wildermuth *et al.*, 2001; Chen *et al.*, 2014). Increased levels of SA cause an alteration of the redox homeostasis resulting in a reduction of disulfide bridges. As a consequence, NPR1 monomers are formed which are transported into the nucleus and function as transcriptional coactivator of TGA transcription factors (Bowling *et al.*, 1997; Mou *et al.*, 2003; Tada *et al.*, 2008). TGAs regulate the transcription of SA-responsive pathogenesis-related (PR) genes, such as the *PATHOGENESIS-RELATED* (*PR)* gene *1* (Uknes *et al.*, 1992; Penninckx *et al.*, 1996; Kombrink and Somssich, 1997; Durner *et al.*, 1997; Thurow *et al.*, 2005). Detailed metabolome and proteome studies of the *A. thaliana* apoplast indentified enhanced concentrations of SA glucoside (SAG) after infection with *V. longisporum* (Floerl *et al.*, 2012). SA and SAG are also present in the xylem sap of roots, hypocotyl and the shoots of *B. napus* plants (Ratzinger *et al.*, 2009) and levels of SA and SAG increase in the xylem sap following the infection with *V. longisporum*. Additionally, several studies verified the expression of SA-dependent pathogenesis-related genes in *A. thaliana* after infection with *V. longisporum* and also *V. dahliae* (Tjamos *et al.*, 2005; Johansson *et al.*, 2006; Ralhan *et al.*, 2012). Remarkably, an unconventionally secreted ICS effector, the isochorismatase VdIsc1, of

V. dahliae was identified to disrupt the SA metabolism pathway (Liu *et al.*, 2014). VdIsc1 is necessary for full pathogenesis of *V. dahliae* on host plants, since it suppresses the salicylate-mediated innate immunity and was shown to hydrolyse isochorismate *in vitro*.

R-gene mediated resistance involving HR is therefore reasonable for counteracting biotrophic pathogens, since HR deprives them of a nutrient source. In contrast, necrotrophic pathogens benefit from plant cell death. Thus, the hypersensitive response is not efficient against necrotrophs. Hence, a different signaling pathway is turned on by necrotrophic pathogen invasion (Beckers and Spoel, 2006; McDowell and Dangl, 2000). During pathogen attack increased levels of JA and ET mediate the expression of defence genes, like the *PLANT DEFENSIN 1.2* (*PDF1.2*) (Penninckx *et al.*, 1996; Ndamukong *et al.*, 2007; Zander *et al.*, 2010). A derivate of JA is the JA-isoleucine-conjugate JA-Ile. In bacteria the phytotoxin coronatine mimics the signaling molecule JA-Ile (Weiler *et al.*, 1994). The protein CORONATINE INSENSITIVE1 (COI1) is the receptor for JA-Ile and is involved in the establishment of susceptibility of *A. thaliana* towards *V. longisporum* and *F. oxysporum* (Thatcher *et al.*, 2009; Ralhan *et al.*, 2012). Infection of the *A. thaliana* JA receptor mutant *coi1-t* with *V. longisporum* results in less infection symptoms compared to inoculated wildtype plants and the JA-biosynthesis mutant *aos*. This was contrary to the expectations, since both mutants are impaired in the JA pathway. Thus, neither in *coi1-t* nor in *aos* mutants JA-mediated defence gene expression against necrotrophic pathogens is activated. In addition, the synthesis of JA-Ile by *V. longisporum* was disproved indicating that COI1 is not activated via JA-Ile after infection (Ralhan *et al.*, 2012). This suggested a JA-Ile-independent function of COI1 which plays a role in the susceptibility towards *V. longisporum*. Grafting experiments confirmed a susceptibility-enhancing function of COI1 in root tissues resulting in the establishment of disease symptoms in the shoot (Ralhan *et al.*, 2012). This lead to the conclusion that a yet unknown root-to-shoot signaling cascade exist which enables *V. longisporum* to induce infection symptoms.

Under natural conditions, plants are exposed to multiple stresses, abiotic and biotic including a simultaneous or successive attack by biotrophic and necrotrophic pathogens. An effective cross talk between the SA and ET/JA pathways was detected and studied in detailed analyses (Ndamukong *et al.*, 2007; Zander *et al.*, 2010). Both pathways have an antagonistic effect on the other and this cross talk constitutes a pivotal mechanism to fine-tune the plants' defence responses and allows to prioritize one signaling cascade over the other (Pieterse *et al.*, 2012).

1.5 Gene expression in eukaryotes is controlled by epigenetic and transposable elements

In eukaryotic organisms gene expression is regulated by various factors, such as the activity of transcription factors as well as structural properties of the DNA. The genome in eukaryotes is arranged in chromosomes and densly packed in highly supercoiled chromatin associated with histones in nucleosomes. This structure limits accessibility of the DNA for transcription factors and RNA polymerases (Phillips, 2008; Madigan and Brock, 2009).

The expression of genes in eukaryotes is activated by transcription factors which have a high affinity for specific promoter motifs and promote the recruitment of the RNA polymerase (Struhl, 1999). The transcription factor target sequences are composed of conserved sequences, e.g. the TATA box, which are recognized by diverse transcription factor families (Madigan and Brock, 2009). Transcription initiation and successful binding of the RNA polymerase often includes enhancer elements to promote the transcription. Enhancers are generally cis-acting elements located 5'-upstream of the gene, but can also be located thousands of nucleotides up- or downstream from the gene (Blackwood and Kadonaga, 1998). Distant enhancer sequences are brought into close vicinity of the promoter due to the supercoiled structure of the DNA. In contrast, negative control of gene expression is achieved by silencer elements in the vicinity of the gene. These genomic regions are usually bound by repressor molecules resulting in the inhibition of the transcription complex and subsequently block recruitment of the RNA polymerase to the promoter (Ogbourne and Antalis, 1998).

In addition to the control of gene expression by cis- and trans-acting factors, transcription is modified epigenetically by the chromatin structure of the DNA. Epigenetic defines the changes in gene function inherited via mitosis and/or meiosis. These changes are not based on alteration of the DNA sequence (Russo *et al.*, 1996). Thus, epigenetic control of gene expression is accomplished without any nucleotide changes by mutation. The best characterized epigenetic mechanisms to control gene expression are DNA methylation and histone modifications. During DNA methylation a methyl group is attached to cytidines of the DNA. The exact role of DNA methylation in gene expression is unknown, but methylation may block promoters impeding proper binding of transcription factors (Phillips, 2008). Histone modification includes the acetylation, methylation, phosphorylation, ubiquitylation, sumoylation and various other types of post-translational modifications of histones which result in alteration of the chromatin structure and thereby affect gene expression (Bannister and Kouzarides, 2011). The methylation of histone H3 lysine 9, for example, regulates the expression of numerous effector proteins of *Leptosphaeria*

maculans during primary infection of oilseed rape (Soyer *et al.*, 2014). It was postulated that epigenetic transcription regulation represents a versatile mechanism to reversibly control and adjust gene expression to environmental conditions (Gijzen *et al.*, 2014). Therefore, epigenetic modifications would allow a fast adaptation of a pathogen to changes in host defence strategies. The combination of transcription factors and regulatory elements as well as epigenetic regulation of gene expression allows eukaryotic organisms to fine-tune the transcription of genes.

Transposable elements, including DNA-transposons and retrotransposons, are mobile genetic elements that change their position within the genome. DNA-transposons insert and excise themselves within the genome via the "cut and paste" mechanism with help of the protein transposase which the transposons encode. Retrotransposons produce RNA transcripts and rely on the action of reverse transcriptase enzymes for reverse transcription into DNA which is subsequently inserted into its target site (Pray, 2008). Transposition results in alteration of the genomic structure. Moreover, transposable elements can insert into genes resulting in gene disruption. Integration of transposons into promoter regions or enhancer and silencer elements would alter gene expression. Likewise, transposable elements can mediate homologous recombination between highly similar elements across the genome (Kang et al., 2001; Lemoine et al., 2005). The activity and recombination of transposable elements, therefore, allows gene insertion and deletion. This affects the genetic structures as well as gene expression of organisms. Therefore, transposable elements are often silenced through epigenetic mechanism.

Transposition of transposable elements and their epigenetic silencing play an important role in genome evolution since they are mechanisms that increase the plasticity of eukaryotic genomes (Fedoroff, 2012). Previous studies elucidated that in particular retrotransposons contribute to genome rearrangements via homologous recombination between elements or by causing chromosomal breaks during excision or insertion (Mieczkowski *et al.*, 2006; Maxwell *et al.*, 2011; Faino *et al.*, 2016). In addition, these dynamic regions may promote gene duplication or facilitate mutational mechanisms and allow pathogens to rapidly adapt to environmental changes or to increase their virulence. Several studies of the genomic structure of filamentous fungi have shown that effector molecules involved in pathogenicity and virulence are encoded in genomic regions which are enriched by transposable elements (Spanu *et al.*, 2010; Jonge *et al.*, 2013). For example, the LS regions in *V. dahliae* strains which are composed of numerous effector genes exhibit a high frequency of repetitive elements (Jonge *et al.*, 2013). In subsequent detailed studies Jonge *et al.* (2013) elucidated that extensive chromosomal reshuffling potentially caused by transposable elements and their homologous recombination is the reason for establishment of LS regions and their dynamic nature. Thus, chromosomal rearrangements play a major role in the

evolution of effector molecules. With regard to the evolutionary arms race between pathogen and host plant, effector genes constantly underlie the natural selection pressure. Since asexual fungal pathogens are not able to recombine their alleles via meisosis, chromosomal rearrangements represent a source for genetic variation. Potentially, this would influence the virulence of asexual fungi, such as *Verticillium*.

1.6 Thesis aims

The *V. longisporum* isolate VL43 and the *V. dahliae* isolate VdJR2 induce clearly distinguishable disease symptoms on *A. thaliana* Col-0 plants (Reusche *et al.*, 2014). VL43 infection results in early senescence and developmental reprogramming of the plant vasculature. In contrast, inoculation with VdJR2 induces plant wilting and enhanced cell wall lignification of genuine xylem vessels. The initial aim of this thesis was to determine whether VL43- and VdJR2-like disease symptoms are *Verticillium* species-specific features. For this purpose, the interaction phenotype of 21 *V. longisporum* and 46 *V. dahliae* isolates with the *A. thaliana* wildtype ecotype Col-0 was systematically analysed. A core collection of haploid *V. dahliae* isolates that induce either robust and strong VL43-like early senescence symptoms or VdJR2-like plant wilting, was studied in an *in-depth* characterization. It was a goal to identify developmental changes of the host plant vascular tissues which are induced by early senescence and wilt inducing *V. dahliae* isolates. Therefore, comparative cytological studies of leaf midribs of infected plants were conducted. QRT-PCR analyses showed that transdifferentiation and hyperplasia formation correlate with induction of the marker genes *VND7* and *AtHB8* (Reusche *et al.*, 2012; Reusche *et al.*, 2014). So, qRT-PCR analyses were included in the *in-depth* characterization. For a comparative analysis of the infection kinetics of both *V. dahliae* subclasses, differences in fungal proliferation and defence gene expression were studied. For this, fungal biomass quantification via qRT-PCR and visualization of fungal structures in the plant's vasculature by staining of hyphae (Diener, 2012) was performed. Defence gene expression was monitored via qRT-PCR of the SA-responsive gene *PR-1* and the JA/ET-responsive gene *PDF1.2* (Penninckx *et al.*, 1996; Glazebrook *et al.*, 1996).

It was postulated that the differential symptom induction, "early senescence" and "wilting", results from *Verticillium* species-specific fungal effector molecule repertoires (Reusche *et al.*, 2014). It was the aim to identify putative fungal effector molecules which are involved in the VL43-like pathogen-induced vascular modifications. Genome sequence comparison studies have the power to identify species-specific effector genes (Kämper *et al.*, 2006; Schirawski *et al.*, 2010; Ma *et al.*, 2010; Jonge *et al.*, 2012). Thus, comparative genome sequence analysis of the

selected *V. dahliae* isolates inducing VL43-like early senescence or VdJR2-like wilting symptoms was performed. Subsequent mapping approaches to the *V. dahliae* reference genomes of wilting and early senescence inducing isolates help to discover “early senescence” subclass-specific genes which may encode fungal effector molecules triggering VL43-like developmental changes. Typically, pathogenic effector proteins are expressed *in planta* upon entry of a pathogen into the plant and subsequent host colonization (Hogenhout *et al.*, 2009; Win *et al.*, 2012; Raffaele and Kamoun, 2012). To identify differentially transcribed genes encoding potential fungal effector proteins, RNA-sequencing was performed on *V. dahliae* strains inducing VL43- or VdJR2-like disease symptoms.

2 Materials and Methods

The following part is divided into two sections. The first section (2.1: Materials) describes the substances, solutions and tools utilized during the thesis at hand. The second section (2.2: Methods) summarizes the methods and describes instructions for the executed experiments.

2.1 Materials

2.1.1 Plant Materials

2.1.1.1 *Arabidopsis thaliana*

The *Arabidopsis thaliana* (*A. thaliana*) accessions used in this study are listed in the following table.

Table 2.1: *Arabidopsis thaliana* accessions used in this study

Accession	Abbr.	Species	Original source	Origin
Columbia-0	Col-0	*A. thaliana*	N1092; NASC[a]	USA

[a]Nottingham *Arabidopsis* Stock Centre, Nottingham, UK

2.1.1.2 Other plant species

During this study *Nicotiana benthamiana* (*N. benthamiana*) plants were used for RNA-sequencing analyses (2.2.8.3). *N. benthamiana* seeds were obtained from the Max-Planck-Institute for Plant Breeding Research (MPIPZ, Cologne, Germany). *Gossypium hisutum* was used for infection studies (2.2.3.1) and seeds were obtained from Sunshine-Seeds (http://www.sunshine-seeds.de; Ahlen, Germany).

2.1.2 Pathogens

The *Verticillium* isolates used in this study are summarized in this section. All isolates were used for infection of *A. thaliana* ecotype Col-0. Wildtype *Verticillium* isolates are listed in Table 2.2 and the genetically modified *Verticillium* line was used for visualization of the fungus in Table 2.3.

Table 2.2: *Verticillium spp* isolates used in this study

Isolate	*Verticillium* species	Isolated from	Origin	Reference
Vl18	*V. longisporum*[1]	*Brassica napus*	Mecklenburg, Germany	Prof. Braus[e]
Vl19	*V. longisporum*[1]	*Brassica napus*	Mecklenburg, Germany	Prof. Braus[e]
Vl32	*V. longisporum*[1]	*Brassica napus*	Mecklenburg, Germany	Prof. Braus[e]
Vl40	*V. longisporum*[1]	*Brassica napus*	Mecklenburg, Germany	Prof. Braus[e]
Vl43	*V. longisporum*[1]	*Brassica napus*	Mecklenburg, Germany	Prof. Braus[e]
Vl60	*V. longisporum*[1]	*Brassica oleracea*	California (CA), USA	Prof. Braus[e]
Vl82	*V. longisporum*[1]	*Brassica napus*	Mecklenburg, Germany	Prof. Braus[e]
Vl83	*V. longisporum*[1]	*Brassica napus*	Mecklenburg, Germany	Prof. Braus[e]
Vl84	*V. longisporum*[1]	*Brassica napus*	Mecklenburg, Germany	Prof. Braus[e]
13	*V. longisporum*[1]	*Gossypium spec.*	Spain	Prof. von Tiedemann[d]
18	*V. longisporum*[1]	*Brassica napus*	Lebckendorf, Germany	Prof. von Tiedemann[d]
22	*V. longisporum*[1]	*Brassica napus*	Rostock, Germany	Prof. von Tiedemann[d]
24	*V. longisporum*[1]	*Brassica napus*	Bandelsdorf, Germany	Prof. von Tiedemann[d]
26	*V. longisporum*[1]	*Centaurea cyanus*	Rostock, Germany	Prof. von Tiedemann[d]
35	*V. longisporum*[1]	*Pisum sativum*	Rostock, Germany	Prof. von Tiedemann[d]
T9	*V. dahliae*[1]	*Gossypium spec.*	California, USA	Prof. von Tiedemann[d]
V1.2	*V. dahliae*[1]	*Vitis vinifera*	Neustadt, Wstr.,Germany	Prof. von Tiedemann[d]
V1.2.3	*V. dahliae*[1]	*Solanum tuberosum*	Wisconsin, USA	Prof. von Tiedemann[d]
V2/87	*V. longisporum*[1]	*Brassica napus*	Poel, Germany	Prof. von Tiedemann[d]
V4.5	*V. longisporum*[1]	*Brassica napus*	Germany	Prof. von Tiedemann[d]
V6/88	*V. longisporum*[1]	*Brassica napus*	Poel, Germany	Prof. von Tiedemann[d]
V10	*V. longisporum*[1]	*Brassica napus*	Rostock, Germany	Prof. von Tiedemann[d]
V40	*V. longisporum*[1]	*Brassica napus*	Hohenlieth, Germany	Prof. von Tiedemann[d]
V76	*V. dahliae*[1]	*Gossypium spec.*	Mexico	Prof. von Tiedemann[d]
V142	*V. dahliae*[1]	*Prunus cerasus*	Hungary	Prof. von Tiedemann[d]
V152	*V. dahliae*[1]	*Quercus spec.*	Hungary	Prof. von Tiedemann[d]
V543b	*V. longisporum*[1]	*Brassica napus*	Braunschweig, Germany	Prof. von Tiedemann[d]
Vd2	*V. dahliae*[1]	*Fragaria x ananassa*	Münsterland, Germany	Prof. von Tiedemann[d]
Vd3	*V. dahliae*[1]	*Fragaria x ananassa*	Münsterland, Germany	Prof. von Tiedemann[d]
Vd4	*V. dahliae*[1]	*Fragaria x ananassa*	Münsterland, Germany	Prof. von Tiedemann[d]
Vd5	*V. dahliae*[1]	*Fragaria x ananassa*	Münsterland, Germany	Prof. von Tiedemann[d]
Vd8	*V. dahliae*[1]	*Solanum tuberosum*	Münsterland, Germany	Prof. von Tiedemann[d]
Vd9	*V. dahliae*[1]	*Solanum tuberosum*	Brandenburg, Germany	Prof. von Tiedemann[d]
Vd13	*V. dahliae*[1]	*Gossypium hirsutum*	Cordoba, Spain	Prof. von Tiedemann[d]
Vd15	*V. dahliae*[1]	*Linum usitatissimum*	Mecklenburg, Germany	Prof. von Tiedemann[d]
Vd16	*V. dahliae*[1]	*Solanum tuberosum*	Mecklenburg, Germany	Prof. von Tiedemann[d]
Vd38	*V. dahliae*[1]	*Helianthus annuus*	Hessen, Germany	Prof. von Tiedemann[d]

Vd39	*V. dahliae*[1]	*Helianthus annuus*	Hessen, Germany	Prof. von Tiedemann[d]
Vd41	*V. dahliae*[1]	*Brassica rapa*	Hessen, Germany	Prof. von Tiedemann[d]
Vd42	*V. dahliae*[1]	*Brassica rapa*	Krasnodas, Russia	Prof. von Tiedemann[d]
Vd49	*V. dahliae*[1]	*Capsicum annuum*	Burgenland, Austria	Prof. von Tiedemann[d]
Vd52	*V. dahliae*[1]	*Capsicum annuum*	Burgenland, Austria	Prof. von Tiedemann[d]
Vd54	*V. dahliae*[1]	*Capsicum annuum*	Burgenland, Austria	Prof. von Tiedemann[d]
Vd57	*V. dahliae*[1]	*Fragaria x ananassa*	Mecklenburg, Germany	Prof. von Tiedemann[d]
Vd73	*V. dahliae*[1]	*Linum usitatissimum*	Mecklenburg, Germany	Prof. von Tiedemann[d]
Vd74	*V. dahliae*[1]	*Helianthus annuus*	Mecklenburg, Germany	Prof. von Tiedemann[d]
Vd85	*V. dahliae*[1]	*Solanum tuberosum*	Mecklenburg, Germany	Prof. von Tiedemann[d]
Vd87	*V. dahliae*[1]	*Solanum tuberosum*	Mecklenburg, Germany	Prof. von Tiedemann[d]
Vd88	*V. dahliae*[1]	*Solanum tuberosum*	Mecklenburg, Germany	Prof. von Tiedemann[d]
Vd89	*V. dahliae*[1]	*Lupinum luteus*	Mecklenburg, Germany	Prof. von Tiedemann[d]
Vd334	*V. longisporum*[1]	*Brassica napus*	France	Prof. von Tiedemann[d]
Vd734	*V. dahliae*[1]	*Gossypium spec.*	France	Prof. von Tiedemann[d]
Vd830	*V. dahliae*[1]	*Solanum tuberosum*	Ohio, USA	Prof. von Tiedemann[d]
Türkei	*V. dahliae*[1]	soil	Turkey	Prof. von Tiedemann[d]
White	*V. dahliae*[1]	*Gossypium spec.*	USA	Prof. von Tiedemann[d]
CBS38166	*V. dahliae*[1]	*Solanum lycopersicum*	Ontario, Canada	Prof. Thomma[f]
DVD-31	*V. dahliae*[1]	*Solanum lycopersicum*	Essex Co., Canada	Prof. Thomma[f]
DVD161	*V. dahliae*[1]	*Solanum tuberosum*	Simcoe Co., Canada	Prof. Thomma[f]
DVD-S26	*V. dahliae*[1]	soil	Essex Co., Canada	Prof. Thomma[f]
DVD-S29	*V. dahliae*[1]	soil	Essex Co., Canada	Prof. Thomma[f]
DVD-S94	*V. dahliae*[1]	soil	Kent Co., Canada	Prof. Thomma[f]
ST100	*V. dahliae*[1]	soil	Belgium	Prof. Thomma[f]
ST14.01	*V. dahliae*[1]	*Pistacia vera*	California, USA	Prof. Thomma[f]
VdJR2	*V. dahliae*[1]	*Solanum lycopersicum*	Ontario, Canada	Prof. Thomma[f]
VdLs17	*V. dahliae*[1]	*Lactuca sativa*	California, USA	Prof. Thomma[f]
VaMs.102	*V. albo-atrum*	*Medicago sativa*	Pennsylvania (PA), USA	Prof. Thomma[f]
V200I	*V. dahliae*[1]	*Gossypium spec.*	Cordoba, Spain	Prof. Jiménez-Díaz[g]
V192I	*V. dahliae*[1]	*Gossypium spec.*	Sevilla, Spain	Prof. Jiménez-Díaz[g]
V138I	*V. dahliae*[1]	*Gossypium spec.*	Cordoba / Spain	Prof. Jiménez-Díaz[g]
V781I	*V. dahliae*[1]	*Olea europaea*	Cordoba / Spain	Prof. Jiménez-Díaz[g]

[1]tested in this study

[d]Division of Plant Pathology and Crop Protection, University of Göttingen, Germany

[e]Department of Molecular Microbiology & Genetics, University of Göttingen, Germany

[f]Laboratory of Phytopathology, University of Wageningen, Netherlands

[g]Department of Plant Pathology, University of Córdoba and Institute of Sustainable Agriculture, Cordoba, Spain

Table 2.3: Genetically modified *V. dahliae* line used in this study

Isolate	Characteristics	Reference/Origin
VdJR2-GFP	GFP-expressing reporter strain of VdJR2	(Reusche *et al.*, 2014)

2.1.3 Oligonucleotides

The design of oligonucleotides was performed with the Geneious® software (Pro v. 8.1.6, http://www.geneious.com, (Kearse *et al.*, 2012)). Production of oligonucleotides was ordered by Invitrogen™ (Karlsruhe, Germany). Oligonucleotides were resuspended in H_2O (nuclease-free) to a stock concentration of 100 µM (100 pmol/µl) for oligonucleotide storage. Oligonucleotide dilutions of 10 µM (10 pmol/µl) concentration were prepared with H_2O (nuclease-free) and subsequently used for polymerase-chain-reactions (PCRs) and sequencing reactions. The oligonucleotides were stored at -20 °C. Oligonucleotides used in this study are listed in Table 2.4.

Table 2.4: Oligonucleotides used in this study

Oligonucleotide name	Sequence (5' → 3')	Characteristics/Use
Amplification and Sequencing		
VTA2 forward	GCGGCCGAGACGACGATACG	For amplification of VTA2 gene from *Verticillium* gDNA
VTA2 reverse	TGGCAGCGGTTGCTGCTGAG	
VDAG05285_promoterregion_for-1	TCCCTGCTTACCAACCTTCA	For amplification of the promoter region of ST100.00067g00160 (VDAG_05285)
VDAG05285_promoterregion_rev-2	GCGGTGAGTCGGAGTAATGA	
VDAG05285_promoterregion_for-3	ACTCGGGACCTACAATGCAT	For sequencing of the amplified promoter region of ST100.00067g00160
VDAG05285_promoterregion_rev-4	AGTTGGAGCCACGTGAATTG	
VDAG05281_promoterregion_for-1	GATGTTGGCCTCCTTCGTTC	For amplification of the promoter region of ST100.01886g00010 (VDAG_05281)
VDAG05281_promoterregion_rev-2	TTGGTAGAGGTTCAGCTCGT	
VDAG05281_promoterregion_for-3	CGGCACCAAGATCAAAATGC	For sequencing of the amplified promoter region of ST100.01886g00010
VDAG05281_promoterregion_rev-4	CCAACTCCCTTGCCTAGTCT	
VDAG06204_promoterregion_for-1	CAAGAGCAGCTAGTCAGGC	For amplification of the promoter region of ST100.00022g00100 (VDAG_06204)
VDAG06204_promoterregion_rev-2	CTGGGATGGGCGTAGATGG	
VDAG06204_promoterregion_for-3	TACACGTGCACTAGTAGCGT	For sequencing of the amplified promoter region of ST100.00022g00100
VDAG06204_promoterregion_rev-4	CCTCCCTTTTATTGATCACGCA	

P1_22g100_for	GCCATGCAAGGTTCAAAGTC	For whole gene amplification and sequencing of ST100.00022g00100
P2_22g100_rev	TTAGACGGCATGGAGGTCAC	
P3_22g100_for	TCGTGATCTCTTGCATGCCC	For sequencing of the amplified gene ST100.00022g00100
P4_22g100_rev	GCATGCAAGAGATCACGAGC	
P1_67g160_for	ATCTCTCACCCTTGCAACGG	For whole gene amplification of ST100.00067g00160 and sequencing
P2_67g160_rev	GGGTCGTATCTCCGCCATAC	
P3_67g160_for	AACAGGCCTTTGGGAGTACC	For sequencing of the amplified gene ST100.00067g00160
P4_67g160_rev	GGTACTCCCAAAGGCCTGTT	
P5_67g160_for	CGATGGGTCAGATGCGGAA	
P6_67g160_rev	CTTCCGCATCTGACCCATCG	
P1_1886g10_for	CGGAGATACAAGAAGAGCAGCT	For whole gene amplification of ST100.01886g00010 and sequencing
P2_1886g10_rev	ACCAATGTGCTTTGTCGTCG	
P3_1886g10_for	TCACCTACAAAGACCGACGA	For sequencing of the amplified gene ST100.01886g00010
P4_1886g10_rev	TCGTCGGTCTTTGTAGGTGA	
Expression studies		
ITSRTI	GTGTTGGGGATCTACGTCTGTA	For fungal biomass detection via (semi-)qRt-PCR
ITSRTr	AGTTCAGCGGGTATTCCTACCT	
hyp_prot_VDAG_05285_for	GCACCGAAGAAAGGAGCGAC	For amplification and expression detection of ST100.00067g00160 (VDAG_05285) via semi-qRt-PCR
hyp_prot_VDAG_05285_rev	GAGTGTCGCAAGCTTCGACG	
ligninase_22g100_for	ACTACGTGCAGACCCTGGAC	For amplification and expression detection of ST100.00022g00100 (VDAG_06204) via semi-qRt-PCR
ligninase_22g100_rev	CGTTGAGATTGTAGGTGCCG	
cons_hyp_prot_VDAG_05281_for	CCGGTCGTCAGTCCTTCTAC	For amplification and expression detection of ST100.01886g00010 (VDAG_05281) via semi-qRt-PCR
cons_hyp_prot_VDAG_05281_rev	CTAACCCAGGTTGTCCATCG	
VND7_for	CACGAATACCGTCTCCAAAACT	For expression detection of VND7 (AT1G71930) via qRt-PCR
VND7_rev	CCTAAATGCTCGACACACCA	
PDF1.2_gatz_forward	CTTGTTCTCTTTGCTGCTTTC	For expression detection of PDF1.2 (AT5G44420) via qRt-PCR
PDF1.2_gatz_reverse	CATGTTTGGCTCCTTCAAG	
PR1_forward	TGATCCTCGTGGGAATTATGT	For expression detection of PR1 (AT2G14610) via qRt-PCR
PR1_reverse	TGCATGATCACATCATTACTTCAT	
AtHB8_forward	CTCAAGAGATTTCACAACCTAACG	For expression detection of AtHB8 (AT4G32880) via qRt-PCR
AtHB8_reverse	TCACTGCTTCGTTGAATCCTT	
UBQ5forw	GACGCTTCATCTCGTCC	For expression detection of UBQ5 (AT3G62250) via qRt-PCR (used as reference)
UBQ5rev	GTAAACGTAGGTGAGTCCA	

For/forw/l/forward: forward primer; rev/r/reverse: reverse primer

2.1.4 Enzymes

2.1.4.1 Nucleic acid modifying enzymes

For standard PCR, cloning purposes and cDNA synthesis different nucleic acid modifying enzymes were used as recommended in the manufacturer's protocols. These enzymes together with their appropriate purposes and producer source are listed in Table 2.5.

Table 2.5: Enzymes used in this study

Enzymes	Use and Description	Source
Taq DNA polymerase	Standard PCR	homemade
DNAse I, RNAse-free	RNA treatment for cDNA preparation	Fermentas (St. Leon-Rot, Germany)
SsoFast™ EvaGreen® supermix	qRT-PCR application	Bio-Rad (Munich, Germany)

2.1.5 Kits

Kits from different manufacturers were used for fragment and vector DNA purification and DNA and RNA extraction from plant derived samples. The kits used in this study with their respective producer source are listed in Table 2.6.

Table 2.6: Kits used in this study

Name	Use and Description	Source
innuPREP Plant RNA Kit	Total RNA extraction from plant samples	Analytic Jena (Jena, Germany)
DNeasy Plant Mini Kit	Total DNA extraction from plant samples	Qiagen (Venlo, Netherlands)
NucleoSpin®Gel and PCR Clean-up	DNA fragment purification	Machery-Nagel (Düren, Germany)
Technovit 7100	Infiltration of plant tissue samples	Kulzer Heraeus (Hanau, Germany)
Technovit 3040	Infiltration of plant tissue samples	Kulzer Heraeus (Hanau, Germany)

2.1.6 Chemicals

All chemicals and reagents used in this thesis were purchased from the companies AppliChem (Darmstadt, Germany), Analytic Jena (Jena, Germany), BD (Franklin Lakes NJ, USA), BD Clontech GmbH (Heidelberg, Germany), Bioline (Luckenwalde, Germany), Bio-Rad (Munich, Germany), Difco (Heidelberg, Germany), Duchefa Biochemie (Haarlem, Netherlands), Fermentas (St. Leon-Rot, Germany), Finnzymes (Espoo, Finland), Fluka (Buchs, Switzerland), GE Healthcare (Munich, Germany), Invitrogen™ (Karlsruhe, Germany), Macherey Nagel (Düren, Germany), Merck (Darmstadt, Germany), New England BioLabs (NEB) (Frankfurt/Main, Germany), Qiagen (Venlo, Netherlands), Roche (Mannheim, Germany), Roth (Karlsruhe, Germany), Serva (Heidelberg, Germany), Sigma-Aldrich (Deisenhofen, Germany), Synchem (Felsberg/Altenburg, Germany) or VWR™ (Darmstadt, Germany) if not otherwise declared.

2.1.7 Antibiotics

Antibiotics were added to selective bacterial or fungal media, liquid or solid. Antibiotic stock solutions were sterile filtrated and added freshly to the autoclaved medium. The stock solutions were stored at -20°C.

Table 2.7: Antibiotics

Antibiotic	Final concentration	Stock-solution
Ampicillin	100 µg/ml	100 mg/ml diluted in dH_2O
Cefotaxim	500 µg/ml	250 mg/ml diluted in dH_2O

2.1.8 Media

Media were prepared with distilled, ultrapure H_2O and sterilized at 121 °C and two bar compression for 20 min. Filter sterilization was used for heat instable components. Heat labile substances such as antibiotics were added after autoclaving when the medium cooled down to about 55 °C.

Arabidopsis thaliana media:

½ Murashige and Skoog (MS)-Medium agar plates (Murashige and Skoog, 1962)

Ingredient	Concentration
MS powder + Vitamins	2.2 g/l
MES (2-(N-morpholino)ethanesulfonic acid)	0.5 g/l
Sucrose	10 g/l
Adjust pH to 5.7 with 1M KOH	
Plant agar	7.5 g/l

H_2O-Agar plates

Ingredient	Concentration
Plant Agar	15 g/l

Verticillium spp media:

Potato Dextrose Broth (PDB) and Czapek Dox Broth (CDB)

Potato Dextrose Broth (PDB) and Czapek Dox Broth (CDB) were prepared according to the manufacturers protocols (Duchefa Biochemie (Haarlem, Netherlands). For solid PDB and CDB agar plates, 15g/l agar was added to the media before autoclaving. To avoid bacterial contamination the antibiotics Ampicillin and Cefotaxim were added to the media in the indicated concentrations (Table 2.7).

2.1.9 Buffers and solutions

In the following section all buffers and solutions used in this study are presented. Recipes are listed according to the method for which they were used. If necessary, the solutions were sterilized at 121 °C and two bar compression for 20 min. Heat instable components were filter sterilized.

Agarose gel electrophoresis

Agarose gel	Agarose	1 % (w/v)
	TAE buffer	1 x
TAE buffer (50 x)	Tris	2 M
	Glacial acetic acid	57.1 ml/l
	EDTA (pH 8.0)	50 mM
Loading dye (6 x)	Orange G	0.25 %
	Xylencyanol FF	0.25 %
	Glycerine	30 %

Polymerase-chain-reaction (PCR)

Taq buffer (10 x)	Tris	100 mM
	KCl	500 mM
	$MgCl_2$	15 mM
	Triton X-100	1 % (w/v)
	pH 9.0 KOH	

Histochemical staining for microscopy

Trypan blue solution	Lactic acid	10 ml

	Glycerine	10 ml
	Phenol	10 ml
	H_2O	10 ml
	Trypan blue	10 mg
	Ethanol (96 %)	40 ml
Chloral hydrate solution	Chloral hydrate	2.5 g/ml

<u>XβD-Glc-NAc staining</u>

XβD-Glc-NAc washing solution	$NaPO_4$ (pH 7.2)	50 mM
	EDTA (pH 8)	500 mM
	Potassium ferrocyanide $K_4[Fe(CN)_6]$	0.5 mM
	Potassium ferrocyanide $K_3[Fe(CN)_6]$	0.5 mM
	Triton X-100	0.2 % (v/v)
	add H_2O	
XβD-Glc-NAc staining solution	$NaPO_4$ (pH 7.2)	50 mM
	EDTA (pH 8)	500 mM
	Potassium ferrocyanide $K_4[Fe(CN)_6]$	0.5 mM
	Potassium ferrocyanide $K_3[Fe(CN)_6]$	0.5 mM
	Triton X-100	0.2 % (v/v)
	XβD-Glc-NAc dissolved in DMF	2 mM
	add H_2O	

<u>Histological plant tissue embedding</u>

FAA	Ethanol	50 % (v/v)
	Acetic acid	5 % (v/v)
	Formaldehyde	3.5 % (v/v)
	add H_2O	
Infiltration solution	Technovit 7100 Hardener I	1 g
	Basic liquid Technovit 7100	100 ml
	Store at 4 °C in the dark (max. 4 weeks)	
Mounting solution	Technovit 3040 powder	4 ml
(~ 3 samples)	Technovit 3040 liquid	2 ml
Polymerisation solution	Technovit 7100 Hardener II	100 µl
(~ 3 samples)	Infiltration solution	1.5 ml
Pre-infiltration solution I	Ethanol	50 % (v/v)
	Basic liquid Technovit 7100	50 % (v/v)

Pre-infiltration solution II	Ethanol	25 % (v/v)
	Basic liquid Technovit 7100	75 % (v/v)
Fungal DNA extraction		
CTAB extraction buffer (CEB)	Tris (pH 8)	100 mM
	EDTA (pH 8)	20 mM
	NaCl	1.4 M
	CTAB	2 % (w/v)
	PVP 40.000	1 % (w/v)
TE buffer	Tris (pH 8)	10 mM
	EDTA (pH 8)	1 mM
Fungal RNA extraction		
Sodium acetate buffer	Sodium acetate	3 M
	pH 5.2 with acetic acid	
Trizol buffer	Phenol	380 ml/l
	Guanidinium thiocyanate	0.8 M
	Ammonium thiocyanate	0.4 M
	Sodium acetate buffer	33.4 ml/l
	Glycerine	5 %
Precipitation buffer	NaCl	1.2 M
	Trisodium citrate	0.8 M

2.1.10 Consumables

All consumables used in this study were obtained from the companies Biozym (Hessisch Oldendorf, Germany), Carl-Roth (Karlsruhe, Germany), Eppendorf (Hamburg, Germany), Hawita Gruppe GmbH (Vechta, Germany), Heinemann (Duderstadt, Germany), Hera (Blaufelden, Germany), Hereaus Holding GmbH (Hanau, Germany), Greiner Bio-One (Frickenhausen, Germany), Kulzer Heraeus (Hanau, Germany), Macherey-Nagel (Düren, Germany), Mars (Viersen, Verden, Germany), Meditrade (Kiefersfelden, Germany), Merck Millipore (Darmstadt, Germany), Nette Papier (Göttingen, Germany), Pack Pack (Jever, Germany), Pechinery Plastic Packaging (Chicago, IL, USA), Sarstedt (Nümbrecht, Germany), Sigma-Aldrich (Steinheim, Germany), Sartorius (Göttingen, Germany), Schott (Mainz, Germany), Th. Geyer (Renningen, Germany), Tölle (Göttingen, Germany), Vitakraft (Bremen, Germany) and VWR (Radnor, PA, USA).

2.1.11 Devices

Device	Model	Manufacturer
Bunsen burner	Phoenix eco	Schuett biotec (Göttingen, Germany)
Carriage	-	Blanco (Leipzig, Germany)
Centrifuge	Pico 21	Thermo Fisher Scientific (Langenselbold, Germany)
Clean bench	Hera safe	Thermo Fisher Scientific (Langenselbold, Germany)
Climate chambers	-	Johnson Controls (Milwaukee, WI, USA)
Computer	Optiplex 760	Dell (Halle (Saale), Germany)
Confokal laser scanning microscope	DM 6000CS	Leica (Wetzlar, Germany)
Counting chamber	Thoma	Optik Labor (Lancing, UK)
Dewer	-	Nalgene (Rochester, NY, USA) / Isotherm KGW (Karlsruhe, Germany)
Digital camera	Lumix FZ150	Panasonic (Hamburg, Germany)
Fluorescence microscope	DM 5000B / CTR HS	Leica (Wetzlar, Germany)
Freezer (-20 °C)	Mediline	Liebherr (Kirchdorf an der Iller, Germany)
Freezer (-80 °C)	Hera freeze	Thermo Fisher Scientific (Langenselbold, Germany)
Gel documentation system	GenoPlex	VWR (Hannover, Germany)
Gel electrophoresis equipment	-	Bio-Rad (Hercules, CA, USA)
Gel running chamber	Sub cell® GT	Bio-Rad (Hercules, CA, USA)
Heating plate	OTS40	Medite (Burgdorf, Germany)
Histoform	S	Kulzer Heraeus (Hanau, Germany)
Ice machine	-	Ziegra (Isernhagen, Germany)
Incubation shakers	Certomat BS-1	Sartorius (Göttingen, Germany)
Incubator	-	Memmert (Schwabach, Germany)
Magnetic stirer	RH basic 2 IKAMAG	IKA (Staufen, Germany)
Microwave	R-26ST	Sharp (Osaka, Japane)
Microtome	Hyrax M55	Zeiss (Göttingen, Germany)
Multifuge	3SR+	Thermo Fisher Scientific (Langenselbold, Germany)
PCR Cycler	MyCycler	Biorad (Hercules, CA, USA)
pH meter	Inolab®	WTW (Weilheim, Germany)

Photometer I	Infinite M200	Tecan (Wiesbaden, Germany)
Photometer II	WPA Biowave II	Biochrom (Cambridge, UK)
Pipet	Research	Eppendorf (Hamburg, Germany)
Pipettor	Easypet	Eppendorf (Hamburg, Germany)
Power pack	Blue Power 500	Serva (Heidelberg, Germany)
Printer I	UP-D897	Sony (Surrey, UK)
Printer II	Aficio MP 2352 SP	Ricoh (Tokio, Japane)
Printer III	Ecosys® FS-C5250DN	Kyocera (Kyoto, Japane)
qRT-PCR Cycler	C100 Touch with CFX96 system	Bio-Rad (Hercules, CA, USA)
Quantum meter	MQ-200	Apogee (Logan, UT, USA)
Refrigerator	Mediline	Liebherr (Kirchdorf an der Iller, Germany)
Rotator	-	Heinemann (Duderstadt, Germany)
Steam sterilizer	Varioklav 75S / 135S	Thermo Fisher Scientific (Langenselbold, Germany)
Stereomicroscope	M165FC	Leica (Wetzlar, Germany)
Thermomixer	Compact / Comfort	Eppendorf (Hamburg, Germany)
Vortexer	VF2	IKA (Staufen, Germany)
Water filter system	Arium® 611 DI	Sartorius (Göttingen, Germany)

2.1.12 Software / Servers

Software	Source
Acrobat Reader	http://get.adobe.com/uk/reader/
AUGUSTUS	Bioinformatics Group of the Institute for Mathematics and Computer Science of the University of Greifswald, http://bioinf.uni-greifswald.de/augustus/, (Stanke *et al.*, 2006)
Bio-Rad CFX Manager 3.0	http://bio-rad.com/pcrsoftware
BlattFlaeche (Datinf® GmbH, Tübingen, Germany)	http://datinf.de/home
Chromas lite v. 2.1.1	Technelysium Pty Ltd (Shannon Co. Clare, Irland)
Geneious™ Pro v. 8.1.6	Biomatters Ltd., (Kearse *et al.*, 2012); http://www.geneious.com/
Genesis v.1.7.7	http://genome.tugraz.at/genesisclient; (Sturn *et al.*, 2002)
GeneSnap v. 7.07	SynGene (Synoptics, Cambridge, UK)
GraphPad	http://www.graphpad.com/

ImageJ	http://rsbweb.nih.gov/ij/
LAS AF v.2.6.7266.0	Leica Application Suite (Leica GmbH, Wetzlar, Deutschland)
LAS v. 3.6	Leica Application Suite (Leica GmbH, Wetzlar, Deutschland)
NCBI BLAST	http://blast.ncbi.nlm.nih.gov/Blast.cgi
NLS-mapper	http://nls-mapper.iab.keio.ac.jp/cgi-bin/NLS_Mapper_form.cgi; (Kosugi *et al.*, 2008; Kosugi *et al.*, 2009a; Kosugi *et al.*, 2009b)
Office 2010	Microsoft
*R*obi*NA* MapMen	http://mapman.gabipd.org/web/guest/robin
SecretomeP 2.0	http://www.cbs.dtu.dk/services/SecretomeP/; (Bendtsen *et al.*, 2004a)
SignalP 3.1	http://www.cbs.dtu.dk/services/SignalP/; (Bendtsen *et al.*, 2004b)
VertiBase	http://biofung.gobics.de:1555/; coordinated by Prof. Dr. G. Braus, Georg-August-University of Göttingen
Verticillium group Database / BROAD Institute	http://www.broadinstitute.org/annotation/genome/verticillium_dahliae/MultiHome.html; (Klosterman *et al.*, 2011)
Yloc+	http://abi.inf.uni-tuebingen.de/Services/ YLoc/webloc.cgi; (Briesemeister *et al.*, 2010a, 2010b)

2.2 Methods

2.2.1 Cultivation and maintenance of plant material

2.2.1.1 Cultivation of *A. thaliana* and *N. benthamiana* seeds on soil

For infection experiments ca. 60 seeds were set on soilin a double-layered, pitted plastic-dish (17.5 cm*13 cm*5.5 cm). Between the two plastic-dishes microcentrifuge tubes (Eppendorf, Hamburg) were arranged to allow aeration. In the upper dish 200 ml of granulated clay (Seramis, Mars GmbH, Mogendorf) were put as a water storage compound. 800 ml of a defined sand/soil-composition (1:1-proportion; sand: Vitakraft, Nr. 12262, Bremen, Germany; damped soil: Frühstorfer Erde, Type T, Archut) were put on top of the granulated clay-layer. Before sowing the seeds, the soil was watered with 250 ml tab water and the surface area was additionally sprayed with 0.1 % fertilizer (Wuxal, Manna, Düsseldorf, Germany). For vernalization and synchronization of the germination process seeds were kept 48 h at 4 °C in the cold chamber. Plants were transferred into a climate chamber (Johnson Controls, Milwaukee, WI, USA) and grown under short day (SD) conditions (8 hours light at 22 °C; 16 hours dark at 18 °C; 65 % relative humidity;

light intensity: ~ 170 µEinsteins m^{-2} sec^{-1}). For seven days plants were covered with a light-transmissive hood. 3 ½ - 4 weeks old seedlings were used for infected.

For seed production, seeds were put directly on soil without sand in round (diameter: 60 mm) or angled (diameter: 80 mm) pots (one seed per round pot; five seeds per angled pot) and plants were grown under long day (LD) conditions (16 hours light at 22 °C; 8 hours dark at 20 °C; 65 % relative humidity; light intensity: ~ 170 µEinsteins m^{-2} sec^{-1}). The upper plant parts were tucked into paper bags in order to collect seeds directly after silique opening. Under SD conditions as well as LD conditions plants were watered every 3 days.

2.2.1.2 *A. thaliana* seed sterilization

The surface of *A. thaliana* seeds was sterilized with 70 % (v/v) ethanol. 100-200 plant seeds were filled into a microcentrifuge tube and incubated with 70 % (v/v) ethanol for 5 min at room temperature under vigorous shaking. After that the liquid was extracted with a sterile pipette and 96 % (v/v) ethanol was added to the seeds. Incubation was continued for another 5 min at room temperature under vigorous shaking. Ethanol was removed and seeds were positioned at the inner surface of the microcentrifuge tube with help of a sterile pipet tip. For evaporation of the residual ethanol and drying of the seeds the tube was placed in a thermo mixer (Eppendorf, Hamburg) for 15-30 min at 35 °C.

2.2.1.3 Sterile cultivation of *A. thaliana* plants on ½-MS-plates

½-MS medium (+ agar) was poured in angled (10 cm * 10 cm) petri dishes positioned with one edge elevated for an inclined position. The medium was cooled down until it was solid. For cultivation of *A. thaliana* plants, seeds were sterilized previously (2.2.1.2) and the sterilized seeds were laid in a row (10 seeds per plate) on the thinner half of the medium. The plates were closed with Millipore tape (Merck, Darmstadt, Germany) and kept at 4 °C in the dark for 2 days for vernalization and synchronization of the germination process. After that the plates were placed upright in a rack in the climate chamber (SD conditions (2.2.1.1)) to allow the roots to grow downwards along the media surface. This was done to facilitate the subsequent inoculation with fungal spores (2.2.3.2). *A. thaliana* plants were grown for 2 ½ weeks under SD conditions until a highly branched root system was formed.

2.2.2 Cultivation and maintenance of *Verticillium spp*

2.2.2.1 Cultivation of *Verticillium spp* for *A. thaliana* and *N. benthamiana* infections

180 ml of PDB were supplemented with Cefotaxim and Ampicillin according to the instructions in 2.1.7 and 2.1.8 and filled into a baffled Erlenmeyer flask (Schott, Mainz). Two pieces (ca. 1 cm * 1 cm) of a Czapek Dox agar plate (Sigma-Aldrich, St. Louis, USA) cultivated with *Verticillium spp* or about 10 µl of a *Verticillium* spore stock culture (2.2.2.3) were added to the medium. The spore suspension was incubated for 1 ½ - 2 weeks at 22 °C and 90 rpm in the dark in an incubation shaker (Certomat BS-1, Sartorius, Göttingen, Germany) until fungal mycelia has formed. The PDB was removed with a sterile pipette leaving the fungal mycelia within the flask. 180 ml fresh CDB with Cefotaxim and Ampicillin according to the instructions in 2.1.7 were added to the mycelia and incubated for about three days at 22 °C and 90 rpm in the dark in an incubation shaker (Certomat BS-1, Sartorius). After that, spores were harvested according to section 2.2.2.2.

2.2.2.2 Harvest of *Verticillium spp* spores

For harvest of fungal spores, a culture established as described in 2.2.2.1 was filtered through sterile filter paper (MN 615 ¼; ⌀ 240 mm; Macherey-Nagel, Düren, Germany). The filtrate was collected in two 50 ml Falcon tubes for centrifugation at 4000 rpm and 4 °C for 15 min (3SR Plus, Thermo Scientific, Waltham, USA). The supernatant was discarded and the pellet including the spores was washed in 35 ml autoclaved ultrapure H_2O. The suspension of spores was centrifuged again at 4000 rpm and 4 °C for 10 min. The supernatant was discarded and the pellet was resuspended in 5 ml autoclaved ultrapure H_2O. The spores were stored at 4 °C. Spore concentration was determined in a diluted sample (1:100) with an Abbe-Zeiss counting cell chamber (depth: 0.1 mm; area: 0.0025 mm²; Optik Labor, Görlitz, Germany) under a stereomicroscope (M165FC, Leica, Wetzlar, Germany).

2.2.2.3 Stock culture preparation of *Verticillium spp*

Verticillium spores were cultivated and harvested under sterile conditions as described above (2.2.2.2). 750 µl of spores were mixed with 250 µl of 65 % (v/v) glycerin and vigorously vortexed immediately. The resulting 1 ml mixture was frozen directly in liquid nitrogen and stored at -80 °C.

2.2.2.4 Growth assay of *Verticillium* on solid medium

For the *Verticillium* growth assay a spore solution of 10.000 spores/ml were dripped in the center of solid Czapek Dox agar plates. After 7, 14 and 21 days after plating the diameter of the growing colonies were measured.

2.2.3 Infection of plants with *Verticillium spp*

2.2.3.1 Inoculation of soil-cultivated plant species with *Verticillium spp*

Inoculation of soil-cultivated plant species with *Verticillium spp* was performed on the basis of a previously published uprooting method (Veronese *et al.*, 2003b). 3 ½ - 4 weeks old *A. thaliana* and 2 ½ - 3 weeks old *N. benthamiana* and *G. hirsutum* seedlings were cautiously isolated from the sand/soil-mixture on which they were cultivated (2.2.1.1) and the roots were mechanically injured via twirling. The required number of plants was infected with a *Verticillium spp* spore solution (2.2.2.1 and 2.2.2.2) adjusted to a concentration of 1 * 10^6 spores/ml. For infection the roots of 10 plants were incubated in one petri dish (92 x 16 mm; Sarstedt AG & Co., Nümbrecht, Germany) for 45 min containing the diluted spore solution. A control group of plants was treated with water after also being injured via twirling of the roots. Afterwards, *A. thaliana* seedlings were planted individually into round pots (⌀ 60 mm) and cultivated under SD conditions. *N. benthamiana* and *G. hirsutum* seedlings were planted into angled pots (8 x 8 mm) and cultivated under LD conditions.

2.2.3.2 Inoculation of ½ MS-cultivated *A. thaliana* plants with *Verticillium spp*

Arabidopsis plants grown for 2 ½ weeks under SD conditions on inclined ½-MS agar plates (2.2.1.3) were transferred to inclined 1 % H_2O-agarose plates and incubated for 1 day under SD conditions prior to infection. Because of the minimal concentration of nutrients in 1 % H_2O-agarose the fungus could hardly grow on the surface of the medium and favored the invasion of the plant roots for nutrition. *Verticillium* spores were harvested as described before (2.2.2.2) and a spore solution was adjusted to a concentration of 100.000 spores/ml. The solution was filled into an aerosol and vigorously vortexed. The root system of the plants was spray-inoculated with the spore solution and the plates were again placed in the climate chamber. After two days, invasion of the fungal hyphae into the plant roots was verified via confocal laser scanning microscopy (2.2.9) of control plants infected with a GFP-tagged reference *Verticillium* strain (VdJR2-GFP; 2.1.2). After 4 days the roots of the plants were harvested and used for RNA extraction (2.2.4.12).

2.2.4 Molecular biological methods

2.2.4.1 DNA sequencing and sequence analysis

Single sequencing reactions of purified plasmids and purified PCR-fragments were performed by SeqLab (Göttingen, Germany) using the Barcode Economy Run Service. For PCR products 18 ng per 100 bp in a volume of 12 µl were added to 3 µl primer (10 µM) to a final volume of 15 µl for sequencing. For sequencing of plasmid DNA 720-1200 ng were combined with 1 µl primer (10 µM). Sequence data was analysed with Chromas lite (v. 2.1.1 Technelysium Pty Ltd, Shannon Co. Clare, Ireland) and Geneious™ Pro software (Pro v. 8.1.6, http://www.geneious.com, Kearse et al., 2012).

2.2.4.2 Genomic DNA isolation of *Verticillium spp* mycelia

Genomic DNA of *Verticillium* mycelia was isolated by use of the cationic detergent cetyl-trimethylammonium bromide (CTAB) (Del Sal *et al.*, 1989). For this, *Verticillium* species were cultivated as described previously (2.2.2.1). The grown mycelia were isolated from the culture by filtering and were dried on paper towels. After that the mycelia were ground with mortar and pistil in liquid nitrogen to a fine powder. About 200 mg of the homogenized mycelia were transferred into 1.5 ml eppendorf tubes. At this point, the ground mycelia were either stored at -80 °C or directly used for DNA extraction. For DNA extraction 700 µl of CEB (+ RNase final concentration: 0.1 mg/ml) were added to 200 mg of ground mycelia and incubated for 10 min at 65 °C on a thermomixer under continuous shaking. After that 700 µl of a chloroform:isoamyl alcohol (ratio 24:1) solution was added to the tubes and the mixture was vigorously vortexed. The samples were then allowed to stand at room temperature (RT) for 2-3 min and after that centrifuged at 21.000 x g for 5 min. The supernatants were transferred to new eppendorf tubes containing 0.7 volume of 100 % isopropanol. The solutions were mixed by inverting the tubes several times and incubated for 10 min at RT. The tubes were again centrifuged at 21.000 x g for 5 min to precipitate the DNA. After that the supernatant was discarded and the liquid was removed thoroughly from the pelleted DNA. To wash the DNA pellet 500 µl of 80 % Ethanol were added and mixed by flipping the tube. Again the tubes were centrifuged for 5 min at 21.000 x g and RT. The supernatant was discarded and the pellet was dried on air for 5-10 min. The DNA was then resuspended in 50 µl Tris-EDTA (TE) buffer (pH 8.0). The DNA was heat treated at 70 °C for 15 min on a thermomixer to inactivate DNases. The DNA concentration was measured with help of a photometer Infinite M200 (Tecan, Wiesbaden, Germany) at an absorbance wavelength of 260 nm.

2.2.4.3 Determination of nucleic acid concentrations

Concentrations of DNA and RNA samples were measured on the NanoQuant plate™ (Tecan, Wiesbaden, Germany) and with the photometer Infinite M200 (Tecan, Wiesbaden, Germany). Nucleic acid concentrations were measured at 260 nm wavelength.1 µl of the sample was used for measurement after standardization of the microplate. For standardization the corresponding elution buffer in which the nucleic acid had been diluted was used.

2.2.4.4 Polymerase chain reaction (PCR)

With polymerase chain reaction (PCR) it is possible to amplify DNA fragments *in vitro* (Mullis and Faloona, 1987). PCR reactions were performed in a PCR cycler MyCycler (BioRad, Hercules, CA, USA). For standard PCR reactions for DNA fragment amplification the home made *Taq* polymerase was used (2.1.4) according to the following recipe:

Ingredient	**Volume [µl]**
Taq buffer	2
dNTPs (10 mM)	0.5
forward primer (10 µM)	0.75
reverse primer (10 µM)	0.75
Taq	0.5
ddH_2O	14.5
DNA (0.1 ng – 50 ng)	1

The following protocol was used for PCR reactions with home made *Taq* polymerase:

Step	**Temperature**	**Time**	
initial denaturation	94 °C	3 min	
denaturation	94 °C	30 sec	35x
annealing	50 °C – 62 °C	30 sec	
extension	72 °C	1 – 3 min (1 min per kbp)	
final extension	72 °C	3 min	

PCR reactions for cloning purposes were carried out with the Phusion High-Fidelity DNA Polymerase (2.1.4.1, manufacturer infos). The Phusion polymerase was used according to the manufacturer's protocol with the following recipe and thermal running protocol:

Ingredient	Volume [µl]
HF buffer (5x)	10
dNTPs (25 mM)	0.4
forward primer (10 µM)	1
reverse primer (10 µM)	1
Phusion	0.25
ddH_2O	x
DNA (10 ng – 100 ng)	x
	50

Step	Temperature	Time	
initial denaturation	98 °C	40 sec	
denaturation	98 °C	15 sec	33x
annealing	62 °C	20 sec	
extension	72 °C	30 sec – 2 min (30 sec per kbp)	
final extension	72 °C	10 min	

2.2.4.5 Agarose gel electrophoresis of DNA fragments

DNA fragments were separated in 1.5 - 3 % (w/v) agarose gels according to the fragment sizes. When fragments with less than 50 bp difference were separated in the same electrophoresis run 3 % agarose gels were used. UltraPure™ Agarose (Biozym, Hessisch Oldendorf, Germany) was dissolved in 1x TAE buffer (Mülhardt, 2009) and boiled up in a microwave. When the agarose was cooled down to ~ 60 °C ethidium bromide solution (10 mg/ml) was added (1 droplet/50 ml) (Sharp *et al.*, 1973). The agarose was then poured in a gel caster (Sub-Cell GT Cell; Biorad, Hercules CA, USA) including a comb and cooled down until the gel was solidified. The gel was placed into a running tank filled with 1x TAE buffer. 6x loading-dye (2.1.9) was added to the DNA samples and the samples were pipetted into the agarose gel-pockets. Electrical current (80-120 volt) was applied in order to create an electrical field. Negatively charged DNA-phosphate groups move according to their conformation and size towards the anode. Sizes of separated DNA-fragments were assigned with help of a marker, the GeneRuler™ 1 kb DNA ladder or GeneRuler™ 100 bp DNA ladder (Fermentas, St. Leon-Roth, Germany). The bands on the agarose gel were then visualized on a 312 nm UV transilluminator (GenoPlex, VWR, Darmstadt, Germany) and photographed with help of the GeneSnap software (version 7.07, Synoptics, Cambridge, UK). For isolation of DNA fragments from agarose gels, bands were visualized with 365 nm wavelength on the UV transilluminator to avoid degradation of DNA fragments and nucleotide mutation. The fragments used for sequencing or cloning purposes were cut with a clean scalpel from the gel and further eluted via the NucleoSpin® Gel and PCR Clean-up Kit (Macherey-Nagel, Düren, Germany). The fragments were eluted in 15 µl elution buffer.

2.2.4.6 DNA isolation of *Verticillium* infected plants for fungal biomass quantification

DNA isolation from the upper plant part (rosette leaves and hypocotyl) of *Verticillium* infected plants was performed by the DNeasy Plant Mini Kit (Qiagen, Hilden, Germany) according to the manufacturer´s instructions. The DNA was eluted in 20 µl elution buffer and the extracted DNA was used in quantitative real-time polymerase-chain-reaction (qRT-PCR) for fungal biomass quantification (2.2.4.7) or stored at -20 °C. The DNA concentration was further measured with help of a photometer at an absorbance of 260 nm.

2.2.4.7 Quantitative real-time PCR (qRT-PCR) for fungal biomass quantification

QRT-PCR reactions were performed in the thermocycler C100 Touch with CFX96 system (Biorad, Hercules CA, USA) and with use of the SsoFast™ EvaGreen® supermix (Bio-Rad, Hercules, CA, USA). For quantification of fungal biomass the expression of the internal transcribed spacer (ITS) region of the nuclear ribosomal RNA gene (rDNA) of *Verticillium spp* was measured. Therefore the primers ITSRTl and ITSRTr were used (2.1.3). For normalization and subsequent calculation of the starting quantity of fungal DNA a calibration scale was pipetted. For the calibration scale specific concentrations of genomic DNA for each *Verticillium* strain tested were used: 8 pg/µl, 16 pg/µl, 32 pg/µl, 64 pg/µl and 128 pg/µl. In qRT-PCR reactions for measurement of fungal biomass 25 ng of total DNA were used as template. Every reaction was pipetted on a Multiplate^{TM} PCR Plate (96-well, clear; Bio-Rad). On the basis of the calibration scale the software Bio-Rad CFX Manager 3.0 (Bio-Rad, Hercules, CA, USA) was used to calculate the starting quantity of fungal DNA in qRT-PCR reactions in ng. As a negative control qRT-PCR reactions with water instead of fungal DNA were performed. The qRT-PCR reactions were mixed according to the following recipe:

Component	Volume [µl]
SsoFast™ EvaGreen® supermix	10
ITS primer mix (4 mM)	2
total DNA (25 ng)	8

QRT-PCR was run according to the following protocol:

Step	Temperature	Time	Cycle number
Initial Denaturation	95 °C	2 min	1x
Denaturation	95 °C	20 sec	
Annealing	60 °C	20 sec	40x
Elongation	72°C	40 sec	
Melting curve	55 °C – 95 °C	10 sec	81x

2.2.4.8 RNA isolation of *Verticillium* infected *A. thaliana* plants for gene expression analyses

For RNA isolation from *Verticillium* infected plant samples the innuPREP Plant RNA Kit (Analytic Jena, Jena, Germany) was used. Total RNA extraction was performed according to the manufacturer's protocol. RNA was eluted in 20 µl RNase-free water and concentrations were measured with a photometer at an absorbance wavelength of 260 nm. Isolated RNA was stored at -80 °C or directly used for cDNA synthesis (2.2.4.9).

2.2.4.9 cDNA synthesis

For cDNA synthesis samples of mRNA were reverse transcribed to cDNA with help of the RevertAid™ H Minus First Strand cDNA Synthesis Kit (Fermentas, St. Leon-Roth). 1 µg of RNA was used for cDNA synthesis and the reactions were performed in RNase-free PCR tubes using a PCR cycler (MyCycler™, Biorad, Hercules CA, USA). Before reverse transcription the samples were digested with DNaseI (Fermentas, St. Leon-Roth) to remove remaining genomic DNA.

DNaseI digestion:

Component	**Concentration**
RNA	1 µg
10x Reaction Buffer with MgCl2	1 µl
DNaseI, RNase-free	1 µl (1 u)
Ribolock™ RNase Inhibitor	0.5 µl
DEPC-treated water	to 10.5 µl

cDNA synthesis

Component	**Volume**
Template RNA	10.5 µl
Oligo $(dT)_{18}$ Primer	1 µl
DEPC-treated water	to 12.5 µl
Chilling on ice for 5 min	
5x Reaction Buffer	4 µl
Ribolock™ RNase Inhibitor (20 u/µl)	0.5 µl
dNTP Mix (10 mM)	2 µl
RevertAid™ H Minus Reverse Transcriptase	1 µl

The reverse transcription was occurred by incubation for 60 min at 42 °C and the reaction was terminated by heating at 70 °C for 5 min. The synthesized cDNA was stored at 4 °C.

2.2.4.10 Semi-quantitative real-time polymerase chain reaction (semi-qRT-PCR)

Semi-qRT-PCR was used for quantification of transcript levels decuced from band intensities after agarose gel electrophoresis (0). Semi-qRT-PCR reactions were performed in a PCR cycler (MyCycler, Biorad, Hercules CA, USA) and as template 1:10-diluted reverse transcribed cDNA was used (2.2.4.9). Semi-qRT-PCR was performed with the home made *Taq* polymerase (see 2.1.6.2) according to the following recipe and thermal running protocol:

Component	**Volume**
Taq Buffer (10x)	2 µl
dNTP mix (10 mM)	0.5 µl
forward primer (10 µM)	0.75 µl
reverse primer (10 µM)	0.75 µl
Taq polymerase	0.5 µl
water, nuclease-free	14.5 µl
cDNA (1:10-dilution)	1 µl

Step	**Temperature**	**Time**	
Initial denaturation	94 °C	4 min	
Denaturation	94 °C	30 sec	33-37x
Annealing	50 °C – 62 °C	30 sec	
Extension	72 °C	1 – 3 min (1 min per kbp)	
Final extension	72 °C	6 min	

2.2.4.11 Quantitative real-time PCR (qRT-PCR) for quantification of gene expression

The qRT-PCR was used to amplify and simultaneously quantify a specific DNA fragment in order to measure gene expression. The expression of a certain gene is thereby quantified relatively to the expression of a reference gene. As reference for *A. thaliana* target genes the Ubiquitin5 gene (UBQ5, At3g62250; primers: UBQ5forw and UBQ5reverse; 2.1.3) was used in this study (Czechowski *et al.*, 2005). The procedure follows the general principle of polymerase chain reaction. Due to the addition of the non-specific fluorescent dye (e.g. SYBR Green) that intercalates with any double-stranded DNA the fluorescence and therefore the concentration of the transcripts could be measured after each cycle during the logarithmic phase in the thermocycler C100 Touch with CFX96 system (Biorad, Hercules CA, USA). The amount of amplified fragments correlates with the amount of template cDNA due to logarithmic measurements. Therefore a threshold value for fluorescence is determined and the cycle number at which the sample reaches this threshold is defined as cycle threshold (ct) value. The higher the ct value the lower the template amount has been in the initial sample. The relative expression of the targeted gene is calculated according to the 2^{-}

$^{\Delta\Delta ct}$ method (Livak and Schmittgen, 2001) in regard to the expression values of the reference gene UBQ5. With the data measured during the qRT-PCR a melt curve is defined to verify that exclusively the target gene was amplified. For quantification of target gene expression the SsoFast™ EvaGreen® supermix (Bio-Rad, Hercules, CA, USA) was used according to the instructions of the manufacturer's protocol and 1 µl of the cDNA 1:10-dilution was used for each reaction (2.2.4.9). For negative control reactions 1 µl water was used instead of cDNA. qRT-PCR reactions were pipetted in a Multiplate™ PCR Plate (96-well, clear; Bio-Rad) with the following components:

Component	**Volume [µl]**
SsoFast™ EvaGreen® supermix	7.5
Primer mix (4 mM)	1.5
dH_2O	5
cDNA (1:10 dilution)	1

QRT-PCR was run according to the following protocol:

Step	**Temperature**	**Time**	**Cycle number**
Initial Denaturation	95 °C	30 sec	1x
Denaturation	95 °C	5 sec	45x
Annealing	55 °C	10 sec	
Melting curve	55 °C – 95 °C	5 sec	81x

2.2.4.12 Total RNA extraction of *Verticillium* infected plants for RNA-sequencing

Total RNA of *Verticillium* infected plants used for RNA-sequencing was isolated with help of the TRIZOL extraction method (Chomczynski, 1993). The plant material was ground to a fine powder in liquid nitrogen and ~200 mg were transferred to a 2 ml eppendorf tube. 1.4 ml of Trizol buffer was added to each tube and incubated for 10 min at RT on a thermoshaker. After that 260 µl chloroform were added to the sample and incubated for 10 min at RT on a thermomixer. The tubes were then centrifuged for 45 min at 4 °C and 13.000 – 15.000 rounds per minute (rpm). ~900 µl of the supernatant were then transferred into new 2 ml tubes in which 400 µl of the precipitation buffer and 400 µl isopropanol have been put. The tubes were then inverted several times to mix and incubated for 10 min at RT. For RNA precipitation the samples were centrifuged again for 30 min at 4 °C and 13.000 – 15.000 rpm and the supernatant was discarded. The pellet was washed in 250 µl 70 % ethanol and centrifuged again for 15 min at RT and and 13.000 – 15.000 rpm. The washing step was repeated twice and the supernatant was discarded. The RNA pellet was air dried for 5 min at RT and after that resuspended in 30 µl ddH_2O. The tubes were incubated at 65 °C for 10 min in a thermomixer to solve the RNA. RNA concentrations were measured with a photometer at an absorbance wavelength of 260 nm. The samples were stored at -80 °C or directly used for RNA-sequencing (2.2.8.3).

2.2.5 Histological methods

2.2.5.1 XβD-Glc-NAc staining, embedding and sectioning of plant tissues

XβD-Glc-NAc staining

The XβD-Glc-NAc staining method was used to visualize fungal structures in different plant tissues (Diener, 2012). The colorimetric substrate 5-bromo-4-chloro-3-indoxyl-2-acetamido-2-deoxy-β-D-glucopyranoside (XβD-Glc-NAc) is converted by the fungal enzyme N-Acetyl-β-D-glucosaminidase into a blue precipitate. First, individual plant tissues (roots, hypocotyl and leaves) were harvested from the plant and immediately immersed in H_2O in brown light-impervious 2 ml microcentrifugation tubes to prevent drying-out. The samples were destained for 20 min in ice-cold aceton. Subsequently, the aceton was removed and the XβD-Glc-NAc washing solution was added and incubated for 10 min (2.1.9). The XβD-Glc-NAc washing solution was discarded and the samples were incubated in the XβD-Glc-NAc staining solution (2.1.9). The solution was vacuum-infiltrated for 1 min with an exsiccator and the samples were kept in the dark at 28 °C over night.

Sample fixation and infiltration:

The following steps were performed under light agitation at room temperature. The staining solution was discarded and 2 ml FAA (2.1.9) was added to the stained samples for fixation. The next day, an ethanol series was used to dehydrate the samples. Increasing ethanol concentrations (50 %, 60 %, 70 %, 85 %, 95 % (v/v)) were added to the samples followed by incubation for 90 min each. The samples were kept in 100 % ethanol over night. Ethanol was replaced by fresh 100 % ethanol the next morning. After 2 h the pre-infiltration solution I was added and incubated for 4 h, followed by incubation with the pre-infiltration solution II over night. The pre-infiltration solution II was exchanged by the filtration solution and the samples were vacuum-infiltrated in an exsiccator for 1.5 h. The samples were kept in the filtration solution for at least 3 days.

Embedding:

Infiltration of the plant tissues was followed by embedding. For this, the Histoform S Kulzer Heraeus (Hanau, Germany) was half-filled with the polymerization solution (2.1.9) and the samples were positioned inside. After 4 h polymerization, the Histoblock was positioned in the recess of the Histoform S. The mounting solution (2.1.9) was poured inside the Histoblock and after the mounting solution solidified (~20 min) the samples were removed from the Histoform. The Histoblock including the samples were stored at 4 °C.

Sectioning via the microtome:

After embedding the samples were sectioned with a microtome (Hyrax M55, Zeiss, Göttingen, Germany). Every Histoblock was cut into sections of 5 µM and 10 µM dimension (sectioning conditions: speed 9 and angle 9 °). The sections were carefully placed directly onto object slides covered with water and were dried on a heating plate (OTS40, Medite, Burgdorf, Germany; 50-60 °C).

Microscopic investigation:

5 µM sections were first investigated under the epifluorescence microscope (DM 5000B, Leica, Wetzlar, Germany) to analyse the autofluorescence level of the samples (ATL filter cube). After examination, the 5 µM sections were stained with 0.1 % (w/v) potassium permanganate (or 0.05 % (w/v) toluidine blue) for 1 min. Potassium permanganate was washed off with water and the object slides were dried at 50-60 °C. The 10 µM sections were stained with 0.05 % (w/v) Safranin-0 for 1 min, the dye was washed off with water and the object slides were dried at 50-60 °C. Finally, the stained slides were mounted with ~100 µl DePeX mounting medium and a cover glass was put on top of the mounting medium. Potassium permanganate and safranin-O stained samples were examined under the epifluorescence microscope (DM 5000B, Leica, Wetzlar, Germany) under bright field conditions with respect to enhanced lignification and fungal colonization, respectively.

2.2.5.2 Trypan blue staining of plant leaves

Trypan blue staining was carried out to illustrate lignified cells and cell death in the leaves. For this, leaves were harvested from Verticillium infected plants and uninfected plants and put into a 50 ml falcon. Trypan blue solution (2.1.9) was filled into the falcons until the leaves were completely covered with the solution. For 5 min the falcons were transferred into a beaker glass with boiling water. After that, trypan blue solution was drained and for destaining 10-15 ml chloral hydrate solution was added to the leaves. Destaining occurred for ~2-3 days at RT. The chloral hydrate solution was exchanged by fresh chloral hydrate solution. This step was repeated several times until no more trypan blue leaked from the samples. The samples were stored in 60 % (v/v) glycerol. The leaves were placed on an object slide and covered with glycerol and a cover glass. The samples were analysed with a fluorescence microscope under bright field and epifluorescence (ATL filter cube) conditions (DM 5000B, Leica, Wetzlar, Germany) for transdifferentiated xylem vessels and lignified structures, respectively.

2.2.6 Leaf area measurement of *A. thaliana*

Pictures of individual plant-rosettes were taken with a digital camera (Lumix FZ150, Panasonic, Hamburg, Germany) at 7 days post infection (dpi), 14 dpi, 21 dpi, 28 dpi and 35 dpi with *Verticilium*. Leaf area of the plants was determined via the image processing by the software BlattFlaeche (Datinf® GmbH, Tübingen). For normalization of leaf area the diameter of the pots was chosen as reference.

2.2.7 Statistical Analyses

Statistics were evaluated with GraphPad QuickCalcs unpaired t-test (http://graphpad.com/quickcalcs/index.cfm).

2.2.8 Bioinformatical methods

2.2.8.1 Whole-genome sequencing of *V. dahliae*

Genome sequencing was done by the Goettingen genomics laboratory (G2L). Shotgun libraries were generated using the Nextera DNA Sample preparation kit following the manufacture instructions. The whole genomes of the different V. dahliae strains were sequenced with the Genome Analyser IIx (Illumina, San Diego, USA). The libraries were sequenced in a 75 bp single read run. The resulting reads were used for genome sequence comparison studies involving a specific mapping strategy (3.4.1). Mappings were performed by the G2L with the software bowtie2 (v. 1.0.0 (Langmead *et al.*, 2009)). Moreover, reads were used for an initial and provisional *de novo* assembly of the diverse *V. dahliae* genomes.
For genome sequence comparison the sequences of DVD31 and DVD-S29 were included. These *V. dahliae* isolates were originally sequenced and *de novo* assembled by the group of Prof. Dr. B. Thomma (University of Wageningen) (Jonge *et al.*, 2012). To perform genome mappings with these isolates which can be compared to the mappings of the other *V. dahliae* isolates, the *de novo* assembled genome had to be artificially split up. The split sequences possessed a length similar to the sequenced reads of the genomes of the other analysed strains. However, due to different sequencing events the number of reads of DVD31 and DVD-S29 were not comparable to that of the other strains which were sequenced in the present study. Therefore, values of mapping reads of DVD31 and DVD-S29 were not specified.

2.2.8.2 Gene prediction of sequenced contigs of *V. dahliae*

Gene prediction was performed with help of the AUGUSTUS software of the Bioinformatics Web Server at the University of Greifswald (http://bioinf.uni-greifswald.de/augustus/, (Stanke *et al.*, 2006)). For gene prediction the pre-trained parameters of *V. longisporum* were used.

2.2.8.3 RNA-sequencing analyses

For RNA-sequencing analyses *Nicotiana benthamiana* plants were cultivated and infected with the *V. dahliae* isolates T9, V76, ST100, V138I, V781I, V192I, VdJR2, VdLs.17, DVD-S29 or DVD31 (2.1.2) as described previously (2.2.1.1 and 2.2.3.1). In addition, *Arabidopsis thaliana* plants were grown on ½-MS agar plates (2.2.1.3) and infected with the same isolates as mentioned above (2.2.3.2). In parallel, *Arabidopsis* plants were infected with the GFP-expressing reporter strain VdJR2-GFP (2.1.2) for confocal microscopy studies to monitor the successful penetration of roots by *Verticillium* (2.2.9). *N. benthamiana* plants were used to isolate the aerial parts of infected and uninfected plants whereas the cultivation of *A. thaliana* served for isolation of infected and uninfected root material. Sampling of the *N. benthamiana* plants occurred 8 days post infection (dpi), 12 dpi and 16 dpi whereas harvest of *Arabiopsis* roots occurred

at 4 dpi. Each sample included the pool of 3 tobacco plants of the same condition (uninfected or infected with one *V. dahliae* isolate) or of 40 *Arabidopsis* root systems of the same condition, respectively. Aerial plant parts or root systems were harvested, collected in a mortar and directly pestled in $N_2^{(l)}$ to a fine powder. RNA was extracted from the samples via TRIZOL method as described previously (2.2.4.12). RNA-sequencing and sample preparation was performed by the Transcriptome and Genome Analysis Laboratory (TAL, Department of Developmental Biochemistry, University of Göttingen, Germany). TruSeq RNA Library Prep Kit v2 (Illumina, San Diego, CA, USA) was used to generate mRNA libraries from total RNA. Furthermore, the TruSeq SR Cluster Kit v3-cBot-HS (Illumina, San Diego, CA, USA) was used for fixation of RNA samples to complementary adapter oligos to guarantee subsequent cluster amplification on single-read flow cells. An indispensable quality control of the RNA-samples was performed via Bioanalyser 2100 software (Agilent technologies, Santa Clara, CA, USA). RNA-sequencing was done with the Illumina HiSeq 2000 Instrument and for each sample ~30-35 million single-end 50 bp reads were obtained. The resulting sequence reads were demultiplexed and transformed into fastq files via the CASAVA v1.8.2 (Illumina, San Diego, CA, USA) software. Fastq files were used for subsequent mapping of the sequencing reads to the transcriptome of *Arabidopsis thaliana* (TAIR10) and *Nicotiana benthamiana* (v1.0.1; Sol Genomics Network), respectively, and to both transcriptomes of *Verticillium dahliae* VdLs.17 (BROAD Institute; (Klosterman *et al.*, 2011)) and *Verticillium dahliae* ST100 (NCBI Sequence Read Archive http://www.ncbi.nlm.nih.gov/sra; BioProject PRJNA169154). The mapping was performed with the software Bowtie2 v2.1.0 (Johns Hopkins University, Baltimore, Maryland, USA (Langmead *et al.*, 2009)).

For subsequent log2FC value calculation one pseudo-read was counted to every expressed gene under every condition. This is indispensable since some genes are not expressed by some *V. dahliae* isolates. To guarantee log2FC calculation the expression value must be >0. The resulting reads per gene were further analysed concerning differential gene expression via the software *R*obi*NA* v1.2.4 (Lohse *et al.*, 2012) and normalization and evaluation of the values was carried out under the conditions of DESeq (Anders and Huber, 2010). The false discovery rate was adjusted using the Benjamini-Hochberg procedure (Benjamini and Hochberg, 1995). Analyses with *R*obi*NA* resulted in the binary logarithm of the fold change (log2FC value) of the gene expression compared between two groups. In parallel, the reads per gene were normalized manually by calculating the reads per million (RPM) in order to compare the resulting log2FC values with that generated by *R*obi*NA* as a control. For correction of log2FC values (total transcription) the RNA-seq reads of gene homologues (ST100 and VdLs.17) were combined. Log2FC values of combined RNA-seq reads were calculated manually.

Candidate genes were analysed concerning the presence of their homologs in the genome of the *Verticillium longisporum* isolate VL43 with help of the Blast Webinterface function of the BioFung Database (VertiBase). In addition, presence of secretion signals and the possibility of unconventional secretion was analysed via SignalP 3.1 Server (Bendtsen *et al.*, 2004b) and SecretomeP 2.0 Server (Bendtsen *et al.*, 2004a), respectively.

2.2.8.4 Heat map generation and hierarchical clustering

Heat map generation for visualization of differential expression as well as hierarchical clustering of expression values was performed with the software Genesis v.1.7.7 (Sturn *et al.*, 2002). For heat map generation the expression profile of log2FC values of candidate genes were visualized. For hierarchical clustering the log2FC values of the Top50 expressed genes for each analysed time point were used.

2.2.9 Confocal laser-scanning microscopy (CLSM)

To monitor the penetration of *Arabidopsis* roots by *V. dahliae* during RNA-sequencing sample cultivation confocal laser-scanning microscopic studies were performed. For this the confocal laser-scanning microscope Leica SP5-DM6000 (Leica GmbH, Wetzlar, Germany) equipped with an argon ion laser as excitation source and the Leica LAS AF software v.2.6.7266.0 was used. An excitation wavelength of 488 nm specific for GFP with detection at 500-540 nm was used. Roots of VdJR2-GFP-infected *A. thaliana* plants were mounted on an object slide, covered first with water and subsequently with a cover glass. Analyses for root penetration were performed 48 hours post infection (hpi).

3 Results

3.1 Classification of a *Verticillium* strain collection based on the type of disease symptoms induced on *A. thaliana* Col-0 plants

Previous studies showed that both, the *V. longisporum* isolate VL43 and the *V. dahliae* isolate VdJR2 induce distinct infection symptoms on *A. thaliana* which may result from species-specific infection strategies and fungal effector molecule repertoires (Reusche *et al.*, 2014). The initial aim of this work was to verify whether the disease symptoms observed for these interactions are indeed species-specific features of the two pathogen species *V. longisporum* and *V. dahliae*. Therefore, a *Verticillium* strain collection was established which allowed to study the interaction phenotypes of various isolates on the *A. thaliana* accession Col-0. The collection consists of 22 *V. longisporum* and 47 *V. dahliae* strains which were isolated from diverse host plant species and also from different geographical regions in Europe and North America (Table 3.1, Figure 3.1). In addition to the initially uncharacterized isolates, the strain collection includes the *V. dahliae* reference strain VdLs17 (Klosterman *et al.*, 2011) and several newly sequenced *V. dahliae* isolates. These isolates were recently subject of a comparative genome sequence analysis aimed at the discovery of the *V. dahliae* effector protein Ave1 (Jonge *et al.*, 2012). Moreover, the *V. longisporum* reference isolates VL43 (A1/D1 lineage) and Vl32 (A1/D3 lineage) are included in the collection which were sequenced in the course of the BioFung project of the University of Göttingen (VertiBase; http://biofung.gobics.de:1555/; coordinated by Prof. Dr. G. Braus, Georg-August-University of Göttingen).

Table 3.1: *Verticillium* isolate collection.

[1]isolates marked with yellow have been sequenced by the group of Prof. Bart Thomma, University of Wageningen, Netherlands (Jonge *et al.*, 2012); genome sequence information of isolates marked with blue (BioFung Database (VertiBase; www.vertibase.org)) or green (BROAD Institute; http://www.broadinstitute.org (Klosterman *et al.*, 2011)) is publicly available; [2]*Verticillium* species (*V. dahliae* or *V. longisporum*) and *V. longisporum* lineages (A1/D1 or A1/D3) of each isolate were identified by sequencing of the ribosomal internal transcribed spacer (ITS) and amplification of the VTA2 sequence; lineage specification of *V. dahliae* is not known and was therefore not performed; [3]host plant species are highlighted in different colors according to their plant families; [4]geographical regions of Europe are highlighted in grey.

Isolate[1]	Species[2]	Lineage[2]	Isolated from[3]	Geographical origin[4]
Vl19	*V. longisporum*	A1/D3	*Brassica napus (Brassicaceae)*	Mecklenburg (Germany)
Vl32	*V. longisporum*	A1/D3	*Brassica napus (Brassicaceae)*	Mecklenburg (Germany)
24	*V. longisporum*	A1/D1	*Brassica napus (Brassicaceae)*	Bandelsdorf (Germany)
V543b	*V. longisporum*	A1/D1	*Brassica napus (Brassicaceae)*	Braunschweig (Germany)
Vd334	*V. longisporum*	A1/D1	*Brassica napus (Brassicaceae)*	France
V4.5	*V. longisporum*	A1/D1	*Brassica napus (Brassicaceae)*	Germany
V40	*V. longisporum*	A1/D1	*Brassica napus (Brassicaceae)*	Hohenlieth (Germany)
18	*V. longisporum*	A1/D1	*Brassica napus (Brassicaceae)*	Lebckendorf (Germany)
Vl18	*V. longisporum*	A1/D1	*Brassica napus (Brassicaceae)*	Mecklenburg (Germany)
Vl82	*V. longisporum*	A1/D1	*Brassica napus (Brassicaceae)*	Mecklenburg (Germany)
Vl84	*V. longisporum*	A1/D1	*Brassica napus (Brassicaceae)*	Mecklenburg (Germany)
Vl40	*V. longisporum*	A1/D1	*Brassica napus (Brassicaceae)*	Mecklenburg (Germany)
Vl43	*V. longisporum*	A1/D1	*Brassica napus (Brassicaceae)*	Mecklenburg (Germany)
Vl83	*V. longisporum*	A1/D1	*Brassica napus (Brassicaceae)*	Mecklenburg (Germany)
V6/88	*V. longisporum*	A1/D1	*Brassica napus (Brassicaceae)*	Poel (Germany)
V2/87	*V. longisporum*	A1/D1	*Brassica napus (Brassicaceae)*	Poel (Germany)
22	*V. longisporum*	A1/D1	*Brassica napus (Brassicaceae)*	Rostock (Germany)
V10	*V. longisporum*	A1/D1	*Brassica napus (Brassicaceae)*	Rostock (Germany)
Vl60	*V. longisporum*	A1/D1	*Brassica oleracea (Brassicaceae)*	California (USA)
13	*V. longisporum*	A1/D1	*Gossypium spec. (Malvaceae)*	Spain
26	*V. longisporum*	A1/D1	*Centaurea cyanus (Asteraceae)*	Rostock (Germany)
35	*V. longisporum*	A1/D1	*Pisum sativum (Fabaceae)*	Rostock (Germany)
Vd41	*V. dahliae*	n.a.	*Brassica rapa (Brassicaceae)*	Hessen (Germany)
Vd42	*V. dahliae*	n.a.	*Brassica rapa (Brassicaceae)*	Krasnodas (Russia)
Vd9	*V. dahliae*	n.a.	*Solanum tuberosum (Solanaceae)*	Brandenburg (Germany)
Vd52	*V. dahliae*	n.a.	*Capsicum annuum (Solanaceae)*	Burgenland (Austria)
Vd54	*V. dahliae*	n.a.	*Capsicum annuum (Solanaceae)*	Burgenland (Austria)
Vd49	*V. dahliae*	n.a.	*Capsicum annuum (Solanaceae)*	Burgenland (Austria)
Vd88	*V. dahliae*	n.a.	*Solanum tuberosum (Solanaceae)*	Mecklenburg (Germany)
Vd16	*V. dahliae*	n.a.	*Solanum tuberosum (Solanaceae)*	Mecklenburg (Germany)
Vd87	*V. dahliae*	n.a.	*Solanum tuberosum (Solanaceae)*	Mecklenburg (Germany)
Vd85	*V. dahliae*	n.a.	*Solanum tuberosum (Solanaceae)*	Mecklenburg (Germany)
Vd8	*V. dahliae*	n.a.	*Solanum tuberosum (Solanaceae)*	Münsterland (Germany)
V138I	*V. dahliae*	n.a.	*Gossypium spec. (Malvaceae)*	Cordoba (Spain)
V200I	*V. dahliae*	n.a.	*Gossypium spec. (Malvaceae)*	Cordoba (Spain)
Vd13	*V. dahliae*	n.a.	*Gossypium hirsutum (Malvaceae)*	Cordoba (Spain)
Vd734	*V. dahliae*	n.a.	*Gossypium spec. (Malvaceae)*	France
V192I	*V. dahliae*	n.a.	*Gossypium spec. (Malvaceae)*	Sevilla (Spain)
Vd39	*V. dahliae*	n.a.	*Helianthus annuus (Asteraceae)*	Hessen (Germany)
Vd38	*V. dahliae*	n.a.	*Helianthus annuus (Asteraceae)*	Hessen (Germany)
Vd74	*V. dahliae*	n.a.	*Helianthus annuus (Asteraceae)*	Mecklenburg (Germany)
Vd89	*V. dahliae*	n.a.	*Lupinum luteus (Fabaceae)*	Mecklenburg (Germany)
V142	*V. dahliae*	n.a.	*Prunus cerasus (Rosaceae)*	Hungary
Vd57	*V. dahliae*	n.a.	*Fragaria x ananassa (Rosaceae)*	Mecklenburg (Germany)
Vd5	*V. dahliae*	n.a.	*Fragaria x ananassa (Rosaceae)*	Münsterland (Germany)

Vd2	*V. dahliae*	n.a.	*Fragaria x ananassa (Rosaceae)*	Münsterland (Germany)
Vd3	*V. dahliae*	n.a.	*Fragaria x ananassa (Rosaceae)*	Münsterland (Germany)
Vd4	*V. dahliae*	n.a.	*Fragaria x ananassa (Rosaceae)*	Münsterland (Germany)
V152	*V. dahliae*	n.a.	*Quercus spec. (Fagaceae)*	Hungary
V781I	*V. dahliae*	n.a.	*Olea europaea (Oleaceae)*	Cordoba (Spain)
ST100	*V. dahliae*	n.a.	Soil	Belgium
Türkei	*V. dahliae*	n.a.	Soil	Turkey
Vd15	*V. dahliae*	n.a.	*Linum usitatissimum (Linaceae)*	Mecklenburg (Germany)
Vd73	*V. dahliae*	n.a.	*Linum usitatissimum (Linaceae)*	Mecklenburg (Germany)
V1.2	*V. dahliae*	n.a.	*Vitis vinifera (Vitaceae)*	Neustadt, Wstr. (Germany)
DVD-31	*V. dahliae*	n.a.	*Solanum lycopersicum (Solanaceae)*	Essex Co.(Canada)
Vd830	*V. dahliae*	n.a.	*Solanum tuberosum (Solanaceae)*	Ohio (USA)
CBS38166	*V. dahliae*	n.a.	*Solanum lycopersicum (Solanaceae)*	Ontario (Canada)
VdJR2	*V. dahliae*	n.a.	*Solanum lycopersicum (Solanaceae)*	Ontario (Canada)
DVD161	*V. dahliae*	n.a.	*Solanum tuberosum (Solanaceae)*	Simcoe Co. (Canada)
V1.2.3	*V. dahliae*	n.a.	*Solanum tuberosum (Solanaceae)*	Wisconsin (USA)
T9	*V. dahliae*	n.a.	*Gossypium spec. (Malvaceae)*	California (USA)
V76	*V. dahliae*	n.a.	*Gossypium spec. (Malvaceae)*	Mexico
White	*V. dahliae*	n.a.	*Gossypium spec. (Malvaceae)*	USA
VdLs.17	*V. dahliae*	n.a.	*Lactuca sativa (Asteraceae)*	California (USA)
ST14.01	*V. dahliae*	n.a.	*Pistacia vera (Anacardiaceae)*	California (USA)
DVD-S26	*V. dahliae*	n.a.	Soil	Essex Co. (Canada)
DVD-S29	*V. dahliae*	n.a.	Soil	Essex Co.(Canada)
DVD-S94	*V. dahliae*	n.a.	Soil	Kent Co. (Canada)

It was essential to verify whether the original classification of the isolates as *V. longisporum* or *V. dahliae* is correct. This was done by amplification of the *Verticillium* transcription activator 2 (VTA2) which was recently used as marker for phylogenetic classification of *Verticillium* (van Tran *et al.*, 2013). *V. longisporum* possesses two VTA2 isogenes which originate from *V. albo-atrum* or *V. dahliae* whereas the genome of *V. dahliae* contains one VTA2 isogene variant (van Tran *et al.*, 2013; Figure S1). It was shown in previous studies that sequencing of the ribosomal internal transcribed spacer (ITS) has the power to distinguish between *V. dahliae* and *V. longisporum* species on the one hand and on the other hand to classify *V. longisporum* isolates into subclades which were formerly assigned to the lineages A1/D1 or A1/D3 (Inderbitzin *et al.*, 2011; van Tran *et al.*, 2013). Therefore, *V. longisporum* strains were further classified into the lineage A1/D1 or A1/D3 via ITS sequencing (Figure S2). Hence, the combination of rDNA type specification and VTA2 isogene pair identification gave information about lineage specificity of *Verticillium* isolates (Figure S1, Figure S2; Table 3.1). A comparable classification for *V. dahliae* isolates is not established and was therefore not performed.

Figure 3.1: Map indicating the geographical origin of the isolates of the *Verticillium* strain collection. Geographical origins of *V. dahliae* and *V. longisporum* isolates are highlighted in green and red circles, respectively. Note that the number of highlighted geographical regions is lower than the number of isolates of the strain collection because geographical origins are marked representatively (green and red circles). The map was generated using BatchGeo LLC (www.batchgeo.com).

A. thaliana Col-0 plants were infected with the *Verticillium* isolates listed in Table 3.1 to further classify the strains based on the macroscopically detectable disease symptom development. In addition, the severity of the induced symptoms was ranked according to the strength of disease induction on *A. thaliana*. This allowed to subdivide the *Verticillium* isolates into three different interaction classes.

3.1.1 *Verticillium* isolates Subclass I induces *V. longisporum* VL43-like infection symptoms on Col-0

Infection of *A. thaliana* Col-0 plants with *V. longisporum* VL43 results in stunted plant growth and the formation of chloroses on plant leaves, followed by the induction of early senescence (Reusche *et al.*, 2012). 17 *Verticillium* isolates of the collection (Table 3.1) induced VL43-like infection symptoms (Table 3.2). Of these isolates, 12 were identified as *V. longisporum* strains (including the reference strain VL43) and five isolates as *V. dahliae* strains (Figure S1; Table 3.2). Therefore, these 17 isolates form the *Verticillium* – *A. thaliana* Col-0 interaction class which is designated in the following as “early senescence”. For greater clarity, the names of isolates belonging to the interaction class “early senescence” are marked in the following with the prefix “s-“. Figure 3.2 shows the infection phenotype and the three different disease intensities on Col-0 plants inoculated with *Verticillium* strains belonging to the interaction class “early senescence”.

Figure 3.2: Infection phenotype of Col-0 plants inoculated with s-Vl60, s-Vl43 and s-ST100 as an example for the three different intensities of early senescence induction. Phenotype of *Verticillium* infected plants was recorded at 28 dpi. Symbols indicate the intensity of disease symptom development: + = moderate symptoms, ++ = strong symptoms, +++ = very strong symptoms. Scale bar: 1 cm.

Comparable to the disease symptoms induced after s-VL43 infection, symptom development after inoculation with the *Verticillium* isolates of the "early senescence" subclass proceeded at 28 dpi and was accompanied by the conversion of chlorotic leaves into necrotic tissues (Figure 3.2; Table 3.2; Reusche *et al.*, 2012). Depending on the intensity of the disease symptom development *Verticillium* strains of the subclass "early senescence" were divided into the three groups "+", "++" and "+++". With respect to the *V. longisporum* isolates the disease intensity ranged from moderate (+) symptoms to very strong (+++) symptom development. However, only one *V. longisporum* isolate, s-Vl83, out of the 12 identified for this subclass was shown to induce very strong symptoms on *Arabidopsis* Col-0 (Table 3.2).

All *V. longisporum* strains of the interaction class "early senescence" carry an A1 ITS sequence closely related to *V. albo-atrum* strain VaMs.102 and were thus identified to belong to the lineage A1/D1 (Figure S2; Inderbitzin *et al.*, 2011; van Tran *et al.*, 2013). In addition, all of these strains, with the exception of strain s-35, were isolated from host plants belonging to the *Bassicaceae* family. Interestingly, these analyses also identified five *V. dahliae* isolates inducing early senescence on *Arabidopsis* Col-0 plants (Table 3.2). The intensity of disease symptom development among these isolates appeared to be stronger than for *V. longisporum* isolates, varying from strong (++) symptoms to very strong (+++) symptom development (Table 3.2).

Four of the five *V. dahliae* isolates, s-T9, s-V76, s-V138I and s-V781I, were originally isolated from geographical regions representing a rather hot and arid climate (Spain, Mexico, California; Table 3.2). Moreover and very interestingly, these strains were isolated from the plant species *Gossypium spec.* and *Olea europaea* and are known to induce defoliation in cotton and olive, respectively (Friebertshauser and DeVay, 1982; Tzeng and Vay, 1985; Parkhi *et al.*, 2010; Collins *et al.*, 2005; personal communication Prof. Rafael M. Jiménez-Díaz, Córdoba, Spain; Figure

3.3). The fifth *V. dahliae* early senescence inducing strain s-ST100 was originally isolated from soil and, consequently, no information on the host plant was available. Therefore, the infectivity and symptom development on cotton in comparison with the *V. dahliae* strains s-V76 and s-T9 was tested. Infection experiments revealed that also s-ST100 is capable of inducing defoliation on cotton (Figure 3.3).

Figure 3.3: Symptom development on *Gossypium hirsutum* upon inoculation with *V. dahliae* isolates s-V76, s-ST100 and s-T9. Phenotype of *Verticillium* infected plants was recorded at 17 dpi. Scale bar: 1 cm.

Notably, *V. dahliae* isolates are able to induce s-VL43-like infection symptoms on *A. thaliana* Col-0 demonstrating that symptoms like chlorotic leaves together with stunted plant growth are not restricted to the species *V. longisporum*. This is important, as it may have implications for the evolution of the near-diploid hybrid species *V. longisporum* and allows more simple molecular analyses in the haploid species *V. dahliae*, such as generation of knock-out mutants and whole-genome sequencing.

Table 3.2: *Verticillium* isolates belonging to the interaction class "early senescence".
[1]isolates marked with yellow have been sequenced by the group of Prof. Bart Thomma, University of Wageningen, Netherlands (Jonge *et al.*, 2012); genome sequence information of isolates marked with blue is publicly available (BioFung Database (VertiBase; www.vertibase.org)); isolates marked with red were selected for further genome sequence comparison and RNA-sequencing studies (3.4); [2]*Verticillium* species were determined via sequencing of the ribosomal internal transcribed spacer (ITS) sequence (Reusche *et al.*, 2012) and *VTA2* amplification (van Tran *et al.*, 2013); [3]*V. longisporum* isolates were classified into A1/D1 or A1/D3 lineage by ITS sequence analyses (van Tran *et al.*, 2013); a comparable classification for *V. dahliae* isolates was not performed (n.a.); *lineage classification was previously established (Zeise and Tiedemann, 2002); [4]symptom development as early senescence refer to s-VL43-like infection symptoms (Reusche *et al.*, 2012); infection phenotype was tested in two independent experiments; cotton/olive defoliation was tested in the present study (Figure 3.3) or other studies (Friebertshauser and DeVay, 1982; Tzeng and Vay, 1985; Parkhi *et al.*, 2010; Collins *et al.*, 2005; personal communication Prof. Rafael M. Jiménez-Díaz, Córdoba, Spain);[5]macroscopically determined intensity of disease symptoms was subdivided into different classes: + = moderate symptoms, ++ = strong symptoms, +++ = very strong symptoms; [6]host plant species are highlighted in different colors according to their plant families; [7]geographical regions in Europe are highlighted in grey.

Isolate[1]	Species[2]	Lineage[3]	Symptoms on *Arabidopsis thaliana* Col-0[4]	Intensity[5]	Isolated from[6]	Geographical origin[7]
s-V4.5	*V. longisporum*	A1/D1	early senescence	+	*Brassica napus (Brassicaceae)*	Germany
s-V543b	*V. longisporum*	A1/D1	early senescence	+	*Brassica napus (Brassicaceae)*	Braunschweig (Germany)
s-22	*V. longisporum*	A1/D1	early senescence	+	*Brassica napus (Brassicaceae)*	Rostock (Germany)
s-Vl60*	*V. longisporum*	A1/D1*	early senescence	+	*Brassica oleracea (Brassicaceae)*	California (USA)
s-35	*V. longisporum*	A1/D1	early senescence	+	*Pisum sativum (Fabaceae)*	Rostock (Germany)
s-Vd334	*V. longisporum*	A1/D1	early senescence	++	*Brassica napus (Brassicaceae)*	France
s-V40	*V. longisporum*	A1/D1	early senescence	++	*Brassica napus (Brassicaceae)*	Hohenlieth (Germany)
s-Vl40*	*V. longisporum*	A1/D1*	early senescence	++	*Brassica napus (Brassicaceae)*	Mecklenburg (Germany)
s-Vl43*	*V. longisporum*	A1/D1*	early senescence	++	*Brassica napus (Brassicaceae)*	Mecklenburg (Germany)
s-V2/87	*V. longisporum*	A1/D1	early senescence	++	*Brassica napus (Brassicaceae)*	Poel (Germany)
s-V10	*V. longisporum*	A1/D1	early senescence	++	*Brassica napus (Brassicaceae)*	Rostock (Germany)
s-Vl83*	*V. longisporum*	A1/D1*	early senescence / cotton defoliating	+++	*Brassica napus (Brassicaceae)*	Mecklenburg (Germany)
s-T9	*V. dahliae*	n.a.	early senescence / cotton defoliating	++	*Gossypium spec. (Malvaceae)*	California (USA)
s-V76	*V. dahliae*	n.a.	early senescence / cotton defoliating	++	*Gossypium spec. (Malvaceae)*	Mexico
s-V138l	*V. dahliae*	n.a.	early senescence / cotton defoliating	++	*Gossypium spec. (Malvaceae)*	Cordoba (Spain)
s-V781l	*V. dahliae*	n.a.	early senescence / olive defoliating	+++	*Olea europaea (Oleaceae)*	Cordoba (Spain)
s-ST100	*V. dahliae*	n.a.	early senescence / cotton defoliating	+++	soil	Belgium

3.1.2 *Verticillium* isolates Subclass II induces VdJR2-like wilting symptoms on *A. thaliana* Col-0 plants

A. thaliana Col-0 infection with *V. dahliae* VdJR2 resulted in stunting and wilted leaves (Reusche *et al.*, 2014). Characterization of the *Verticillium* isolate collection identified 36 *V. dahliae* strains that induce VdJR2-like wilting and stunted plant growth on Col-0 plants (Table 3.3). Moreover, VdJR2 infection caused suppression of apical dominance resulting in the formation of numerous side branches (Reusche *et al.*, 2014). To classify the *Verticillium* interaction class "wilting" the combination of the robust disease phenotypes wilting and stunted plant growth were used (Table 3.3). The names of isolates belonging to the interaction class "wilting" are marked in the following with the prefix "w-".

Infection severity was ranked from mild (-/+) to very strong (+++) symptom development. Figure 3.4 illustrates the disease symptoms as well as the infection severities of representative wilt inducing *Verticillium* isolates.

Figure 3.4: Infection phenotypes of Col-0 plants inoculated with the *V. dahliae* isolates w-V192I, w-VdLs.17, w-ST14.01 and w-VdJR2 as examples for the four different symptom development intensities of stunted plant growth and wilting. Phenotype of *Verticillium* infected plants was recorded at 28 dpi. Symbols indicate the intensity of disease symptom development: -/+ = mild symptoms, + = moderate symptoms, ++ = strong symptoms, +++ = very strong symptoms. Boxes show enlargement of wilted leaves. Scale bar: 1 cm.

Remarkably, only *V. dahliae* and no *V. longisporum* isolates fall into the interaction class "wilting" (Table 3.3). This result correlated with earlier findings that wilt induction is the hallmark of *V. dahliae* infections (Tjamos and Beckman, 1989).

In contrast to isolates of the "early senescence" interaction class, wilt inducing *Verticillium* strains were originally isolated from diverse host plant families, e.g. *Solanaceae*, *Malvaceae* and

Rosaceae (Table 3.3). Moreover, isolates of this interaction class were found in diverse geographical regions of Europe, the USA and Canada.

Two wilt inducing *V. dahliae* isolates, w-V192I and w-V200I, were originally isolated from *Gossypium spec.* (Table 3.3). Contrarily to the *V. dahliae* isolates s-T9, s-V76 and s-V138I of the "early senescence" interaction class, w-V192I and w-V200I were previously identified as cotton non-defoliating *Verticillium* strains (Collins *et al.*, 2005). In the present study these isolates were shown to induce mild wilting of *A. thaliana* Col-0.

Table 3.3: *Verticillium* isolates belonging to the interaction class "wilting".

[1]isolates marked with yellow have been sequenced by the group of Prof. Bart Thomma, University of Wageningen, Netherlands (Jonge *et al.*, 2012); genome sequence information of isolates marked with green is publicly available (BROAD Institute; http://www.broadinstitute.org (Klosterman *et al.*, 2011)); isolates marked with red were selected for further genome sequence comparison and RNA-sequencing studies (3.4); [2]*Verticillium* species were determined via sequencing of the ribosomal internal transcribed spacer (ITS) sequence (Reusche *et al.*, 2012) and *VTA2* amplification (van Tran *et al.*, 2013); *classification was previously established (Zeise and Tiedemann, 2002); [3]a lineage classification for *V. dahliae* isolates was not performed; [4]symptom development as wilting refer to w-VdJR2-like infection symptoms (Reusche *et al.*, 2014); infection phenotype was tested in two independent experiments; cotton non-defoliation was tested in previous studies (Collins *et al.*, 2005; personal communication Prof. Rafael M. Jiménez-Díaz, Córdoba, Spain); [5]macroscopically determined intensity of disease symptom development was subdivided into different classes: -/+ = mild symptoms, + = moderate symptoms, ++ = strong symptoms, +++ = very strong symptoms; [6]host plant species are highlighted in different colors according to their plant families; [7]geographical regions in Europe are highlighted in grey.

Isolate[1]	Species[2]	Lineage[3]	Symptoms on *Arabidopsis thaliana* Col-0[4]	Intensity[5]	Isolated from[6]	Geographical origin[7]
w-Vd49*	*V. dahliae*	n.a.	wilting	-/+	*Capsicum annuum (Solanaceae)*	Burgenland (Austria)
w-Vd9*	*V. dahliae*	n.a.	wilting	-/+	*Solanum tuberosum (Solanaceae)*	Brandenburg (Germany)
w-Vd88*	*V. dahliae*	n.a.	wilting	-/+	*Solanum tuberosum (Solanaceae)*	Mecklenburg (Germany)
w-Vd16*	*V. dahliae*	n.a.	wilting	-/+	*Solanum tuberosum (Solanaceae)*	Mecklenburg (Germany)
w-Vd830*	*V. dahliae*	n.a.	wilting	-/+	*Solanum tuberosum (Solanaceae)*	Ohio (USA)
w-DVD161	*V. dahliae*	n.a.	wilting	-/+	*Solanum tuberosum (Solanaceae)*	Simcoe Co. (Canada)
w-V1.2.3	*V. dahliae*	n.a.	wilting	-/+	*Solanum tuberosum (Solanaceae)*	Wisconsin (USA)
w-Vd5*	*V. dahliae*	n.a.	wilting	-/+	*Fragaria x ananassa (Rosaceae)*	Münsterland (Germany)
w-V200I	*V. dahliae*	n.a.	wilting / cotton non-defoliating	-/+	*Gossypium spec. (Malvaceae)*	Cordoba (Spain)
w-V192I	*V. dahliae*	n.a.	wilting / cotton non-defoliating	-/+	*Gossypium spec. (Malvaceae)*	Sevilla (Spain)
w-Vd734	*V. dahliae*	n.a.	wilting	-/+	*Gossypium spec. (Malvaceae)*	France
w-White	*V. dahliae*	n.a.	wilting	-/+	*Gossypium spec. (Malvaceae)*	USA
w-DVD-S94	*V. dahliae*	n.a.	wilting	-/+	soil	Kent Co. (Canada)
w-Vd2*	*V. dahliae*	n.a.	wilting	+	*Fragaria x ananassa (Rosaceae)*	Münsterland (Germany)
w-V142	*V. dahliae*	n.a.	wilting	+	*Prunus cerasus (Rosaceae)*	Hungary

w-Vd13*	*V. dahliae*	n.a.	wilting	+	*Gossypium hirsutum (Malvaceae)*	Cordoba (Spain)
w-Vd74*	*V. dahliae*	n.a.	wilting	+	*Helianthus annuus (Asteraceae)*	Mecklenburg (Germany)
w-VdLs.17	*V. dahliae*	n.a.	wilting	+	*Lactuca sativa (Asteraceae)*	California (USA)
w-Vd15*	*V. dahliae*	n.a.	wilting	+	*Linum usitatissimum (Linaceae)*	Mecklenburg (Germany)
w-Vd87*	*V. dahliae*	n.a.	wilting	+	*Solanum tuberosum (Solanaceae)*	Mecklenburg (Germany)
w-V1.2*	*V. dahliae*	n.a.	wilting	+	*Vitis vinifera (Vitaceae)*	Neustadt, Wstr. (Germany)
w-Türkei	*V. dahliae*	n.a.	wilting	+	soil	Turkey
w-DVD-S26	*V. dahlia*	n.a.	Wilting	+	soil	Essex Co. (Canada)
w-Vd41*	*V. dahliae*	n.a.	wilting	++	*Brassica rapa (Brassicaceae)*	Hessen (Germany)
w-Vd3*	*V. dahliae*	n.a.	wilting	++	*Fragaria x ananassa (Rosaceae)*	Münsterland (Germany)
w-Vd4*	*V. dahliae*	n.a.	wilting	++	*Fragaria x ananassa (Rosaceae)*	Münsterland (Germany)
w-Vd38*	*V. dahliae*	n.a.	wilting	++	*Helianthus annuus (Asteraceae)*	Hessen (Germany)
w-ST14.01	*V. dahliae*	n.a.	wilting	++	*Pistacia vera (Anacardiaceae)*	California (USA)
w-CBS38166	*V. dahliae*	n.a.	wilting	++	*Solanum lycopersicum (Solanaceae)*	Ontario (Canada)
w-Vd85*	*V. dahlia*	n.a.	Wilting	++	*Solanum tuberosum (Solanaceae)*	Mecklenburg (Germany)
w-Vd57*	*V. dahliae*	n.a.	wilting	+++	*Fragaria x ananassa (Rosaceae)*	Mecklenburg (Germany)
w-Vd73*	*V. dahliae*	n.a.	wilting	+++	*Linum usitatissimum (Linaceae)*	Mecklenburg (Germany)
w-Vd89*	*V. dahliae*	n.a.	wilting	+++	*Lupinum luteus (Fabaceae)*	Mecklenburg (Germany)
w-VdJR2	*V. dahliae*	n.a.	wilting	+++	*Solanum lycopersicum (Solanaceae)*	Ontario (Canada)
w-DVD-31	*V. dahliae*	n.a.	wilting	+++	*Solanum lycopersicum (Solanaceae)*	Essex Co.(Canada)
w-DVD-S29	*V. dahliae*	n.a.	wilting	+++	soil	Essex Co.(Canada)

3.1.3 *Verticillium* isolates Subclass III causes asymptomatic interactions with *A. thaliana* Col-0 upon infection

Infection of *A. thaliana* Col-0 plants with 10 *V. longisporum* and 6 *V. dahliae* isolates resulted in symptom free plant phenotypes after inoculation. These 16 isolates form the "asymptomatic" interaction class (Table 3.4). In the following, the names of isolates belonging to this interaction class are marked with the prefix "a-". The phenotype of Col-0 plants infected with two different *Verticillium* strains belonging to the "asymptomatic" interaction class is shown in Figure 3.5. Even at 28 dpi no macroscopically detectable disease symptoms became visible.

Figure 3.5: Infection phenotype of plants inoculated with a-Vd8 and a-Vl32 illustrating the asymptomatic interaction of *Verticillium* with *A. thaliana* Col-0. Phenotype of *Verticillium* infected plants was recorded at 28 dpi. Scale bar: 1 cm.

Table 3.4: *Verticillium* isolates belonging to the interaction class "asymptomatic".

[1]genome sequence information is publicly available of isolates marked with blue (BioFung Database (VertiBase; www.vertibase.org)); isolates marked with red were selected for further genome sequence comparison and RNA-sequencing studies (3.4); [2]*Verticillium* species were determined via sequencing of the ribosomal internal transcribed spacer (ITS) sequence (Reusche *et al.*, 2012) and *VTA2* amplification (van Tran *et al.*, 2013); *classification was previously established (Zeise and Tiedemann, 2002); [3]*V. longisporum* isolates were classified into A1/D1 or A1/D3 lineage by ITS sequence analyses (van Tran *et al.*, 2013); *lineage classification was previously established (Zeise and Tiedemann, 2002); a comparable classification for *V. dahliae* isolates was not performed; [4]symptom development as asymptomatic refer to no symptom induction after infection; infection phenotype was tested in two independent experiments; [5]determination of disease symptom development intensities was not applicable for the asymptomatic interaction (n.a.); [6]host plant species are highlighted in different colors according to their plant families; [7]geographical regions in Europe are highlighted in grey.

Isolate[1]	Species[2]	Lineage[3]	Symptoms on *Arabidopsis thaliana* Col-0[4]	Intensity[5]	Isolated from[6]	Geographical origin[7]
a-Vl19*	*V. longisporum*	A1/D3*	asymptomatic	n.a.	*Brassica napus (Brassicaceae)*	Mecklenburg (Germany)
a-Vl32*	*V. longisporum*	A1/D3*	asymptomatic	n.a.	*Brassica napus (Brassicaceae)*	Mecklenburg (Germany)
a-24	*V. longisporum*	A1/D1	asymptomatic	n.a.	*Brassica napus (Brassicaceae)*	Bandelsdorf (Germany)
a-18	*V. longisporum*	A1/D1	asymptomatic	n.a.	*Brassica napus (Brassicaceae)*	Lebckendorf (Germany)
a-Vl18*	*V. longisporum*	A1/D1*	asymptomatic	n.a.	*Brassica napus (Brassicaceae)*	Mecklenburg (Germany)
a-Vl82*	*V. longisporum*	A1/D1*	asymptomatic	n.a.	*Brassica napus (Brassicaceae)*	Mecklenburg (Germany)
a-Vl84*	*V. longisporum*	A1/D1*	asymptomatic	n.a.	*Brassica napus (Brassicaceae)*	Mecklenburg (Germany)
a-V6/88	*V. longisporum*	A1/D1	asymptomatic	n.a.	*Brassica napus (Brassicaceae)*	Poel (Germany)
a-26	*V. longisporum*	A1/D1	asymptomatic	n.a.	*Centaurea cyanus (Asteraceae)*	Rostock (Germany)
a-13	*V. longisporum*	A1/D1	asymptomatic	n.a.	*Gossypium spec. (Malvaceae)*	Spain
a-Vd42*	*V. dahliae*	n.a.	asymptomatic	n.a.	*Brassica rapa (Brassicaceae)*	Krasnodas (Russia)
a-Vd52*	*V. dahliae*	n.a.	asymptomatic	n.a.	*Capsicum annuum (Solanaceae)*	Burgenland (Austria)
a-Vd54*	*V. dahliae*	n.a.	asymptomatic	n.a.	*Capsicum annuum (Solanaceae)*	Burgenland (Austria)
a-Vd8*	*V. dahliae*	n.a.	asymptomatic	n.a.	*Solanum tuberosum (Solanaceae)*	Münsterland (Germany)
a-Vd39*	*V. dahliae*	n.a.	asymptomatic	n.a.	*Helianthus annuus (Asteraceae)*	Hessen (Germany)
a-V152	*V. dahliae*	n.a.	asymptomatic	n.a.	*Quercus spec. (Fagaceae)*	Hungary

3.2 Comparative *in-depth* characterization of *V. dahliae* isolates inducing early senescence or wilting on *A. thaliana* Col-0

The characterization of the *Verticillium* strain collection resulted in the identification of five *V. dahliae* isolates, s-T9, s-V76, s-ST100, s-V138I and s-V781I, which induce early senescence disease symptoms on *A. thaliana* Col-0 similar to that of s-VL43 (Reusche *et al.*, 2012). Since haploid *V. dahliae* strains pose a great advantage in contrast to *V. longisporum* concerning subsequent studies such as genome sequence comparison of *Verticillium* isolates and transcriptome analyses, for further experiments these *V. dahliae* isolates were used.

A detailed *in-depth* characterization of these isolates and *V. dahliae* strains w-VdJR2, w-V192I and w-V200I of the "wilting" interaction class was performed. W-VdJR2 was selected as reference strain for the "wilting" interaction class, since comparable infection experiments with this isolate were conducted in a previous study (Reusche *et al.*, 2014). The isolates w-V192I and w-V200I were included in the characterization because they were identified as cotton non-defoliating isolates whereas strains s-T9, s-V76, s-ST100, s-V138I and s-V781I are capable to induce defoliation of cotton or olive plants, respectively (Collins *et al.*, 2005; personal communication Prof. Rafael M. Jiménez-Díaz, Córdoba, Spain; Figure 3.3). A direct comparison of these isolates in an *in-depth* characterization would allow to distinguish the symptom development induced by the two classes on *A. thaliana* with regard to their symptom induction on cotton/olive plants.

The *in-depth* characterization was performed to elucidate whether the interaction classes differ in fungal proliferation *in planta* indicating diverse infection kinetics. The fungal proliferation was quantified *in planta* as well as qualitatively detected *in situ* within the plant vasculature and compared among the *Verticillium* strains.

To verify whether early senescence inducing *V. dahliae* strains are also capable to induce s-VL43-like developmental reprogramming in the leaf vasculature of *Arabidopsis* (Reusche *et al.*, 2014) leaf veins and leaf midrib cross-sections of infected plants were microscopically investigated. Vascular reprogramming patterns and structural differences were directly compared to that induced by the "wilting" interaction class. In addition, for the comparison of symptom development induced by *V. dahliae* isolates of the "early senescence" interaction class the reference strain s-VL43 was included in the *in-depth* characterization. To support the observation of developmental changes the expression of marker genes for vascular reprogramming and cambial activity was analysed on molecular level. Moreover, the expression of marker genes for

biotic stress was detected on molecular level to reveal differences in plant defence responses induced by strains of the "wilting" and "early senescence" interaction class.

Due to the large number of *Verticillium* isolates included in the studies and the resulting amount of experimental samples infection studies and *in-depth* characterization of the isolates were separated and analysed in two experiments (Experiment I: Figure 3.6, Figure 3.8, Figure 3.10, Figure 3.12, Figure 3.14, Figure 3.16, Figure 3.18; Experiment II: Figure 3.7, Figure 3.9, Figure 3.11, Figure 3.13, Figure 3.15, Figure 3.17 and Figure 3.19). The macroscopic disease symptom development of mock-treated and infected plants of both experiments is illustrated in Figure S3. Expression studies of the specific marker genes and fungal DNA quantification were conducted with the same samples including the same harvested plant material.

3.2.1 *V. dahliae* isolates of the "early senescence" interaction class induce stronger stunting of *A. thaliana* Col-0 than isolates of the "wilting" interaction class

Verticillium isolates of both the "wilting" and "early senescence" interaction class induce stunted plant growth on *A. thaliana* Col-0 plants (3.1.1; 3.1.2). Stunting was monitored by measurements of the leaf area (2.2.6). To identify differences in stunting intensities induced by the two interaction classes, *A. thaliana* Col-0 plants were infected with the selected *Verticillium* isolates and the leaf area of mock-treated and inoculated plants was tested in a time course experiment. The experimental time course included the time points 7 dpi, 14 dpi, 21 dpi and 28 dpi.

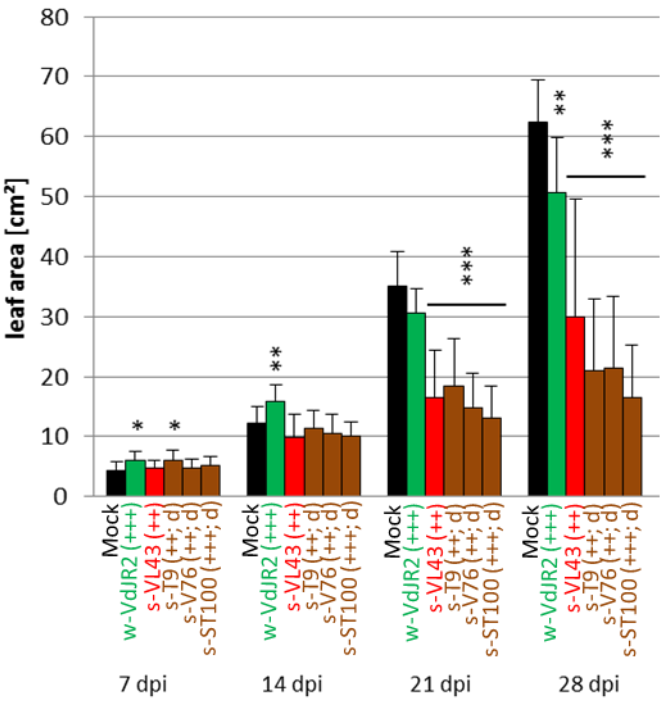

Figure 3.6: Leaf area measurements of *A. thaliana* Col-0 infected with *V. dahliae* isolates s-T9, s-V76 and s-ST100 in comparison to s-VL43 and w-VdJR2 inoculated plants. *V. dahliae* isolates representing the "early senescence" interaction class are highlighted in **brown**. The reference isolates s-VL43 and w-VdJR2 are highlighted in **red** and **green**, respectively. Early senescence inducing isolates are marked with the prefix s-. Wilt inducing isolates are marked with the prefix w-. Symbols indicate the intensity of disease symptom development: ++ = strong symptoms, +++ = very strong symptoms. d = cotton/olive defoliating. Bars represent leaf area measurement of mock-treated and infected plants (n=16) in the time course of the experiment. Error bars show standard deviation. Asterisks indicate statistical significance between *Verticillium* infections and mock-treated plants (t-test; * p≤0.05, ** p≤0.01, *** p≤0.001). Experiments were repeated three times and representative data are shown.

Stunted plant growth was generally less severe in plants infected with the *V. dahliae* isolates of the "wilting" interaction class as compared to plants inoculated with the early senescence inducing isolates (Figure 3.6; Figure 3.7). Plant stunting of Col-0 plants infected with the early senescence inducing isolates first appeared at 21 dpi and continued during the time course until 28 dpi (Figure 3.6; Figure 3.7). This resulted in an about 3-fold reduction of the leaf area of these plants compared to mock-treated plants (Figure 3.6; Figure 3.7). In contrast to that, only a slight reduction in leaf area was detected for w-VdJR2 inoculated plants at 21 dpi (Figure 3.6; Figure 3.7). With regard to w-V192I and w-V200I infected plants no leaf area reduction was measured at 21 dpi (Figure 3.7). A reduction in leaf area of w-VdJR2, w-V192I and w-V200I inoculated plants was observed at 28 dpi (Figure 3.6; Figure 3.7). Thus, plant stunting was induced earlier and stronger by *Verticillium* isolates of the "early senescence" interaction class.

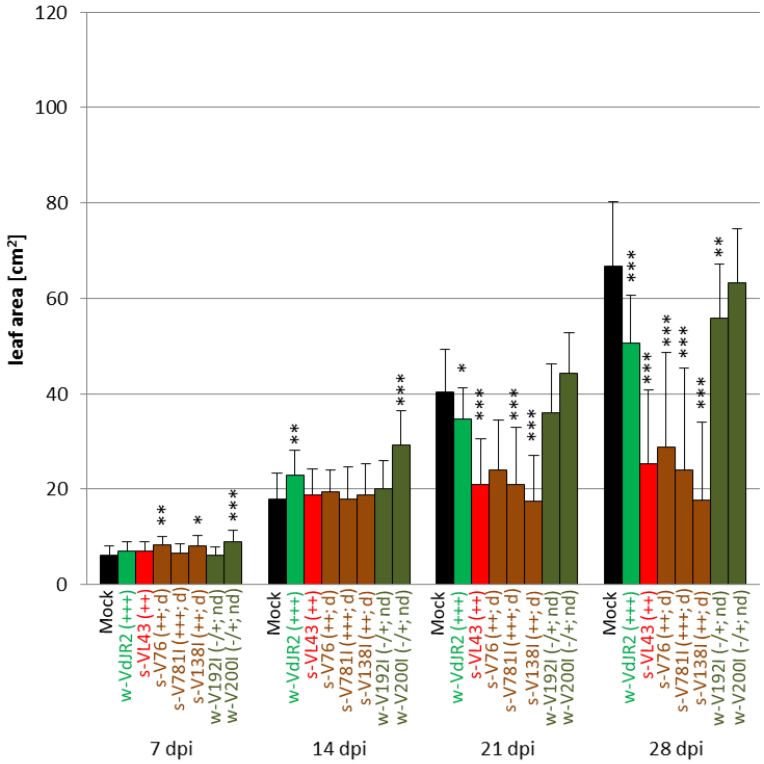

Figure 3.7: Leaf area measurements of *A. thaliana* Col-0 infected with *V. dahliae* isolates s-V76, s-V781I, s-V138I, w-V192I and w-V200I in comparison to s-VL43 and w-VdJR2 inoculated plants. *V. dahliae* isolates representing the "early senescence" interaction class are highlighted in **brown**. *V. dahliae* isolates representing the "wilting" interaction class are highlighted in **dark green**. The reference isolates s-VL43 and w-VdJR2 are highlighted in **red** and **green**, respectively. Early senescence inducing isolates are marked with the prefix s-. Wilt inducing isolates are marked with the prefix w-. Symbols indicate the intensity of disease symptom development: -/+ = mild symptoms, ++ = strong symptoms, +++ = very strong symptoms. d = cotton/olive defoliating, nd = cotton non-defoliating. Bars represent leaf area measurement of mock-treated and infected plants (n=16) in the time course of the experiment. Error bars show standard deviation. Asterisks indicate statistical significance between *Verticillium* infections and mock-treated plants (t-test; * p≤0.05, ** p≤0.01, *** p≤0.001). Experiment was performed once.

3.2.2 Early senescence inducing *V. dahliae* isolates produce higher *in planta* biomass compared to wilt inducing isolates.

To assess differences in fungal proliferation among the two interaction classes "early senescence" and "wilting" as well as between the two *Verticillium* species *V. dahliae* and *V. longisporum* the fungal biomass was quantified *in planta*. For fungal biomass detection, expression of the ribosomal internal transcribed spacer (ITS) was measured in the infected plants via qRT-PCR (2.2.4.7). The biomass was detected in a time course including the time points 7 dpi, 14 dpi, 21 dpi and 28 dpi.

QRT-PCR results indicated that the fungal biomass of every *V. dahliae* isolate increased continuously during the time course of the experiments (Figure 3.8A; Figure 3.9). Particularly between 14 dpi and 21 dpi a gain in fungal proliferation can be observed for all *Verticillium* isolates (Figure 3.8A; Figure 3.9). The early senescence inducing *V. dahliae* isolates proliferated faster and to a much stronger extent in Col-0 plants than isolates triggering plant wilting (Figure 3.8A; Figure 3.9). Isolates s-T9, s-V76 and s-ST100 reached an about 7-, 5- and 1.5-fold increase in DNA content from 21 dpi to 28 dpi respectively, resulting in up to ~33 ng/µg total DNA (Figure 3.8A). In contrast, isolate w-VdJR2 never attained a DNA content higher than 0.7 ng/µg total DNA (Figure 3.8A).

Remarkably, also the wilt inducing isolates w-V192I and w-V200I proliferated within *Arabidopsis* to a much lower extent than the early senescence inducing isolates s-V76, s-V781I and s-V138I (Figure 3.9). At 28 dpi w-V192I and w-V200I infected plants contained about 63 times and 190 times lower fungal biomass, respectively, in comparison to plants infected with the isolate s-V76 (Figure 3.9). Also the reference strain w-VdJR2 exhibited a 19-fold lower *in planta* proliferation at 28 dpi compared to s-V76 (Figure 3.9).

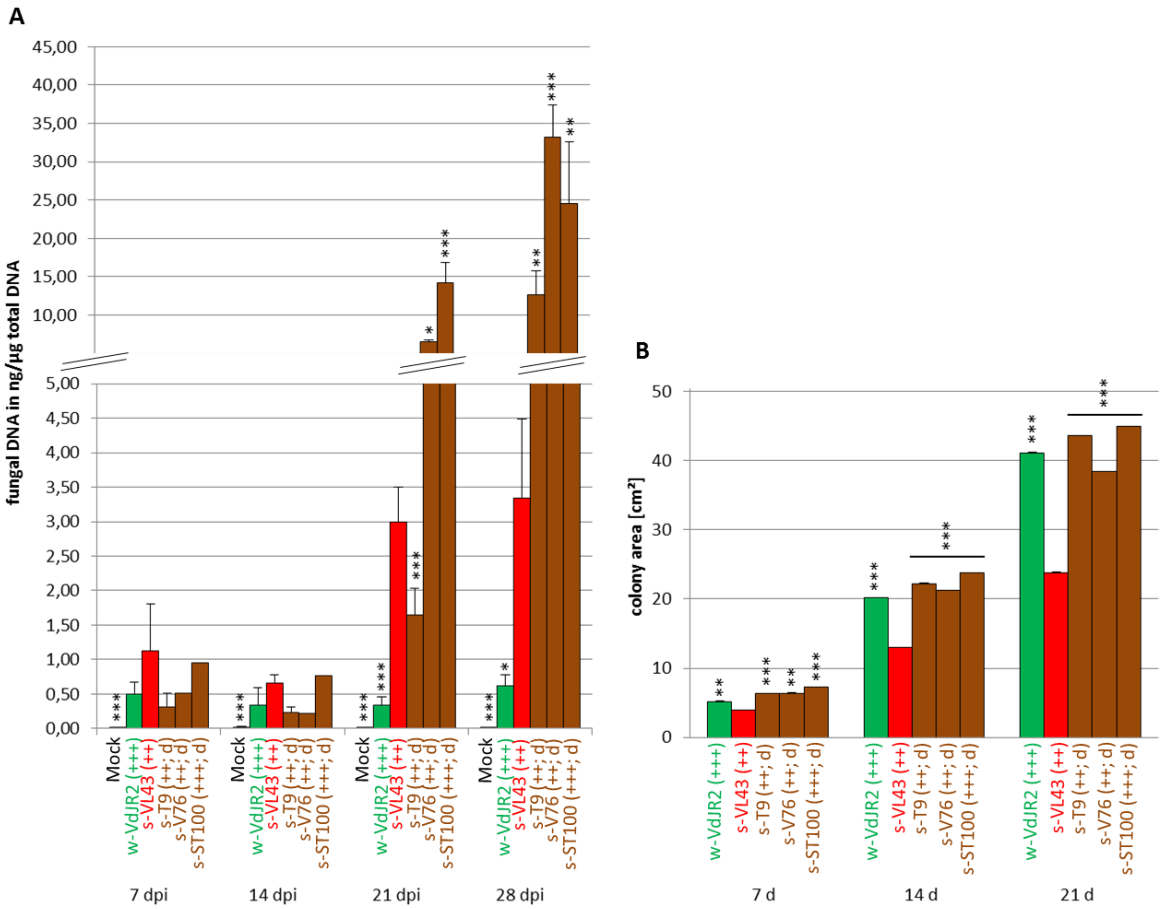

Figure 3.8: Proliferation of *V. dahliae* isolates w-VdJR2, s-T9, s-V76 and s-ST100 in comparison to *V.longisporum* isolate s-VL43 *in planta* and *in vitro* on solid CDB medium. *V. dahliae* isolates representing the "early senescence" interaction class are highlighted in **brown**. The reference isolates s-VL43 and w-VdJR2 are highlighted in **red** and **green**, respectively. Early senescence inducing isolates are marked with the prefix s-. Wilt inducing isolates are marked with the prefix w-. Symbols indicate the intensity of disease symptom development: ++ = strong symptoms, +++ = very strong symptoms. d = cotton/olive defoliating. **A:** Bars represent fungal biomass quantification via qRT-PCR of mock-treated and infected plants (n=4; pools of 4 plants) in the time course of the experiment. Error bars show standard deviation. Asterisks indicate statistical significance between *V. dahliae* and s-VL43 infected plants (t-test; * p≤0.05, ** p≤0.01, *** p≤0.001). Experiments were repeated three times and representative data are shown. **B:** Growth assay of *Verticillium* isolates on solid CDB medium. *Verticillium* spore solutions were plated on CDB plates and the diameter of the colonies was measured at 7, 14 and 21 days after plating (n=3). Error bars show standard deviation. Asterisks indicate statistical significance between *V. dahliae* and s-VL43 diameter (t-test; * p≤0.05, ** p≤0.01, *** p≤0.001). Experiment was performed once.

Interestingly, the *in planta* proliferation of *V. dahliae* isolates s-V76 and s-ST100 was significantly stronger and faster than that of the *V. longisporum* reference strain s-VL43 at later time points (21 dpi and 28 dpi; Figure 3.8A; Figure 3.9). In comparison to the previously mentioned 5- and 1.5-fold increase of s-V76 and s-ST100 biomass between 21 dpi and 28 dpi, s-VL43 only showed a 1.1-fold enrichment of fungal DNA for these time points (Figure 3.8A). The measured DNA content of s-V76 infected plants at 28 dpi was the highest DNA amount detected in *Verticillium* infected plants in this study (~950 ng/µg total DNA; Figure 3.9). The DNA content of s-V76 was ~1.7 times higher than the biomass level of s-VL43 (Figure 3.9).

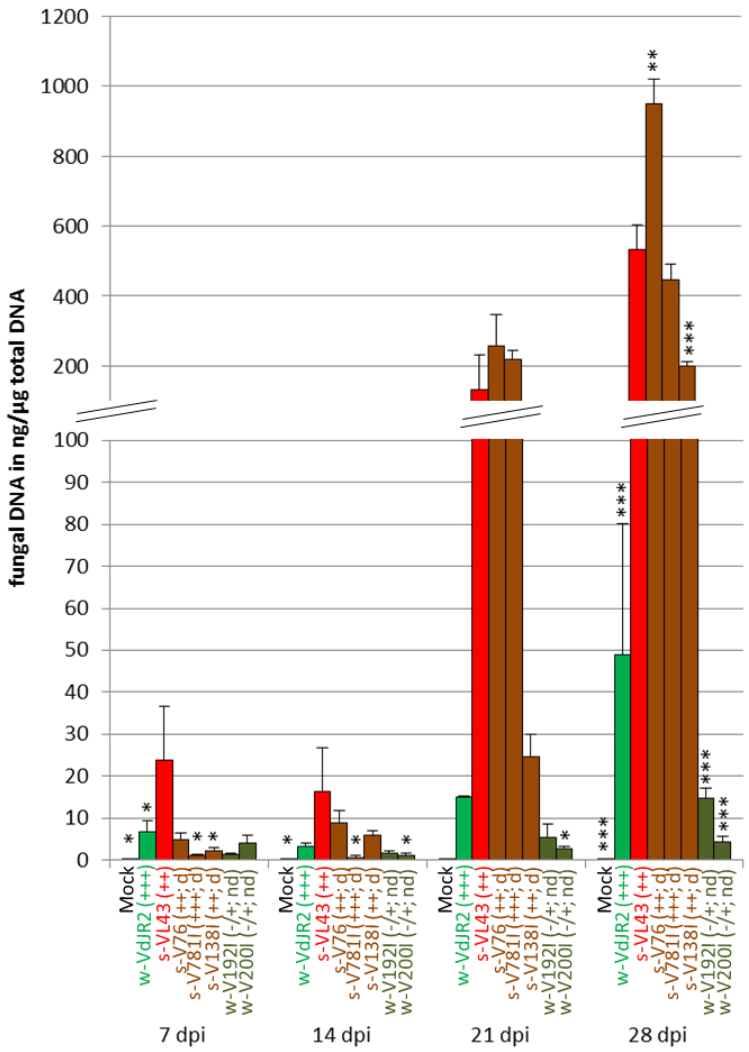

Figure 3.9: Proliferation of *V. dahliae* isolates w-VdJR2, s-V76, s-V781I, s-V138I, w-V192I and w-V200I in comparison to *V. longisporum* isolate s-VL43 *in planta*. *V. dahliae* isolates representing the "early senescence" interaction class are highlighted in **brown**. *V. dahliae* isolates representing the "wilting" interaction class are highlighted in **dark green**. The reference isolates s-VL43 and w-VdJR2 are highlighted in **red** and **green**, respectively. Early senescence inducing isolates are marked with the prefix s-. Wilt inducing isolates are marked with the prefix w-. Symbols indicate the intensity of disease symptom development: -/+ = mild symptoms, ++ = strong symptoms, +++ = very strong symptoms. d = cotton/olive defoliating, nd = cotton non-defoliating. Bars represent fungal biomass quantification via qRT-PCR of mock-treated and infected plants (n=4; pools of 4 plants) in the time course of the experiment. Error bars show standard deviation. Asterisks indicate statistical significance between *V. dahliae* and s-VL43 infected plants (t-test; * p≤0.05, ** p≤0.01, *** p≤0.001). Experiment was performed once.

To test whether early senescence inducing *V. dahliae* and *V. longisporum* isolates in comparison to their *in planta* proliferation also indicate differences in *in vitro* growth on solid medium spore solutions of s-T9, s-V76, s-ST100 and s-VL43 were plated on CDB agar plates and the colony diameter was measured at 7, 14 and 21 days after plating (Figure 3.8B). The isolate w-VdJR2 served as a growth control for the "wilting" interaction class and was included in this plate assay.

Notably, the previously mentioned enhanced *in planta* proliferation of s-T9, s-V76 and s-ST100 in comparison to s-VL43 was also reflected in their *in vitro* growth (Figure 3.8B). While early senescence inducing *V. dahliae* isolates possessed in average a colony diameter of ~6 cm at 7 days after plating, colonies of s-VL43 exhibited a diameter of only 4 cm (Figure 3.8B). This difference between *V. dahliae* and *V. longisporum* isolates of the "early senescence" interaction class was even more severe at later time points resulting in an about 1.75-fold smaller colony diameter of s-VL43 than that of the *V. dahliae* isolates at 21 days after plating (Figure 3.8B). In general, colony diameters of *V. dahliae* isolates of the "early senescence" interaction class did not differ from the diameter of w-VdJR2 colonies (Figure 3.8B).

3.2.3 *In situ* detection of fungal proliferation does not correlate with the *in planta* biomass quantification of *V. dahliae*

To support the previous quantification of the *in planta* fungal proliferation*, Verticillium* growth was also detected qualitatively *in situ* in infected Col-0 plants. For this purpose cytological studies of the leaf midrib vasculature were conducted. Leaf midribs of mock-treated Col-0 plants and plants 28 days post inoculation were cross-sectioned and embedded in plastic (2.2.5.1). In order to visualize fungal structures the cross-sections were stained histochemically with the chlorometric substrate XβD-Glc-NAc (2.2.5.1). The staining procedure was adapted from a previously published protocol to visualize structures of filamentous fungi (Diener, 2012). The substrate is converted by fungal hydrolases into a blue precipitate. Thus, fungal hyphae were colored in blue. For enhancement of the contrast between leaf tissues and *Verticillium* hyphae, samples were counterstained with safranin-O.

An extensive colonization of the leaf midrib was observed for w-VdJR2 infected plants (Figure 3.10B; Figure 3.11B). Xylem vessels seemed to be clogged by the fungal hyphae (Figure 3.10B; Figure 3.11B; magnification). Leaf midribs of w-V192I, w-V200I and s-V138I infected Col-0 plants were also frequently colonized comparable to w-VdJR2 infected plants (Figure 3.11F-H). Contrarily, significantly fewer hyphae of s-T9 were detected in the midrib vasculature (Figure 3.10D). Only in one out of the two experiments s-V76 was discovered to colonize the leaf midrib vasculature (Figure 3.10E; Figure 3.11D). Remarkably, no fungal structures were identified in leaf midribs of s-ST100, s-V781I and s-VL43 infected plants (Figure 3.10C, F; Figure 3.11C, E).

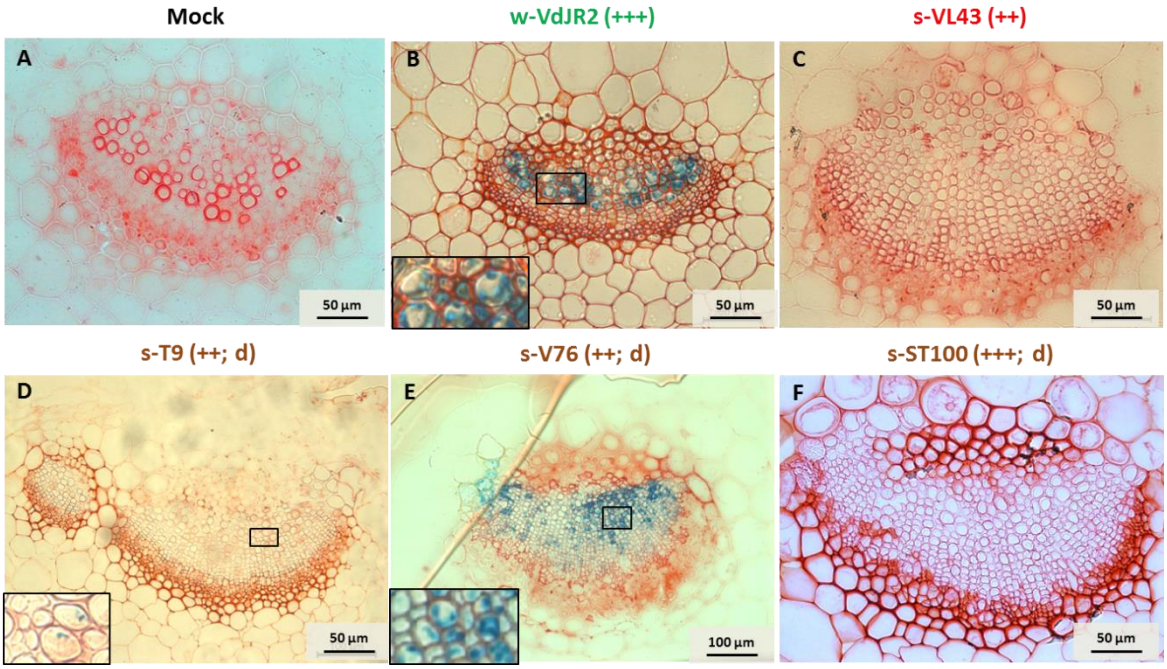

Figure 3.10: Cytological analyses to monitor fungal proliferation of w-VdJR2, s-VL43, s-T9, s-V76 and s-ST100 in infected Col-0 plants. *V. dahliae* isolates representing the "early senescence" interaction class are highlighted in **brown**. The reference isolates s-VL43 and w-VdJR2 are highlighted in **red** and **green**, respectively. Early senescence inducing isolates are marked with the prefix s-. Wilt inducing isolates are marked with the prefix w-. Symbols indicate the intensity of disease symptom development: ++ = strong symptoms, +++ = very strong symptoms. d = cotton/olive defoliating. Cross-sections of leaf midribs of mock-treated (A), w-VdJR2 (B), s-VL43 (C), s-T9 (D), s-V76 (E) and s-ST100 (F) infected plants. Midribs were harvested at 28 dpi. Fungal hyphae were visualized via XβD-Glc-Nac staining and plant tissues were counterstained with safranin-O. Boxes mark the position of insets. Insets show magnifications of tissues containing fungal hyphae. Experiment was performed twice involving two analysed midribs per experiment. Representative data are shown.

These results are conflicting with the in parallel performed *in planta* quantification of *Verticillium* proliferation. Since fungal DNA of early senescence inducing *V. dahliae* isolates was quantified to much greater extents than for wilt inducing isolates it was expected to detect *in situ* an enhanced abundance of fungal structures of the "early senescence" interaction class (Figure 3.8A; Figure 3.9; Figure 3.10C-F; Figure 3.11C-F). However, *in situ* studies revealed a much stronger leaf midrib colonization by w-VdJR2, w-V192I and w-V200I, although qRT-PCR data suggested a significantly lower growth of these isolates at 28 dpi compared to early senescence inducing *V. dahliae* strains (Figure 3.8A; Figure 3.9; Figure 3.10B; Figure 3.11B, G-H).

Possible reasons for the discordance between the data of *in planta* fungal biomass quantification and *in situ* detection will be discussed in section 4.4.

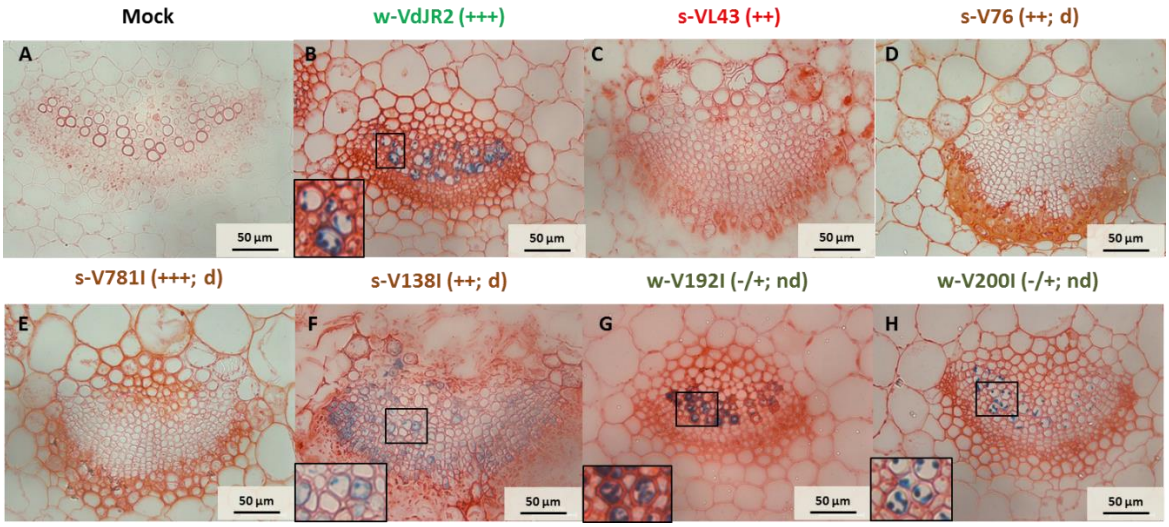

Figure 3.11: Cytological analyses to monitor fungal proliferation of w-VdJR2, s-VL43, s-V76, s-V781I, s-V138I, w-V192I and w-V200I in infected Col-0 plants. *V. dahliae* isolates representing the "early senescence" interaction class are highlighted in **brown**. *V. dahliae* isolates representing the "wilting" interaction class are highlighted in **dark green**. The reference isolates s-VL43 and w-VdJR2 are highlighted in **red** and **green**, respectively. Early senescence inducing isolates are marked with the prefix s-. Wilt inducing isolates are marked with the prefix w-. Symbols indicate the intensity of disease symptom development: -/+ = mild symptoms, ++ = strong symptoms, +++ = very strong symptoms. d = cotton/olive defoliating, nd = cotton non-defoliating. Cross-sections of leaf midribs of mock-treated (A), w-VdJR2 (B), s-VL43 (C), s-V76 (D), s-V781I (E), s-V138I (F), w-V192I (G) and w-V200I (H) infected plants. Midribs were harvested at 28 dpi. Fungal hyphae were visualized via XβD-Glc-Nac staining and plant tissues were counterstained with safranin-O. Boxes mark the position of insets. Insets show magnifications of tissues containing fungal hyphae. Experiment was performed once involving two analysed midribs. Representative data are shown.

3.2.4 Early senescence inducing *V. dahliae* isolates trigger bundle sheath cell transdifferentiation in Col-0 leaf midribs accompanied by enhanced expression of the VASCULAR-RELATED NAC DOMAIN7 (VND7) transcription factor

Previous infection experiments showed that inoculation of Col-0 plants with s-VL43 and w-VdJR2 are accompanied by different structural reprogramming patterns of the plants' vasculature (Reusche *et al.*, 2014). Whereas infection with *V. longisporum* s-VL43 involves the replacement of bundle sheath cells surrounding the leaf vascular tissue with *de novo* formed xylem vessels, no transdifferentiation of bundle sheath cells was observed for w-VdJR2 infected plants (Reusche *et al.*, 2014).

To elucidate whether early senescence disease symptoms are generally accompanied by s-VL43-like bundle sheath cell transdifferentiation microscopic analyses were performed. At 28 dpi leaves were harvested from infected and mock-treated Col-0 plants and stained with trypan-blue in order to detect dead cells which include tracheary elements (TEs) of xylem tissues. Moreover, to support the detection of bundle sheath cell transdifferentiation the expression of the VASCULAR-RELATED NAC DOMAIN7 (VND7) gene which participates in developmental reprogramming in leaf vasculatures was measured (Reusche *et al.*, 2012).

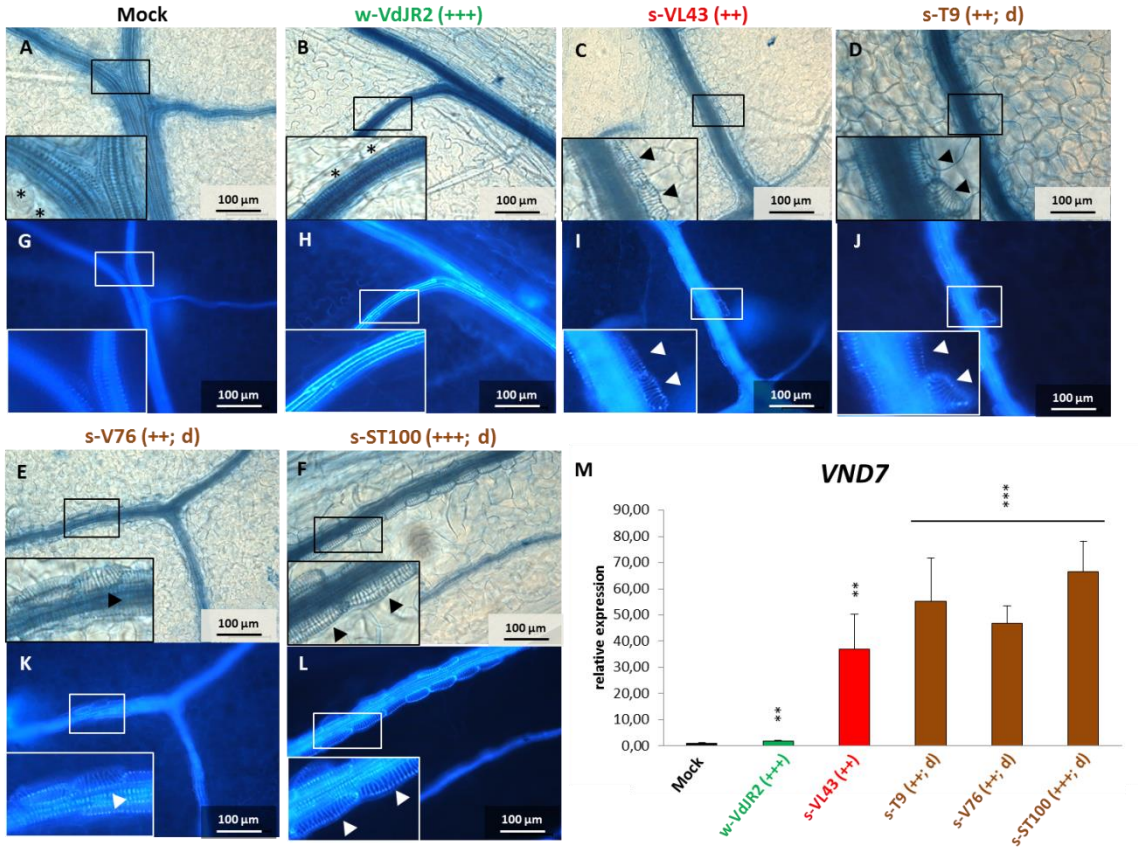

Figure 3.12: Detection of bundle sheath cell transdifferentiation into TEs in Col-0 after infection with *Verticillium* isolates s-VL43, w-VdJR2, s-T9, s-V76 and s-ST100. *V. dahliae* isolates representing the "early senescence" interaction class are highlighted in **brown**. The reference isolates s-VL43 and w-VdJR2 are highlighted in **red** and **green**, respectively. Early senescence inducing isolates are marked with the prefix s-. Wilt inducing isolates are marked with the prefix w-. Symbols indicate the intensity of disease symptom development: ++ = strong symptoms, +++ = very strong symptoms. d = cotton/olive defoliating. **A-L:** Microscopic investigation of trypan-blue stained leaves of mock-treated plants and plants inoculated with *Verticillium*. Boxes mark the position of insets. Insets show magnifications of leaf veins containing *de novo* formed xylem vessels indicated by arrowheads. Leaves were harvested at 28 dpi. Experiment was performed three times involving three analysed leaves and representative data are shown. **A-F:** Bright-field images of leaf veins of either mock-treated or *Verticillium* infected plants. Bundle sheath cells are marked with asterisks. **G-L:** Autofluorescence detection of leaf xylem vessels of mock-treated or *Verticillium* infected plants. **M:** Bars represent the relative expression levels of *VND7* of mock-treated or *Verticillium* infected plants measured via qRT-PCR. For qRT-PCR the aerial plant parts were harvested (n=4; pool of 4 plants) at 28 dpi. Error bars show standard deviation. Asterisks indicate statistical significance between mock-treated and *V. dahliae* infected plants (t-test; * p≤0.05, ** p≤0.01, *** p≤0.001). Experiment was performed three times and representative data are shown.

Vasculature in non-infected plant leaf veins was composed of TEs surrounded by a continuous layer of bundle sheath cells (Figure 3.12A; Figure 3.13A). Moreover, the xylem of leaf veins in mock-treated *A. thaliana* plants usually show a generally elevated level of fluorescence due to incorporation of autofluorescent polyphenolics (e.g. lignins) into their cell walls (Figure 3.12G; Figure 3.13I). As expected, the inoculation of Col-0 plants with s-VL43 resulted in transdifferentiation of bundle sheath cells into TEs (Figure 3.12C, I; Figure 3.13C, K; arrowheads). Accordingly, also leaves of plants infected with the early senescence inducing *V. dahliae* isolates s-T9, s-V76, s-ST100, s-V781I and s-V138I showed bundle sheath cell layers which were

interrupted by discontinuous segments of *de novo* formed xylem cells (Figure 3.12D-F, J-L; Figure 3.13D-F, L-N; arrowheads). In contrast to that, leaf veins of w-VdJR2, w-V192I and w-V200I inoculated plants are surrounded by a continuous layer of bundle sheath cells and no transdifferentiation into TEs was discovered (Figure 3.12B, H; Figure 3.13B, G-H, J, O-P).

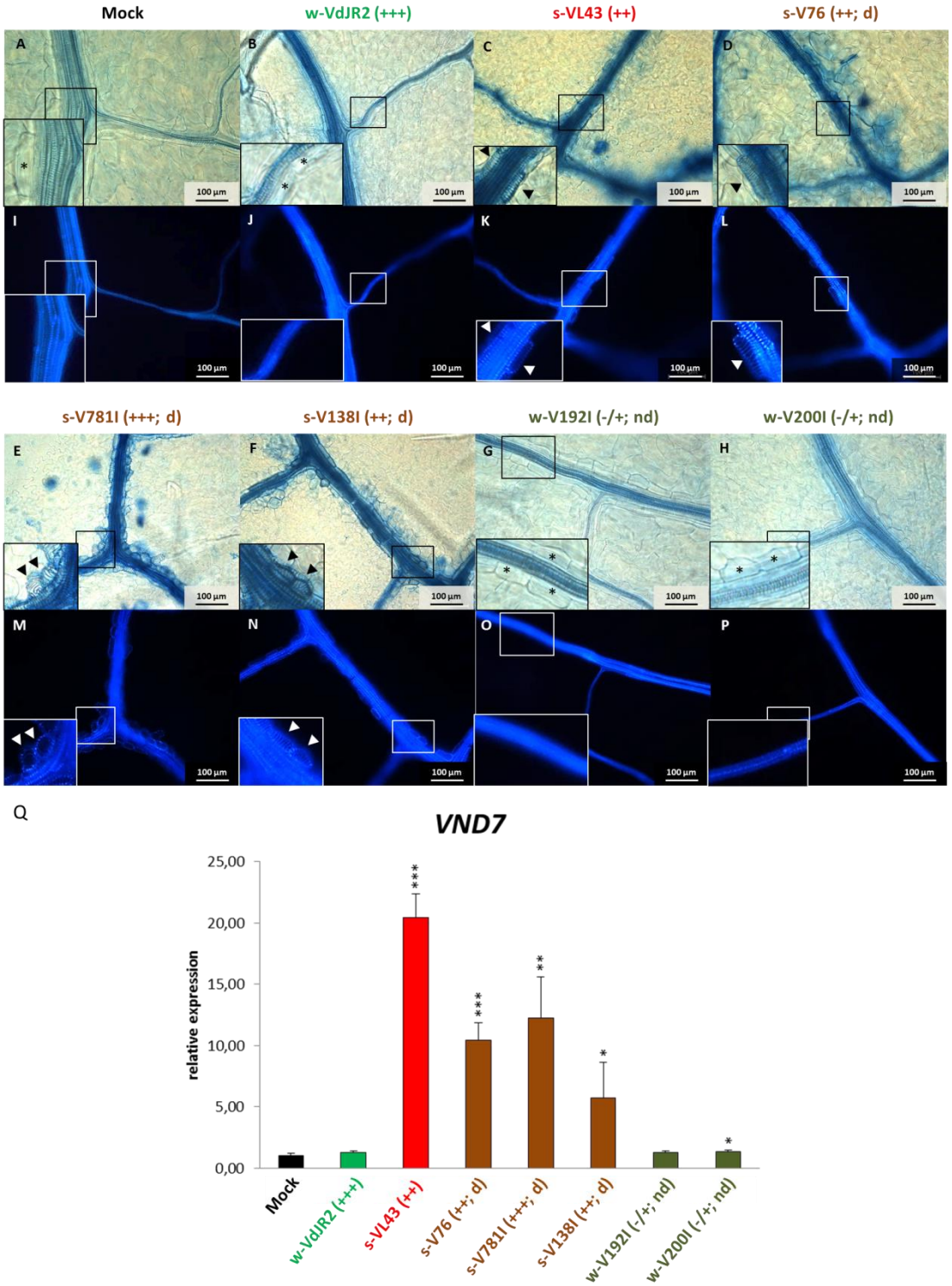

Figure 3.13: Detection of bundle sheath cell transdifferentiation into TEs and *VND7* expression analysis in Col-0 after infection with *Verticillium* isolates s-VL43, w-VdJR2, s-V76, s-V781I, s-V138I, w-V192I and w-V200I. *V. dahliae* isolates representing the "early senescence" interaction class are highlighted in **brown**. *V. dahliae* isolates representing the "wilting" interaction class are highlighted in **dark green**. The reference isolates s-VL43 and w-VdJR2 are highlighted in **red** and **green**, respectively. Early senescence inducing isolates are marked with the prefix s-. Wilt inducing isolates are marked with the prefix w-. Symbols indicate the intensity of disease symptom development: -/+ = mild symptoms, ++ = strong symptoms, +++ = very strong symptoms. d = cotton/olive defoliating, nd = cotton non-defoliating. **A-P:** Microscopic investigation of trypan-blue stained leaves of mock-treated plants and plants inoculated with *Verticillium*. Boxes mark the position of insets. Insets show magnifications of leaf veins containing *de novo* formed xylem vessels indicated by arrowheads. Leaves for microscopic investigation were harvested at 28 dpi. Experiment was perfomed once involving three analysed leaves. Representative data are shown. **A-H:** Bright-field images of leaf veins of either mock-treated or *Verticillium* infected plants. Bundle sheath cells are marked with asterisks. **I-P:** Autofluorescence detection of leaf xylem vessels of mock-treated or *Verticillium* infected plants. **Q:** Bars represent the relative expression levels of *VND7* of mock-treated or *Verticillium* infected plants measured via qRT-PCR. For qRT-PCR the aerial plant parts were harvested (n=4; pool of 4 plants) at 28 dpi. Error bars show standard deviation. Asterisks indicate statistical significance between mock-treated and *V. dahliae* infected plants (t-test; * p≤0.05, ** p≤0.01, *** p≤0.001). Experiments were performed once.

The identification of *de novo* xylem vessel formation in *A. thaliana* Col-0 plants was supported by expression analysis of the VASCULAR-RELATED NAC DOMAIN7 (VND7) gene (Figure 3.12M; Figure 3.13Q), which was recently found to be associated with the *Verticillium*-induced transdifferentiation process (Reusche *et al.*, 2012). S-T9, s-V76, s-ST100, s-V781I and s-V138I infected plants as well as plants inoculated with the reference strain s-VL43 exhibited a significantly higher *VND7* expression than mock-treated plants (Figure 3.12M; Figure 3.13Q). *VND7* expression in s-VL43 infected plants was 21-fold induced in comparison to mock-treated plants (Figure 3.13Q). In the first experiment *VND7* expression was even more elevated and 35-fold induced than in mock-treated plants (Figure 3.12M). Plants inoculated with s-T9, s-V76 and s-ST100 possessed even stronger expression of *VND7* than s-VL43 infected plants, indicating a ~55-, ~45- and ~65-fold induction compared to mock-treated plants (Figure 3.12M). In s-V138I and s-V781I infected plants *VND7* expression was ~6-fold and ~12-fold induced, respectively (Figure 3.13Q).

Moreover, for plants infected with isolates w-VdJR2, w-V192I and w-V200I which did not induce bundle sheath cell transdifferentiation, no upregulation in *VND7* expression was detected (Figure 3.12M; Figure 3.13Q). Although, *VND7* expression in w-VdJR2 and w-V200I inoculated plants was calculated to be significantly increased the expression was detected to a similar level as in mock-treated and w-V192I infected plants, respectively (Figure 3.12M; Figure 3.13Q).

3.2.5 Infection with *V. dahliae* isolates of the "early senescence" interaction class results in the development of a hyperplastic xylem in leaf midribs accompanied by enhanced upregulation of the cambial marker gene *AtHB8*

As previously mentioned diverse structural and developmental changes of the plants' vasculature were identified after w-VdJR2 and s-VL43 infection. This included the formation of hyperplastic xylem tissues in the vascular bundles of leaf midribs after s-VL43 infection which was not detected in *V. dahliae* w-VdJR2 infected plants (Reusche *et al.*, 2014). Hyperplasia formation was discussed to be caused by the transdifferentiation of xylem parenchyma cells into novel xylem vessels on the one hand and by a reactivated cambial activity on the other hand (Reusche *et al.*, 2014). Moreover, an enhanced cell wall lignification of genuine xylem cells was discovered in w-VdJR2 inoculated plants, but not after s-VL43 infection (Reusche *et al.*, 2014).

To elucidate whether early senescence disease symptoms and plant wilting are usually accompanied by hyperplasia development and elevated levels of xylem cell wall lignification, respectively, leaf midribs of mock-treated and *Verticillium* infected plants were cross-sectioned and microscopically analysed. To substantiate the detection of a hyperplastic xylem, xylem cells in leaf midribs were counted. In addition, the expression of the cambial marker gene *AtHB8* was measured via qRT-PCR in mock-treated and *Verticillium* infected Col-0 plants at 14 dpi (Reusche *et al.*, 2014). For visualization of fungal structures leaf midribs were stained with the substrate XβD-Glc-NAc according to a previously published staining protocol (2.2.5.1; Diener, 2012). Epifluorescence microscopy was used to monitor autofluorescent cell wall lignification patterns. In addition, lignified xylem structures were monitored via potassium permanganate staining and investigated by bright field microscopy. Potassium permanganate staining in combination with XβD-Glc-Nac treatment allows to simultaneously identify lignified cells and the presence of fungal hyphae (Reusche *et al.*, 2014). This would answer the question whether fungal structures mainly occur in genuine xylem vessels possessing enhanced lignification or whether hyphae are distributed similarly in xylem vessels and xylem parenchyma cells in leaf midribs.

As expected, the inoculation with s-VL43 resulted in the development of an unusually high number of lignified xylem vessels, a pathogen-induced hyperplasia (Figure 3.14C, I; Figure 3.15C, K). Radial files of xylem cells were highly produced and derange the vascular tissue borders as it was previously observed after s-VL43 infection (Reusche *et al.*, 2012; Reusche *et al.*, 2014). According to the s-VL43-like symptom development, hyperplastic xylem formation was also observed in leaf midribs of plants infected with early senescence inducing *V. dahliae* isolates s-T9, s-V76, s-ST100, s-V781I and s-V138I (Figure 3.14D-F, J-L; Figure 3.15D-F, L-N). Contrarily, no

transdifferentiation of xylem parenchyma cells into novel xylem vessels was detected in leaves of w-VdJR2, w-V192I and w-V200I infected plants (Figure 3.14B, H; Figure 3.15B, G-H, J, O-P).

Hyperplasia formation was confirmed by quantification of the xylem cells per midrib section: leaf midribs of plants infected with the isolates of the "early senescence" interaction class, s-VL43, s-T9, s-V76, s-ST100, s-V781I and s-V138I, exhibited a significantly higher number of xylem cells than mock-treated plants (Figure 3.14M; Figure 3.15Q). In contrast to that, w-VdJR2, w-V192I and w-V200I infected plants exhibited a number of leaf midrib xylem vessels which was comparable to mock-treated plants (Figure 3.14M; Figure S9Q).

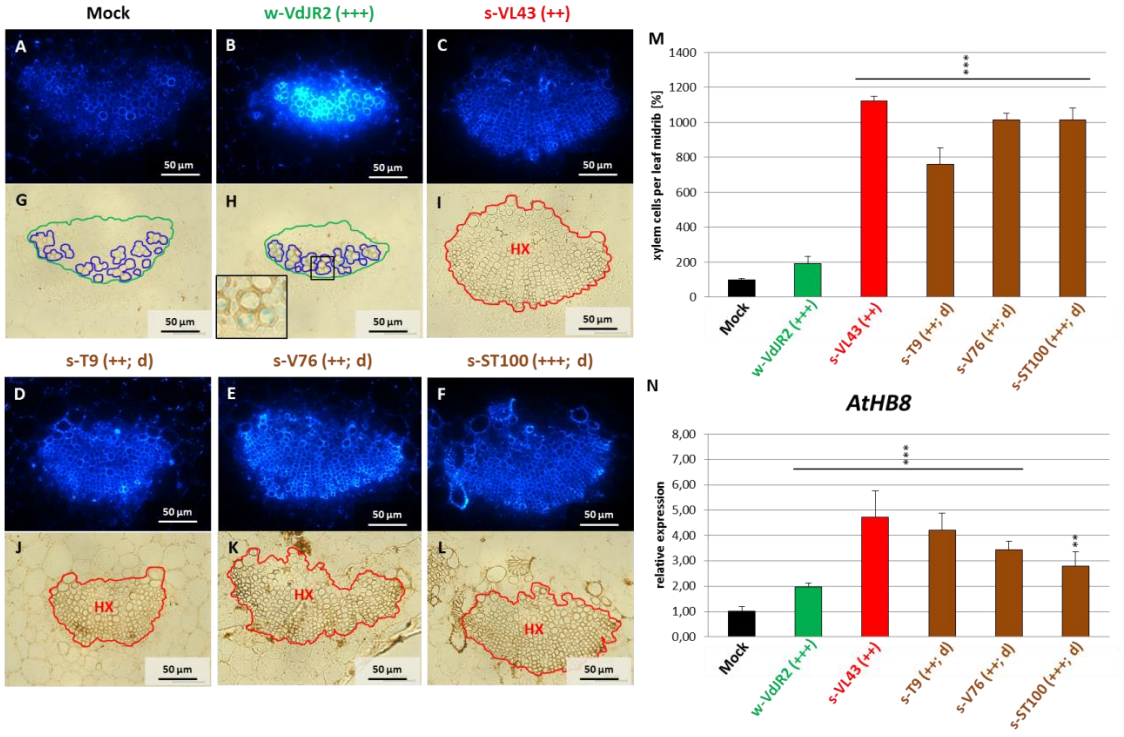

Figure 3.14: Histological analyses and xylem cell counting of Col-0 leaf midribs as well as *AtHB8* expression measurements for the identification of hyperplasia induction after infection with the *Verticillium* isolates s-VL43, w-VdJR2, s-T9, s-V76 and s-ST100. *V. dahliae* isolates representing the "early senescence" interaction class are highlighted in **brown**. The reference isolates s-VL43 and w-VdJR2 are highlighted in **red** and **green**, respectively. Early senescence inducing isolates are marked with the prefix s-. Wilt inducing isolates are marked with the prefix w-. Symbols indicate the intensity of disease symptom development: ++ = strong symptoms, +++ = very strong symptoms. d = cotton/olive defoliating. **A-L:** Microscopic investigation of potassium permanganate stained midribs and midrib autofluorescence of mock-treated plants or plants inoculated with *Verticillium*. Bordered cells indicate positions of different cell types: Red: hyperplastic xylem, green: xylem parenchyma, blue: xylem. HX = hyperplastic xylem. Tissues were examined at 40x magnification. Box indicates position of magnified tissues. Magnification indicates w-VdJR2 hyphae in lignified vessels. Leaves for microscopic investigation were harvested at 28 dpi. Experiment was performed twice involving two analysed midribs per experiment. Representative data are shown. **A-F:** Autofluorescence detection of leaf midrib tissues. **G-L:** Bright field microscopy of leaf midrib tissues. **M:** Quantification of xylem cells per midrib section by counting in mock-treated and infected plants (n=4). Experiment was performed once. Error bars show standard deviation. Asterisks indicate statistical significance between mock-treated and *Verticillium* infected plants (t-test; * p≤0.05, ** p≤0.01, *** p≤0.001). **N:** Bars represent the relative expression levels of *AtHB8* in mock-treated or *Verticillium* infected plants measured via qRT-PCR. For qRT-PCR the aerial plant parts were harvested (n=4; pools of 4 plants) at 14 dpi. Error bars show standard deviation. Asterisks indicate statistical significance between mock-treated and *Verticillium* infected plants (t-test; * p≤0.05, ** p≤0.01, *** p≤0.001). Experiments were performed twice and representative data are shown.

Since it was postulated that the formation of a hyperplastic xylem is the consequence of an enhanced cambial activity (Reusche *et al.*, 2014), the expression of *AtHB8* as a marker of cambial activity (Scarpella *et al.*, 2004) was monitored for mock-treated and infected plants. Hyperplastic xylem formation in plants infected with *Verticillium* isolates of the "early senescence" interaction class clearly correlated with an increased *AtHB8* expression (Figure 3.14N; Figure 3.15R). Contrarily, *AtHB8* expression in w-VdJR2, w-V192I and w-V200I infected plants was considerably lower which supports the lack of hyperplasia development in leaf midribs (Figure 3.14B, H, N; Figure 3.15B, G-H, J, O-P, R).

Autofluorescence detection in leaf midribs of w-VdJR2 infected plants revealed intense lignification of xylem cell walls of already existing xylem vessels (Figure 3.14B; Figure 3.15B). In contrast to these findings, no enhanced lignification of the leaf vasculature was detected in mock-treated plants and plants infected with the early senescence inducing *Verticillium* isolates and the autofluorescence level was comparable to mock-treated plants (Figure 3.14A, C-F; Figure 3.15A, C-F). An increase in autofluorescence levels was discovered for xylem cell walls in leaf vasculatures of w-V192I and w-V200I inoculated plants (Figure 3.15G-H). However, the lignification intensity was lower than in leaf midribs of w-VdJR2 inoculated plants (Figure 3.15B). The discrepancy of different lignification levels between w-VdJR2, w-V192I and w-V200I infected plants may be explained by the different symptom development intensities induced by the strains of the "wilting" interaction class. Since w-VdJR2 triggered more severe wilting symptoms on Col-0 plants than w-V192I and w-V200I (Figure S3; Table 3.3), this might also be reflected in the strength of lignification events.

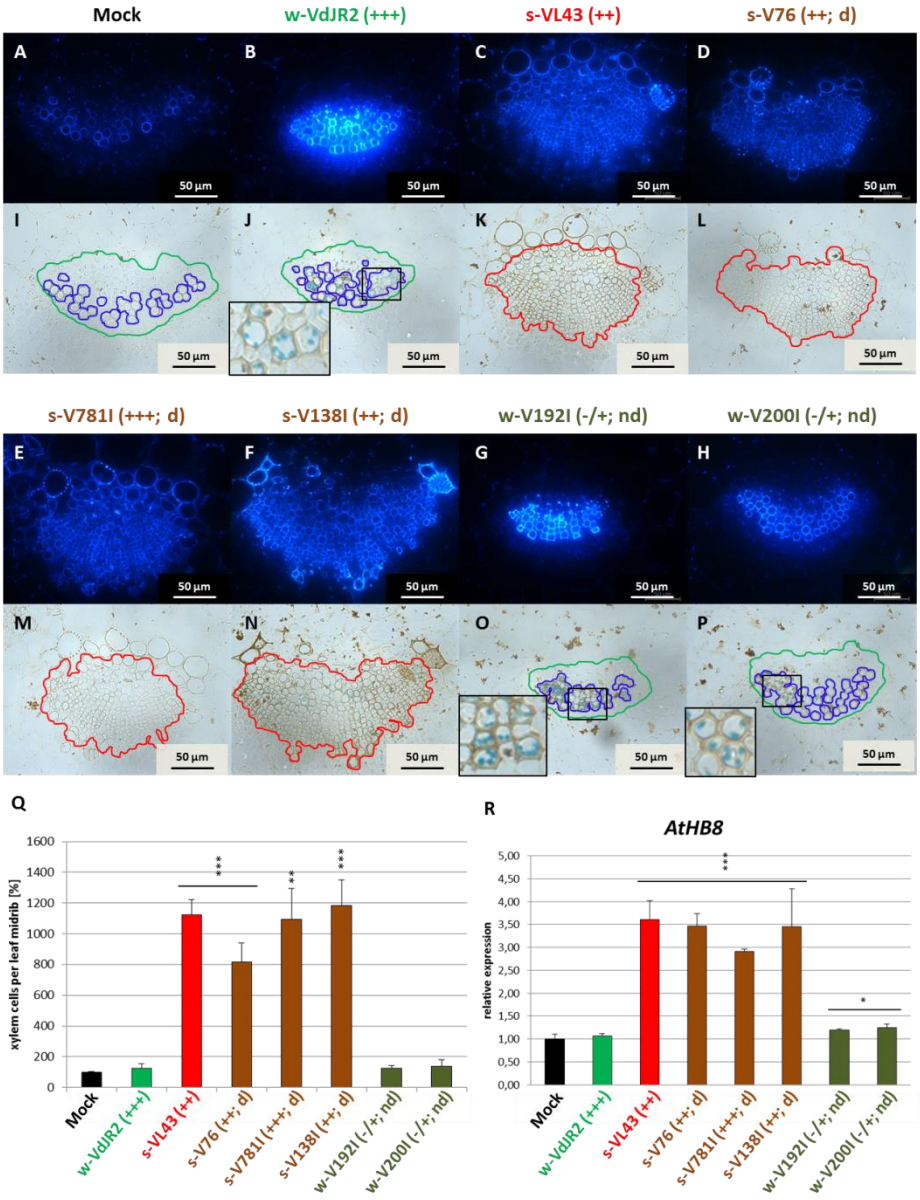

Figure 3.15: Histological analyses and xylem cell counting of Col-0 leaf midribs as well as *AtHB8* expression measurements for the identification of hyperplasia induction after infection with the *Verticillium* isolates s-VL43, w-VdJR2, s-V76, s-V781I, s-V138I, w-V192I and w-V200I. *V. dahliae* isolates representing the "early senescence" interaction class are highlighted in **brown**. *V. dahliae* isolates representing the "wilting" interaction class are highlighted in **dark green**. The reference isolates s-VL43 and w-VdJR2 are highlighted in **red** and **green**, respectively. Early senescence inducing isolates are marked with the prefix s-. Wilt inducing isolates are marked with the prefix w-. Symbols indicate the intensity of disease symptom development: -/+ = mild symptoms, ++ = strong symptoms, +++ = very strong symptoms. d = cotton/olive defoliating, nd = cotton non-defoliating. **A-P:** Microscopic investigation of potassium permanganate stained midribs and autofluorescence of mock-treated plants or plants inoculated with *Verticillium*. Bordered cells indicate positions of different cell types: Red: hyperplastic xylem, green: xylem parenchyma, blue: xylem. HX = hyperplastic xylem. Tissues were examined at 40x magnification. Box indicates position of magnified tissues. Magnification indicates w-VdJR2 hyphae in lignified vessels. Leaves for microscopic investigation were harvested at 28 dpi. Experiment was performed once involving three analysed midribs per experiment. Representative data are shown. **A-H:** Autofluorescence detection of leaf midrib tissues. **I-P:** Bright field microscopy of leaf midrib tissues. **Q:** Quantification of xylem cells per midrib section by counting in mock-treated and infected plants (n=3). Error bars show standard deviation. Asterisks indicate statistical significance between mock-treated and *Verticillium* infected plants (t-test; * p≤0.05, ** p≤0.01, *** p≤0.001). Experiment was performed once. **R:** Bars represent the relative expression levels of *AtHB8* in mock-treated or *Verticillium* infected plants measured via qRT-PCR. For qRT-PCR the aerial plant parts were harvested (n=4; pools of 4 plants) at 14 dpi. Error bars show standard deviation. Asterisks indicate statistical significance between mock-treated and *Verticillium* infected plants (t-test; * p≤0.05, ** p≤0.01, *** p≤0.001). Experiment was performed once.

Remarkably, fungal structures of w-VdJR2, w-V192I and w-V200I were solely discovered in xylem cells which are intensely stained by potassium permanganate indicating an increased lignification (Figure 3.14H; Figure 3.15J, O-P; magnification). This hypothesizes that the enhanced lignification is directly linked to the presence of fungal hyphae in the midrib vasculature. In contrast, no fungal hyphae of the early senescence inducing strains were discovered in the leaf midrib cross-sections used for the potassium permanganate staining (Figure 3.14I-L; Figure 3.15K-N). Nevertheless, the previous cytological studies for *in situ* detection of fungal hyphae also indicated a large amount of newly build xylem cells which only in case of s-T9, s-V76 and s-V138I infected plants harbored fungal structures (Figure 3.10D-E; Figure 3.11F). The observation of hyperplasia formation without the detection of any fungal hyphae in the newly formed cells points towards the independence of xylem parenchyma transdifferentiation and cambial reactivation from the presence of fungal hyphae.

3.2.6 Expression of the *Arabidopsis* biotic stress marker genes *PR-1* and *PDF1.2* was stronger in early senescence than in wilt inducing *V. dahliae* isolates

To answer the question whether plant hormone signaling involved in plant defence responses might be differently regulated in plants infected with *Verticillium* isolates of the “wilting” or the “early senescence” interaction classes, the expression of two marker genes was analysed: expression of the *PATHOGENESIS-RELATED* (*PR*) gene *1* is triggered by the signaling cascade of the salicylic acid (SA) pathway (Uknes *et al.*, 1992; Penninckx *et al.*, 1996; Kombrink and Somssich, 1997; Durner *et al.*, 1997) whereas expression of the marker gene *PLANT DEFENSIN 1.2* (*PDF1.2*) is induced by jasmonic acid (JA) and ethylene (ET) (Penninckx *et al.*, 1996). *PR-1* and *PDF1.2* expression was measured in a time course including the time points 7 dpi, 14 dpi, 21 dpi and 28 dpi.

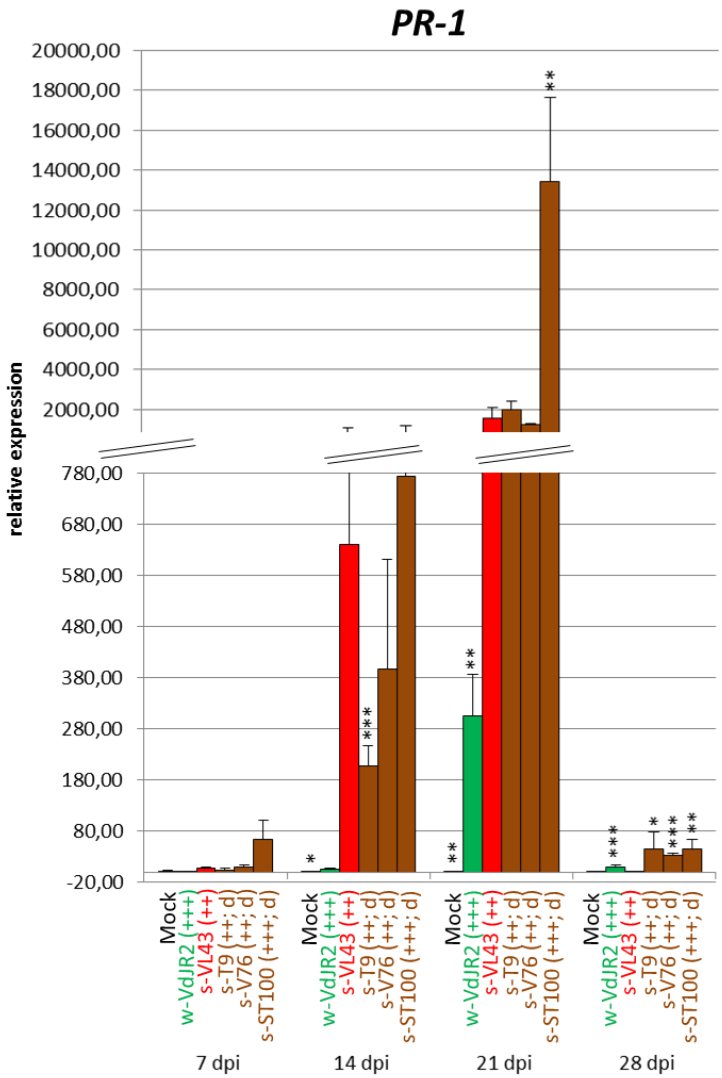

Figure 3.16: Expression analysis of *PR-1* in mock-treated and w-VdJR2, s-VL43, s-T9, s-V76 and s-ST100 infected plants. *V. dahliae* isolates representing the "early senescence" interaction class are highlighted in **brown**. The reference isolates s-VL43 and w-VdJR2 are highlighted in **red** and **green**, respectively. Early senescence inducing isolates are marked with the prefix s-. Wilt inducing isolates are marked with the prefix w-. Symbols indicate the intensity of disease symptom development: ++ = strong symptoms, +++ = very strong symptoms. d = cotton/olive defoliating. Bars represent relative expression of *PR-1* in mock-treated and *Verticillium* infected plants measured via qRT-PCR (n=4; pool of 4 plants). Error bars show standard deviation. Asterisks indicate statistical significance between *V. longisporum* s-VL43 infected and mock-treated or *V. dahliae* infected plants (t-test; * p≤0.05, ** p≤0.01, *** p≤0.001). Experiment was repeated three times. A supplementary *PR-1* expression measurement monitoring no intense upregulation of *PR-1* for s-ST100 inoculated plants at 21 dpi is illustrated in Figure S4.

In general, the expression of *PR-1* in plants infected with w-VdJR2, s-VL43, s-T9, s-V76 and s-ST100 continuously increased from 7 dpi to 21 dpi during the time course reaching a maximum *PR-1* expression at 21 dpi (Figure 3.16). Interestingly, *PR-1* expression of plants infected with the *Verticillium* isolates which induce early senescence on *A. thaliana* Col-0 was higher than *PR-1* expression in w-VdJR2 inoculated plants at every time point (Figure 3.16). An extremely elevated level of *PR-1* expression was detected in s-ST100 inoculated plants at 21 dpi resulting in a ~6.7-

fold expression induction in comparison to s-VL43 infected plants (Figure 3.16). However, this intense upregulation of *PR-1* was not confirmed in a repetition of the experiment (Figure S4). No clear trend of *PR-1* expression was discovered in s-V781I, s-V138I, w-V192I and w-V200I infected plants during the time course (Figure 3.17). Nevertheless, from 14 dpi to 21 dpi plants inoculated with the *V. dahliae* isolates s-V781I and s-V138I of the "early senescence" interaction class exhibited stronger *PR-1* expression than plants infected with the wilt isolates w-VdJR2, w-V192I and w-V200I (Figure 3.17).

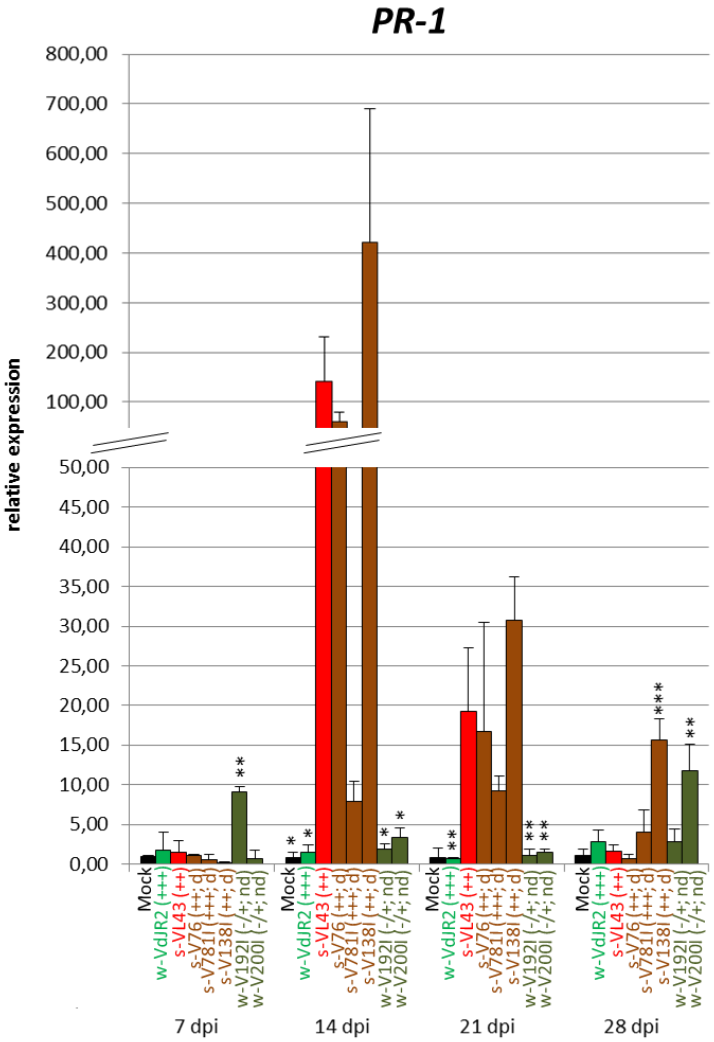

Figure 3.17: Expression analysis of *PR-1* in w-VdJR2, s-VL43, s-V76, s-V781I, s-V138I, w-V192I and w-V200I infected plants. *V. dahliae* isolates representing the "early senescence" interaction class are highlighted in **brown**. *V. dahliae* isolates representing the "wilting" interaction class are highlighted in **dark green**. The reference isolates s-VL43 and w-VdJR2 are highlighted in **red** and **green**, respectively. Early senescence inducing isolates are marked with the prefix s-. Wilt inducing isolates are marked with the prefix w-. Symbols indicate the intensity of disease symptom development: -/+ = mild symptoms, ++ = strong symptoms, +++ = very strong symptoms. d = cotton/olive defoliating, nd = cotton non-defoliating. Bars represent relative expression of *PR-1* in mock-treated and *Verticillium* infected plants measured via qRT-PCR (n=4; pools of 4 plants). Error bars show standard deviation. Asterisks indicate statistical significance between *V. longisporum* s-VL43 infected and mock-treated or *V. dahliae* infected plants (t-test; * p≤0.05, ** p≤0.01, *** p≤0.001). Experiment was performed once.

To analyse the regulation of the JA signaling pathway in *Verticillum* infected plants, expression of the JA/ET marker gene *PDF1.2* was studied. The highest marker gene expression was detected for almost every infected plant at 28 dpi, except for s-ST100 infected plants which showed the strongest upregulation of *PDF1.2* at 21 dpi (Figure 3.18; Figure 3.19). This finding was confirmed by a repetition of the expression analysis which as well detected an intense *PDF1.2* expression in s-ST100 inoculated plants at 21 dpi (Figure S5). Simultaneously, these plants possessed a dramatic increase in *PR-1* expression indicating that both biotic stress marker genes were strongly induced by s-ST100 infection (Figure 3.16). However, intense expression of biotic stress marker genes do not result from exceedingly high fungal biomass of s-ST100 *in planta* since the isolate proliferated lesser than s-V76 (Figure 3.8A).

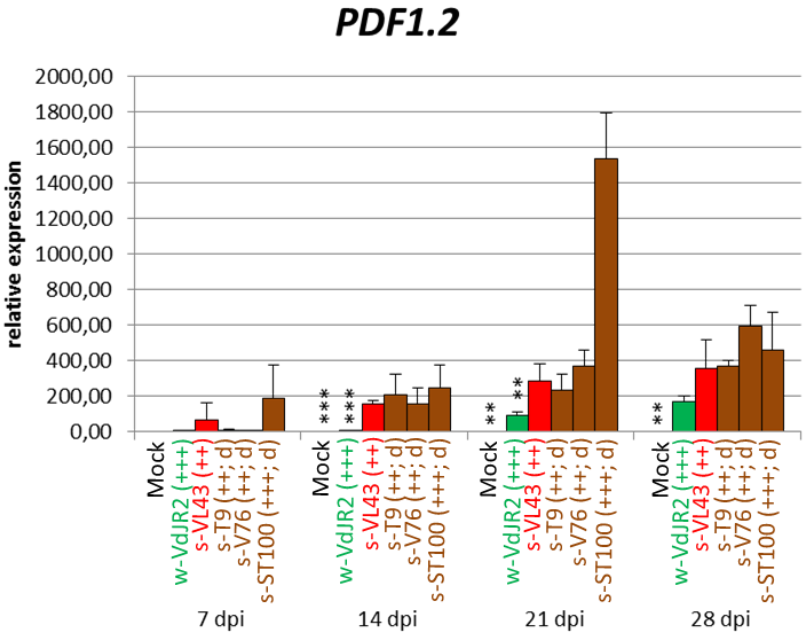

Figure 3.18: Expression analysis of *PDF1.2* in mock-treated and w-VdJR2, s-VL43, s-T9, s-V76 and s-ST100 infected plants. *V. dahliae* isolates representing the "early senescence" interaction class are highlighted in **brown**. The reference isolates s-VL43 and w-VdJR2 are highlighted in **red** and **green**, respectively. Early senescence inducing isolates are marked with the prefix s-. Wilt inducing isolates are marked with the prefix w-. Symbols indicate the intensity of disease symptom development: ++ = strong symptoms, +++ = very strong symptoms. d = cotton/olive defoliating. Bars represent relative expression of *PDF1.2* in mock-treated and *Verticillium* infected plants measured via qRT-PCR (n=4; pools of 4 plants). Error bars show standard deviation. Asterisks indicate statistical significance between *V. longisporum* s-VL43 infected and mock-treated or *V. dahliae* infected plants (t-test; * p≤0.05, ** p≤0.01, *** p≤0.001). Experiment was repeated three times. A supplementary *PDF1.2* expression measurement monitoring similar intense upregulation of *PDF1.2* for s-ST100 inoculated plants at 21 dpi is illustrated in Figure S5.

Notably, between 14 dpi and 21 dpi the level of *PDF1.2* expression was significantly elevated in plants infected with the *Verticillium* isolates of the "early senescence" interaction class compared to plants inoculated with isolates of the "wilting" class (Figure 3.18; Figure 3.19). Moreover, *PDF1.2* expression increased more rapidly during the time course in plants inoculated with strains of the "early senescence" class than in plants infected with w-VdJR2, w-V192I or w-V200I (Figure 3.18; Figure 3.19).

Generally, *PDF1.2* expression persisted longer during the time course of the experiments than the expression of *PR-1.* In addition, the maximum of *PDF1.2* expression was reached about 7 to 14 days later in infected plants than the expression maximum of *PR-1*.

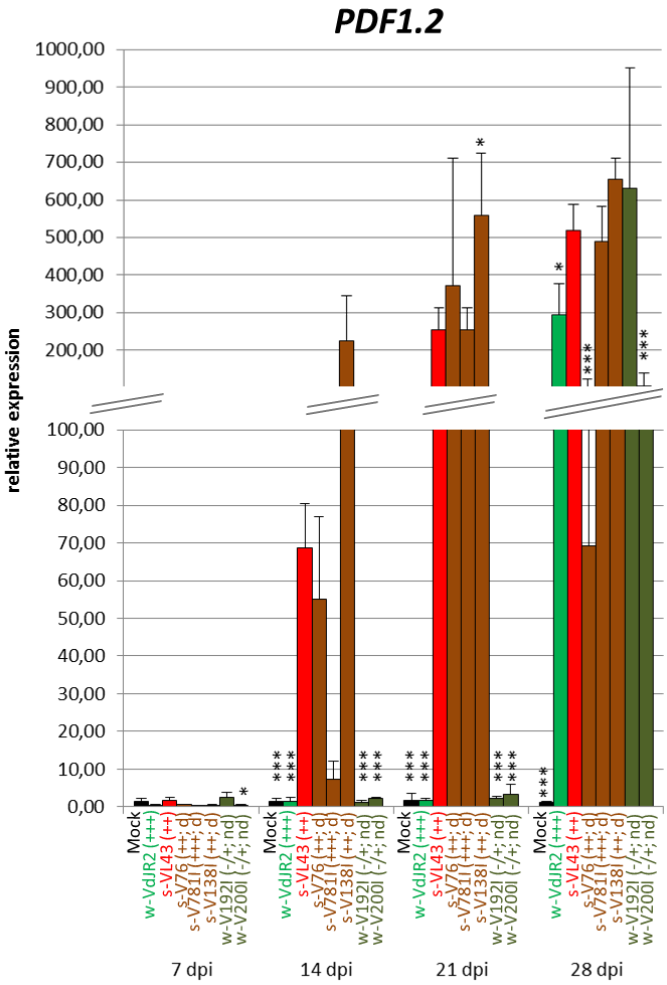

Figure 3.19: Expression analysis of *PDF1.2* in mock-treated and w-VdJR2, s-VL43, s-V76, s-V781I, s-V138I, w-V192I and w-V200I infected plants. *V. dahliae* isolates representing the "early senescence" interaction class are highlighted in **brown**. *V. dahliae* isolates representing the "wilting" interaction class are highlighted in **dark green**. The reference isolates s-VL43 and w-VdJR2 are highlighted in **red** and **green**, respectively. Early senescence inducing isolates are marked with the prefix s-. Wilt inducing isolates are marked with the prefix w-. Symbols indicate the intensity of disease symptom development: -/+ = mild symptoms, ++ = strong symptoms, +++ = very strong symptoms. d = cotton/olive defoliating, nd = cotton non-defoliating. Bars represent relative expression of *PDF1.2* in mock-treated and *Verticillium* infected plants measured via qRT-PCR (n=4; pools of 4 plants). Error bars show standard deviation. Asterisks indicate statistical significance between *V. longisporum* s-VL43 infected and mock-treated or *V. dahliae* infected plants (t-test; * p≤0.05, ** p≤0.01, *** p≤0.001). Experiment was performed once.

3.3 Analysis of macroscopic disease symptom induction and bundle sheath cell transdifferentiation induced by *V. dahliae* on *N. benthamiana* plants

As discovered in section 3.2.4 and 3.2.5 *V. dahliae* isolates of the "early senescence" interaction class induce *de novo* xylem formation in the leaf vasculature of *A. thaliana* Col-0, resulting in hyperplasia formation and bundle sheath cell transdifferentiation (Figure 3.12C-F; Figure 3.13C-F; Figure 3.14I-L; Figure 3.15K-N). It was suggested that fungal effector molecules potentially are involved in the induction of the observed developmental changes (Reusche *et al.*, 2014). Comparative transcriptome studies should shed light on the presence of candidate effector molecules which are upregulated *in planta* by early senescence inducing *V. dahliae* isolates in comparison to wilt inducing isolates. In previous and comparable *in planta* RNA-sequencing studies *Nicotiana benthamiana* was used as host plant for *V. dahliae* infections since the authors postulated that *N. benthamiana* plants accommodate higher levels of fungal biomass than other host plants as for instance *A. thaliana* (Faino *et al.*, 2012).

To verify whether *N. benthamiana* serves as host for the selected *V. dahliae* isolates of the "early senescence" and "wilting" interaction class plants were infected with the strains s-VL43, s-T9, s-V76, s-ST100, s-V781I, s-V138I, w-VdJR2, w-V192I, w-DVD-S29, w-DVD31 and w-VdLs.17. Symptom development was studied in a time course at 8 dpi, 12 dpi and 16 dpi. Moreover, the presence of transdifferentiated bundle sheath cells into TEs was analysed via microscopic investigation to elucidate whether *de novo* xylem formation is also induced in *N. benthamiana* by the "early senescence" interaction class. Hyperplasia formation as well as differences in xylem cell wall lignification levels in leaf midribs of *N. benthamiana* plants was not investigated.

Notably, infections with the analysed isolates of both *Verticillium* interaction classes "wilting" and "early senescence" induced macroscopic disease symptoms. Already at 8 dpi, a clear stunting phenotype was detectable and first chlorotic leaves developed (Figure 3.20). These symptoms became more prominent over time and lead to completely chlorotic plants at 16 dpi. These results suggested that *N. benthamiana* represents a good host for both *V. dahliae* groups. However, no clear differences in the macroscopically detected infection symptoms were discovered between the two interaction classes, which means that wilting could not be observed.

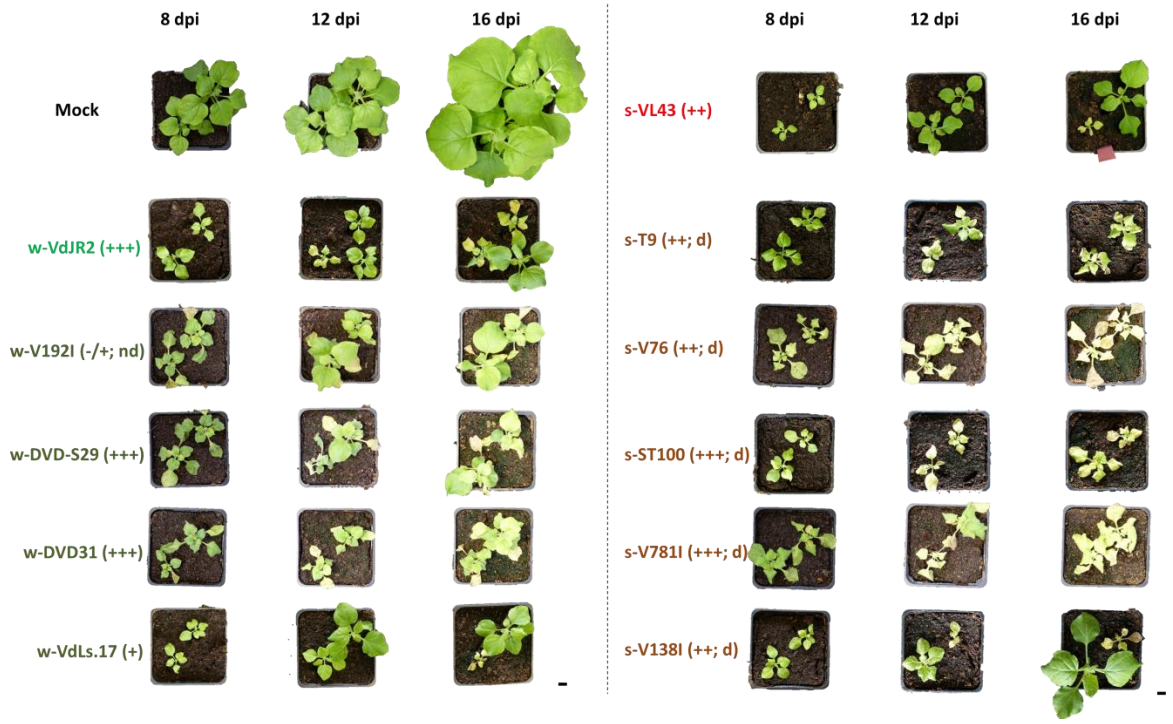

Figure 3.20: Disease symptom development of *N. benthamiana* plants infected with *V. dahliae* isolates usually inducing either wilting or early senescence on *A. thaliana* Col-0. *V. dahliae* isolates representing the "early senescence" interaction class are highlighted in **brown**. *V. dahliae* isolates representing the "wilting" interaction class are highlighted in **dark green**. The reference isolates s-VL43 and w-VdJR2 are highlighted in **red** and **green**, respectively. Early senescence inducing isolates are marked with the prefix s-. Wilt inducing isolates are marked with the prefix w-. Symbols indicate the intensity of disease symptom development: -/+ = mild symptoms, + = moderate symptoms, ++ = strong symptoms, +++ = very strong symptoms. d = cotton/olive defoliating, nd = cotton non-defoliating. Phenotype of *Verticillium* infected plants was recorded at 8 dpi, 12 dpi or 16 dpi. Left panel: mock-treated *N. benthamiana* plants (upper row) or *N. benthamiana* inoculated with *V. dahliae* isolates usually inducing wilting on Col-0 plants. Right panel: *N. benthamiana* plants inoculated with *Verticillium* isolates usually inducing early senescence on Col-0 plants. Scale bar = 1 cm. Experiments were performed once and representative plants are shown.

In order to find out whether *V. dahliae* isolates of the "early senescence" interaction class trigger developmental reprogramming in *N. benthamiana* plants bundle sheath cell transdifferentiation was analysed in mock-treated and *Verticillium* infected plants. Moreover, it was important to verify whether *de novo* xylem formation in leaf midribs is also an "early senescence" interaction class-specific disease symptom in the plant species *N. benthamiana* and not induced by strains of the "wilting" interaction class. This would allow to use *N. benthamiana* plants for transcriptomic analyses aiming for the identification of potential fungal effector molecules which are involved in developmental changes.

Microscopic investigation showed that infection with the early senescence inducing *Verticillium* isolates resulted in leaf *de novo* xylem formation due to bundle sheath cell transdifferentiation in plants (Figure 3.21, right panel). In contrast, leaves of *N. benthamiana* plants inoculated with isolates of the "wilting" interaction class still possessed continuous segments of bundle sheath cells surrounding the leaf vasculature (Figure 3.21, left panel). These

results lead to the conclusion that *N. benthamiana* is suitable for *in planta* transcriptome studies to identify candidate fungal effector molecules presumably triggering *de novo* xylem formation in the plants' leaf vasculature.

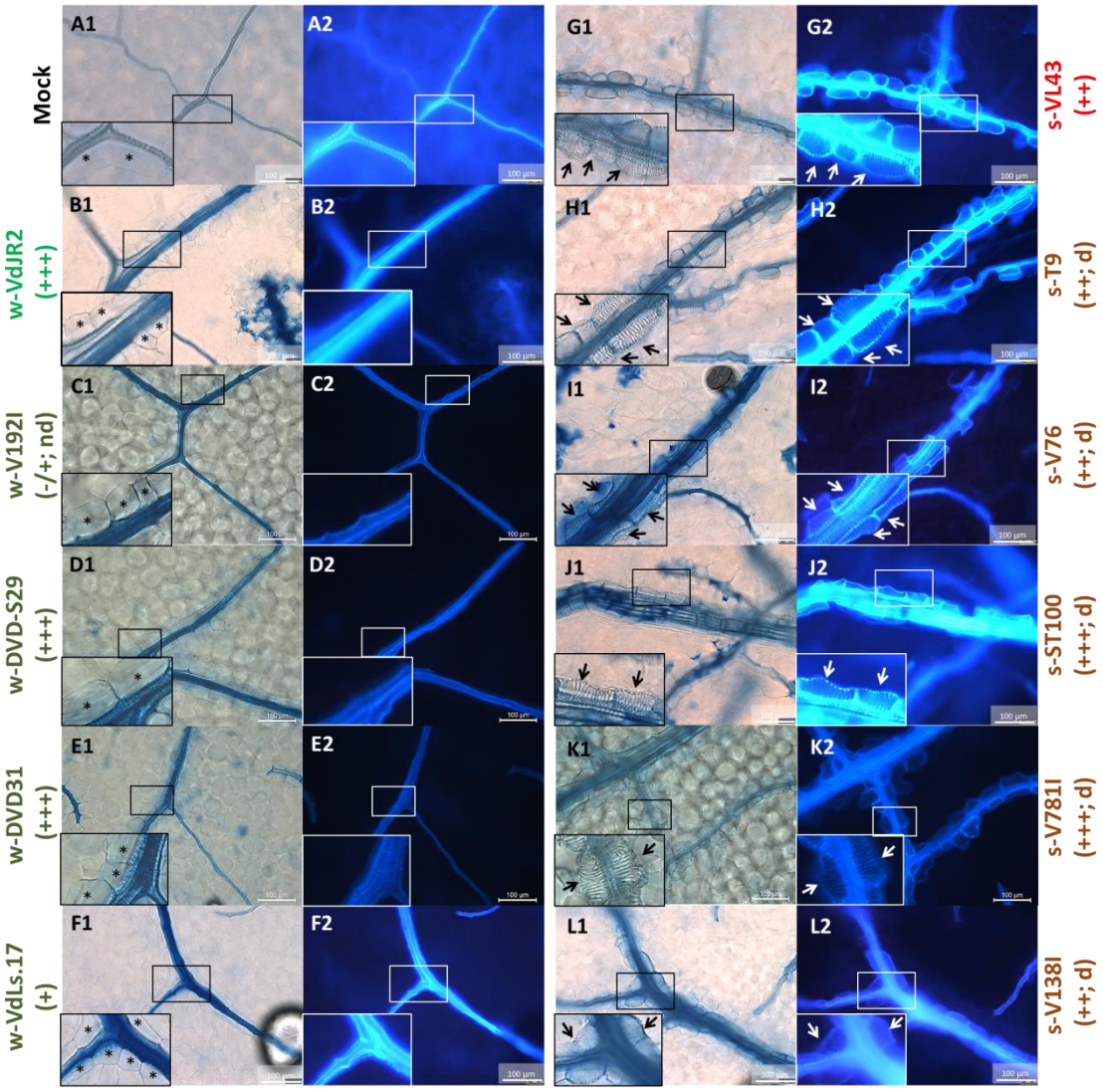

Figure 3.21: Detection of bundle sheath cell transdifferentiation into TEs in *N. benthamiana* plants infected with *V. dahliae* isolates usually inducing either wilting or early senescence on *A. thaliana* Col-0. *V. dahliae* isolates representing the "early senescence" interaction class are highlighted in **brown**. *V. dahliae* isolates representing the "wilting" interaction class are highlighted in **dark green**. The reference isolates s-VL43 and w-VdJR2 are highlighted in **red** and **green**, respectively. Early senescence inducing isolates are marked with the prefix s-. Wilt inducing isolates are marked with the prefix w-. Symbols indicate the intensity of disease symptom development: -/+ = mild symptoms, + = moderate symptoms, ++ = strong symptoms, +++ = very strong symptoms. d = cotton/olive defoliating, nd = cotton non-defoliating. Microscopic investigation of trypan-blue stained leaves of mock-treated (left panel, upper row) *N. benthamiana* plants or inoculated with wilting inducing (left panel) or early senescence inducing (right panel) *Verticillium* isolates. Boxes mark the position of insets. Insets show magnifications of leaf veins containing bundle sheath cells or rather *de novo* formed TEs. **A1-L1:** Bright-field images of leaf veins of either mock-treated or *Verticillium* infected plants. Bundle sheath cells are marked with asterisks. *De novo* formed TEs are marked by arrows. **A2-L2:** Autofluorescence detection of leaf xylem vessels of mock-treated or *Verticillium* infected plants. Bundle sheath cells are marked with asterisks. *De novo* formed TEs are marked by arrows. Scale bar = 100 µm. Microscopic studies were done at 16 dpi. Experiments were performed once involving three analysed leaves and representative leaves are shown.

3.4 Next-Generation Sequencing analyses for the identification of *V. dahliae* effector candidates involved in the establishment of the early senescence phenotype

The *V. dahliae* – *A. thaliana* Col-0 "wilting" and "early senescence" interaction classes are characterized by clearly distinguishable disease symptom development (3.2), e.g. pathogen-induced developmental reprogramming of the vascular system differed between the two classes. A typical symptom caused by the early senescence class is transdifferentiation of bundle sheath cells and xylem parenchyma in leaf midribs resulting in *de novo* xylem vessel and hyperplasia formation, respectively. In contrast, strains of the "wilting" interaction class do not induce these developmental symptoms in the leaf midrib. It is conceivable to postulate that these different symptoms potentially result from the activity of fungal effector molecules, which are exclusively produced by the "early senescence" interaction class.

The following section focuses on the identification of effector molecule candidates which are involved in the "early senescence" symptom development and which play a role in the induction of the observed vascular changes. Comparative genome sequencing allows to discover genomic sequences which are shared by isolates of the "early senescence" interaction class and which are absent in the "wilting" interaction class. A similar comparative genomic approach was performed by the group of Prof. Dr. B. Thomma (University of Wageningen). This lead to the identification of lineage-specific (LS) regions within the genomes of *V. dahliae* classes which had been grouped according to their pathogenicity on tomato (Jonge *et al.*, 2012). Accompanying RNA-sequencing studies showed an upregulation of the *Ave1* gene during tomato infections. *Ave1* encodes a fungal effector protein which is located in one of these LS regions and functions as an avirulence factor in resistant tomato plants producing the corresponding immune receptor Ve1 (Jonge *et al.*, 2012). Similarly, in this work, RNA-sequencing was used to identify fungal genes exclusively upregulated *in planta* by the early senescence inducing *V. dahliae* isolates, with the rationale that the proteins encoded by these genes may play a role in s-VL43-like disease development. This strategy was backed by comparative genomic analyses. To this end, next generation DNA sequencing reads were used for comparative mapping to annotated *Verticillium* reference genomes and *de novo* assembly of selected *V. dahliae* genomes. Furthermore, RNA-seq reads encoding candidate genes were subsequently mapped to the *de novo* assembled *V. dahliae* genomes (3.4.1), with the aim to analyse whether the transcribed genes are present in all genomes of the "early senescence" interaction class and absent in the genomes of the "wilting" interaction class.

3.4.1 Genome sequence comparison identified sequences exclusively present in the *V. dahliae* genomes of the "early senescence" interaction class

Whole genome sequencing (WGS) and genome comparison of the three different *V. dahliae* – *A. thaliana* interaction classes was performed to identify genomic sequences which are exclusively contained in the genomes of *V. dahliae* isolates of the "early senescence" interaction class. Therefore, a core collection of strains which strongly and robustly induced early senescence and wilting symptoms, respectively, was established. All of these strains were chosen on the basis of the previous classification of the *Verticillium* strain collection (3.1) and the *in-depth* characterization described in detail in section 3.2 (Table 3.5). Moreover, the strains w-DVD31 and w-DVD-S29 were included in the core collection as they cause strong wilting symptoms on *A. thaliana* plants and because genomic sequence information for both isolates was already available in the lab of our collaborator Prof. Dr. B. Thomma (University of Wageningen) (Jonge *et al.*, 2012) (3.1.2). In addition, strains were included which are asymptomatic on *Arabidopsis* (Table 3.5) (Master thesis, I. Sjuts, 2014). Finally, w-VdJR2 and s-ST100 were used as reference strains for genome sequence comparison since they represent strong and robust isolates of the "wilting" and "early senescence" interaction class, respectively, and genome sequences are publically available (Jonge *et al.*, 2012; Jonge *et al.*, 2013).

WGS and genome sequence comparison was carried out by the Göttingen Genomics Laboratory (G2L, University of Göttingen, Head of the department: Prof. Dr. R. Daniel). Genomic DNA was isolated from each *V. dahliae* isolate to create shotgun libraries which were used for single-end Illumina sequencing. WGS of the diverse isolates resulted in comparable amounts of total single-end reads ranging from ~10 million to ~27 million sequenced reads per isolate (Table S1). For WGS approaches an about 30-40x genome coverage was required and was achieved for every isolate. Approximately 11 million paired-end Illumina reads each were obtained for the genomes of w-DVD-S29, w-DVD31 and w-VdJR2 resulting in a 30x genome coverage (Jonge *et al.*, 2012). To discover sequences which potentially encode effectors triggering the s-VL43-like symptom development in *A. thaliana*, a specific mapping strategy was developed. In the first step the genomic reads of each *V. dahliae* isolate were aligned to the reference genome of the wilt inducing strain w-VdJR2. Reads which successfully mapped to the genome of w-VdJR2 were discarded with the rationale that sequences encoding for effectors responsible for s-VL43-like symptoms are not contained in the reference genome of the "wilting" interaction class. In order to identify effector candidate genes specific for the "early senescence" interaction class, all w-VdJR2 unaligned sequences were retained and aligned to the genome of the "early senescence" interaction class reference strain s-ST100.

Table 3.5: *V. dahliae* isolates of the three interaction classes used for genome sequence comparison. [1]isolates marked in yellow have been sequenced by the group of Prof. Dr. B. Thomma, University of Wageningen, Netherlands (Jonge *et al.*, 2012); asymptomatic isolates are marked with the prefix a-; early senescence inducing isolates are marked with the prefix s-; wilt inducing isolates are marked with the prefix w-; d = cotton/olive defoliating, nd = cotton non-defoliating; [2]isolates s-ST100 and w-VdJR2 were used as reference strains for genome sequence comparison studies; [3]macroscopically determined intensity of disease symptom development was subdivided into different classes: -/+ = mild symptoms, ++ = strong symptoms, +++ = very strong symptoms; determination of disease symptom development intensities was not applicable for the asymptomatic interaction (n.a.).

Isolate[1]	Species	Symptoms on *Arabidopsis thaliana* Col-0	Intensity[3]
a-Vd8	*V. dahliae*	asymptomatic	n.a.
a-Vd39	*V. dahliae*	asymptomatic	n.a.
a-Vd42	*V. dahliae*	asymptomatic	n.a.
a-Vd52	*V. dahliae*	asymptomatic	n.a.
a-V152	*V. dahliae*	asymptomatic	n.a.
s-V76 (d)	*V. dahliae*	early senescence / cotton defoliating	++
s-T9 (d)	*V. dahliae*	early senescence / cotton defoliating	++
s-V138I (d)	*V. dahliae*	early senescence / cotton defoliating	++
s-V781I (d)	*V. dahliae*	early senescence / olive defoliating	+++
s-ST100[2] (d)	*V. dahliae*	early senescence / cotton defoliating	+++
w-V192I (nd)	*V. dahliae*	wilting / cotton non-defoliating	-/+
w-V200I (nd)	*V. dahliae*	wilting / cotton non-defoliating	-/+
w-DVD-S29	*V. dahliae*	wilting	+++
w-DVD31	*V. dahliae*	wilting	+++
w-VdJR2[2]	*V. dahliae*	wilting	+++

On average 94.3 % of the w-VdJR2 genome was covered by the genomic reads of the asymptomatic and the wilt inducing isolates (Table 3.6, column B). Moreover, on average 93.6 % of the w-VdJR2 genome was covered by sequences of early senescence inducing isolates (Table 3.6, column B). Thus, despite the fact that the three classes induce different or no symptoms on *Arabidopsis* a relatively high percentage of the genome of the wilt inducing strain w-VdJR2 was covered by genome sequences of all three interaction classes. This supports the idea of a core genome of the species *V. dahliae* which is shared among the diverse isolates. Alignment of sequences of the genomes of the "early senescence" interaction class resulted in a smaller coverage of the w-VdJR2 genome in comparison to wilt inducing and asymptomatic isolates (Table 3.6, column B). This suggests genomic regions in the genomes of wilt inducing and asymptomatic isolates that are absent in isolates of the "early senescence" interaction class.

W-VdJR2 unspecific sequences were retained and aligned to the early senescence reference genome s-ST100. The alignment resulted in approximately 61 % of genomic reads from the early senescence inducing isolates that aligned to the s-ST100 reference genome (Table 3.6, column D). In comparison, only about 52 % and 51 % of w-VdJR2 unspecific genomic sequences of the wilt inducing and asymptomatic isolates, respectively, aligned to the genome of s-ST100

(Table 3.6, column D). This indicates that a higher percentage of w-VdJR2 unspecific genomic sequences of isolates of the "early senescence" interaction class shares sequence similarities to s-ST100 compared to genomic reads of the two other interaction classes. This result supports the idea that the "early senescence" interaction class harbors an interaction class-specific effector molecule repertoire which is shared by all isolates of this class.

W-VdJR2 unspecific, but s-ST100 genome-aligning sequences deriving from the genomes of early senescence inducing isolates were suggested to encode for fungal effector proteins which are involved in the early senescence disease phenotype. To identify fungal effector genes which are potentially harbored by these sequences, w-VdJR2 unspecific, but s-ST100 genome aligning genomic reads of the different *V. dahliae* isolates were further assembled into longer contiguous genomic sequences. This resulted in contigs with lengths > 500 base pairs (bp), but also smaller contigs with lengths between 100 bp and 500 bp (Table 3.6, column E). Effector molecules are classified as small secreted proteins that are able to alter the host cell structure and function (Raffaele and Kamoun, 2012; Hacquard *et al.*, 2012). Usually, during genome annotation no specific functions are assigned to effector proteins, thus, they are annotated as (conserved) hypothetical or predicted proteins (Klosterman *et al.*, 2011). Initially, the aim was to identify effector proteins via open reading frame (ORF) prediction on genomic contigs and selection of genes which encode hypothetical proteins. However, gene prediction on the various contigs was not feasible since frequently no ORFs could not determined for these short sequences. Moreover, motif detection could not be used in this study to identify effector molecules in genomic contig sequences, since motifs comparable to the conserved Arg-X-Leu-Arg (RXLR) motif of oomycete effectors (Whisson *et al.*, 2007) are not known for filamentous fungi.

Table 3.6: Coverage of the reference genomes of w-VdJR2 and s-ST100 by sequenced reads of the *V. dahliae* core collection.
Information about the asymptomatic *V. dahliae* isolates marked in blue, about the early senescence inducing isolates in brown and the wilt inducing isolates in green; [1]isolates marked with yellow background color have been sequenced by the group of Prof. Bart Thomma, University of Wageningen, Netherlands (Jonge *et al.*, 2012); asymptomatic isolates are marked with the prefix a-; early senescence inducing isolates are marked with the prefix s-; wilt inducing isolates are marked with the prefix w-; symbols indicate the intensity of disease symptom development: -/+ = mild symptoms, ++ = strong symptoms, +++ = very strong symptoms; d = cotton/olive defoliating, nd = cotton non-defoliating; [2]genomes of w-DVD31 and w-DVD-S29 were artificially split up into contigs which do not represent the *de novo* sequenced reads (2.2.8.1), hence, numbers of effectively mapping reads to the reference genomes were not available.

		A		B		C	D		E		
Isolate[1]	Interaction class	Reads aligned to w-VdJR2		w-VdJR2 genome size covered by aligned reads		Reads not aligned to w-VdJR2	Reads not aligned to w-VdJR2 but aligned to s-ST100		s-ST100 genome size covered by aligned reads		
		[No.]	[%]	[Mb]	[%]	[No.]	[No.]	[%]	contigs ≥ 500 bp [Mb] (No.)	contigs 100 bp-500 bp [Mb] (No.)	sum contigs [Mb] (No.)
a-Vd8	asymptomatic	8.073.444	77,18	31,1	93,1	1.859.822	1.181.288	63,95	0,17 (140)	0,74 (3.996)	0,91 (4.136)
a-Vd39	asymptomatic	19.834.614	86,73	31,2	93,4	2.058.037	1.109.411	53,91	0,29 (208)	0,87 (3.872)	1,16 (4.080)
a-Vd42	asymptomatic	19.759.121	77,61	32,1	93,1	4.114.711	1.197.505	29,10	0,18 (138)	0,87 (4.687)	1,05 (4.825)
a-Vd52	asymptomatic	24.064.762	89,27	32,2	96,4	1.631.694	900.415	55,18	0,13 (65)	0,31 (1.252)	0,44 (1.317)
a-V152	asymptomatic	16.473.700	88,63	32	95,8	1.197.790	642.093	53,61	0,11 (56)	0,26 (979)	0,37 (1.035)
s-V76 (++; d)	early senescence	22.393.135	86,68	31,2	93,4	2.198.637	1.474.112	67,05	0,62 (298)	1,3 (4.449)	1,92 (4.747)
s-T9 (++; d)	early senescence	16.416.507	82	31,7	94,9	3.603.869	2.220.832	62,00	0,95 (605)	2,2 (8.675)	3,15 (9.280)
s-V138I (++; d)	early senescence	17.619.232	87,88	31,1	93,1	1.524.528	948.698	62,23	0,52 (254)	1,1 (3.727)	1,62 (3.981)
s-V781I (+++; d)	early senescence	16.235.686	85,63	31,1	93,1	1.856.689	977.082	52,62	0,53 (260)	1,1 (4.156)	1,63 (4.416)
w-V192I (-/+; nd)	wilting	21.783.282	89,9	31,3	93,7	1.352.460	578.851	42,80	0,11 (88)	0,52 (2.787)	0,63 (2.875)
w-V200I (-/+; nd)	wilting	18.033.830	82,16	31,7	94,9	3.061.164	1.875.790	61,28	0,18 (126)	0,7 (3.216)	0,88 (3.342)
w-DVD-S29[2] (+++)	wilting	n.a.[2]	95,6	30,6	n.a.[2]	n.a.[2]	n.a.[2]	n.a.[2]	0,05 (39)	0,13 (553)	0,18 (592)
w-DVD31[2] (+++)	wilting	n.a.[2]	95,8	30,6	n.a.[2]	n.a.[2]	n.a.[2]	n.a.[2]	0,07 (56)	0,15 (598)	0,22 (654)

Between 1.62 to 3.15 (on average 2.1) Mb of the s-ST100 reference genome was covered by the remaining contigs deriving from the four distinct isolates that belong to the "early senescence" interaction class (Table 3.6, column E). This coverage was on average ~2.6-fold and ~4.4-fold higher than the genome size of s-ST100 covered by contigs of asymptomatic or wilt inducing *V. dahliae* strains, respectively (Table 3.6, column E). This difference in s-ST100 reference genome coverage by the three different interaction classes confirmed the initial working hypothesis, that early senescence inducing *V. dahliae* isolates harbor genome sequences which are specific for this interaction class and not for wilt inducing or asymptomatic strains. Due to the complexity of the data analysis it was not possible to determine the sequences homologous to the s-ST100 genomic regions in each strain of the "early senescence" interaction class. Hence, for the confirmation that selected candidate effector genes exist in the genomes of every early senescence inducing isolate, genes have to be identified in the *de novo* assembled genomes. For this purpose sequencing reads from the diverse *V. dahliae* strain genomes were used for a first and provisional *de novo* genome assembly. With help of subsequent RNA-sequencing studies (3.4.2) RNA-seq reads representing selected candidate genes can be mapped to the *de novo* assembled genomes. This will allow to detect candidate genes which exclusively occur in the genomes of the "early senescence" interaction class.

3.4.2 Analyses of the *in planta V. dahliae* transcriptome for the identification of proteins putatively involved in the *A. thaliana* Col-0 vascular reprogramming

In the next step, fungal RNA-sequencing analyses were conducted for comparative *in planta* time course transcript profiling with *V. dahliae* strains of the "early senescence" and the "wilting" interaction class. The rationale behind this strategy was that effector candidates with a potential role in interaction class-specific symptom development should exhibit differential abundance of transcript levels in the respective interaction class, i.e. high levels in the "early senescence" and low levels in the "wilting" interaction class, or vice versa.

For RNA-sequencing 4 dpi old root material of *V. dahliae* infected *A. thaliana* Col-0 plants was used since similar experiments were performed by the group of Prof. Dr. C. Gatz (Dissertation, Dr. J. Schmitz, 2015) using the *V. longisporum* isolate s-VL43 for *Arabidopsis* inoculation. RNA-sequencing data generated in the present study were compared to the gene expression data obtained by Dr. Schmitz. For *Arabidopsis* infections in this study a plate system was used (Dissertation, Dr. M. Reusche, 2011). Moreover, the aerial parts of *V. dahliae* infected *Nicotiana benthamiana* plants were harvested and used for RNA-sequencing approaches. *N. benthamiana* was used, because these plants can accommodate greater *V. dahliae* biomasses

than other host plants as for instance *A. thaliana* (Faino *et al.*, 2012). Infection of *N. benthamiana* with *V. dahliae* isolates of the "wilting" and "early senescence" interaction class resulted in disease symptom development such as yellow leaf formation and plant stunting indicating that *N. benthamiana* can serve as host plant for these *V. dahliae* isolates (3.3; Figure 3.20). Moreover, *de novo* xylem formation due to bundle sheath cell transdifferentiation as it was previously observed in *Arabidopsis* (Figure 3.12C-F; Figure 3.13C-F) was discovered in *N. benthamiana* after inoculation with isolates of the "early senescence" interaction class (Figure 3.21). Thus, it was expected that fungal effector proteins involved in developmental changes of the leaf vasculature show enhanced levels of transcript abundance during *N. benthamiana* infection in the "early senescence" pathosystem in comparison to the "wilting" pathosystem. *N. benthamiana* seedlings were cultivated on soil and inoculated with *Verticillium* spores via the uprooting method (2.2.1.1; 2.2.3.1). Infected plant material was harvested in a time course at 8 dpi, 12 dpi and 16 dpi as described in Faino *et al.* (2012).

N. benthamiana and *A. thaliana* Col-0 plants were infected with the early senescence as well as the wilt inducing *V. dahliae* strains of the core collection (3.4.1), with the exception of w-V200I. In addition to that, the reference isolates s-ST100, w-VdJR2 and w-VdLs.17 were included in the RNA-sequencing studies. Thus, five different *V. dahliae* isolates for the two interaction classes were included in the RNA-sequencing studies.

RNA sample preparation and sequencing was done by the Transcriptome and Genome Analysis Laboratory (TAL, Department of Developmental Biochemistry, University of Göttingen, Germany) as described in the Methods section (2.2.8.3). The resulting sequencing reads were mapped either to the transcriptome of *Arabidopsis thaliana* (TAIR10) or *Nicotiana benthamiana* (Sol Genomics Network) to identify the transcript abundance of plant-derived genes. Differential levels of relative transcript abundance of *A. thaliana* and *N. benthamiana* genes were not analysed in the present study. Furthermore, RNA-seq reads were mapped to the transcriptomes of both *Verticillium dahliae* strains w-VdLs.17 (BROAD Institute; Klosterman *et al.*, 2011) and s-ST100 (NCBI Sequence Read Archive http://www.ncbi.nlm.nih.gov/sra; BioProject PRJNA169154). The transcriptomes of w-VdLs.17 and s-ST100 were used to include reference genomes of both "wilting" and "early senescence" interaction class. Moreover, the genomes of w-VdLs.17 and s-ST100 are currently the best annotated *V. dahliae* strains which are assigned to the two interaction classes.

3.4.2.1 RNA-seq analyses identified *V. dahliae* genes which exhibit enhanced transcript abundance in plants infected with the "early senescence" interaction class compared with the "wilting" class

Differential gene expression was calculated via the software *R*obi*NA* (v1.2.4_build656; Lohse *et al.*, 2012). The binary logarithm of the fold change (log2FC value) was calculated for genes expressed by the "early senescence" interaction class in direct comparison to their expression by the "wilting" interaction class. Positive log2FC values, thus, represent increased transcript abundance and negative log2FC values reduced transcript abundance of fungal genes in the "early senescence" pathosystem in comparison to the "wilting" pathosystem.

In planta induced fungal genes of the *V. dahliae* "early senescence" interaction class were of special interest in this study since it was assumed that some of these genes may encode fungal effector molecules which trigger disease symptoms specific for the "early senescence" class. For each analysed time point 50 *Verticillium* genes which showed the highest relative transcript abundance in the "early senescence" pathosystem compared to the "wilting" pathosystem (log2FC) (Top50; Table S2) were selected for further analyses. To identify potential effector molecules, peptide prediction and hierarchical clustering based on transcription profiles was done. The Top50 included genes coding i.e. for proteins involved in cellular development, metabolic processes, mRNA translation, and cell-wall degradation (Table S2). Several genes encode hypothetical and predicted proteins to which no specific functions were assigned (Table S2). Hierarchical clustering of the log2FC values for the Top50 genes was performed with the software Genesis v.1.7.7 (Sturn *et al.*, 2002) and indicated that specific transcription profiles exist (Figure S6). The Top50 gene lists were examined for potential effector candidates and their transcription profiles were subsequently studied in detail.

Fungal effectors are classified as proteins which are expressed during host colonization and which are mainly involved in suppression of the host defence (Hogenhout *et al.*, 2009; Jonge *et al.*, 2011). Effector proteins can have enzymatic functions like cell wall degrading enzymes (CWDEs), but mostly they are defined as small (< 400 amino acids), secreted proteins. Frequently, the function of these proteins is unknown and they are annotated as "(conserved) hypothetical proteins" or "predicted proteins" (Klosterman *et al.*, 2011; Raffaele and Kamoun, 2012; Hacquard *et al.*, 2012; Santhanam and Thomma, 2013). The analyses, therefore, focused on proteins with these characteristics. To mediate plant vascular reprogramming, fungal effector molecules have to be secreted by the fungus into the plants' apoplast or translocated into the cytoplasm. Thus, only proteins were considered as candidate effectors which either featured a secretion signal or

were predicted to be non-classically secreted. The probability of classical or non-classical secretion was analysed via the SignalP 3.1 Server (http://www.cbs.dtu.dk/services/SignalP/; (Bendtsen *et al.*, 2004b)) and the SecretomeP 2.0 Server (http://www.cbs.dtu.dk/services/SecretomeP/; (Bendtsen *et al.*, 2004a)), respectively. Since the early senescence phenotype and *de novo* xylem formation in leaf vasculatures were initially discovered in *V. longisporum* s-VL43 infected plants, it was assumed that homologues of selected candidate genes have to be encoded within the genome of s-VL43. Homologues of candidate effector genes in the genome of s-VL43 were detected with the help of the Blast Webinterface function of the BioFung Database (VertiBase; http://biofung.gobics.de:1555/; coordinated by Prof. Dr. G. Braus, Georg-August-University of Göttingen). Since up to now, the genome of s-VL43 is not entirely annotated it was important to also consider s-VL43 homologues on the scaffolds of the genome. Considering these criteria, 12 fungal candidate effectors were selected (Table 3.7; Table S2). These candidate effector (CE) proteins were designated as CE1-CE12.

Testing CEs for presence of a predicted mono- or bipartite nuclear localization signal (NLS) motif and their subcellular localization in plants allowed interpretation for possible functions of the candidate effector proteins. For this, the NLS-mapper tool (http://nls-mapper.iab.keio.ac.jp/cgi-bin/NLS_Mapper_form.cgi; (Kosugi *et al.*, 2008; Kosugi *et al.*, 2009a; Kosugi *et al.*, 2009b)) and the subcellular localization prediction tool Yloc+ (http://abi.inf.uni-tuebingen.de/Services/ YLoc/webloc.cgi; (Briesemeister *et al.*, 2010a, 2010b)) were used. For analysis of subcellular localization of CEs in plants the protein sequence without signal peptide was used simulating signal peptide cleavage during fungal secretion. Most of the CEs were predicted to be localized in the cytoplasm or the nucleus within the plant cell (Table 3.8). Moreover, for CE1 a monopartite NLS was predicted indicating that CE1 potentially is transported into the plant's nucleus (Table 3.8).

Table 3.7: Candidate effectors with their corresponding properties.

Candidate effector (CE) genes with enhanced transcript abundance in the "early senescence" pathosystem in comparison to the "wilting" pathosystem (log2FC values; Table S2) were named as *CEL* for the detected ligninase H8 and *CE1-CE13* for secreted, (conserved) hypothetical or predicted proteins; [1]Peptide prediction was performed via Custom BLAST analyses via the software Geneious™ (Pro v. 8.1.6; Biomatters Ltd., (Kearse et al. 2012)) against the w-VdLs.17 proteome (BROAD Institute; (Klosterman *et al.*, 2011)); if no BLAST hit was discovered in the w-VdLs.17 proteome protein sequences were analysed via the NCBI BLASTP suite; [2]Presence of secretion signals or the probability of non-classical secretion was tested via SignalP 3.1 server (http://www.cbs.dtu.dk/services/SignalP/; (Bendtsen *et al.*, 2004b)) or the SecretomeP 2.0 Server (http://www.cbs.dtu.dk/services/SecretomeP/; (Bendtsen *et al.*, 2004a)), respectively; [3]The presence of s-VL43 homologues was detected with the Blast Webinterface function of the BioFung Database (VertiBase; http://biofung.gobics.de:1555/) on protein and scaffold level; [4]Score (Bits) and E-value indicate the homology of both genes in s-ST100 and w-VdLs.17 genome to each other.

Candidate effector (CE)	GeneID	Peptide prediction[1]	Length [aa]	Secretion signal[2]	s-VL43 homologue (protein)[3]	Score (Bits) / E-value[4]	s-VL43 homologue (scaffold)[3]	Score (Bits) / E-value[4]
CEL	ST100.00022g00100	VDAG_06204T0 | *Verticillium dahliae* VdLs.17 **ligninase H8**	352	Yes	vl43-au16.g5158.t1	727 / 0.0	v.longisporum-43_au16: VL43Ass51Scaf276	1836 / 0.0
CE1	ST100.00067g00160	VDAG_05285T0 | *Verticillium dahliae* VdLs.17 **hypothetical protein**	571	Non-classically secreted	No	-	v.longisporum-43_au16: VL43Ass51Scaf416	2625 / 0.0
CE2	ST100.00358g00100	VDAG_02735T0 | *Verticillium dahliae* VdLs.17 **conserved hypothetical protein**	155	Yes	vl43-au16.g15664.t1	258 / 7e-70	v.longisporum-43_au16: VL43Ass51Scaf66	494 / e-139
CE3	ST100.00508g00020	VDAG_10515T0 | *Verticillium dahliae* VdLs.17 **predicted protein**	127	Yes	vl43-au16.g6402.t1	249 / 2e-67	v.longisporum-43_au16: VL43Ass51Scaf332	698 / 0.0
CE4	ST100.00552g00080	VDAG_04352T0 | *Verticillium dahliae* VdLs.17 **conserved hypothetical protein**	338	Non-classically secreted	vl43-au16.g4353.t1	639 / 0.0	v.longisporum-43_au16: VL43Ass51Scaf272	835 / 0.0
CE5	ST100.00260g00060	VDAG_02155T0 | *Verticillium dahliae* VdLs.17 **hypothetical protein**	100	Non-classically secreted	vl43-au16.g8518.t1	106 / 3e-24	v.longisporum-43_au16: VL43Ass51Scaf362	184 / 5e-46

CE6	ST100.00212g00110	VDAG_04125T0 | *Verticillium dahliae* VdLs.17 **hypothetical protein**	187	Yes	No	-	v.longisporum-43_au16: VL43Ass51Scaf491	751 / 0.0
CE7	ST100.00737g00020	**hypothetical protein** S40288_11089 [Stachybotrys chartarum IBT 40288]	248	Non-classically secreted	No	-	v.longisporum-43_au16: VL43Ass51Scaf491	759 / 0.0
CE8	ST100.00205g00130	VDAG_00454T0 | *Verticillium dahliae* VdLs.17 **hypothetical protein**	64	Non-classically secreted	No	-	v.longisporum-43_au16: VL43Ass51Scaf487	210 / 5e-54
CE9	ST100.00088g00030	VDAG_03129T0 | *Verticillium dahliae* VdLs.17 **hypothetical protein**	106	Non-classically secreted	vl43-au16.g20721.t1	169 / 3e-43	v.longisporum-43_au16: VL43Ass51Scaf470	200 / 8e-51
CE10	ST100.00314g00060	VDAG_04407T0 | *Verticillium dahliae* VdLs.17 **conserved hypothetical protein**	196	Yes	vl43-au16.g20726.t1	330 / 3e-91	v.longisporum-43_au16: VL43Ass51Scaf73	438 / e-122
CE11	ST100.00104g00140	**hypothetical protein** BN1708_010982 [*Verticillium longisporum*]	126	Non-classically secreted	No	-	v.longisporum-43_au16: VL43Ass51Scaf254	622 / e-178
CE12	ST100.00992g00010	VDAG_05263T0 | *Verticillium dahliae* VdLs.17 **conserved hypothetical protein**	282	Non-classically secreted	No	-	v.longisporum-43_au16: VL43Ass51Scaf416	888 / 0.0
CE13	ST100.01886g00010	VDAG_05281T0 | *Verticillium dahliae* VdLs.17 **conserved hypothetical protein**	193	Non-classically secreted	No	-	v.longisporum-43_au16: VL43Ass51Scaf416	928 / 0.0

Table 3.8: Predicted subcellular localization of candidate effectors within the plant and the presence of a NLS. NLS and subcellular localization were predicted with the online available NLS-mapper tool (http://nls-mapper.iab.keio.ac.jp/cgi-bin/NLS_Mapper_form.cgi; (Kosugi *et al.*, 2008; Kosugi *et al.*, 2009a; Kosugi *et al.*, 2009b)) and the subcellular localization prediction tool Yloc+ (http://abi.inf.uni-tuebingen.de/Services/YLoc/webloc.cgi; (Briesemeister *et al.*, 2010a, 2010b)), respectively; Nu = nucleus, Cy = cytoplasm, Pm = plasma membrane, Ex = extracellular space, Va = vacuole, Go = golgi apparatus.

Candidate effector (CE)	Yloc+ prediction	NLS prediction
CEL	Nu, Cy	No
CE1	Nu, Cy	Yes, monopartite
CE2	Cy	No
CE3	Cy	No
CE4	Pm, Cy	No
CE5	Nu, Cy	No
CE6	Nu, Cy	No
CE7	Nu, Cy	No
CE8	Nu, Cy, Ex	No
CE9	Nu, Ex	No
CE10	Nu, Cy, Ex	No
CE11	Nu, Cy	No
CE12	Va, Go, Cy, Pm	No
CE13	Nu, Cy	No

Apart from small secreted proteins with unknown function the Top50 also included plant cell wall degrading enzymes (CWDEs) which are predicted to be secreted (Table S2). For three endoglucanases as well as two glucan 1,3-beta-glucosidases and a glucosidase higher transcript levels were detected in the “early senescence” pathosystem compared to the “wilting” pathosystem (Table S2). These enzymes are predicted to be involved in the hydrolysis of cellulose and beta-glucan which are components of the plant cell wall. Additionally, a mannan endo-1,6-alpha-mannosidase and a polysaccharide deacetylase family protein which are involved in cell wall polysaccharide degradation exhibited enhanced transcript abundance in the “early senescence” pathosystem (Table S2). Moreover, high transcript abundance of a gene encoding for a ligninase H8 were detected in the “early senescence” pathosystem (Table S2). Ligninases catalyse the degradation of lignin, a main component of the secondary plant cell wall. This enzyme is of interest for the present study, since less lignification levels in xylem cell walls of plants infected with the early senescence inducing *V. dahliae* isolates were discovered in comparison to leaf midribs of Col-0 plants inoculated with the wilt inducing isolates (3.2). A transcript abundance of the ligninase H8 gene in the “early senescence” strain may, thus, be a

reason for lower lignification observed in leaf midribs of plants inoculated with the early senescence inducing isolates compared with the wilt inducing isolates. Therefore, the ligninase H8 was included as a potential CE in the following studies and was named CEL (Table 3.7).

In most cases RNA-seq reads obtained from strains of the “early senescence” interaction class map to the reference transcriptome of s-ST100 due to high sequence homology. This is reflected by the Top50 which were all exclusively mapped to the s-ST100 reference transcriptome (Table S2). In contrast, RNA-seq reads deriving from the "wilting" interaction class mainly mapped to the corresponding homologue of the w-VdLs.17 reference transcriptome (data not shown). However, closer inspection revealed for all selected CEs with homologues in both genome classes (i.e. all except for *CE7* and *CE11*; see below) a variable and restricted number of raw reads that were assigned to the reference transcriptome of the other interaction class. This resulted from single-nucleotide polymorphisms (SNPs) in gene homologues of the w-VdLs.17 and s-ST100 transcriptomes which give rise to locally restricted higher homology of individual sequence reads to corresponding sequence stretches in the reference genomes of the other interaction class. As a consequence, the number of RNA-seq reads belonging to the same gene were split to map to the homologues occurring in the two different reference genomes. To correct the discrepancies of the mapping bias, RNA-seq reads mapping to homologous genes were combined resulting in their total gene transcription (Table 3.9). The corrected values were used for the subsequent heat map construction and transcript profile analysis (Figure 3.22).

To identify the closest homologues of the selected CEs in the genome of w-VdLs.17 subsequent BLAST analyses were performed. Custom BLAST analyses were conducted via the software Geneious^{TM} (Pro v. 8.1.6; Biomatters Ltd., Kearse *et al.*, 2012) against the w-VdLs.17 transciptome (BROAD Institute; (Klosterman *et al.*, 2011)). Except for *CE7* and *CE11* putative homologues were identified for all candidate effector genes (Table 3.9). The E-values for the BLAST hits which were calculated from the percentage of identical sites as well as the query coverage of both homologues indicated that the candidate effector genes were closely related to the genes encoded by the w-VdLs.17 reference genome (Table 3.9). The resulting total transcription values of the candidate effectors were illustrated in a heat map to identify genes with similar transcription profiles (Figure 3.22A).

Table 3.9: Selected candidate effectors with their putative w-VdLs.17 homologues and their corresponding total transcription.

RNA-seq reads mapping to homologous genes of the selected candidate effectors (CEs) were combined and the log2FC for each CE was calculated resulting in their total transcription (log2FC); log2FC values of the total transcription of CEs were used for heat map generation and subsequent transcription profile analysis (Figure 3.22); [1]Gene prediction was performed via Custom BLAST analyses with the software Geneious™ (Pro v. 8.1.6; Biomatters Ltd., (Kearse et al. 2012)) against the w-VdLs.17 transcriptome (BROAD Institute; (Klosterman *et al.*, 2011)); #NV = no homolog in w-VdLs.17 found.

		Log2FC							
Candidate effector (CE)	**s-ST100 GeneID**	**4 dpi**	**8 dpi**	**12 dpi**	**16 dpi**	**w-VdLs.17 homologue[1]**	**Identical sites**	**Query coverage**	**E-Value**
CEL	ST100.00022g00100	**-0.39**	**1.84**	**2.20**	**0.27**	VDAG_06204 | **ligninase H8**	99%	92%	0.0
CE1	ST100.00067g00160	**-0.44**	**3.79**	**4.70**	**5.02**	VDAG_05285 | **hypothetical protein**	99%	84%	0.0
CE2	ST100.00358g00100	**-0.49**	**-3.80**	**-0.26**	**3.55**	VDAG_02735 | **conserved hypothetical protein**	99%	72%	1E-170
CE3	ST100.00508g00020	**-0.58**	**1.52**	**1.13**	**-0.21**	VDAG_10515 | **predicted protein**	100%	100%	0.0
CE4	ST100.00552g00080	**-1.81**	**0.73**	**1.23**	**2.30**	VDAG_04352 | **conserved hypothetical protein**	100%	42%	0.0
CE5	ST100.00260g00060	**5.34**	**1.89**	**2.37**	**4.88**	VDAG_02155 | **conserved hypothetical protein**	98%	15%	1,01E-14
CE6	ST100.00212g00110	**-1.04**	**0.55**	**1.73**	**4.08**	VDAG_04125 | **hypothetical protein**	99%	73%	0.0
CE7	ST100.00737g00020	**6.56**	**3.10**	**4.87**	**6.85**	#NV	#NV	#NV	#NV
CE8	ST100.00205g00130	**-2.19**	**-0.67**	**-0.09**	**2.00**	VDAG_00454 | **hypothetical protein**	99%	56%	4,59E-51
CE9	ST100.00088g00030	**-3.03**	**-0.41**	**0.77**	**2.31**	VDAG_03129 | **hypothetical protein**	100%	31%	1,71E-47
CE10	ST100.00314g00060	**-0.47**	**0.81**	**1.99**	**3.41**	VDAG_04407 | **conserved hypothetical protein**	97%	100%	0.0
CE11	ST100.00104g00140	**5.39**	**2.26**	**3.30**	**6.61**	#NV	#NV	#NV	#NV
CE12	ST100.00992g00010	**0.13**	**0.58**	**2.17**	**5.37**	VDAG_05263 | **conserved hypothetical protein**	97%	61%	0.0
CE13	ST100.01886g00010	**1.62**	**0.93**	**1.67**	**3.16**	VDAG_05281 | **conserved hypothetical protein**	98%	80%	0.0

The heat map of relative transcript abundance for the selected candidate effector genes indicates that the candidate genes can be assigned to three different transcription profiles (A, B and C) (Figure 3.22A). *CEL* and *CE3* grouped into the transcription profile A showing an enhanced gene transcript abundance in aerial parts of *N. benthamiana* plants which first increased during the infection, followed by downregulation of transcript abundance (Figure 3.22A, B upper panel). In *A. thaliana* roots transcript abundance of *CEL* and *CE3* increased in plants inoculated with isolates of the "wilting" interaction class in comparison to roots infected with early senescence inducing strains (Figure 3.22A, B upper panel).

CE1, *CE4*, *CE6*, *CE8*, *CE9, CE10* and *CE12* grouped into the transcription profile B during the experimental time course (Figure 3.22A, B, middle panel). Transcript abundance of these genes continuously increased during the investigated time interval. Whereas *CE4*, *CE6*, *CE8*, *CE9* and *CE10* reached a maximum log2FC value of ~2 to 4 the transcript levels of *CE1* and *CE12* were higher with a log2FC value of ~5 – 5.5 at 16 dpi (Table 3.9; Figure 3.22B, middle panel). The high transcript abundance of *CE1* in the "early senescence" pathosystem compared to the "wilting" pathosystem may result from its absence in the genomes of the wilt inducing isolates w-DVD-S29, w-DVD31 and w-V192I. This correlated with the lack of RNA-seq reads in plants infected with w-DVD-S29, w-DVD31 and w-V192I mapping to *CE1* (Table S3). Moreover, no transcripts of a gene with the gene identification (GeneID) ST100.01886g00010 were detected in these three isolates of the "wilting" interaction class (Table S3). In addition, transcripts of this gene were not detected in the reference strain w-VdLs.17 (Table S3), although a homolog of this gene was annotated to exist within the genome of this isolate (GeneID: VDAG_05281; Table 3.9). Thus, this gene was included into further analyses and named as *CE13*. Interestingly, no transcripts of *CE5*, *CE7* and *CE11* were identified in every wilt inducing isolate (Table S3). Additionally, no homologues of *CE7* and *CE11* were identified in the genome of the reference strain w-VdLs.17 (Table 3.9). This suggests that *CE7* and *CE11* may not exist in the genomes of the wilt inducing isolates. *CE2, CE5, CE7, CE11* and *CE13* could be assigned to the transcription profile C (Figure 3.22A, B, lower panel). Genes grouped into this profile started with higher transcript levels at 4 dpi in *A. thaliana* Col-0 root material (Figure 3.22B, lower panel). In aerial parts of *N. benthamiana* plants transcript abundance were significantly lower at 8 dpi but increased continuously from 8 dpi to 16 dpi reaching a maximum log2FC values of ~3 – 7 at 16 dpi (Table 3.9; Figure 3.22B, lower panel).

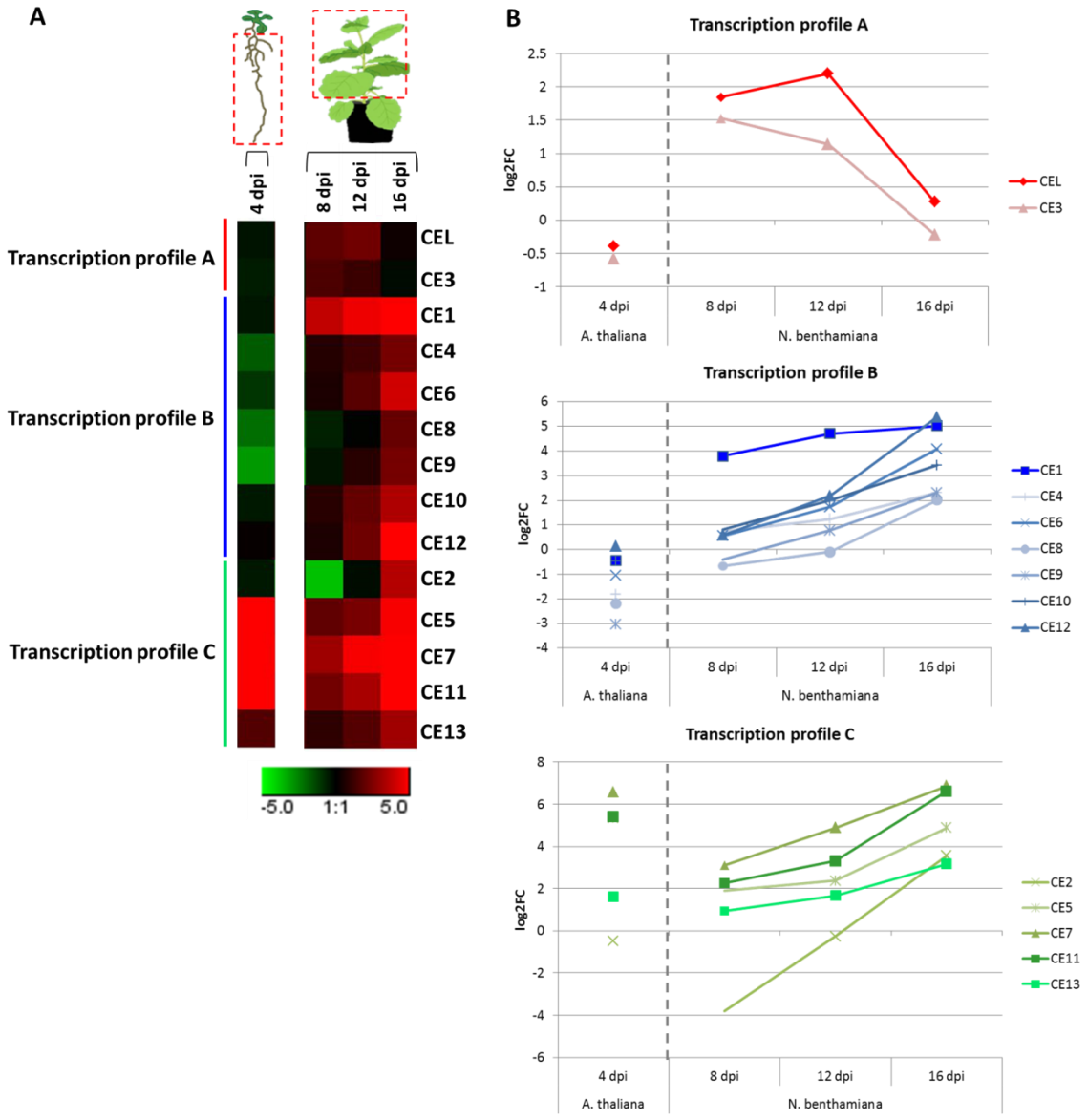

Figure 3.22: Heat map generation of the total transcription of selected candidate effectors CEL and CE1-13 identified three different transcription profiles. A: Heat map was generated with log2FC values of total transcript abundance of s-ST100 and w-VdLs.17 gene homologues of candidate effectors CEL and CE1-13 (Table 3.9). The transcriptome data of *A. thaliana* Col-0 roots (4 dpi) and the aerial parts of *N. benthamiana* plants (8 dpi, 12 dpi and 16 dpi) were used. For heat map coloration the upper maximum was set to log2FC = 5 and the lower maximum was set to log2FC = -5. Heat map generation indicated that candidate effectors can be assigned to three different transcription profiles and was performed via the software Genesis v.1.7.7 (Sturn *et al.*, 2002). **B:** log2FC values of total transcript abundance of the s-ST100 and w-VdLs.17 homologues of *CEL* and *CE1-13* (Table 3.9) were plotted in diagrams corresponding to the three different transcription profiles. *CE13* was not identified among the Top50 upregulated genes (Table S2) but was included in expression studies as described in 3.4.2.1.

In summary, a repertoire of potential fungal effector molecules was identified which exhibited higher transcript abundance *in planta* in the "early senescence" pathosystem in comparison to the "wilting" pathosystem. Transcription kinetics of the selected candidate effectors could be assigned to three different transcription profiles. RNA-seq reads of *CE5*, *CE7* and *CE11* were not identified in transcriptomes of the "wilting" pathosystem and no homologues

of *CE7* and *CE11* were identified in the reference genome w-VdLs.17 of the "wilting" interaction class. Likewise, three wilt inducing *V. dahliae* isolates exhibited no transcripts of the candidate effector genes, *CE1* and *CE13*. Moreover, enhanced transcript levels of a ligninase, CEL, were identified in aerial parts of plants inoculated with strains inducing *de novo* xylem formation, but no enhanced lignin deposition in leaf midribs. Due to its sequence homology to a ligninase H8 protein and its potential effect on lignin hydrolysis in the plants' vasculature, this protein represents an interesting candidate for further analyses.

3.4.2.2 Enhanced transcript abundance of candidate effectors CEL and CE1 in plants infected with *V. dahliae* isolates of the "early senescence" interaction class was confirmed in semi-qRT-PCR analyses

Further analyses focused on two candidate genes: *CEL* encoding a putative ligninase as well as *CE1* coding for a non-classically secreted, putative effector protein. *CEL* was selected because lignin is a crucial component of the plant cell wall and it was suggested that ligninases may be involved in the structural differences observed in leaf midribs of plants infected with early senescence and wilt inducing isolates (Figure 3.14B-F; Figure 3.15B-H). *CE1* was selected due to its potential absence in the genomes of wilt inducing isolates w-V192I, w-DVD-S29 and w-DVD31 (Table S3). Additionally, *CE1* exhibits very high transcript levels in the "early senescence" pathosystem in comparison to the "wilting" pathosystem which continuously increased in aerial plant tissues during the time course (Figure 3.22B middle panel).

The *in planta* transcription of *CEL* and *CE1* was additionally analysed via semi-qRT-PCR analyses. For cDNA synthesis and subsequent semi-qRT-PCR the samples which were previously used for RNA-sequencing approaches were used. The amplification of the ribosomal internal transcribed spacer (ITS) served as a loading control.

Semi-qRT-PCR analyses showed an transcriptional induction of *CEL* and *CE1* in *N. benthamiana* plants inoculated with *V. dahliae* isolates s-V76 and s-V781I of the "early senescence" interaction class (Figure 3.23). In contrast to that, *CEL* was only slightly transcribed in *N. benthamiana* plants infected with the wilt inducing isolates w-DVD31, w-DVD-S29 and w-V192I (Figure 3.23, first row). No expression of *CE1* was detected in w-DVD31, w-DVD-S29 and w-V192I inoculated plants (Figure 3.23, second row). This finding correlates with the low amount of normalized RNA-seq reads in plants infected with these isolates indicating no RNA-seq reads corresponding to *CE1* (Table S3). This substantiated the hypothesis that *CE1* is not present in the genomes of w-DVD31, w-DVD-S29 and w-V192I.

The transcription of *CEL* and *CE1* was only marginally detectable in *A. thaliana* root material (Figure 3.23). This correlates with the low transcript abundance of both genes detected at 4 dpi (Figure 3.22B, upper and middle panel). Semi-qRT-PCR analyses of plants inoculated with the early senescence inducing *V. dahliae* strains s-ST100, s-T9 and s-V138I and the wilt inducing isolates w-VdJR2 and w-VdLs.17 were not taken into account since the ITS loading control was not uniform (Figure S7).

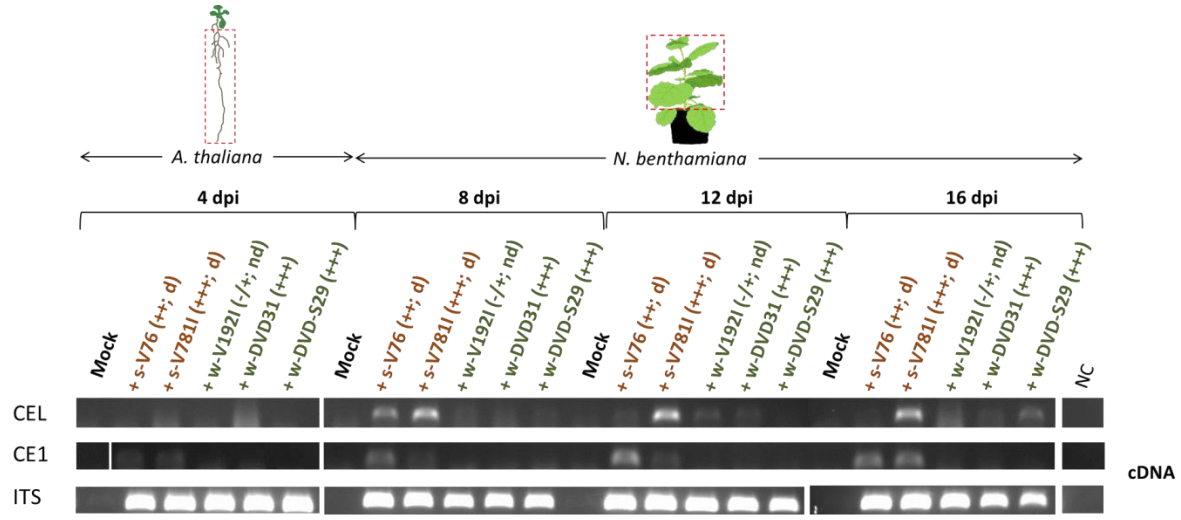

Figure 3.23: Agarose gels of semi-qRT-PCRs for transcription detection of *CEL* and *CE1* on cDNA samples. Samples of *V. dahliae* isolates of the "early senescence" interaction class are highlighted in **brown** and of the "wilting" interaction class in **dark green**. Semi-qRT-PCR for transcription detection of *CEL* (first row) and *CE1* (second row) via cDNA generated from the same RNA samples which were used for RNA-sequencing. 4 dpi samples derived from infected *A. thaliana* roots and 8 dpi, 12 dpi and 16 dpi derived from aerial tissues of infected *N. benthamiana* plants. Boxes with dotted red lines indicate from which plant tissues RNA was extracted. Early senescence inducing isolates are marked with the prefix s-. Wilt inducing isolates are marked with the prefix w-. Symbols indicate the intensity of disease symptom development: -/+ = mild symptoms, ++ = strong symptoms, +++ = very strong symptoms. d = cotton/olive defoliating, nd = cotton non-defoliating. Semi-qRT-PCR with samples of plant tissues infected with s-T9, s-ST100, s-V138I, w-VdJR2 and w-VdLs.17 are shown in Figure S7. Amplification of ITS sequence was used as a loading control (third row). NC = no template control, cDNA = complementary DNA. The experiment was repeated three times. Representative data are shown.

3.4.2.3 *CE1* is not present in the genomes of the wilt inducing *V. dahliae* isolates w-DVD31 and w-DVD-S29

Semi-qRT-PCR analyses confirmed the RNA-seq data that *CEL* as well as *CE1* are highly transcribed *in planta* by early senescence inducing *V. dahliae* isolates in comparison to wilt inducing isolates (Figure 3.23). In the case of *CE1* no transcription was detected in plants infected with the strains w-V192I, w-DVD31 and w-DVD-S29 (Table S3; Figure 3.23). The identified differences in transcript abundance indicate that this gene is potentially absent from the genomes of some of the wilt inducing isolates. To verify the presence or absence of *CEL* and *CE1*, PCR analysis on genomic DNA of the *V. dahliae* isolates of the two interaction classes "early senescence" and "wilting" using

gene specific primers was performed. Primers were designed which amplify both homologues of *CEL* and *CE1* annotated in the w-VdLs.17 and s-ST100 reference genomes (Table 3.9). Genomic DNA was isolated from the strains which had been used for transcriptome studies: s-V76, s-V781I, s-V138I, s-T9 and s-ST100 of the "early senescence" interaction class and w-V192I, w-DVD31, w-DVD-S29, w-VdJR2 and w-VdLs.17 of the "wilting" interaction class. Moreover, the *V. longisporum* "early senescence" reference strain s-VL43 was used for PCR analysis. In addition to PCR-analysis the absence or presence of *CEL* and *CE1* in the genomes of *V. dahliae* isolates of the "wilting" and "early senescence" interaction classes was confirmed via comparison of the genome sequencing data of the core collection. For this, the RNA reads representing the selected candidate genes were mapped on the provisionally *de novo* assembled *V. dahliae* genomes which were studied in section 3.4.1. Coverage of the candidate genes only by short RNA-seq reads represents unspecific mapping indicating that the genes may be absent in the genomes (personal communication G2L, University of Göttingen, Head of the department: Prof. Dr. R. Daniel).

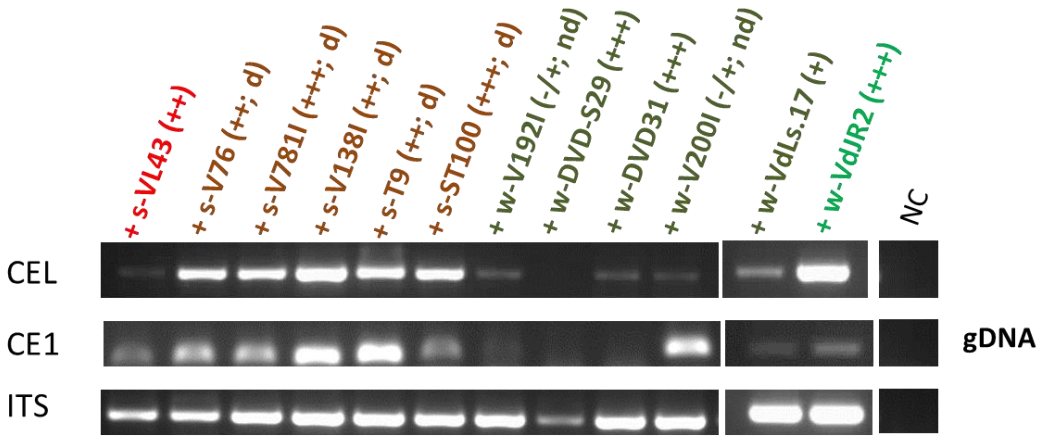

Figure 3.24: Agarose gels of PCR reactions for amplification of *CEL* and *CE1* on gDNA of *Verticillium* isolates of the "early senescence" and "wilting" interaction class. Amplification of the *CEL* (first row) and *CE1* (second row) from genomic DNA of diverse *Verticillium* isolates falling into the two interaction classes. *V. dahliae* isolates of the "early senescence" interaction class are highlighted in **brown** and of the "wilting" interaction class in **dark green**. The reference isolates s-VL43 and w-VdJR2 are highlighted in **red** and **green**, respectively. Early senescence inducing isolates are marked with the prefix s-. Wilt inducing isolates are marked with the prefix w-. Symbols indicate the intensity of disease symptom development: -/+ = mild symptoms, + = moderate symptoms, ++ = strong symptoms, +++ = very strong symptoms. d = cotton/olive defoliating, nd = cotton non-defoliating. Amplification of ITS sequence (third row) was used as control for proper amplification. NC = no template control, gDNA = genomic DNA. Experiment was repeated three times and representative data are shown.

RNA-seq reads (≥ 90 bp) of *CE1* (Gene ID ST100.00067g00160) aligned to the genomes of the early senescence inducing *V. dahliae* isolates s-V76, s-T9, s-V781I and s-V138I (Table S4). In contrast, only short (≤ 23 bp) RNA-seq reads of *CE1* mapped to the genomes of w-DVD31 and w-DVD-S29 (Table S4). This indicates that larger parts of *CE1* of the "early senescence" interaction class are covered by RNA-seq reads whereas only short sequences mapped to *CE1* in the wilt

inducing isolates w-DVD31 and w-DVD-S29. Thus, *CE1* may be absent in genomes of wilt inducing isolates w-DVD31 and w-DVD-S29. This result was supported by PCR-analysis since *CE1* was not amplified from the genomes of w-DVD31 and w-DVD-S29 (Figure 3.24, second row). Moreover, this finding verified the results of the semi-qRT-PCR analysis and RNA-seq read detection of the transcriptome data indicating no transcription of these genes by w-DVD31 and w-DVD-S29 (Figure 3.23; Table S3). Only a low amount of *CE1* was amplified from the genome of w-V192I (Figure 3.24, second row). In contrast, RNA-seq reads with a length > 100 bp aligned to *CE1* of the genome of the wilt inducing strain w-V192I (Table S4) indicating that *CE1* is encoded in the genome of w-V192I, but not expressed *in planta* by this isolate (Table S3; Figure 3.23). Longer RNA-seq reads (≥ 90 bp) of *CEL* mapped to every *de novo* assembled *V. dahliae* genome of the "wilting" and "early senescence" interaction class (Table S4). Also, PCR-analysis revealed that *CEL* is present in all tested isolates, except for the wilt inducing isolate w-DVD-S29 (Figure 3.24, first row). This finding was contradictory to the results of the RNA-seq read mapping to the *de novo* assembled genomes (Table S4). Moreover, it is unlikely that CEL is not encoded in the genome of w-DVD-S29 since expression of this gene was detected in plants infected with this isolate (Table S3; Figure 3.23, upper row). With respect to the amplification of the ITS a lower amount of the internal transcribed spacer was amplified from the genome of w-DVD-S29 than for the other genomes (Figure 3.24, third row). Therefore, a lower amount of genomic DNA of w-DVD-S29 may be applied what may have been the cause for the low amplification of *CEL*.

In summary, PCR-analysis and comparison of the genome sequencing data supported the hypothesis that genes encoding for the potential candidate effector CE1 do not exist in the genomes of w-DVD31 and w-DVD-S29 of the "wilting" interaction class.

3.4.2.4 Protein sequences of CEL contain interaction class-specific amino acid substitution whereas *CEL* and *CE1* promoter regions do not contain interaction class-specific motifs

As shown in section 3.4.2.1 and 3.4.2.2 the two candidate effector genes *CEL* and *CE1* are differentially expressed *in planta* in the "early senescence" interaction class compared to the "wilting" interaction class. Differences in the nucleotide composition of the promoter regions may be the reason for the differential regulation of the genes in the two interaction classes. SNPs in promoter regions consistently shared by isolates of the "early senescence" interaction class which are not present in promoter regions of wilt inducing isolates may hint for the presence or absence of enhancer or repressor elements or for certain transcription factor binding sites. About 500 bp

of the 5'-upstream region of *CEL* and *CE1* from the genomes of the different *Verticillium* strains for analysis of the promoter region were aligned with each other. Moreover, nonsynonymous nucleotide substitutions within the coding region of a gene may represent nonsense or missense mutations resulting in an alteration of the amino acid sequence. This may alter the functionality of enzymes. Therefore, the amino acid sequence of the ORF of the ligninase, *CEL*, in the "early senescence" and "wilting" interaction class was analysed. Ligninases can be classified concerning their kinetic and physical features as peroxidases (Kuila *et al.*, 1985; Tien *et al.*, 1986). Peroxidases contain two conserved histidine residues and a conserved arginine residue which are crucial for their activity (Dunford and Stillman, 1976; Poulos *et al.*, 1986). The proximal histidine is the axial ligand of the haem, the cofactor in the active site of peroxidases, whereas the distal histidine and arginine are important for charge stabilization during H_2O_2-dependent substrate oxidation (Poulos and Kraut, 1980). These conserved amino acid residues were all identified in the ligninase H8 protein of the lignin-degrading white-rot fungus *Phanerochaete chrysosporium* (Tien and Tu, 1986). The proximal histidine (His252) and the distal histidine (His127) and arginine (Arg123) also exist in the protein sequence of CEL in all tested *Verticillium* isolates of the "early senescence" and "wilting" interaction class (Figure 3.25A, B, blue bars; Figure S8). Additionally, the predicted protein domains of CEL were analysed. In cooperation with the group of Prof. Dr. B. Thomma (University of Wageningen), the sequences of CEL and the promoter regions of *CEL* and *CE1* within the genomes of *V. dahliae* isolates of the "early senescence" and "wilting" interaction class of the core collection were identified (Table 3.5). Here, the *V. dahliae* reference isolates w-VdJR2 and w-VdLs.17 were included in the core collection since genome sequence information of both strains are available (BioFung Database, VertiBase; www.vertibase.org and BROAD Institute; Klosterman *et al.*, 2011). In addition, the *V. longisporum* reference strain s-VL43 was included in this study and homologous gene sequences were extracted from the BioFung Database (VertiBase; www.vertibase.org). Alignments were performed using the software Geneious™ Pro v. 8.1.6; Biomatters Ltd., (Kearse *et al.*, 2012). Protein domains were predicted with help of the InterProScan plugin in Geneious™ (Quevillon *et al.*, 2005).

For none of the two effector candidate genes coherent differences in the promoter regions of the genomes of the "early senescence" interaction class were identified which differed to that of the "wilting" interaction class (data not shown). Thus, no SNPs were detected that may explain the differential regulation of the transcription of *CEL* and *CE1* in the two pathosystems "early senescence" and "wilting". This lead to the conclusion that the transcription is regulated epigenetically or by transposable elements.

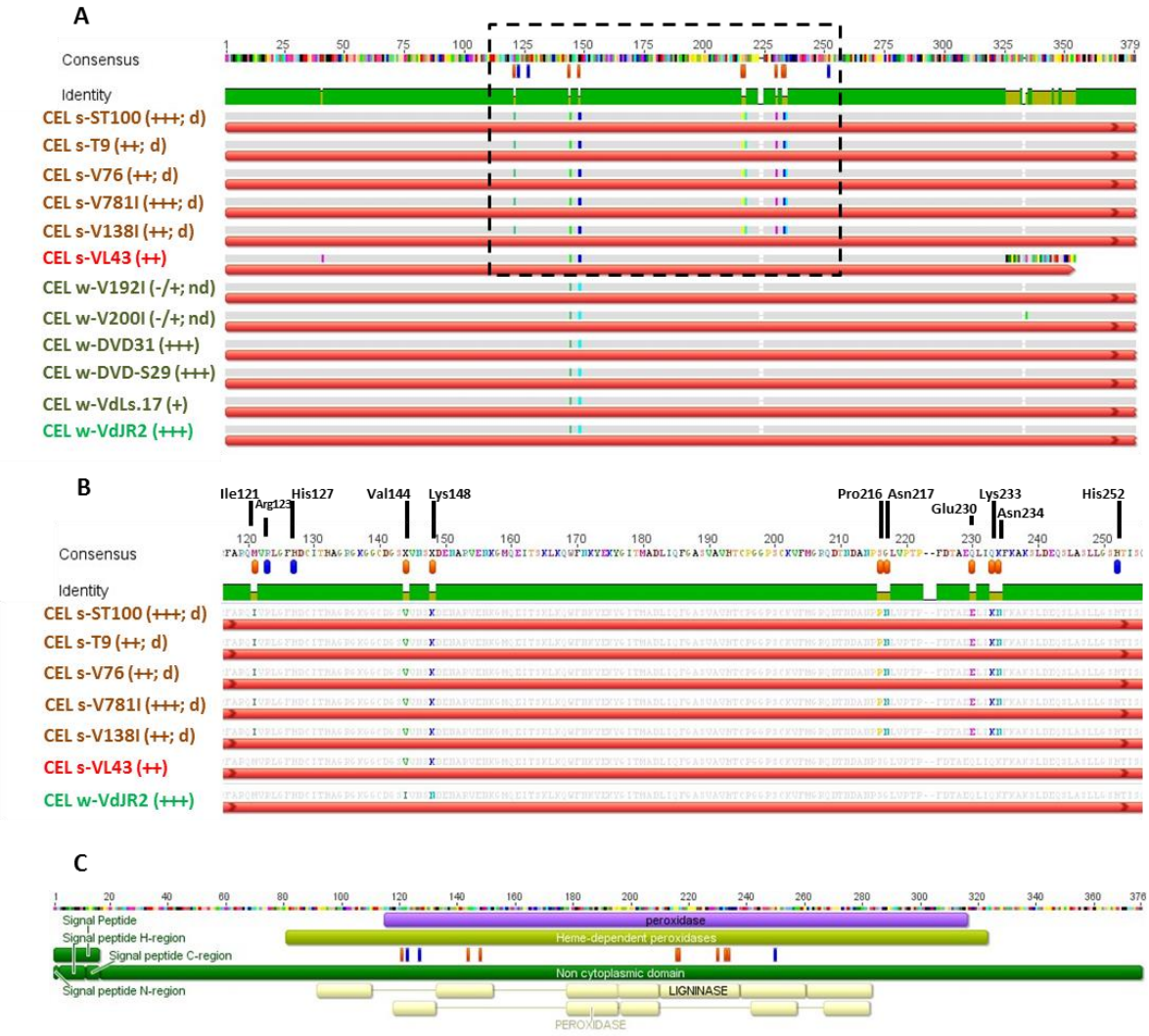

Figure 3.25: Amino acid sequence alignment and protein domain prediction of CEL encoded by the different *Verticillium* isolates of the two interaction classes. *V. dahliae* isolates of the "early senescence" interaction class are highlighted in **brown** and of the "wilting" interaction class in **dark green**. The reference isolates s-VL43 and w-VdJR2 are highlighted in **red** and **green**, respectively. Early senescence inducing isolates are marked with the prefix s-. Wilt inducing isolates are marked with the prefix w-. Symbols indicate the intensity of disease symptom development: -/+ = mild symptoms, + = moderate symptoms, ++ = strong symptoms, +++ = very strong symptoms. d = cotton/olive defoliating, nd = cotton non-defoliating. **Orange** bars indicate amino acid substitution between isolates of the "early senescence" and "wilting" interaction class (Ile121, Val144, Lys148, Pro216, Asn217, Glu230, Lys233 and Asn234). **Blue** bars indicate the two histidine residues (His127 and His252) and the arginine residue (Arg123) essential for peroxidase activity which are present in the protein sequence of CEL of every tested *Verticillium* isolate. **A:** Amino acid sequence alignment of CEL from the different *Verticillium* genomes. Sequence region encircled with black dashed lines marks the magnification illustrated in B. **B:** Magnification of amino acid similarities and differences of CEL of the early senescence inducing *Verticillium* isolates. **C:** Representative protein domains predicted consistently for all CEL proteins of the *Verticillium* isolates. Used databases: Lilac = Pfam, light green = superfamily, green = Phobius, light yellow = Prints. Alignments were done via the software Geneious™ Pro v. 8.1.6; Biomatters Ltd., (Kearse *et al.*, 2012). Protein domain prediction was done via the InterProScan plugin in Geneious™ (Quevillon *et al.*, 2005).

The amino acid sequence alignment of CEL of the two interaction classes shows few amino acid substitution which were consistently shared by all *V. dahliae* isolates of the "early senescence" interaction class, but not by isolates of the "wilting" interaction class (Figure 3.25A,

B, orange bars). However, only two of the substituted amino acids, Val144 and Lys148, also exist in the protein sequence of CEL of the early senescence inducing *V. longisporum* isolate s-VL43 (Figure 3.25A, B). CEL of all wilt inducing strains exhibit a uniform amino acid sequence (Figure 3.25A). The dissimilarities in the CEL protein sequences between the two interaction classes do not result in differences of the prediction of protein domains (Figure 3.25C). All tested isolates possess a ligninase which is predicted to be composed of the same domains including a ligninase and peroxidase domain. However, the detected amino acid substitution are located in the predicted peroxidase and ligninase domains (Figure 3.25B, C, orange bars). Moreover, the amino acids substitution are in close proximity of the conserved amino acids Arg123, His127 and His252 which are proposed to be essential for peroxidase activity (Figure 3.25 blue and orange bars). Hence, the amino acids substitution may alter the catalytic activity of CEL encoded in the genomes of the two interaction classes possibly due to changes in protein folding or substrate binding capacity.

4 Discussion

Previous studies showed that the *V. longisporum* isolate s-VL43 and the *V. dahliae* isolate w-VdJR2 induce clearly distinguishable disease symptoms on *A. thaliana* Col-0 plants (Reusche *et al.*, 2014). It was postulated that the differential symptom induction results from *Verticillium* species-specific fungal effector molecule repertoires (Reusche *et al.*, 2014). This work focused on the identification of fungal effector molecules which are involved in the induction of s-VL43-like developmental reprogramming of the host plant's vasculature. Characterization of a *Verticillium* strain collection revealed that symptom development induced by various *V. dahliae* and *V. longisporum* strains are comparable with the disease induction observed for either s-VL43 or w-VdJR2 ("early senescence" interaction class, Table 3.2; "wilting" interaction class, Table 3.3). Moreover, a third interaction class, named "asymptomatic", was identified, which contains *Verticillium* isolates inducing no symptoms at all on Col-0 plants (Table 3.4). Symptoms induced by strains of the "early senescence" interaction class included stunting, early senescence, hyperplasia development and bundle sheath cell transdifferentiation in *Arabidopsis* (Figure S3; Figure 3.6; Figure 3.7; Figure 3.12C-F; Figure 3.13C-F; Figure 3.14I-L; Figure 3.15K-N). *De novo* xylem vessel formation was also induced in *N. benthamiana* plants after infection with these isolates (Figure 3.21). Genome sequence comparison of *V. dahliae* isolates assigned to the three interaction classes gave evidence for the existence of sequences which are exclusively present in the genomes of early senescence inducing isolates, but not in asymptomatic or wilt inducing isolates (Table 3.6). *In planta* transcriptome studies showed high transcript abundance of potential candidate fungal effectors in strains of the "early senescence" interaction class compared to strains of the "wilting" interaction class (Figure 3.22; Table 3.9). With the help of *de novo* assembled *V. dahliae* genomes a candidate effector gene with high transcript abundance in the "early senescence" pathosystem was identified which does not exist in two wilt inducing *V. dahliae* isolates. Together, the results of comparative genomic and transcriptomic studies support the hypothesis that "early senescence" interaction class-specific effector molecules exist which are presumably involved in the s-VL43-like symptom development. For discussion of the transcriptome data the simplifying assumption was made that the *V. dahliae – A. thaliana* and *V. dahliae – N. benthamiana* pathosystems are equivalent. This assumption is based on the fact that *Verticillium* strains of the "early senescence" interaction class induce *de novo* xylem formation in both plant species to the same extent.

4.1 *De novo* xylem formation is not a compensatory plant response to counteract vessel clogging, but rather a strategy of an adapted pathogen

Infection of *A. thaliana* Col-0 plants with *V. longisporum* s-VL43 results in early senescence of the plant accompanied by hyperplasia development and bundle sheath cell transdifferentiation in leaves (Reusche *et al.*, 2012; Reusche *et al.*, 2014; Figure 3.12C; Figure 3.13C; Figure 3.14C; Figure 3.15C). In contrast, infection with w-VdJR2 does not trigger *de novo* xylem cell formation, but wilting of plant leaves (Reusche *et al.*, 2012; Reusche *et al.*, 2014; Figure 3.12B; Figure 3.13B; Figure 3.14B; Figure 3.15B). Talboys (1958) postulated that xylem vessel occlusion via fungal structures of *V. albo-atrum* and tyloses (novel cell-wall material rising into the lumen of the vessel) formation in the vasculature of hop plants is accompanied by renewed or prolonged cambial activity. Vessel occlusion subsequently results in the development of a hyperplastic xylem (Talboys, 1958; Baayen, 1986). Finally, the formation of novel xylem cells would maintain the water storage and transport which is impaired by obstruction of genuine vessels.

The present study confirms the observation that the induction of early senescence symptoms is accompanied by *de novo* xylem development: *A. thaliana* infection with the *Verticillium* isolates s-VL43, s-V76, s-T9, s-ST100, s-V781I and s-V138I of the “early senescence” interaction class triggered hyperplasia formation as well as bundle sheath cell transdifferentiation in leaves (Figure 3.12C-F; Figure 3.13C-F; Figure 3.14I-L, M; Figure 3.15K-N, Q). This finding was substantiated by the identification of enhanced cell wall material production *in planta* including increased lignification in *A. thaliana* plants after s-VL43 infection (Floerl *et al.*, 2012). Upon inoculation with the wilt inducing isolates w-VdJR2, w-V192I and w-V200I no novel xylem vessels are formed (Figure 3.12B; Figure 3.13B, G-H; Figure 3.14H, M; Figure 3.15J, O-P, Q). However, neither massive amounts of fungal structures resulting in vessel clogging nor tyloses formation after infection were observed in plants inoculated with isolates of the “early senescence” interaction class (Figure 3.10C-F, I-L; Figure 3.11C-F, K-N). Moreover, *in planta* proliferation of wilt inducing isolates causes vessel clogging without triggering hyperplasia formation or bundle sheath cell transdifferentiation (Figure 3.10B; Figure 3.11B, G-H; Figure 3.14H; Figure 3.15J, O-P). Thus, vessel clogging *per se* does not result in *de novo* xylem formation. The results of the present study, therefore, disprove the hypothesis of Talboys (1958). Moreover, this leads to the suggestion that hyperplasia formation and bundle sheath cell transdifferentiation are components of a strategy of the pathogen, presumably induced by the activity of secreted effector proteins, rather than a compensatory plant response to counteract xylem vessel obstruction.

It was postulated that the early senescence inducing *V. longisporum* isolate s-VL43 forms a conditionally mutualistic interaction with *Arabidopsis* (Reusche *et al.*, 2012). *De novo* xylem formation results in an enhanced drought-stress tolerance of the host plant (Zhang *et al.*, 2009; Reusche *et al.*, 2012). Also *Verticillium* would benefit from an enhanced drought-stress tolerance of the plant since the fungus can nourish on the plant's nutrients for a longer time period under abiotic stress conditions. In contrast, infection with w-VdJR2 causes wilting, but no improved drought-stress tolerance since w-VdJR2 does not induce *de novo* xylem development (Reusche *et al.*, 2012). Under natural conditions combining abiotic and biotic stresses both organisms, plant and pathogen, benefit from the pathogen-induced reprogramming of the plants' vasculature. Interestingly, *V. dahliae* strains s-V76, s-T9, s-V138I and s-V781I were isolated from geographical regions exhibiting arid and hot climates (Mexico, California and Spain; Table 3.2). Especially in hot and dry climates it is crucial to counteract drought stress with enhanced water storage capacities. It has to be tested whether infection with s-V76, s-T9, s-ST100, s-V138I and s-V781I does also result in enhanced drought-stress tolerance in *A. thaliana*.

4.2 Developmental reprogramming in the leaf midrib is an "early senescence" interaction class-specific disease symptom

It was postulated that disease symptoms, such as early senescence accompanied by developmental changes in the leaf midrib induced by *V. longisporum* s-VL43 and plant wilting triggered by *V. dahliae* w-VdJR2 infection are *Verticillium* species-specific features (Reusche *et al.*, 2014). Strikingly, *Verticillium* strain collection characterization conducted in this thesis identified five *V. dahliae* isolates, s-V76, s-T9, s-ST100, s-V781I and s-V138I, which induce s-VL43-like disease symptoms. All of these isolates triggered the formation of a hyperplastic xylem in *A. thaliana* leaf midribs as well as transdifferentiation of leaf bundle sheath cells into *de novo* xylem vessels (Figure 3.12C-F, I-L; Figure 3.13C-F, K-N; Figure 3.14I-L; Figure 3.15K-N). Expression measurements of the VASCULAR-RELATED NAC DOMAIN7 (VND7) gene participating in developmental reprogramming in leaf vasculatures as well as the cambial marker gene *AtHB8* gave supportive evidence for bundle sheath cell transdifferentiation and hyperplasia formation, respectively (Figure 3.12M; Figure 3.13Q; Figure 3.14N; Figure 3.15R). Also counting of newly formed xylem cells in the leaf midrib clearly proved that massive amounts of xylem cells were formed in plants infected with the isolates of the "early senescence" interaction class (Figure 3.14M; Figure 3.15Q). This demonstrates that s-VL43-like disease symptom induction is not restricted to the species *V. longisporum,* but is also triggered by certain *V. dahliae* strains. However, *de novo* xylem formation

within leaf midribs was never observed upon infection with the wilt inducing *V. dahliae* strains (Figure 3.12B, H; Figure 3.13B, G-H, J, O-P; Figure 3.14B, H; Figure 3.15B, G-H, J, O-P). Thus, *Verticillium* strains can be assigned to different interaction classes.

Moreover, the identification of haploid *V. dahliae* isolates inducing s-VL43-like infection symptoms indicates that early senescence symptom development already existed before origination of the hybrid species *V. longisporum* via parasexual hybridization (Inderbitzin *et al.,* 2011). The *V. dahliae* strains of the "early senescence" interaction class might, therefore, be related to one of the ancestral species which gave rise to the *V. longisporum* lineage A1/D1. This lineage consists of *V. longisporum* strains of the "early senescence" interaction class including s-VL43 (Table 3.2; Inderbitzin *et al.*, 2011). A1 and D1 designate the species which hybridized and built the near-diploid species *V. longisporum*. It is more likely that the *V. dahliae* isolates of the early senescence interaction class are related to D1, since it is assumed that the A1 species was related to *V. albo-atrum* (Inderbitzin *et al.*, 2011). Likewise, putative fungal effector molecules accounting for the developmental reprogramming in leaf midribs must have already been encoded in the genomes of the *V. dahliae* isolates before the parasexual hybridization gave rise to the *V. longisporum* lineage A1/D1. Previous studies already hypothesized that parasexual recombination affects the transfer of effector genes between parental and evolving lineages (Noguchi *et al.*, 2006; Chuma *et al.*, 2011). Laboratory studies of parasexual recombinants of *Magnaporthe oryzae* evidenced that hyphal anastomosis and transient diploid formation between *Oryza* isolates results in DNA exchange.

4.3 Enhanced lignification of xylem cell walls in *A. thaliana* leaf midribs correlates with the presence of fungal hyphae and low transcript abundance of *CEL*

Notably, an enhanced lignification of the cell walls of original xylem vessels in leaf midribs was observed in *A. thaliana* plants inoculated with the wilt inducing *V. dahliae* isolates (Figure 3.14B, H; Figure 3.15B, G-H, J, O-P). Interestingly, specifically these lignified cells contained fungal structures (Figure 3.14H; Figure 3.15J, O-P). Reusche *et al.* (2014) also discovered fungal hyphae of w-VdJR2 in single genuine xylem vessels of the hypocotyl vasculature which exhibited higher lignin levels in the secondary cell walls. Lignin is proposed to form a barrier against mechanical penetration by plant pathogens as well as to hamper the degradation of plant cell walls via fungal enzymes (Millett *et al.*, 1976; Ride, 1978). Lignification is involved in the resistance of cotton against *V. dahliae* (Xu *et al.*, 2011). Xu et al (2011) showed that a resistant cultivar of *Gossypium*

barbadense exhibits an increased expression of lignin synthesis-related genes and accumulates high levels of lignin. Moreover, lignification plays a central role in a *V. dahliae* resistant line of *Solanum lycopersicum*. This tomato line exhibits a significantly faster increase in lignin synthesis after infection than susceptible plants (Gayoso *et al.*, 2010). A recent study involving metabolite fingerprinting of *Arabidopsis* leaves also verified the accumulation of metabolites synthesized via the phenylpropanoid pathway after infection with *V. longisporum* s-VL43 (König *et al.*, 2014). These soluble phenylpropanoids include sinapoyl glucosides, coniferin, syringin and lignans and were postulated to contribute to the defence response of *Arabidopsis* against *V. longisporum*. Notably, proteome and metabolome analysis of the *Arabidopsis* apoplast identified an increased abundance of *V. longisporum*-responsive peroxidases after infection (Floerl *et al.*, 2012). Peroxidases are involved in the formation and the consumption of H_2O_2, e.g. during the synthesis of lignin. Hence, lignification may be an active defence response of the plant against *Verticillium* infection. Moreover, reinforcement of xylem cell walls would limit the access of fungal hyphae to the plant's nutrients which are necessary for fungal proliferation. Eynck et al. (2009) proved that cell wall reinforcement and lignification in the hypocotyl of a resistant *B. napus* cultivar upon infection with *V. longisporum* results in limited fungal spread (Eynck *et al.*, 2009). This leads to the assumption that fortification of xylem cell walls via lignin deposition is a defence response of *A. thaliana* to suppress the fungal spread of wilt inducing *V. dahliae* isolates and to restrict the hyphae to the already infested xylem cells.

Ligninases are glycosylated peroxidases that can directly oxidize non-phenolic aromatic lignin compounds, like veratryl alcohol, in the presence of H_2O_2 resulting in lignin break down (Tien and Kirk, 1984; Lin *et al.*, 1997; Wong, 2009). Early studies indicated that white-rot basidiomycete fungi, such as *Phanerocheate chrysosporium*, are capable of degrading lignin via secretion of lignin peroxidases (Kirk and Farrell, 1987; Wariishi *et al.*, 1989). Likewise, the fungal pathogen *Fusarium solani f. sp. glycines* produces lignin peroxidases and is able to degrade lignin what may be important during its infection of soybean (Lozovaya *et al.*, 2006). In fact, RNA-sequencing analyses of the present study revealed a higher transcript abundance of *CEL,* encoding a secreted ligninase H8, in *V. dahliae* strains of the "early senescence" interaction class in comparison to the wilt inducing strains in aerial plant parts (Figure 3.22A, B upper panel;Table 3.9). Moreover, a previous study revealed that CEL was strongly expressed in the root tissues of s-VL43-GFP inoculated *A. thaliana* plants in comparison to s-VL43-GFP grown on solid medium (Dissertation J. Schmitz, 2015). This indicates that CEL is particularly expressed *in planta.* This conclusion is substantiated by a recent study identifying a lignin degrading peroxidase, VnaPRX1.1277, which is highly expressed *in planta* and secreted to hop xylem sap by *Verticillium*

nonalfalfae (Flajsman *et al.*, 2016). Blast analysis showed that the nucleotide sequence of *VnaPRX1.1277* exhibit similarity (99 % coverage, 62 % identity) to the *CEL* homologue of *V. dahliae* VdLs.17 (Flajsman *et al.*, 2016). Expression of CEL may play a role in lignin degradation during infection and, thus, influence the different lignification patterns identified in leaf midribs of plants infected with wilt and early senescence inducing *Verticillium* isolates.

Moreover, amino acid substitutions were identified which are located in the catalytic domains of CEL in strains of the "early senescence" interaction class compared to strains of the "wilting" interaction class (Figure 3.25C). These amino acid substitutions are in close proximity to the proximal histidine (His252) and the distal histidine (His127) and arginine (Arg123) residues which are postulated to be essential for the catalytic activity of lignin peroxidases (Figure 3.25B; Figure S8 (Poulos and Kraut, 1980; Tien and Tu, 1986; Poulos *et al.*, 1986)). Thus, the amino acids differing in the protein sequence of CEL of the "early senescence" interaction class may have an influence on the catalytic activity of the ligninase, e.g. by an altered protein folding and enhanced substrate binding capacity. Subsequently, this may result in enhanced lignin hydrolysis in the "early senescence" pathosystem and potentially result in the diverse lignification levels in leaf midribs of the "early senescence" and "wilting" pathosystems (Figure 3.14; Figure 3.15).

4.4 *V. dahliae* isolates of the "early senescence" interaction class exhibit enhanced proliferation presumably resulting in a rapid fungal life cycle completion

Leaf area measurements of *A. thaliana* showed that stunting of plants was more severe after inoculation with isolates of the "early senescence" interaction class compared with plants infected with isolates of the "wilting" interaction class (Figure 3.6; Figure 3.7). A difference in the capacity to induce stunting of plants was already shown for the "wilting" and "early sencescence" reference strains w-VdJR2 and s-VL43, respectively (Reusche *et al.*, 2014). Moreover, a slower disease progression was detected for w-VdJR2 infected plants compared to s-VL43 infected plants. In the w-VdJR2-*Arabidopsis* pathosystem first wilting symptoms appeared at 21 dpi whereas chlorosis formation induced by s-VL43 infection already occurred at 14 dpi (Reusche *et al.*, 2014). These data indicate faster proliferation of *Verticillium* isolates inducing early senescence compared with isolates inducing wilting symptoms. Strikingly, qRT-PCR analyses to determine *in planta* fungal biomass showed that *Verticillium* isolates inducing early senescence on *A. thaliana* exhibit a faster *in planta* proliferation than wilt inducing isolates (Figure 3.8A; Figure 3.9).

One reason for the different *in planta* proliferation rates of early senescence and wilt inducing isolates may be an inherent difference in the growth rates of both interaction classes. However, no significant differences in colony growth rates on solid media was discovered between w-VdJR2 and the early senescence inducing *V. dahliae* isolates s-V76, s-T9 and s-ST100 (Figure 3.8B). Thus, it can be concluded that no differences in growth rates *per se* of *V. dahliae* isolates of the two interaction classes exist.

Cell wall degrading enzymes (CWDEs) catalyse the hydrolysis of plant cell wall polymers. Thus, secretion of fungal CWDEs into the apoplast aids pathogenic invasion into the plant's cell and nutrient acquisition (Walton, 1994; Gibson *et al.*, 2011). Moreover, it was proposed that the production of CWDEs, like pectin-degrading enzymes, facilitate the colonization of the plant vasculature by *Verticillium* (Klosterman *et al.*, 2011; Yadeta and Thomma, 2014). Transcriptomic studies of *Ustilago maydis* infected *A. thaliana* plants revealed the upregulation of genes encoding for cellulose and hemicellulose degrading enzymes (Martínez-Soto *et al.*, 2014). In addition, transcriptome profiling of the rice blast fungus *Magnaporthe oryzae* showed enhanced expression levels of CWDEs *in planta* during infection in comparison to the *in vitro* situation (Mathioni *et al.*, 2011). Due to the high redundancy of CWDEs in the genome of fungi, there exist only few studies verifying that these hydrolytic enzymes contribute to fungal virulence (Doehlemann and Hemetsberger, 2013). Nonetheless, knock-down experiments of celluloses and xylanases, respectively, in the hemibiotroph *M. oryzae* proved the participation of CWDEs in fungal virulence during infection (Nguyen *et al.*, 2011; van Vu *et al.*, 2012). Other studies provided evidence for the importance of carbohydrate degrading enzymes, such as the endoglucanase VdEG-1, in pathogenicity or early xylem colonization of *V. dahliae* (Novo *et al.*, 2006; Maruthachalam *et al.*, 2011; Liu *et al.*, 2013). The sucrose non-fermenting 1 protein, VdSNF1, plays a role in expression regulation of some CWDE genes (Tzima *et al.*, 2011). Notably, deletion of *VdSNF1* resulted in an impaired virulence of *V. dahliae* on tomato and eggplant. Moreover, these mutant lines showed a reduced colonization of tomato plants. Indeed, RNA-sequencing analyses identified secreted CWDEs, such as glucan 1,3-beta-glucosidases and endoglucanases, which showed high transcript abundance in the early senescence pathosystem and which are involved in the decomposition of cellulose and hemicellulose (Table S2 (Bayer *et al.*, 1998; Kubicek *et al.*, 2014)). Breakdown of xylem cell walls possibly facilitates the entry and exit of fungal hyphae in xylem vessels to enable fungal spread and proliferation. The results support CWDEs as virulence factors required to promote fungal colonization of host plants.

Verticillium is a hemibiotroph with a biotrophic phase in which the fungus feeds from nutrients of the xylem sap and a necrotrophic phase in which it nourishes from senescing tissues

(Fradin and Thomma, Bart P H J, 2006). Enhanced proliferation as it is assumed for the "early senescence" interaction class would, thus, presumably result in a faster entrance into the necrotrophic phase. Data on transcript levels of the marker genes for biotrophic and necrotrophic pathogen attack, *PR-1* and *PDF1.2,* respectively (Penninckx *et al.*, 1996; Koornneef and Pieterse, 2008; Zander *et al.*, 2010), support this presumed scenario*. PR-1* showed the highest expression levels at early time points between 7 dpi and 21 dpi (Figure 3.16; Figure 3.17). Downregulation of *PR-1* expression at 28 dpi and simultaneous upregulation of *PDF1.2* expression indicated that *Verticillium* switches to a necrotrophic life style at later infection stages (Figure 3.18; Figure 3.19). Remarkably, plants inoculated with the early senescence inducing isolates exhibited a more elevated level of *PDF1.2* expression during the time course and upregulation of that marker gene started earlier, already at 14 dpi (Figure 3.18; Figure 3.19). This strongly supports the hypothesis that *Verticillium* isolates of the "early senescence" interaction class enter the necrotrophic phase much faster than wilt inducing isolates potentially resulting in a more rapid life cycle completion.

In situ detection of fungal proliferation in leaf midrib vasculatures did not correlate with the *in planta* biomass quantification of *V. dahliae* isolates of the "early senescence" and "wilting" interaction class (Figure 3.8A; Figure 3.9; Figure 3.10; Figure 3.11). An explanation for the discrepancies between *in situ* studies and qRT-PCR with respect to assessment of fungal proliferation might be that *in situ* examinations do not represent the actual biomass level of *Verticillium.* In this study *Verticillium* isolates have been stained with the colometric substrate XβD-Glc-Nac. XβD-Glc-Nac is a chromogenic substrate for N-Acetyl-β-D-glucosaminidases and its hydrolysis results in the production of a blue precipitate (Diener, 2012). Thus, the amount of stained fungal structures might be dependent on the copy number of N-Acetyl-β-D-glucosaminidase genes in the genomes of the different isolates. Also, the expression levels of N-Acetyl-β-D-glucosaminidase genes might differ between interaction classes. It has to be verified with the *de novo* assembled *V. dahliae* genomes whether diverse copy numbers of N-Acetyl-β-D-glucosaminidase genes exist in different *V. dahliae* isolates.

4.5 Identification of interaction-class specific sequences by genome sequence comparison

The genome sequence comparison study revealed that a large part of the w-VdJR2 reference genome is covered by genomic sequences of wilt inducing, early senescence inducing and asymptomatic *V. dahliae* isolates (Table 3.6). Therefore, it was conceivable to postulate that

isolates of all interaction classes share a core genome probably including a large amount of homologous genes. This gene repertoire presumably encodes for proteins involved in house-keeping functions, such as cell growth and the metabolism of *V. dahliae* as well as the maintenance of fungal reproduction. The low degree of genomic diversity between various *V. dahliae* strains was expected, since *Verticillium* propagates asexually. The absence of meiotic recombination limits the generation of novel genetic combinations (Burt, 2000; McDonald and Linde, 2002). De Jonge et al. (2013) identified in a previous genome comparison study of a *V. dahliae* population genome nucleotide diversities between *V. dahliae* isolates of maximal 0.5 % (Jonge *et al.*, 2013). This supports the results of the present study and indicates that *V. dahliae* strains of the different interaction classes are highly related to each other despite their distinct disease symptom induction.

In addition, the genome sequence comparison study gives evidence for "early senescence" interaction class-specific sequences since significantly higher s-ST100 genome coverage was discovered for this interaction class in comparison to the "wilting" and "asymptomatic" interaction class (Table 3.6). As discussed in 4.1 *de novo* xylem formation is supposed to be a pathogen-induced disease symptom. Potentially, "early senescence" interaction class-specific sequences harbor genes encoding certain enzymes and fungal effector molecules which are involved in the induction of vascular developmental reprogramming in *A. thaliana*. Nonetheless, it cannot be ruled out that proteins playing a role in the early senescence symptom development may also be encoded in the genomes of wilt inducing and asymptomatic *V. dahliae* isolates but their transcription is suppressed.

Recent studies of de Jonge *et al*. (2013) support the hypothesis of *Verticillium* class-specific genes since they identified ~4 Mb large lineage-specific (LS) regions in the genomes of several *V. dahliae* isolates. These LS regions were either unique for the strains or shared by only a subset of *V. dahliae* isolates assigned to race 1. In addition, these regions overrepresent *in planta* induced genes. Importantly, the LS region of race 1 strains harbors the fungal effector gene *Ave1* which is crucial for disease development on tomato plants. Hence, LS regions might contribute to the pathogenicity on host plants (Jonge *et al.*, 2012; Jonge *et al.*, 2013). Also in *Fusarium oxysporum* LS genomic regions were identified (Ma *et al.*, 2010). Four entire chromosomes composed the LS regions and harbor a number of proteins, including the *SIX* (secreted in xylem) genes, which are involved in pathogenicity of *Fusarium*. Genome sequence comparison of the present study give supportive evidence for the putative presence of interaction class-specific genes. It has to be clarified in future analyses whether the genomic sequences are present in each isolate of the different interaction classes and which proteins they encode. Moreover, it should be

verified whether interaction class-specific genes are arranged in specific regions of their genomes, comparable to the LS-regions identified by de Jonge *et al.* (2012). Up to now it was not possible to answer this question, since genomes of the *V. dahliae* isolates sequenced in the present study are only provisionally *de novo* assembled.

4.6 Developmental reprogramming in leaf midribs is accompanied by enhanced transcript abundance of a repertoire of potential fungal effector molecules and cell-wall degrading enzymes

As discussed in 4.1 *de novo* xylem formation is presumed to be triggered by *Verticillium*-derived secreted fungal effector molecules. Effectors are molecules defined as small (< 400 amino acids) proteins that lack any characteristic signatures concerning their function. Therefore, they are mostly designated as hypothetical or predicted proteins (Hogenhout *et al.*, 2009; Klosterman *et al.*, 2011; Santhanam and Thomma, 2013). Upon host penetration and colonization the expression of effector molecules is induced to facilitate pathogenic *in planta* propagation via alteration of the plant immunity and reprogramming of host cells (Stergiopoulos and Wit, 2009). The secretion of effector molecules into host cells, thus, is essential for their action. Many fungal effector molecules possess a secretion signal in order to be delivered from the fungal cells (Hogenhout *et al.*, 2009; Raffaele and Kamoun, 2012). However, effector proteins can also be secreted unconventionally via the non-classical secretory pathway (Bendtsen *et al.*, 2004a; Liu *et al.*, 2014). The aim of the present study was to identify *V. dahliae* effector molecules which are potentially involved in vascular developmental reprogramming of the host plant after infection with the "early senescence" interaction class. *In planta* transcriptomic studies identified a repertoire of fungal genes exhibiting higher transcript levels in the "early senescence" interaction class compared to the "wilting" interaction class (Table S2). 13 genes were selected that encode proteins possessing the described characteristics of fungal effector molecules and, thus, potentially play a role in the early senescence symptom development (Table 3.7). CE1-CE13 are annotated as (conserved) hypothetical or predicted proteins and for most of the candidate effectors a length < 400 amino acids (aa) is predicted (Table 3.7). Only CE1 is larger, 571 aa, but was included into the study due to *CE1* absence in the genomes of the wilt inducing isolates w-DVD31 and w-DVD-S29 (Figure 3.24; Table S4). Every candidate effector was encoded in the s-VL43 "early senescence" reference genome indicating that they may play a role in establishment of the s-VL43-like infection symptoms (Table 3.7). Moreover, CE1-CE13 are predicted to be secreted, nine of them via the non-classical secretory pathway and four candidate effectors

possess a secretion signal. Thus, a repertoire of 13 candidate effector proteins was identified which presumably is delivered in the plant's apoplast or inside the host cell.

The *V. dahliae* reference isolate VdLs.17 contains 10.535 protein-coding genes whereof about one-tenth was predicted to be secreted (Klosterman *et al.*, 2011). Of these secreted proteins 127 were identified as CWDEs and to 387 proteins no annotated functional domain could be assigned (Klosterman *et al.*, 2011; Lo Presti *et al.*, 2015). In necrotrophic and hemibiotrophic fungi, such as *Verticillium*, a large proportion of CWDEs was identified and this proportion is higher than in biotrophic pathogens (O'Connell *et al.*, 2012; Kubicek *et al.*, 2014; Zhao *et al.*, 2014). Especially at late invasion stages and in the necrotrophic phase of the pathogenic lifestyle these enzymes are assumed to be important for the induction of plant cell damage in order to utilize the liberated nutrients for growth and proliferation (Gibson *et al.*, 2011; Kubicek *et al.*, 2014). Moreover, it was postulated that hemibiotrophs initially require effector proteins that suppress the plant defences in the apoplast during plant colonization and later need effectors, like CWDEs, that kill plant cells (Lo Presti *et al.*, 2015). Transcriptomic studies of *Colletotrichum* with respect to its lifestyle transition during host plant infection elucidated that genes coding for secreted proteins without a functional annotation are primarily expressed during the initial biotrophic phase (O'Connell *et al.*, 2012). In contrast, secreted CWDEs showed enhanced expression in the subsequent necrotrophic phase (O'Connell *et al.*, 2012). Also in the present study CWDEs were expressed *in planta* with the highest transcript abundance at the latest time point of the analysed time course (Table S2). Also the *Verticillium nonalfalfae* lignin degrading peroxidase VnaPRX1.1277 showed increasing *in planta* expression during the progress of colonization. The authors, therefore, postulated that this peroxidase is involved in pathogenicity of *V. nonalfalfae*. (Flajsman *et al.*, 2016). Hence, it is reasonable that the expression of CWDEs in the *Verticillium* "early senescence" pathosystem increases and it is likely that CWDEs play a role in the *Verticillium* proliferation and the proceeding colonization of the host plant.

Candidate effectors of the transcription profile A, CE3 as well as CEL, exhibit enhanced transcript abundance *in planta* at the early infection time points 8 dpi and 12 dpi in the "early senescence" pathosystem compared to the "wilting" pathosystem (Figure 3.22B, upper panel). At the later time point (16 dpi) the transcript levels significantly decrease indicating that CE3 and CEL are particularly expressed during the initial host colonization presumably to suppress host plant defences. Specifically expression of CEL was postulated to be important for the reduced lignin levels in xylem cell walls in order to guarantee fungal spread and proliferation (4.3). In the biotrophic basidiomycete *U. maydis* the effector molecule Pep1 was discovered to be necessary for effective invasion of the fungal hyphae into maize epidermis cells (Doehlemann *et al.*, 2009).

Pep1 disruption mutants develop typical infection structures, however, hyphal penetration is arrested. Moreover, these mutants elicit plant defence responses, since downregulation of several plant genes which are involved in the plant defence does not occur when the effector gene *Pep1* is disrupted (Doehlemann *et al.*, 2009). Likewise, i*n planta* microarray data of barley plants 72 hours post infection (hpi) with *M. oryzae* identified expression of fungal genes which are most likely involved in successful invasive hyphal growth and penetration (Mathioni *et al.*, 2011). Thus, suppression of host defence responses potentially is also important at very early infection time points during root tissue penetration and invasion by *Verticillium*. Candidate effectors assigned to the transcription profile C exhibit high transcript levels in the "early senescence" interaction class at the early infection time point (4 dpi) in *A. thaliana* roots. Reusche *et al.* (2014) recently monitored the fungal growth of the early senescence inducing strain s-VL43 and the wilt inducing strain w-VdJR2 into the *A. thaliana* root tissues in a time course experiment. At 4 dpi fungal hyphae of both *Verticillium* species successfully penetrated the rhizodermis and colonized the vascular cylinder (Reusche *et al.*, 2014). Thus, candidate effectors selected in this study are potentially not involved in lysis of root cell walls. Yet, the effectors may be crucial for the establishment of the biotrophic interaction in root tissues by suppression of plant defence responses.

Candidate effector genes assigned to the transcription profile B and C exhibited increasing transcript abundance in aerial tissues of *N. benthamiana* plants inoculated with the "early senescence" interaction class (Figure 3.22B, middle and lower panel). These candidate effector genes obtained the maximal transcript levels of the analysed time course at 16 dpi when bundle sheath cell transdifferentiation was detected in *N. benthamiana* leaves (Figure 3.21). Thus, they may be involved in the induction of developmental reprogramming of the plant's vasculature. One possible scenario of candidate effector function is the regulation of gene expression involved in *de novo* xylem formation, like the *A. thaliana* NAC domain transcription factor gene *VND7* (Kubo *et al.*, 2005; Reusche *et al.*, 2012). Expression measurements of *VND7* support this hypothesis since the marker gene is strongly induced in *A. thaliana* upon infection with the "early senescence" interaction class (Figure 3.12M; Figure 3.13Q). Candidate effectors may be translocated or secreted into the cytoplasm of the host cell and may be further transported to the nucleus. Subsequently, they may alter the structure and function of the cell. Indeed, the subcellular localization tool Yloc+ predicted a nuclear localization for nine of the candidate effectors of the transcription profile B and C (Table 3.8). Moreover, CE1 possesses a nuclear localization signal (NLS) and, thus, is most likely transported into the nucleus (Table 3.8). In the bacterial plant pathogen *Xanthomonas spp* an effector family, the *T*ranscription *A*ctivator-*L*ike

(TAL) effectors, was identified which bind to the promoters of specific host target genes and activate their expression. These TAL effectors possess unique DNA binding domains which resemble no classic DNA binding domain (Scholze and Boch, 2010). The TAL effector AvrBs3 of *Xanthomonas campestris* pv. *vesicatoria,* for example, is secreted into the host cells of susceptible *Capsicum annuum* varieties and enhances the expression of the cell size regulator *upa20* (Kay *et al.*, 2007). This results in developmental reprogramming of the host cells in pepper. Deletion of CEs of transcription profile B and C in the early senescence inducing *V. dahliae* isolates and subsequent *A. thaliana* and *N. benthamiana* infection studies with these knock-out lines would reveal if these candidate effectors are involved in leaf developmental reprogramming.

4.7 Early senescence symptom development by *V. dahliae* infection correlates with induction of defoliation on *Gossypium spec.* or *Olea europaea*

Notably, the four early senescence inducing *V. dahliae* strains s-V76, s-T9, s-V138I and s-V781I were isolated from *Gossypium spec.* or *Olea europaea* and were previously shown to induce defoliation on cotton or olive plants, respectively (Friebertshauser and DeVay, 1982; Tzeng and Vay, 1985; Parkhi *et al.*, 2010; Collins *et al.*, 2005; personal communication Prof. Rafael M. Jiménez-Díaz, Córdoba, Spain; Table 3.2). The *V. dahliae* isolate s-ST100 was isolated from soil in Belgium and, thus, the host plant and the symptom development by infection with this isolate was not known. Here, it was shown that s-ST100 infects cotton plants and causes defoliation as well (Figure 3.3). The hypothesis was put up that the induction of early senescence symptoms on *A. thaliana* correlates with the induction of defoliation on cotton or olive plants. In contrast, the wilt inducing strains w-V192I and w-V200I infect cotton without induction of defoliation (Collins *et al.*, 2005; personal communication Prof. Rafael M. Jiménez-Díaz, Córdoba, Spain; Table 3.3). The question arises whether fungal effector molecules which showed high transcript abundance in the "early senescence" pathosystem and are postulated to trigger the early senescence phenotype are similarly responsible for defoliation induction on cotton or olive plants.

Early senescence of *A. thaliana* after infection with *V. longisporum* s-VL43 is associated to decreased levels of the hormone cytokinin (Reusche *et al.*, 2013). Notably, the expression of cytokinin oxidases/dehydrogenases was induced in infected plants compared to non-infected plants. Therefore, it was postulated that the reduction of cytokinin is affected by an induction of cytokinin oxidases resulting in early senescence (Reusche *et al.*, 2013). The senescence of leaves in cotton and olive plants may subsequently result in the plant's defoliation. It should be verified

whether infection with the early senescence inducing *V. dahliae* strains s-V76, s-T9, s-ST100, s-V138I and s-V781I also results in reduced cytokinin levels in *A. thaliana*, but also in *Gossypium spec.* and *Olea europaea* plants. This would answer the question whether the induction of early senescence in *A. thaliana* correlates with defoliation of cotton and olive plants. Moreover, RNA-sequencing approaches with *V. dahliae* infected cotton or olive plants would help in the identification of potential effector proteins which are involved in the induction of early senescence. Genes encoding for these effector proteins would show high transcript abundance in cotton or olive and can be compared with the already existing *V. dahliae* transcriptome in *A. thaliana* Col-0 and *N. benthamiana*.

4.8 Differential transcription of *CEL* and *CE1* may be controlled by transposable elements or epigenetics

On bases of their *in planta* transcription profiles in early senescence inducing isolates two effector candidate genes, *CEL* and *CE1*, were selected which are possibly involved in the early senescence disease symptom induction. Candidate gene promoter sequences specific for the "early senescence" or "wilting" interaction class may regulate the differential expression of the candidate genes in both interaction classes (Figure 3.22). However, a nucleotide sequence in the promoter regions of *CEL* and *CE1* which was uniformly present in the genomes of early senescence inducing *Verticillium* strains and not in the "wilting" interaction class was not discovered (data not shown). This led to the hypothesis that expression of *CEL* and *CE1* is controlled epigenetically or by transposable elements.

Proteins involved in pathogenicity, such as effector proteins are often encoded in close proximity of transposable elements like in telomeric and centromeric regions or on dispensable chromosomes (Orbach *et al.*, 2000; Haas *et al.*, 2009; Schmidt and Panstruga, 2011; Balesdent *et al.*, 2013). It was suggested before that these highly dynamic genomic regions result in improved adaptation to the environment and in pathogenic diversity (Van de Wouw, Angela P *et al.*, 2010; Raffaele *et al.*, 2010a; Raffaele and Kamoun, 2012). Especially, transposable elements, such as retro- and DNA-transposons, are assumed to provide a chromosomal plasticity for development of new virulence traits in diverse plant pathogens, like *Magnoporthe oryzae*, *Leptosphaeria maculans*, *Phythophthora infestans* and also *Verticillium dahliae* (Raffaele *et al.*, 2010b; Rouxel *et al.*, 2011; Chuma *et al.*, 2011; Faino *et al.*, 2016). In *M. grisea* the insertion of the Pot3 transposon into the promoter region of an *AVR-Pita* gene results in gain of virulence of the pathogen on a rice cultivar (Chuma *et al.*, 2011). Thus, transposition of Pot3 in the promoter of *AVR-Pita* was

supposed to mutate this region and subsequently silence the gene. Without expression of *AVR-Pita* the plant does not recognize pathogenic invasion resulting in alteration of the virulence of *M. grisea* (Kang *et al.*, 2001). In addition, transposable elements in the proximity of the *UhAvr1* effector gene in *Ustilago hordei* altered its expression via transposition in the promoter region of *UhAvr1* (Ali *et al.*, 2014). In case of the different transcript abundance of *CEL* and *CE1* in the "early senescence" and "wilting" interaction class it is unlikely that transposable elements translocated in the promoter regions, since no ambivalent sequences between both interaction classes were identified (data not shown). Perhaps, transposable elements may have inserted in enhancer or silencer elements which originally regulated the transcription of the genes. E.g. translocation of transposons in enhancer elements of *CEL* and *CE1* of the wilt inducing isolates would result in mutation of this region. The binding capacity of the corresponding activator would be disturbed by transposon insertion resulting in reduced transcription of *CEL* and *CE1* in the "wilting" interaction class compared to the "early senescence" interaction class. Likewise, genomic regions enriched in transposable elements are commonly linked to highly condensed chromatin (heterochromatin). Heterochromatin limits the transcription of genes as well as the activity of transposons (Lewis *et al.*, 2009; Connolly *et al.*, 2013; Galazka and Freitag, 2014). Thus, transposable elements which are located in close proximity of genes would affect their expression by directing heterochromatin formation. It has to be analysed with help of the *de novo* assembled genomes of the *V. dahliae* isolates (Table 3.5) if the candidate effectors are encoded in a region which is enriched in transposable elements in the different interaction classes. This would verify whether transposable elements might play a role in the different transcript levels of *CEL* and *CE1*.

Transcription of *CEL* and *CE1* in the two interaction classes may also be controlled epigenetically via histone modifications or DNA methylation. Histone modification may result in structural changes of genomic regions harboring *CEL* and *CE1* and hence alter the promoter accessibility. This subsequently affects the expression of the candidate effector genes. Histone modifications, such as methylation, was identified, for example, in the plant pathogenic fungus *Leptosphaeria maculans*. Histone H3 lysine 9 methylation represses the expression of numerous effector proteins of *L. maculans* during vegetative growth. In contrast, expression of effector proteins was strongly induced during infection of *B. napus* (Soyer *et al.*, 2014).

DNA methylation mostly results in gene silencing (Rich *et al.*, 1984; Razin, 1998). Hence, DNA methylation of the promoter regions of *CEL* and *CE1* in the "wilting" interaction class would perturb the promoter accessibility to the transcription factors resulting in the low transcript abundance of *CEL* and *CE1* discovered for the "wilting" interaction class (Figure 3.22). Importantly, the level of DNA methylation can vary among isolates of the same species, as it was discovered for

the ascomycete *Ophiostoma novo-ulmi* (Binz *et al.*, 1998). Hence, it is possible that variations in DNA methylation and thus, variations in gene silencing also exist within the species *V. dahliae* and may be the cause for the detected differential expression of the *CEL* and *CE1* between isolates of the "early senescence" and the "wilting" interaction class.

4.9 The absence/presence polymorphism of candidate effector genes in *V. dahliae* genomes may result from chromosomal rearrangements

PCR analyses in combination with genomic mapping approaches via RNA-seq reads revealed that the potential candidate effector gene *CE1* is not present in all analysed wilt inducing *V. dahliae* isolates. *CE1* is absent in the genomes of w-DVD31 and w-DVD-S29 (Table S4; Figure 3.24). Nonetheless, the candidate effector gene exist in the genomes of early senescence inducing *Verticillium* isolates as well as all other tested wilt inducing strains (Table S4; Figure 3.24). Moreover, the lack of RNA-seq reads mapping to *CE7* and *CE11* in all transciptomes of plants infected with the wilt inducing isolates (Table S3) hints for the absence of both candidate effector genes in genomes of the "wilting" interaction class. In addition, no homologue of *CE7* and *CE11* was identified in the reference genome w-VdLs.17 (Table 3.9). It has to be verified via PCR analysis and genomic sequence investigation whether *CE7* and *CE11* are absent in the genomes of the tested wilt inducing isolates. If this holds true CE7 and CE11 may represent interaction class-specific effector proteins presumably involved in the early senescence infection symptoms.

Effector genes were claimed to rapidly evolve in the genomes of plant pathogens since their existence might either suppress the plant immune system or be recognized by R proteins resulting in ETI (Win *et al.*, 2012). Hence, their existence may have a positive or negative influence on the pathogen's fitness. Therefore, the evolution of pathogenic effector genes is highly dynamic to guarantee a fast adaptation to its host plant (Jones and Dangl, 2006; Raffaele and Kamoun, 2012). Asexual fungi, such as *Verticillium*, are claimed as evolutionary dead ends since they do not recombine their alleles via meiosis (Burt, 2000; McDonald and Linde, 2002). Thus, asexual fungi have a lower evolutionary potential due to a lower potential of gene flow in comparison to sexually reproducing fungi. This would result in a reduced ability to create genetic variation and adapt to changing environmental conditions (Heitman, 2006). Evolutionary mechanisms such as random mutations and chromosomal instability have to occur within genomes of asexual fungi in order to enable their arms race with host plants. Chromosomal rearrangements have the power to promote changes in the virulence profile of pathogens and lead to a variation of individual pathogen lineages or species (Anderson *et al.*, 2010).

Extensive chromosomal reshuffling was identified in a previous study in a *V. dahliae* isolate population (Jonge *et al.*, 2013). The authors discovered complex intra- and interchromosomal rearrangements between highly similar *V. dahliae* strains. The rearrangements evidenced chromosomal plasticity and induced local sequence variation within the population. Sequence variation included the enrichment or loss of effector genes, as it was discovered for the *Ave1* effector in race 1 and race 2 *V. dahliae* strains, respectively (Jonge *et al.*, 2012; Jonge *et al.*, 2013). Presumably this would increase the adaptive capability of the fungus to host plant responses. With regard to the present study genome sequence comparison of *V. dahliae* isolates of the different interaction classes indicated the existence of interaction class-specific sequences (Table 3.6; section 4.5). This leads to the suggestion that chromosomal rearrangements also occur in the genomes of *V. dahliae* isolates tested in this thesis. Strikingly, the potential effector candidate gene *CE1* is not present in the genomes of the wilt inducing isolates w-DVD31 and w-DVD-S29, but in all other *Verticillium* strains of the "wilting" and "early senescence" interaction class (Figure 3.24; Table S4). Chromosomal rearrangements can result in the insertion, the duplication and also the deletion of genomic regions (Seidl and Thomma, 2014). Thus, *CE1* may be located in plastic genomic regions and its absence or presence in isolate genomes may be mediated by the flexible and instable structure of dynamic chromosome regions. Potentially, during chromosomal rearrangements of isolates w-DVD31 and w-DVD-S29 *CE1* got lost.

Notably, *Verticillium* effector genes which are strongly upregulated *in planta* after infection of *N. benthamiana* are often flanked by transposable elements in lineage-specific (LS) regions (Jonge *et al.*, 2013). Gene-flanking transposable elements can mediate homologous recombination between highly similar elements across the genome (Kang *et al.*, 2001; Lemoine *et al.*, 2005). Subsequent transposition cause the deletion of genes or they are inserted to/inversed by other genomic regions. The *AVR-Pita* effector gene family of *Magnaporthe oryzae* corresponds to the disease resistance gene *Pita* (Chuma *et al.*, 2011). The effector genes are located in the genome in a subtelomeric region and are flanked by a retrotransposon. This retrotransposon was suggested to play a role in the multiple translocation and genomic dispersion of the *AVR-Pita* genes. Frequent deletion and recovery of the avirulence genes due to the high mobility of retrotransposons might contribute to a rapid adaptation towards the rice *Pita* resistance genes (Chuma *et al.*, 2011). Moreover, transposable elements can cause DNA breaks during excision which would also result in gene deletion (Seidl and Thomma, 2014; Faino *et al.*, 2016). It is likely that the absence/presence polymorphism of *CE1* may also be mediated by the recombination or the activity of transposable elements.

4.10 Outlook

The findings presented in this study revealed that the developmental reprogramming within the leaf vasculature of *A. thaliana* and *N. benthamiana* plants are exclusively induced by *Verticillium* isolates of the "early senescence" interaction class. Moreover, *de novo* xylem formation in leaves is accompanied by the upregulation of a potential fungal effector molecule repertoire.

To assess whether candidate effectors (CEs) are involved in the vascular developmental reprogramming and the enhanced pathogenicity of the "early senescence" interaction class knock-out mutants of CEs are currently generated. *CE* genes should be deleted in representative isolates inducing robust and strong infection symptoms, such as s-ST100 and s-V76. *A. thaliana* infection studies with the mutant and wildtype strains and subsequent microscopic investigations should reveal if they play a role in hyperplasia formation and bundle sheath cell transdifferentiation. Likewise, qRT-PCR analysis should identify differences in proliferation and infection kinetics between mutant and wildtype strains.

Histological analysis discovered enhanced lignification levels in leaf midribs of *A. thaliana* plants infected with the wilt inducing *V. dahliae* isolates whereas infection with early senescence inducing isolates does not increase lignin deposition. Moreover, transcriptomic studies identified high transcript levels of *CEL* in the "early senescence" pathosystem. Generation of *cel* knock-out mutants in the strains s-ST100 and s-V76 and subsequent *A. thaliana* infection studies should elucidate if this enzyme is involved in changes of xylem cell wall lignification patterns and give evidence for its general importance in fungal virulence. In addition, it is necessary to verify in histological analyses whether leaf midribs of *N. benthamiana* plants infected with the "wilting" interaction class possess enhanced lignification levels in comparison to plants infected with the "early senescence" interaction class. This would support the hypothesis that high transcript abundance of *CEL* in aerial tissues of *N. benthamiana* inoculated with the "early senescence" interaction class correlates with reduced xylem cell wall lignification.

Furthermore, it would be interesting to identify the targets of selected candidate effectors in *A. thaliana.* The identification of effector protein interactors would shed light on their function during infection establishment. For this purpose transgenic *V. dahliae* strains expressing GFP-tagged *CE* genes should be generated. GFP-Trap®-mediated pull-down experiments and subsequent LC-MS/MS analyses provide a powerful tool for identification of interaction partners. Besides, expression of *CE-GFP* in early senescence inducing *V. dahliae* isolates during plant infection should verify their predicted subcellular localization. With help of confocal laser

scanning microscopy this should prove whether CEs, like CE1, are transported to the nucleus and may influence the expression of genes regulating xylem cell transdifferentiation.

Genome sequence comparison verified the existence of interaction class-specific genomic sequences. To elucidate whether interaction class-specific sequences are arranged in particular genomic regions the chromosomal structure of the *de novo* assembled genomes of the *V. dahliae* core collection should be further investigated. Moreover, it should be analysed which genes are represented by the "early senescence" interaction class-specific sequences. This would help to assess if these unique sequences have a function in the symptom development.

Likewise, detailed investigation of the genome structure of early senescence inducing *V. dahliae* isolates should reveal whether effector proteins are encoded in clusters. If *ce* single knock-outs would have no effect on the symptom development, effector gene clusters should be deleted or downregulated to avoid functional redundancy of the effector proteins. The CRISPR/Cas9 system (Jinek *et al.*, 2012) as well as RNA interference (RNAi) (Fire *et al.*, 1998)would provide powerful tools for the deletion or downregulation of fungal gene clusters, respectively.

5 References

Abramovitch RB, Anderson JC, Martin GB. 2006. Bacterial elicitation and evasion of plant innate immunity. *Nature Reviews Molecular Cell Biology* **7,** 601–611.

Agerbirk N, Vos M de, **Kim JH, Jander G.** 2009. Indole glucosinolate breakdown and its biological effects. *Phytochemistry Reviews* **8,** 101–120.

Agrios GN. 1997. *Plant Pathology. Ed ke-4*: San Diego: Academic Press.

Ali S, Laurie JD, Linning R, Cervantes-Chávez JA, Gaudet D, Bakkeren G. 2014. An immunity-triggering effector from the barley smut fungus Ustilago hordei resides in an Ustilaginaceae-specific cluster bearing signs of transposable element-assisted evolution. *PLoS Pathog* **10,** e1004223.

Anders S, Huber W. 2010. Differential expression analysis for sequence count data. *Genome biology* **11,** R106.

Anderson JP, Gleason CA, Foley RC, Thrall PH, Burdon JB, Singh KB. 2010. Plants versus pathogens: an evolutionary arms race. *Functional plant biology FPB* **37,** 499–512.

Annis SL, Goodwin PH. Recent advances in the molecular genetics of plant cell wall-degrading enzymes produced by plant pathogenic fungi. *European Journal of Plant Pathology* **103,** 1–14.

Annis SL, Goodwin PH. 1997. Recent advances in the molecular genetics of plant cell wall-degrading enzymes produced by plant pathogenic fungi. *European Journal of Plant Pathology* **103,** 1–14.

Baayen RP. 1986. Regeneration of vascular tissues in relation to Fusarium wilt resistance of carnation. *Netherlands Journal of Plant Pathology* **92,** 273–285.

Balesdent M, Fudal I, Ollivier B *et al.* 2013. The dispensable chromosome of Leptosphaeria maculans shelters an effector gene conferring avirulence towards Brassica rapa. *The New phytologist* **198,** 887–898.

Bannister AJ, Kouzarides T. 2011. Regulation of chromatin by histone modifications. *Cell research* **21,** 381–395.

Barbara D. 2003. Verticillium Wilts. *Physiological and Molecular Plant Pathology* **62,** 51–52.

Barbara DJ, Clewes E. 2003. Plant pathogenic Verticillium species: how many of them are there? *Molecular plant pathology* **4,** 297–305.

Bayer EA, Chanzy H, Lamed R, Shoham Y. 1998. Cellulose, cellulases and cellulosomes. *Current opinion in structural biology* **8,** 548–557.

Beckers GJM, Spoel SH. 2006. Fine-Tuning Plant Defence Signalling: Salicylate versus Jasmonate. *Plant biology (Stuttgart, Germany)* **8,** 1–10.

Bendtsen JD, Jensen LJ, Blom N, Heijne G von, **Brunak S.** 2004a. Feature-based prediction of non-classical and leaderless protein secretion. *Protein engineering, design & selection PEDS* **17,** 349–356.

Bendtsen JD, Nielsen H, Heijne G von, **Brunak S.** 2004b. Improved prediction of signal peptides: SignalP 3.0. *Journal of molecular biology* **340,** 783–795.

Benjamini Y, Hochberg Y. 1995. Controlling the false discovery rate: a practical and powerful approach to multiple testing. *Journal of the Royal Statistical Society. Series B (Methodological),* 289–300.

Binz T, D'Mello N, Horgen PA. 1998. A Comparison of DNA Methylation Levels in Selected Isolates of Higher Fungi. *Mycologia* **90,** 785.

Birch PRJ, Rehmany AP, Pritchard L, Kamoun S, Beynon JL. 2006. Trafficking arms: oomycete effectors enter host plant cells. *Trends in microbiology* **14,** 8–11.

Bishop CD, Cooper RM. 1983. An ultrastructural study of root invasion in three vascular wilt diseases. *Physiological plant pathology* **22,** 15-IN13.

Blackwood EM, Kadonaga JT. 1998. Going the distance: a current view of enhancer action. *Science* **281,** 60–63.

Boch J, Scholze H, Schornack S *et al.* 2009. Breaking the code of DNA binding specificity of TAL-type III effectors. *Science* **326,** 1509–1512.

Bowling SA, Clarke JD, Liu Y, Klessig DF, Dong X. 1997. The cpr5 mutant of Arabidopsis expresses both NPR1-dependent and NPR1-independent resistance. *The Plant Cell* **9,** 1573–1584.

Brefort T, Tanaka S, Neidig N, Doehlemann G, Vincon V, Kahmann R. 2014. Characterization of the largest effector gene cluster of Ustilago maydis. *PLoS pathogens* **10,** e1003866.

Briesemeister S, Rahnenführer J, Kohlbacher O. 2010a. Going from where to why—interpretable prediction of protein subcellular localization. *Bioinformatics* **26,** 1232–1238.

Briesemeister S, Rahnenführer J, Kohlbacher O. 2010b. YLoc—an interpretable web server for predicting subcellular localization. *Nucleic acids research* **38,** W497-W502.

Burt A. 2000. Perspective: sex, recombination, and the efficacy of selection—was Weismann right? *Evolution* **54,** 337–351.

Cao H, Bowling SA, Gordon AS, Dong X. 1994. Characterization of an Arabidopsis mutant that is nonresponsive to inducers of systemic acquired resistance. *The Plant Cell* **6,** 1583–1592.

Carpita NC, Gibeaut DM. 1993. Structural models of primary cell walls in flowering plants: consistency of molecular structure with the physical properties of the walls during growth. *The Plant Journal* **3,** 1–30.

Chatterjee S, Chaudhury S, McShan AC, Kaur K, Guzman RN de. 2013. Structure and biophysics of type III secretion in bacteria. *Biochemistry* **52,** 2508–2517.

Chen L, Hou B, Lalonde S *et al.* 2010. Sugar transporters for intercellular exchange and nutrition of pathogens. *Nature* **468,** 527–532.

Chen Z, Zheng Z, Huang J, Lai Z, Fan B. 2014. Biosynthesis of salicylic acid in plants. *Plant Signaling & Behavior* **4,** 493–496.

Chisholm ST, Coaker G, Day B, Staskawicz BJ. 2006. Host-microbe interactions: shaping the evolution of the plant immune response. *Cell* **124,** 803–814.

Chomczynski P. 1993. A reagent for the single-step simultaneous isolation of RNA, DNA and proteins from cell and tissue samples. *BioTechniques* **15,** 532-4, 536-7.

Chuma I, Isobe C, Hotta Y *et al.* 2011. Multiple translocation of the AVR-Pita effector gene among chromosomes of the rice blast fungus Magnaporthe oryzae and related species. *PLoS pathogens* **7,** e1002147.

Collins A, Mercado-Blanco J, Jimenez-Diaz RM, Olivares C, Clewes E, Barbara DJ. 2005. Correlation of molecular markers and biological properties in Verticillium dahliae and the possible origins of some isolates. *Plant Pathology* **54,** 549–557.

Connolly LR, Smith KM, Freitag M. 2013. The Fusarium graminearum histone H3 K27 methyltransferase KMT6 regulates development and expression of secondary metabolite gene clusters. *PLoS Genet* **9,** e1003916.

Czechowski T, Stitt M, Altmann T, Udvardi MK, Scheible W. 2005. Genome-wide identification and testing of superior reference genes for transcript normalization in Arabidopsis. *Plant physiology* **139,** 5–17.

Dangl JL, Jones JDG. 2001. Plant pathogens and integrated defence responses to infection. *Nature* **411,** 826–833.

Davis EL, Hussey RS, Mitchum MG, Baum TJ. 2008. Parasitism proteins in nematode–plant interactions. *Current opinion in plant biology* **11,** 360–366.

Del Sal G, Manfioletti G, Schneider C. 1989. The CTAB-DNA precipitation method: a common mini-scale preparation of template DNA from phagemids, phages or plasmids suitable for sequencing. *BioTechniques* **7,** 514–520.

Deslandes L, Rivas S. 2012. Catch me if you can: bacterial effectors and plant targets. *Trends in Plant Science* **17,** 644–655.

Diener A. 2012. Visualizing and quantifying Fusarium oxysporum in the plant host. *Molecular Plant-Microbe Interactions* **25,** 1531–1541.

Doehlemann G, Hemetsberger C. 2013. Apoplastic immunity and its suppression by filamentous plant pathogens. *New Phytologist* **198,** 1001–1016.

Doehlemann G, van der Linde K, Assmann D *et al.* 2009. Pep1, a secreted effector protein of Ustilago maydis, is required for successful invasion of plant cells. *PLoS pathogens* **5,** e1000290.

Dunford HB, Stillman JS. 1976. On the function and mechanism of action of peroxidases. *Coordination chemistry reviews* **19,** 187–251.

Durner J, Shah J, Klessig DF. 1997. Salicylic acid and disease resistance in plants. *Trends in Plant Science* **2,** 266–274.

Eynck C, Koopmann B, Grunewaldt-Stoecker G, Karlovsky P, Tiedemann A von. 2007. Differential interactions of Verticillium longisporum and V. dahliae with Brassica napus detected with molecular and histological techniques. *European Journal of Plant Pathology* **118,** 259–274.

Eynck C, Koopmann B, Karlovsky P, Tiedemann A von. 2009. Internal resistance in winter oilseed rape inhibits systemic spread of the vascular pathogen Verticillium longisporum. *Phytopathology* **99,** 802–811.

Faino L, Jonge R de, **Thomma, Bart P. H. J.** 2012. The transcriptome of Verticillium dahliae-infected Nicotiana benthamiana determined by deep RNA sequencing: Plant Signaling & Behavior. *Plant Signaling & Behavior* **7,** 1065–1069.

Faino L, Seidl MF, Shi-Kunne X *et al.* 2016. How transposons drive evolution of virulence in a fungal pathogen. *bioRxiv*.

Fan W, Dong X. 2002. In vivo interaction between NPR1 and transcription factor TGA2 leads to salicylic acid–mediated gene activation in Arabidopsis. *The Plant Cell* **14,** 1377–1389.

Fedoroff NV. 2012. Transposable Elements, Epigenetics, and Genome Evolution. *Science* **338,** 758–767.

Fire A, Xu S, Montgomery MK, Kostas SA, Driver SE, Mello CC. 1998. Potent and specific genetic interference by double-stranded RNA in Caenorhabditis elegans. *Nature* **391,** 806–811.

Flajsman M, Mandelc S, Radisek S *et al.* 2016. Identification of novel virulence - associated proteins secreted to xylem by Verticillium nonalfalfae during colonization of hop plants. *Molecular plant-microbe interactions MPMI*.

Floerl S, Druebert C, Aroud HI, Karlovsky P, Polle A. 2010. Disease symptoms and mineral nutrition in Arabidopsis thaliana in response to Verticillium longisporum VL43 infection. *Journal of Plant Pathology,* 693–700.

Floerl S, Druebert C, Majcherczyk A, Karlovsky P, Kües U, Polle A. 2008. Defence reactions in the apoplastic proteome of oilseed rape (Brassica napus var. napus) attenuate Verticillium longisporum growth but not disease symptoms. *BMC plant biology* **8,** 129.

Floerl S, Majcherczyk A, Possienke M *et al.* 2012. Verticillium longisporum Infection Affects the Leaf Apoplastic Proteome, Metabolome, and Cell Wall Properties in Arabidopsis thaliana. *PLoS One* **7,** e31435.

Fradin EF, Thomma, Bart P H J. 2006. Physiology and molecular aspects of Verticillium wilt diseases caused by V. dahliae and V. albo-atrum. *Molecular plant pathology* **7,** 71–86.

Friebertshauser GE, DeVay JE. 1982. Differential effects of the defoliating and nondefoliating pathotypes of Verticillium dahliae upon the growth and development of Gossypium hirsutum [Verticillium wilt]. *Phytopathology (USA)*.

Galazka JM, Freitag M. 2014. Variability of chromosome structure in pathogenic fungi—of 'ends and odds'. *Current opinion in microbiology* **20,** 19–26.

Gayoso C, Pomar F, Novo-Uzal E, Merino F, Ilárduya OM de. 2010. The Ve-mediated resistance response of the tomato to Verticillium dahliae involves H2O2, peroxidase and lignins and drives PAL gene expression. *BMC plant biology* **10,** 232.

Gibson DM, King BC, Hayes ML, Bergstrom GC. 2011. Plant pathogens as a source of diverse enzymes for lignocellulose digestion. *Current opinion in microbiology* **14,** 264–270.

Gijzen M, Ishmael C, Shrestha SD. 2014. Epigenetic control of effectors in plant pathogens. *Frontiers in plant science* **5,** 638.

Giraldo MC, Valent B. 2013. Filamentous plant pathogen effectors in action. *Nature Reviews Microbiology* **11,** 800–814.

Glazebrook J. 2005. Contrasting mechanisms of defense against biotrophic and necrotrophic pathogens. *Annu. Rev. Phytopathol.* **43,** 205–227.

Glazebrook J, Rogers EE, Ausubel FM. 1996. Isolation of Arabidopsis mutants with enhanced disease susceptibility by direct screening. *Genetics* **143,** 973–982.

Greenberg JT, Yao N. 2004. The role and regulation of programmed cell death in plant–pathogen interactions. *Cellular microbiology* **6,** 201–211.

Haas BJ, Kamoun S, Zody MC *et al.* 2009. Genome sequence and analysis of the Irish potato famine pathogen Phytophthora infestans. *Nature* **461,** 393–398.

Hacquard S, Joly DL, Lin Y *et al.* 2012. A comprehensive analysis of genes encoding small secreted proteins identifies candidate effectors in Melampsora larici-populina (poplar leaf rust). *Molecular Plant-Microbe Interactions* **25,** 279–293.

HEALE JB. 2000. Diversification and speciation in Verticillium-an overview. *Advances in Verticillium Research and Disease Management,* 1–14.

Heitman J. 2006. Sexual reproduction and the evolution of microbial pathogens. *Current Biology* **16,** R711-R725.

Hogenhout SA, Van der Hoorn, Renier A L, Terauchi R, Kamoun S. 2009. Emerging concepts in effector biology of plant-associated organisms. *Molecular plant-microbe interactions MPMI* **22,** 115–122.

Houterman PM, Ma L, van Ooijen G *et al.* 2009. The effector protein Avr2 of the xylem-colonizing fungus Fusarium oxysporum activates the tomato resistance protein I-2 intracellularly. *The Plant Journal* **58,** 970–978.

Inderbitzin P, Davis RM, Bostock RM, Subbarao KV. 2011. The ascomycete Verticillium longisporum is a hybrid and a plant pathogen with an expanded host range. *PLoS One* **6,** e18260.

Jinek M, Chylinski K, Fonfara I, Hauer M, Doudna JA, Charpentier E. 2012. A programmable dual-RNA–guided DNA endonuclease in adaptive bacterial immunity. *Science* **337,** 816–821.

Johansson A, Staal J, Dixelius C. 2006. Early responses in the Arabidopsis-Verticillium longisporum pathosystem are dependent on NDR1, JA- and ET-associated signals via cytosolic NPR1 and RFO1. *Molecular plant-microbe interactions MPMI* **19,** 958–969.

Jones JDG, Dangl JL. 2006. The plant immune system. *Nature* **444,** 323–329.

Jonge R de, **Bolton MD, Kombrink A, van den Berg, Grardy C M, Yadeta KA, Thomma, Bart P H J.** 2013. Extensive chromosomal reshuffling drives evolution of virulence in an asexual pathogen. *Genome research* **23,** 1271–1282.

Jonge R de, **Bolton MD, Thomma, Bart P H J.** 2011. How filamentous pathogens co-opt plants: the ins and outs of fungal effectors. *Current opinion in plant biology* **14,** 400–406.

Jonge R de, **van Esse HP, Kombrink A *et al.*** 2010. Conserved fungal LysM effector Ecp6 prevents chitin-triggered immunity in plants. *Science (New York, N.Y.)* **329,** 953–955.

Jonge R de, **van Esse HP, Maruthachalam K *et al.*** 2012. Tomato immune receptor Ve1 recognizes effector of multiple fungal pathogens uncovered by genome and RNA sequencing. *Proceedings of the National Academy of Sciences* **109,** 5110–5115.

Jonkers W, Rodrigues CDA, Rep M. 2009. Impaired colonization and infection of tomato roots by the Δ frp1 mutant of Fusarium oxysporum correlates with reduced CWDE gene expression. *Molecular Plant-Microbe Interactions* **22,** 507–518.

Kale SD, Gu B, Capelluto DG *et al.* 2010. External Lipid PI3P Mediates Entry of Eukaryotic Pathogen Effectors into Plant and Animal Host Cells. *Cell* **142,** 284–295.

Kale SD, Tyler BM. 2011. Entry of oomycete and fungal effectors into plant and animal host cells. *Cellular microbiology* **13,** 1839–1848.

Kamoun S. 2007. Groovy times: filamentous pathogen effectors revealed. *Current opinion in plant biology* **10,** 358–365.

Kämper J, Kahmann R, Bölker M *et al.* 2006. Insights from the genome of the biotrophic fungal plant pathogen Ustilago maydis. *Nature* **444,** 97–101.

Kang S, Lebrun MH, Farrall L, Valent B. 2001. Gain of virulence caused by insertion of a Pot3 transposon in a Magnaporthe grisea avirulence gene. *Molecular plant-microbe interactions MPMI* **14,** 671–674.

Karapapa VK, Bainbridge BW, HEALE JB. 1997. Morphological and molecular characterization of Verticillium longisporum comb, nov., pathogenic to oilseed rape. *Mycological Research* **101,** 1281–1294.

Karapapa VK, Typas MA. 2001. Molecular characterization of the host-adapted pathogen Verticillium longisporum on the basis of a group-I intron found in the nuclear SSU-rRNA gene. *Current microbiology* **42,** 217–224.

Kay S, Hahn S, Marois E, Hause G, Bonas U. 2007. A bacterial effector acts as a plant transcription factor and induces a cell size regulator. *Science (New York, N.Y.)* **318,** 648–651.

Kearse M, Moir R, Wilson A *et al.* 2012. Geneious Basic: an integrated and extendable desktop software platform for the organization and analysis of sequence data. *Bioinformatics* **28,** 1647–1649.

Kirk TK, Farrell RL. 1987. Enzymatic" combustion": the microbial degradation of lignin. *Annual Reviews in Microbiology* **41,** 465–501.

Klimes A, Dobinson KF, Thomma BP, Klosterman SJ. 2015. Genomics Spurs Rapid Advances in Our Understanding of the Biology of Vascular Wilt Pathogens in the Genus Verticillium. *Annual Review of Phytopathology* **53,** 181–198.

Klosterman SJ, Atallah ZK, Vallad GE, Subbarao KV. 2009. Diversity, pathogenicity, and management of Verticillium species. *Annual review of phytopathology* **47,** 39–62.

Klosterman SJ, Subbarao KV, Kang S *et al.* 2011. Comparative genomics yields insights into niche adaptation of plant vascular wilt pathogens. *PLoS Pathog* **7,** e1002137.

Kombrink E, Somssich IE. 1997. Pathogenesis-Related Proteins and Plant Defense. In: Carroll GC, Tudzynski P, eds. *Plant Relationships*. Berlin, Heidelberg: Springer Berlin Heidelberg, 107–128.

König S, Feussner K, Kaever A *et al.* 2014. Soluble phenylpropanoids are involved in the defense response of Arabidopsis against Verticillium longisporum. *New Phytologist* **202,** 823–837.

Koornneef A, Pieterse CMJ. 2008. Cross talk in defense signaling. *Plant physiology* **146,** 839–844.

Kosugi S, Hasebe M, Entani T, Takayama S, Tomita M, Yanagawa H. 2008. Design of peptide inhibitors for the importin α/β nuclear import pathway by activity-based profiling. *Chemistry & biology* **15,** 940–949.

Kosugi S, Hasebe M, Matsumura N *et al.* 2009a. Six classes of nuclear localization signals specific to different binding grooves of importin α. *Journal of Biological Chemistry* **284,** 478–485.

Kosugi S, Hasebe M, Tomita M, Yanagawa H. 2009b. Systematic identification of cell cycle-dependent yeast nucleocytoplasmic shuttling proteins by prediction of composite motifs. *Proceedings of the National Academy of Sciences* **106,** 10171–10176.

Kubicek CP, Starr TL, Glass NL. 2014. Plant Cell Wall–Degrading Enzymes and Their Secretion in Plant-Pathogenic Fungi. *Annual Review of Phytopathology* **52,** 427–451.

Kubo M, Udagawa M, Nishikubo N *et al.* 2005. Transcription switches for protoxylem and metaxylem vessel formation. *Genes & development* **19,** 1855–1860.

Kuila D, Tien M, Fee JA, Ondrias MR. 1985. Resonance Raman spectra of extracellular ligninase: evidence for a heme active site similar to those of peroxidases. *Biochemistry* **24,** 3394–3397.

Langmead B, Trapnell C, Pop M, Salzberg SL. 2009. Ultrafast and memory-efficient alignment of short DNA sequences to the human genome. *Genome biol* **10,** R25.

Lemoine FJ, Degtyareva NP, Lobachev K, Petes TD. 2005. Chromosomal translocations in yeast induced by low levels of DNA polymerase: a model for chromosome fragile sites. *Cell* **120,** 587–598.

Lewis ZA, Honda S, Khlafallah TK *et al.* 2009. Relics of repeat-induced point mutation direct heterochromatin formation in Neurospora crassa. *Genome research* **19,** 427–437.

Lin Q, Li JK, Lam HP. 1997. Improved heterologous expression of the white-rot fungal ligninase H8 by crossover linker mutagenesis. *Applied Biochemistry and Biotechnology* **66,** 269–279.

Liu S, Chen J, Wang J *et al.* 2013. Molecular characterization and functional analysis of a specific secreted protein from highly virulent defoliating Verticillium dahliae. *Gene* **529,** 307–316.

Liu T, Song T, Zhang X *et al.* 2014. Unconventionally secreted effectors of two filamentous pathogens target plant salicylate biosynthesis. *Nature communications* **5,** 4686.

Livak KJ, Schmittgen TD. 2001. Analysis of relative gene expression data using real-time quantitative PCR and the 2− ΔΔCT method. *methods* **25,** 402–408.

Lo Presti L, Lanver D, Schweizer G *et al.* 2015. Fungal Effectors and Plant Susceptibility. *Annual Review of Plant Biology* **66,** 513–545.

Lohse M, Bolger AM, Nagel A *et al.* 2012. RobiNA: a user-friendly, integrated software solution for RNA-Seq-based transcriptomics. *Nucleic acids research* **40,** W622-7.

Lozovaya VV, Lygin AV, Zernova OV, Li S, Widholm JM, Hartman GL. 2006. Lignin degradation by Fusarium solani f. sp. glycines. *Plant Disease* **90,** 77–82.

Ma L, Van Der Does, H Charlotte, Borkovich KA *et al.* 2010. Comparative genomics reveals mobile pathogenicity chromosomes in Fusarium. *Nature* **464,** 367–373.

Madigan MT, Brock TD. 2009. *Brock biology of microorganisms,* 12. ed., internat. ed. San Francisco, Calif.: Pearson/Benjamin Cummings.

Martínez-Soto D, Robledo-Briones AM, Estrada-Luna AA, Ruiz-Herrera J. 2014. Transcriptomic analysis of Ustilago maydis infecting Arabidopsis reveals important aspects of the fungus pathogenic mechanisms. *Plant Signaling & Behavior* **8,** e25059.

Maruthachalam K, Klosterman SJ, Kang S, Hayes RJ, Subbarao KV. 2011. Identification of pathogenicity-related genes in the vascular wilt fungus Verticillium dahliae by Agrobacterium tumefaciens-mediated T-DNA insertional mutagenesis. *Molecular biotechnology* **49,** 209–221.

Mathioni SM, Beló A, Rizzo CJ, Dean RA, Donofrio NM. 2011. Transcriptome profiling of the rice blast fungus during invasive plant infection and in vitro stresses. *BMC genomics* **12,** 49.

Maxwell PH, Burhans WC, Curcio MJ. 2011. Retrotransposition is associated with genome instability during chronological aging. *Proceedings of the National Academy of Sciences* **108,** 20376–20381.

McDonald BA, Linde C. 2002. Pathogen population genetics, evolutionary potential, and durable resistance. *Annual review of phytopathology* **40,** 349–379.

McDowell JM, Dangl JL. 2000. Signal transduction in the plant immune response. *Trends in biochemical sciences* **25,** 79–82.

Mieczkowski PA, Lemoine FJ, Petes TD. 2006. Recombination between retrotransposons as a source of chromosome rearrangements in the yeast Saccharomyces cerevisiae. *DNA repair* **5,** 1010–1020.

Millett MA, Baker AJ, Satter LD. 1976. *Pretreatments to enhance chemical, enzymatic, and microbiological attack of cellulosic materials*: US Department of Agriculture, Forest Service, Forest Products Laboratory.

MOL L, SCHOLTE K, VOS J. 1995. Effects of crop rotation and removal of crop debris on the soil population of two isolates of Verticillium dahliae. *Plant Pathology* **44,** 1070–1074.

Mou Z, Fan W, Dong X. 2003. Inducers of plant systemic acquired resistance regulate NPR1 function through redox changes. *Cell* **113,** 935–944.

Mülhardt C. 2009. *Der Experimentator: Molekularbiologie, Genomics*: Springer.

Mullis KB, Faloona FA. 1987. Specific synthesis of DNA in vitro via a polymerase-catalyzed chain reaction. *Methods in enzymology* **155,** 335.

Murashige T, Skoog F. 1962. A Revised Medium for Rapid Growth and Bio Assays with Tobacco Tissue Cultures. *Physiologia Plantarum* **15,** 473–497.

Ndamukong I, Abdallat AA, Thurow C *et al.* 2007. SA-inducible Arabidopsis glutaredoxin interacts with TGA factors and suppresses JA-responsive PDF1. 2 transcription. *The Plant Journal* **50,** 128–139.

Nguyen QB, Itoh K, van Vu B, Tosa Y, Nakayashiki H. 2011. Simultaneous silencing of endo-β-1, 4 xylanase genes reveals their roles in the virulence of Magnaporthe oryzae. *Molecular microbiology* **81,** 1008–1019.

Nicholson RL, Hammerschmidt R. 1992. Phenolic compounds and their role in disease resistance. *Annual review of phytopathology* **30,** 369–389.

Noguchi MT, Yasuda N, Fujita Y. 2006. Evidence of Genetic Exchange by Parasexual Recombination and Genetic Analysis of Pathogenicity and Mating Type of Parasexual Recombinants in Rice Blast Fungus, Magnaporthe oryzae. *Phytopathology* **96,** 746–750.

Novo M, Pomar F, Gayoso C, Merino F. 2006. Cellulase activity in isolates of Verticillium dahliae differing in aggressiveness. *Plant Disease* **90,** 155–160.

Nürnberger T, Lipka V. 2005. Non-host resistance in plants: new insights into an old phenomenon. *Molecular plant pathology* **6,** 335–345.

O'Connell RJ, Thon MR, Hacquard S *et al.* 2012. Lifestyle transitions in plant pathogenic Colletotrichum fungi deciphered by genome and transcriptome analyses. *Nature Genetics* **44,** 1060–1065.

Ogbourne S, Antalis TM. 1998. Transcriptional control and the role of silencers in transcriptional regulation in eukaryotes. *The Biochemical journal* **331 (Pt 1),** 1–14.

Orbach MJ, Farrall L, Sweigard JA, Chumley FG, Valent B. 2000. A telomeric avirulence gene determines efficacy for the rice blast resistance gene Pi-ta. *The Plant Cell* **12,** 2019–2032.

Parkhi V, Kumar V, Le Campbell AM, Bell AA, Rathore KS. 2010. Expression of Arabidopsis NPR1 in Transgenic Cotton Confers Resistance to Non-defoliating Isolates of Verticillium dahliae but not the Defoliating Isolates. *Journal of Phytopathology* **158,** 822–825.

Pegg GF, Brady BL. 2002. *Verticillium wilts*. Wallingford, Oxon, UK, New York: CABI Pub.

Penninckx IA, Eggermont K, Terras FR *et al.* 1996. Pathogen-induced systemic activation of a plant defensin gene in Arabidopsis follows a salicylic acid-independent pathway. *The Plant Cell* **8,** 2309–2323.

Petersen TN, Brunak S, Heijne G von, **Nielsen H.** 2011. SignalP 4.0: discriminating signal peptides from transmembrane regions. *Nature methods* **8,** 785–786.

Petre B, Kamoun S. 2014. How do filamentous pathogens deliver effector proteins into plant cells? *PLoS Biol* **12,** e1001801.

Phillips T. 2008. Regulation of transcription and gene expression in eukaryotes. *Nature Education* **1,** 199.

Pieterse CMJ, van der Does D, Zamioudis C, Leon-Reyes A, Van Wees, Saskia C M. 2012. Hormonal modulation of plant immunity. *Annual review of cell and developmental biology* **28,** 489–521.

Plett JM, Kemppainen M, Kale SD *et al.* 2011. A Secreted Effector Protein of Laccaria bicolor Is Required for Symbiosis Development. *Current Biology* **21,** 1197–1203.

Poulos TL, Finzel BC, Howard AJ. 1986. Crystal structure of substrate-free Pseudomonas putida cytochrome P-450. *Biochemistry* **25,** 5314–5322.

Poulos TL, Kraut J. 1980. A hypothetical model of the cytochrome c peroxidase. cytochrome c electron transfer complex. *Journal of Biological Chemistry* **255,** 10322–10330.

Pray LA. 2008. Transposons: The jumping genes. *Nature Education* **1,** 204.

Quevillon E, Silventoinen V, Pillai S *et al.* 2005. InterProScan: protein domains identifier. *Nucleic acids research* **33,** W116-20.

Raffaele S, Farrer RA, Cano LM *et al.* 2010a. Genome evolution following host jumps in the Irish potato famine pathogen lineage. *Science (New York, N.Y.)* **330,** 1540–1543.

Raffaele S, Kamoun S. 2012. Genome evolution in filamentous plant pathogens: why bigger can be better. *Nature reviews. Microbiology* **10,** 417–430.

Raffaele S, Win J, Cano LM, Kamoun S. 2010b. Analyses of genome architecture and gene expression reveal novel candidate virulence factors in the secretome of Phytophthora infestans. *BMC genomics* **11,** 637.

Ralhan A, Schöttle S, Thurow C *et al.* 2012. The vascular pathogen Verticillium longisporum requires a jasmonic acid-independent COI1 function in roots to elicit disease symptoms in Arabidopsis shoots. *Plant physiology* **159,** 1192–1203.

Ratzinger A, Riediger N, Tiedemann A von, **Karlovsky P.** 2009. Salicylic acid and salicylic acid glucoside in xylem sap of Brassica napus infected with Verticillium longisporum. *Journal of Plant Research* **122,** 571–579.

Razin A. 1998. CpG methylation, chromatin structure and gene silencing-a three-way connection. *The EMBO journal* **17,** 4905–4908.

Rep M, Van Der Does, H Charlotte, Meijer M *et al.* 2004. A small, cysteine-rich protein secreted by Fusarium oxysporum during colonization of xylem vessels is required for I-3-mediated resistance in tomato. *Molecular microbiology* **53,** 1373–1383.

Reusche M, Klásková J, Thole K *et al.* 2013. Stabilization of cytokinin levels enhances Arabidopsis resistance against Verticillium longisporum. *Molecular plant-microbe interactions MPMI* **26,** 850–860.

Reusche M, Thole K, Janz D *et al.* 2012. Verticillium infection triggers VASCULAR-RELATED NAC DOMAIN7–dependent de novo xylem formation and enhances drought tolerance in arabidopsis. *The Plant Cell* **24,** 3823–3837.

Reusche M, Truskina J, Thole K *et al.* 2014. Infections with the vascular pathogens Verticillium longisporum and Verticillium dahliae induce distinct disease symptoms and differentially affect drought stress tolerance of Arabidopsis thaliana. *Environmental and Experimental Botany* **108,** 23–37.

Rich A, Razin A, Cedar H, Riggs AD. 1984. *DNA Methylation*. New York, NY: Springer New York.

Ride JP. 1978. Role of cell wall alterations in resistance to fungi. *Annals of Applied Biology*.

Rouxel T, Grandaubert J, Hane JK *et al.* 2011. Effector diversification within compartments of the Leptosphaeria maculans genome affected by Repeat-Induced Point mutations. *Nature communications* **2,** 202.

Russo VEA, Martienssen RA, Riggs AD. 1996. *Epigenetic mechanisms of gene regulation*: Cold Spring Harbor Laboratory Press.

Saitou N, Nei M. 1987. The neighbor-joining method: a new method for reconstructing phylogenetic trees. *Molecular biology and evolution* **4,** 406–425.

Santhanam P, Thomma BP. 2013. Verticillium dahliae Sge1 differentially regulates expression of candidate effector genes. *Molecular Plant-Microbe Interactions* **26,** 249–256.

Scarpella E, Francis P, Berleth T. 2004. Stage-specific markers define early steps of procambium development in Arabidopsis leaves and correlate termination of vein formation with mesophyll differentiation. *Development (Cambridge, England)* **131,** 3445–3455.

Schirawski J, Mannhaupt G, Münch K *et al.* 2010. Pathogenicity determinants in smut fungi revealed by genome comparison. *Science (New York, N.Y.)* **330,** 1546–1548.

Schmidt SM, Houterman PM, Schreiver I *et al.* 2013. MITEs in the promoters of effector genes allow prediction of novel virulence genes in Fusarium oxysporum. *BMC genomics* **14,** 119.

Schmidt SM, Panstruga R. 2011. Pathogenomics of fungal plant parasites: what have we learnt about pathogenesis? *Current opinion in plant biology* **14,** 392–399.

Scholze H, Boch J. 2010. TAL effector-DNA specificity. *Virulence* **1,** 428–432.

Scholze H, Boch J. 2011. TAL effectors are remote controls for gene activation. *Current opinion in microbiology* **14,** 47–53.

Seidl MF, Thomma BP. 2014. Sex or no sex: evolutionary adaptation occurs regardless. *Bioessays* **36,** 335–345.

Shabab M, Shindo T, Gu C *et al.* 2008. Fungal effector protein AVR2 targets diversifying defense-related cys proteases of tomato. *The Plant Cell* **20,** 1169–1183.

Sharp PA, Sugden B, Sambrook J. 1973. Detection of two restriction endonuclease activities in Haemophilus parainfluenzae using analytical agarose-ethidium bromide electrophoresis. *Biochemistry* **12,** 3055–3063.

Showalter AM. 1993. Structure and function of plant cell wall proteins. *The Plant Cell* **5,** 9–23.

Soyer JL, El Ghalid M, Glaser N *et al.* 2014. Epigenetic control of effector gene expression in the plant pathogenic fungus Leptosphaeria maculans. *PLoS genetics* **10,** e1004227.

Spanu PD, Abbott JC, Amselem J *et al.* 2010. Genome expansion and gene loss in powdery mildew fungi reveal tradeoffs in extreme parasitism. *Science (New York, N.Y.)* **330,** 1543–1546.

Stanke M, Keller O, Gunduz I, Hayes A, Waack S, Morgenstern B. 2006. AUGUSTUS: ab initio prediction of alternative transcripts. *Nucleic acids research* **34,** W435-9.

Stergiopoulos I, Wit PJ de. 2009. Fungal effector proteins. *Annual review of phytopathology* **47,** 233–263.

Struhl K. 1999. Fundamentally different logic of gene regulation in eukaryotes and prokaryotes. *Cell* **98,** 1–4.

Sturn A, Quackenbush J, Trajanoski Z. 2002. Genesis: cluster analysis of microarray data. *Bioinformatics* **18,** 207–208.

Tada Y, Spoel SH, Pajerowska-Mukhtar K, Mou Z, Song J, Dong X. 2008. Plant immunity requires conformational changes of NPR1 via S-nitrosylation and thioredoxins. *Science*.

Takken F, Rep M. 2010. The arms race between tomato and Fusarium oxysporum. *Molecular plant pathology* **11,** 309–314.

Talboys PW. 1958. Association of tylosis and hyperplasia of the xylem with vascular invasion of the hop by Verticillium albo-atrum. *Transactions of the British Mycological Society* **41,** 249-IN8.

Tamura K, Nei M. 1993. Estimation of the number of nucleotide substitutions in the control region of mitochondrial DNA in humans and chimpanzees. *Molecular biology and evolution* **10,** 512–526.

Textor S, Gershenzon J. 2009. Herbivore induction of the glucosinolate–myrosinase defense system: Major trends, biochemical bases and ecological significance. *Phytochemistry Reviews* **8,** 149–170.

Thatcher LF, Manners JM, Kazan K. 2009. Fusarium oxysporum hijacks COI1-mediated jasmonate signaling to promote disease development in Arabidopsis. *The Plant Journal* **58,** 927–939.

Thurow C, Schiermeyer A, Krawczyk S, Butterbrodt T, Nickolov K, Gatz C. 2005. Tobacco bZIP transcription factor TGA2.2 and related factor TGA2.1 have distinct roles in plant defense responses and plant development. *The Plant Journal* **44,** 100–113.

Tien M, Kirk TK. 1984. Lignin-degrading enzyme from Phanerochaete chrysosporium: purification, characterization, and catalytic properties of a unique H2O2-requiring oxygenase. *Proceedings of the National Academy of Sciences* **81,** 2280–2284.

Tien M, Kirk TK, Bull C, Fee JA. 1986. Steady-state and transient-state kinetic studies on the oxidation of 3, 4-dimethoxybenzyl alcohol catalyzed by the ligninase of Phanerocheate chrysosporium Burds. *Journal of Biological Chemistry* **261,** 1687–1693.

Tien M, Tu CP. 1986. Cloning and sequencing of a cDNA for a ligninase from Phanerochaete chrysosporium. *Nature* **326,** 520–523.

Tischner R, Koltermann M, Hesse H, Plath M. 2010. Early responses of Arabidopsis thaliana to infection by Verticillium longisporum. *Physiological and Molecular Plant Pathology* **74,** 419–427.

Tjamos EC, Beckman CH. 1989. *Vascular Wilt Diseases of Plants*. Berlin, Heidelberg: Springer Berlin Heidelberg.

Tjamos SE, Flemetakis E, Paplomatas EJ, Katinakis P. 2005. Induction of resistance to Verticillium dahliae in Arabidopsis thaliana by the biocontrol agent K-165 and pathogenesis-related proteins gene expression. *Molecular plant-microbe interactions MPMI* **18,** 555–561.

Typas MA, HEALE JB. 1980. DNA Content of Germinating Spores, Individual Hyphal Cells and Resting Structure Cells of Verticillium spp. Measured by Microdensitometry. *Microbiology* **121,** 231–242.

Tzeng DD, Vay JE de. 1985. Physiological responses of Gossypium hirsutum L. to infection by defoliating and nondefoliating pathotypes of Verticillium dahliae Kleb. *Physiological plant pathology* **26,** 57–72.

Tzima AK, Paplomatas EJ, Rauyaree P, Ospina-Giraldo MD, Kang S. 2011. VdSNF1, the sucrose nonfermenting protein kinase gene of Verticillium dahliae, is required for virulence and expression of genes involved in cell-wall degradation. *Molecular Plant-Microbe Interactions* **24,** 129–142.

Uknes S, Mauch-Mani B, Moyer M *et al.* 1992. Acquired resistance in Arabidopsis. *The Plant Cell* **4,** 645–656.

Van de Wouw, Angela P, Cozijnsen AJ, Hane JK *et al.* 2010. Evolution of linked avirulence effectors in Leptosphaeria maculans is affected by genomic environment and exposure to resistance genes in host plants. *PLoS pathogens* **6,** e1001180.

van Esse HP, van't Klooster JW, Bolton MD *et al.* 2008. The Cladosporium fulvum virulence protein Avr2 inhibits host proteases required for basal defense. *The Plant Cell* **20,** 1948–1963.

van Tran T, Braus-Stromeyer SA, Timpner C, Braus GH. 2013. Molecular diagnosis to discriminate pathogen and apathogen species of the hybrid Verticillium longisporum on the oilseed crop Brassica napus. *Applied microbiology and biotechnology* **97,** 4467–4483.

van Vu B, Itoh K, Nguyen QB, Tosa Y, Nakayashiki H. 2012. Cellulases belonging to glycoside hydrolase families 6 and 7 contribute to the virulence of Magnaporthe oryzae. *Molecular Plant-Microbe Interactions* **25,** 1135–1141.

Vance CP, Kirk TK, Sherwood RT. 1980. Lignification as a mechanism of disease resistance. *Annual review of phytopathology* **18,** 259–288.

VanderMolen GE, Labavitch JM, Strand LL, DeVay JE. 1983. Pathogen-induced vascular gels: Ethylene as a host intermediate. *Physiologia Plantarum* **59,** 573–580.

Vellosillo T, Vicente J, Kulasekaran S, Hamberg M, Castresana C. 2010. Emerging complexity in reactive oxygen species production and signaling during the response of plants to pathogens. *Plant physiology* **154,** 444–448.

Veronese P, Narasimhan ML, Stevenson RA *et al.* 2003a. Identification of a locus controlling Verticillium disease symptom response in Arabidopsis thaliana. *The Plant Journal* **35,** 574–587.

Veronese P, Narasimhan ML, Stevenson RA *et al.* 2003b. Identification of a locus controlling Verticillium disease symptom response in Arabidopsis thaliana. *The Plant Journal* **35,** 574–587.

Walton JD. 1994. Deconstructing the cell wall. *Plant physiology* **104,** 1113.

Wariishi H, Valli K, Gold MH. 1989. Oxidative cleavage of a phenolic diarylpropane lignin model dimer by manganese peroxidase from Phanerochaete chrysosporium. *Biochemistry* **28,** 6017–6023.

Weiler EW, Kutchan TM, Gorba T, Brodschelm W, Niesel U, Bublitz F. 1994. The Pseudomonas phytotoxin coronatine mimics octadecanoid signalling molecules of higher plants. *FEBS letters* **345,** 9–13.

Whisson SC, Boevink PC, Moleleki L *et al.* 2007. A translocation signal for delivery of oomycete effector proteins into host plant cells. *Nature* **450,** 115–118.

Wildermuth MC, Dewdney J, Wu G, Ausubel FM. 2001. Isochorismate synthase is required to synthesize salicylic acid for plant defence. *Nature* **414,** 562–565.

Win J, Chaparro-Garcia A, Belhaj K *et al.* 2012. Effector biology of plant-associated organisms: concepts and perspectives. *Cold Spring Harbor symposia on quantitative biology* **77,** 235–247.

Witzel K, Hanschen FS, Klopsch R, Ruppel S, Schreiner M, Grosch R. 2015. Verticillium longisporum infection induces organ-specific glucosinolate degradation in Arabidopsis thaliana. *Frontiers in plant science* **6**.

Wong DWS. 2009. Structure and action mechanism of ligninolytic enzymes. *Applied Biochemistry and Biotechnology* **157,** 174–209.

Xu L, Zhu L, Tu L *et al.* 2011. Lignin metabolism has a central role in the resistance of cotton to the wilt fungus Verticillium dahliae as revealed by RNA-Seq-dependent transcriptional analysis and histochemistry. *Journal of experimental botany* **62,** 5607–5621.

Yadeta KA, Thomma BP. 2014. The xylem as battleground for plant hosts and vascular wilt pathogens. *Induced plant responses to microbes and insects,* 110.

Zander M, La Camera S, Lamotte O, Métraux J, Gatz C. 2010. Arabidopsis thaliana class-II TGA transcription factors are essential activators of jasmonic acid/ethylene-induced defense responses. *The Plant Journal* **61,** 200–210.

Zeise K, Tiedemann A von. 2002. Host Specialization among Vegetative Compatibility Groups of Verticillium dahliae in Relation to Verticillium longisporum. *Journal of Phytopathology* **150,** 112–119.

Zhang W, Li C, Qian C, Cao L. 2009. Studies on the responses of root, shoot and drought resistance in the seedlings of forage triticale to water stress. *Journal of Agricultural Science* **1,** 50.

Zhao Z, Liu H, Wang C, Xu J. 2014. Correction: Comparative analysis of fungal genomes reveals different plant cell wall degrading capacity in fungi. *BMC genomics* **15,** 6.

6 Supplemental material

Table S1: Whole-genome sequencing (WGS) properties of the *V. dahliae* isolate core collection.
Isolates of the diverse interaction classes used for genome sequencing were listed with their corresponding amount total sequences reads and the obtaines sequencing coverage. Information about the asymptomatic *V. dahliae* isolates marked in blue, about the early senescence inducing isolates in brown and the wilt inducing isolates in green.
[1]isolates marked with yellow background color have been sequenced by the group of Prof. Bart Thomma, University of Wageningen, Netherlands (Jonge *et al.*, 2012); asymptomatic isolates are marked with the prefix a-; early senescence inducing isolates are marked with the prefix s-; wilt inducing isolates are marked with the prefix w-; symbols indicate the intensity of disease symptom development: -/+ = mild symptoms, ++ = strong symptoms, +++ = very strong symptoms; d = cotton/olive defoliating, nd = cotton non-defoliating; [2]isolates s-ST100 and w-VdJR2 were used as reference strains for genome sequence comparison studies; [3]contigs of WGS approaches performed in this work were only provisionally *de novo* assembled, hence genome size was not available; [4] (Jonge *et al.*, 2012); [5](Jonge *et al.*, 2013); [6]information about sequenced reads and coverage of s-ST100 was not available.

Isolate[1]	Interaction class	Genome size [Mb]	Sequenced reads (in total)	Coverage (x-fold)
a-Vd8	asymptomatic	n.a.[3]	10.461.034	27
a-Vd39	asymptomatic	n.a.[3]	22.870.160	47
a-Vd42	asymptomatic	n.a.[3]	25.458.142	73
a-Vd52	asymptomatic	n.a.[3]	26.955.868	55
a-V152	asymptomatic	n.a.[3]	18.586.420	38
s-V76 (++; d)	early senescence	n.a.[3]	18.565.557	38
s-T9 (++; d)	early senescence	n.a.[3]	21.254.265	56
s-V138I (++; d)	early senescence	n.a.[3]	20.048.619	41
s-V781I (+++; d)	early senescence	n.a.[3]	18.960.701	38
w-V192I (-/+; nd)	wilting	n.a.[3]	24.231.235	49
w-V200I (-/+; nd)	wilting	n.a.[3]	21.829.282	44
w-DVD-S29 (+++)	wilting	34.1[4]	~11.000.000[4]	~30[4]
w-DVD31 (+++)	wilting	34[4]	~11.000.000[4]	~30[4]
s-ST100[2] (+++; d)	early senescence	35[5]	n.a.[6]	n.a.[6]
w-VdJR2[2] (+++; nd)	wilting	35.1[4]	~11.000.000[4]	~30[4]

Table S2: Top50 induced genes of the „early senescence“ or “wilting” pathosystem for the four different time points analysed in transcriptome studies.
Note that the incorporation of the Top50 induced genes for every time point resulted in a gene number larger than 50 (122 genes), since the Top50 candidates were only partially congruent among the diverse time points. Peptide prediction and identification of the corresponding w-VdLs.17 homologues was performed via CustomBlast with Geneious softwareTM (Pro v. 8.1.6; Biomatters Ltd., (Kearse et al., 2012)) against w-VdLs.17 transcriptome (BROAD Institute; (Klosterman et al., 2011)). (Conserved) hypothetical or predicted proteins with a length ≤ 400 aa which encode for possible candidate effectors are marked in **pink.** Possible cell wall modifying proteins are marked in **green**. Secretion signal presence or the possibility of non-classical secretion was studied for (conserved) hypothetical proteins ≤ 400 aa and cell wall modifying proteins via the SignalP 3.1 Server (http://www.cbs.dtu.dk/services/SignalP/; (Bendtsen et al., 2004b)) and the SecretomeP 2.0 Server (http://www.cbs.dtu.dk/services/SecretomeP/; (Bendtsen et al., 2004a)). N.t.: presence of secretion signal not tested. Selected CEs and CEL with their corresponding homologs were marked in **red.** Log2FC values for all Top50 induced genes and all four time points were scheduled. The log2FC values of the Top50 genes for the corresponding time points were marked in **bold.**

			Prediction				log2FC			
	Candidate effector (CE)	GeneID	w-VdLs.17 homologue	Putative function	Length [aa]	Secretion	4 dpi	8 dpi	12 dpi	16 dpi
induced in the "early senescence" pathosystem in comparison to "wilting" pathosystem		ST100.00190g00130	-	-	273	n.t.	5,7	**3,38**	**4,5**	**7,39**
		ST100.00196g00160	VDAG_01223T0	40S ribosomal protein S23	142	n.t.	4,97	**4,04**	**4,11**	**7,27**
		ST100.00077g00060	VDAG_10491T0	40S ribosomal protein S26E	122	n.t.	**6,22**	**2,85**	**4,37**	**7,67**
		ST100.00357g00100	VDAG_07532T0	40S ribosomal protein S5-B	280	n.t.	2,19	2,11	**3,84**	**6,3**
		ST100.00099g00090	VDAG_03283T0	60S acidic ribosomal protein P2	111	n.t.	5,63	2,32	**3,92**	**6,34**
		ST100.00138g00130	VDAG_01079T0	60S ribosomal protein L20	175	n.t.	0,96	2,1	2,85	**6,76**
		ST100.00160g00060	VDAG_06316T0	60S ribosomal protein L28	159	n.t.	**6**	**2,81**	**3,91**	**6,54**
		ST100.00273g00060	VDAG_04489T0	60S ribosomal protein L33-B	110	n.t.	5,93	**2,85**	**4,21**	6,28
		ST100.00373g00100	VDAG_02494T0	60S ribosomal protein L37	98	n.t.	2,67	2,04	3,53	**6,49**
		ST100.00048g00150	VDAG_08793T0	60S ribosomal protein L9	194	n.t.	5,6	1,49	**4,03**	**6,31**
		ST100.00011g00110	VDAG_02332T0	aconitate hydratase	789	n.t.	**6,56**	2,07	3,06	6,02
		ST100.00022g00320	VDAG_06226T0	alcohol dehydrogenase	342	n.t.	**6,13**	2,43	3,64	4,78
		ST100.00018g00260	VDAG_05976T0	alpha-amylase A type-1/2	463	n.t.	**7,21**	**2,93**	3,41	3,93
		ST100.00781g00030	VDAG_09411T0	amidohydrolase family protein	476	n.t.	-0,32	**2,65**	1,99	3,93
		ST100.00105g00120	VDAG_03160T0	ammonium transporter MEP1	519	n.t.	**6,92**	1,14	**4,75**	4,96
		ST100.00003g00320	VDAG_02041T0	aspartyl-tRNA synthetase	870	n.t.	4,73	2,28	3,57	**6,46**
		ST100.00201g00190	VDAG_02505T0	ATP synthase D chain, mitochondrial	174	n.t.	**6,26**	2,32	3,41	5,82
		ST100.00008g00400	VDAG_10347T0	ATP synthase subunit alpha	554	n.t.	5,88	2,49	3,55	**6,42**
		ST100.00179g00150	VDAG_09882T0	beta-Ig-H3/Fasciclin	348	n.t.	**6,56**	-0,49	0,57	2,38
		ST100.00005g00170	VDAG_02201T0	biotin synthase	414	n.t.	**6,73**	1,93	2,18	4,07
		ST100.00022g00120	VDAG_06207T0	carboxylesterase	563	n.t.	2,87	**3,38**	**6,36**	**7,08**
		ST100.00411g00030	VDAG_03371T0	carboxylic acid transport protein	520	n.t.	-0,8	**3,36**	3,52	5,38
		ST100.00037g00300	VDAG_07290T0	carboxypeptidase B	414	n.t.	**6,18**	0,49	-0,02	0,7
		ST100.00006g00520	VDAG_03661T0	catalase-1	755	n.t.	2,97	0,36	2,7	**6,29**
		ST100.00025g00120	VDAG_02980T0	cell wall protein PhiA	194	n.t.	2,4	0,26	1,91	**6,42**

induced in the "early senescence" pathosystem in comparison to "wilting" pathosystem										
	ST100.00739g00010	VDAG_09779T0	cell wall surface anchor signal protein	307	n.t.	**6,59**	0,85	**3,77**	6,2
	ST100.00024g00430	VDAG_02670T0	cerevisin	527	n.t.	**6,23**	2	2,91	5,98
	ST100.00012g00090	VDAG_07266T0	choline dehydrogenase	617	n.t.	**6,37**	2,2	2,75	4,29
	ST100.00149g00140	VDAG_05050T0	choline monooxygenase	422	n.t.	1,85	**3**	3,31	4,14
	ST100.00011g00350	VDAG_02308T0	coatomer subunit alpha	768	n.t.	3,17	**2,62**	**4,18**	**6,52**
	ST100.00201g00160	VDAG_02508T0	conserved hypothetical protein	104	no	2,84	0,26	1,83	**6,75**
	ST100.00167g00030	VDAG_07930T0	conserved hypothetical protein	155	no	2,65	**2,7**	3,7	5,64
CE2	ST100.00358g00100	VDAG_02735T0	conserved hypothetical protein	156	SignalP3.1	4,14	**3**	**5,54**	**10,18**
	ST100.00549g00050	VDAG_04712T0	conserved hypothetical protein	180	non-classically secreted	0,56	-0,26	1,91	**6,52**
CE10	ST100.00314g00060	VDAG_04407T0	conserved hypothetical protein	197	SignalP3.1	5,86	**4,38**	**4,81**	**6,86**
	ST100.00052g00080	VDAG_01121T0	conserved hypothetical protein	205	No	**6,21**	1,14	2,12	4,47
	ST100.00018g00330	VDAG_05983T0	conserved hypothetical protein	215	SignalP3.1	4,33	**3,68**	3,24	2,54
	ST100.00018g00200	VDAG_05970T0	conserved hypothetical protein	235	SignalP3.1	**6,86**	0,26	1,24	4,67
	ST100.00073g00020	VDAG_01288T0	conserved hypothetical protein	273	No	**6,17**	0	-0,02	-0,15
CE12	ST100.00992g00010	VDAG_05263T0	conserved hypothetical protein	282	non-classically secreted	5,18	1,46	**4,15**	**6,55**
	ST100.00244g00050	VDAG_02906T0	conserved hypothetical protein	292	SignalP3.1	3,52	**2,77**	1,91	1,41
	ST100.00008g00190	VDAG_10367T0	conserved hypothetical protein	295	SignalP3.1	4,26	**2,89**	2,91	4,43
	ST100.00612g00020	VDAG_02029T0	conserved hypothetical protein	314	SignalP3.1	**9,18**	0,68	0,66	1,74
CE4	ST100.00552g00080	VDAG_04352T0	conserved hypothetical protein	339	non-classically secreted	**6,9**	2	2,79	4,7
	ST100.00012g00100	VDAG_07265T0	conserved hypothetical protein	385	non-classically secreted	5,3	**3**	3,12	2,3
	ST100.00127g00090	VDAG_01339T0	conserved hypothetical protein	425	n.t.	**7,87**	2,26	**5,03**	**7,93**
	ST100.00499g00030	VDAG_09230T0	conserved hypothetical protein	426	n.t.	0,21	**3,69**	**3,93**	1,92
	ST100.00561g00090	VDAG_03755T0	conserved hypothetical protein	449	n.t.	2,55	1,85	**3,83**	5,87
	ST100.00034g00080	VDAG_09574T0	conserved hypothetical protein	491	n.t.	3,02	2,07	**3,97**	5,42
	ST100.00032g00110	VDAG_09529T0	conserved hypothetical protein	519	n.t.	0,03	1,25	**4,07**	4,49
	ST100.00133g00250	VDAG_02776T0	conserved hypothetical protein	567	n.t.	**6,36**	1	**3,96**	5,38
	ST100.00817g00010	VDAG_00424T0	conserved hypothetical protein	732	n.t.	4,86	**3,19**	**4,1**	**7,09**
	ST100.00067g00020	VDAG_05288T0	conserved hypothetical protein	764	n.t.	**6,63**	2,58	**4,1**	6
	ST100.00067g00130	VDAG_05257T0	conserved hypothetical protein	810	n.t.	**6,78**	2,49	**4,07**	**6,86**
	ST100.00725g00010	VDAG_05724T0	conserved hypothetical protein	932	n.t.	**6,43**	1,14	2,56	5,61
	ST100.00516g00140	VDAG_06395T0	conserved hypothetical protein	1425	n.t.	1,23	**2,72**	**4,72**	5,95
	ST100.00310g00150	VDAG_05375T0	covalently-linked cell wall protein	365	n.t.	2,61	1,38	2,36	**7,34**
	ST100.00259g00220	VDAG_10113T0	cross-pathway control protein	222	n.t.	**6,98**	**3,83**	**5,41**	**7,04**
	ST100.00060g00190	VDAG_03943T0	cyclopentanone 1,2-monooxygenase	565	n.t.	3,05	0	0,98	**6,94**
	ST100.00060g00130	VDAG_03938T0	cytochrome P450 52E2	529	n.t.	2,38	**2,85**	3,39	2,67

induced in the "early senescence" pathosystem in comparison to "wilting" pathosystem										
	ST100.00041g00210	VDAG_01531T0	diaminohydroxyphosphoribosylamino-pyrimidine deaminase	179	n.t.	**6,03**	1,93	3,24	4,25
	ST100.00205g00060	VDAG_00461T0	elongation factor 2	845	n.t.	1,8	1,42	3,36	**6,41**
	ST100.00085g00280	VDAG_07406T0	endoglucanase-1	303	non-classically secreted	**6,98**	1	1,75	4,25
	ST100.00025g00300	VDAG_02959T0	endoglucanase-4	363	SignalP3.1	2,91	0,68	**4,37**	5,93
	ST100.00023g00010	VDAG_06254T0	endoglucanase-5	324	SignalP3.1	**7,97**	0,49	1,12	4,76
	ST100.00194g00030	VDAG_07185T0	glucan 1,3-beta-glucosidase	358	SignalP3.1	3,27	**2,85**	2,66	2,45
	ST100.00200g00100	VDAG_09510T0	glucan 1,3-beta-glucosidase	405	SignalP3.1	2,1	2,1	**4,33**	**7,76**
	ST100.00443g00070	VDAG_03528T0	glucoamylase	636	n.t.	**6,53**	2,14	0,83	1,5
	ST100.00544g00060	VDAG_01467T0	glucose-repressible gene protein	72	n.t.	**7,79**	1	**3,89**	**7,44**
	ST100.00320g00060	VDAG_01819T0	glutamate decarboxylase	560	n.t.	**6,29**	1,85	1,75	4,95
	ST100.00096g00140	VDAG_05026T0	glutamyl-tRNA synthetase	627	n.t.	2,92	2,14	3,03	**6,3**
	ST100.00118g00010	VDAG_02710T0	high-affinity glucose transporter SNF3	556	n.t.	**7,64**	0,85	2,75	5,14
	ST100.00576g00020	VDAG_09414T0	histone H2A	135	n.t.	**6,28**	**3,56**	**4,76**	**6,75**
	ST100.00114g00090	VDAG_06910T0	hsp70-like protein	657	n.t.	**8,84**	2,49	**4,32**	**7,81**
	ST100.00567g00050	-	hypothetical protein	66	SignalP3.1	0,2	**2,78**	1,89	4,47
CE11	ST100.00104g00140	-	hypothetical protein	127	non-classically secreted	5,39	2,26	3,3	**6,61**
	ST100.00018g00090	-	hypothetical protein	198	No	0,9	**4,36**	2,43	**7,96**
CE7	ST100.00737g00020	-	hypothetical protein	249	non-classically secreted	**6,88**	**3,1**	**4,86**	**6,67**
CE8	ST100.00205g00130	VDAG_00454T0	hypothetical protein	65	non-classically secreted	**6,59**	**2,63**	3,47	5,56
	ST100.00841g00020	VDAG_04926T0	hypothetical protein	71	non-classically secreted	**5,99**	2,07	3,59	5,87
CE5	ST100.00260g00060	VDAG_02155T0	hypothetical protein	101	non-classically secreted	**8,37**	**2,85**	3,36	5,94
CE9	ST100.00088g00030	VDAG_03129T0	hypothetical protein	107	non-classically secreted	5,87	**2,58**	**3,94**	**6,23**
	ST100.00068g00250	VDAG_02103T0	hypothetical protein	145	SignalP3.1	0,71	0	**4,08**	6,12
CE6	ST100.00212g00110	VDAG_04125T0	hypothetical protein	188	SignalP3.1	**7,75**	**3,38**	**5,3**	**7,57**
	ST100.00586g00040	VDAG_04046T0	hypothetical protein	348	SignalP3.1	**6,13**	0,26	1,83	4,56
CE1	ST100.00067g00160	VDAG_05285T0	hypothetical protein	572	non-classically secreted	0,8	**4,61**	**6,06**	**6,51**
	ST100.00572g00020	VDAG_10047T0	ice nucleation protein	404	n.t.	4,58	2,26	**4,34**	**7,32**
	ST100.00212g00080	VDAG_04122T0	inorganic pyrophosphatase	486	n.t.	5,54	1,94	3,48	**7,23**
	ST100.00630g00010	VDAG_07280T0	LEA domain-containing protein	1239	n.t.	4,42	0	2,41	**6,51**
CEL	ST100.00022g00100	VDAG_06204T0	ligninase H8	353	SignalP3.1	1,81	**7,16**	**6,88**	5,02
	ST100.00533g00020	VDAG_01771T0	low affinity copper transporter	198	n.t.	**6,33**	0	1,12	3,01
	ST100.00024g00230	VDAG_02649T0	mannan endo-1,6-alpha-mannosidase DCW1	561	SignalP3.1	**6,36**	1,38	3,49	**6,85**
	ST100.00369g00010	VDAG_05354T0	metalloproteinase	387	n.t.	5,25	**3,58**	**4,33**	4,59
	ST100.00605g00020	VDAG_05293T0	multidrug resistance protein CDR1	1471	n.t.	1,16	**2,84**	3,12	2,85
	ST100.00102g00060	VDAG_05703T0	NAD-specific glutamate dehydrogenase	1083	n.t.	0,21	**2,65**	2,31	4,75

induced in the "early senescence" pathosystem in comparison to "wilting" pathosystem		ST100.00009g00400	VDAG_02834T0	peroxidase/catalase	763	n.t.	1,73	**2,94**	3,43	4,73
		ST100.00222g00160	VDAG_03328T0	phosphoglucomutase	554	n.t.	**6,05**	0,49	3,08	5,77
		ST100.00016g00340	VDAG_07727T0	polysaccharide deacetylase family protein	436	non-classically secreted	2,89	**3,64**	**4,66**	6,03
		ST100.00156g00210	VDAG_02705T0	predicted protein	73	SignalP3.1	1,8	**4,68**	**3,82**	3,74
	CE3	ST100.00508g00020	VDAG_10515T0	predicted protein	128	SignalP3.1	0,85	**5,02**	**4,03**	2,26
		ST100.00395g00100	VDAG_01905T0	predicted protein	177	SignalP3.1	0,81	**2,77**	1,74	2,49
		ST100.00129g00100	VDAG_02371T0	predicted protein	211	non-classically secreted	2,64	**2,72**	1,47	3,12
		ST100.00458g00030	VDAG_10210T0	predicted protein	295	No	5,3	1,85	**3,81**	6,06
		ST100.00002g00420	VDAG_08213T0	predicted protein	696	n.t.	2,75	**3,14**	**4**	5,76
		ST100.00458g00070	VDAG_09170T0	protein kinase domain-containing protein	443	n.t.	**5,99**	2,54	**3,98**	5,81
		ST100.00217g00160	VDAG_06028T0	rds1	466	n.t.	0,69	0	1,36	**6,99**
		ST100.00421g00110	VDAG_04042T0	regulatory protein cys-3	276	n.t.	**6,36**	1,26	3,33	5,26
		ST100.00529g00030	VDAG_06717T0	S-(hydroxymethyl)glutathione dehydrogenase	532	n.t.	0,08	-1	3,02	**6,71**
		ST100.00062g00230	VDAG_07969T0	secreted glucosidase	338	SignalP3.1	1,69	**3,26**	2,41	1,58
		ST100.00032g00140	VDAG_09532T0	serine 3-dehydrogenase	261	n.t.	3,28	2	**4,45**	4,49
		ST100.00100g00110	VDAG_00824T0	serine hydroxymethyltransferase	484	n.t.	5,81	**2,72**	3,72	**7,32**
		ST100.00429g00020	VDAG_06310T0	serine/threonine-protein kinase ksp1	635	n.t.	**6,68**	**2,96**	3,56	6,05
		ST100.00670g00030	VDAG_09836T0	sodium transport ATPase	1073	n.t.	**7,17**	**2,85**	**4,75**	**6,59**
		ST100.00214g00160	VDAG_03786T0	TOXD	345	n.t.	1,96	1,14	2,03	**6,47**
		ST100.00343g00010	VDAG_03738T0	translationally-controlled tumor protein	171	n.t.	**6,23**	2,32	3,33	**6,37**
		ST100.00029g00010	VDAG_04559T0	transport protein SEC23	949	n.t.	5,87	**2,72**	3,56	**6,44**
		ST100.00034g00100	VDAG_09572T0	TRI15	311	n.t.	2,43	2,07	**4,49**	5,29
		ST100.00794g00010	VDAG_09498T0	trichothecene 3-O-acetyltransferase	297	n.t.	0,44	1,93	**4,54**	5,95
		ST100.00593g00030	VDAG_02764T0	urea active transporter	685	n.t.	**6,3**	0,68	0,24	0,51
		ST100.00015g00150	VDAG_06686T0	WD repeat-containing protein 5B	320	n.t.	**6,17**	**3,41**	**4,05**	**6,51**
		ST100.00462g00020	VDAG_00057T0	zinc-regulated transporter 1	317	n.t.	**8,27**	0,68	0,66	4,05
		VDAG_04886	-	1-aminocyclopropane-1-carboxylate synthase	425	n.t.	-6,95	-1,77	-2,69	**-3,86**
		VDAG_01223	-	40S ribosomal protein S23	142	n.t.	**-9,11**	**-4,33**	**-5,17**	**-5,06**
		VDAG_10491	-	40S ribosomal protein S26E	122	n.t.	**-8,3**	**-3,61**	**-4,16**	**-5,05**
		VDAG_07532	-	40S ribosomal protein S5-B	213	n.t.	**-7,97**	**-2,7**	-2,92	-3,1
		VDAG_03591	-	40S ribosomal protein S7	202	n.t.	-7,8	-2,32	**-3,3**	**-3,82**
		VDAG_02440	-	40S ribosomal protein S9	192	n.t.	**-7,82**	-2,62	-2,42	-3,31
		VDAG_04294	-	60S acidic ribosomal protein P0	313	n.t.	-7,76	**-3,5**	**-4**	**-4,6**
		VDAG_06690	-	60S ribosomal protein L19	194	n.t.	-7,82	**-3**	**-3,36**	**-4,81**
		VDAG_01079	-	60S ribosomal protein L20	210	n.t.	-7,46	**-2,91**	**-3,56**	**-3,93**

induced in the "wilting" pathosystem in comparison to "early senescence" pathosystem										
	VDAG_02441	-	60S ribosomal protein L21-B	161	n.t.	-7,36	-2,26	**-3,04**	**-4,17**
	VDAG_04489	-	60S ribosomal protein L33-B	110	n.t.	-7,34	-2,38	-2,85	**-3,76**
	VDAG_02494	-	60S ribosomal protein L37	98	n.t.	**-8,13**	**-3,72**	**-4,51**	**-5,06**
	VDAG_05789	-	60S ribosomal protein L39	52	n.t.	**-8,04**	-2,58	**-3,41**	**-4,09**
	VDAG_09104	-	ABC transporter CDR4	1510	n.t.	**-8,13**	-2,07	-2,44	-3,67
	VDAG_07535	-	ADP,ATP carrier protein	311	n.t.	-7,41	**-3,71**	**-3,56**	-2,86
	VDAG_09583	-	alcohol oxidase	650	n.t.	-0,59	-2,7	**-3,72**	-2,18
	VDAG_03160	-	ammonium transporter MEP1	515	n.t.	**-8,26**	-1,77	-1,85	-3,46
	VDAG_10347	-	ATP synthase subunit alpha	554	n.t.	-7	-1,42	**-3,3**	**-3,96**
	VDAG_07681	-	ATP-binding cassette sub-family G member 5	626	n.t.	-5,08	**-3,1**	**-3,12**	-3,6
	VDAG_04288	-	ATP-dependent RNA helicase eIF4A	398	n.t.	-7,07	-2,38	-2,46	**-3,95**
	VDAG_05014	-	calcium-transporting ATPase	1057	n.t.	-1,53	-0,68	-1,59	**-4,02**
	VDAG_02935	-	calcium-transporting ATPase	1084	n.t.	-5,78	**-3**	**-3,72**	**-4,36**
	VDAG_06207	-	carboxylesterase	563	n.t.	-1,61	-2,26	**-3,04**	-2,82
	VDAG_09727	-	cellulose-growth-specific protein	436	SignalP3.1	-5,14	-1,26	-2,77	**-4,18**
	VDAG_09386	-	CipC protein	130	n.t.	**-8,07**	-1,26	-1,39	-2,25
	VDAG_02308	-	coatomer subunit alpha	1199	n.t.	-7,35	**-2,93**	-2,93	**-3,97**
	VDAG_05411	-	cobW domain-containing protein	553	n.t.	**-8,33**	0	-0,02	-0,61
	VDAG_06662	-	conserved hypothetical protein	66	n.t.	-4,47	**-2,77**	-2,27	-2,68
	VDAG_07701	-	conserved hypothetical protein	139	SignalP3.1	**-9,07**	-1,58	-2,34	-3,07
	VDAG_00215	-	conserved hypothetical protein	151	non-classically secreted	-5,05	-1,26	-1,78	**-4,05**
CE2	VDAG_02735	-	conserved hypothetical protein	156	SignalP3.1	-3,75	**-6,96**	**-6,09**	**-6,82**
	VDAG_07229	-	conserved hypothetical protein	159	No	**-8,85**	0	-0,28	-0,95
CE10	VDAG_04407	-	conserved hypothetical protein	197	SignalP3.1	-5,43	**-3,51**	-2,68	**-3,56**
	VDAG_04894	-	conserved hypothetical protein	305	No	**-10,09**	**-3,32**	**-3,78**	**-4,37**
	VDAG_03242	-	conserved hypothetical protein	309	non-classically secreted	-7,51	**-3,1**	-2,38	**-3,86**
CE4	VDAG_04352	-	conserved hypothetical protein	339	non-classically secreted	**-8,02**	-1	-1,27	-2,68
	VDAG_01109	-	conserved hypothetical protein	362	SignalP3.1	-5,88	**-3,14**	-2,6	-2,84
	VDAG_06039	-	conserved hypothetical protein	389	SignalP3.1	**-7,97**	-1,58	-2,21	-2,32
	VDAG_01339	-	conserved hypothetical protein	419	n.t.	**-8,19**	-1,87	**-3,52**	**-5,01**
	VDAG_09803	-	conserved hypothetical protein	477	n.t.	**-8,26**	0	-0,28	-0,95
	VDAG_09574	-	conserved hypothetical protein	491	n.t.	-6,22	**-4,22**	**-3,64**	-2,99
	VDAG_09230	-	conserved hypothetical protein	572	n.t.	**-8**	**-3,2**	**-3,17**	**-3,81**
	VDAG_02399	-	conserved hypothetical protein	780	n.t.	**-8,03**	-0,26	-0,53	-0,78
	VDAG_10113	-	cross-pathway control protein	222	n.t.	**-8,33**	**-4,1**	**-4,67**	**-5,26**

induced in the "wilting" pathosystem in comparison to "early senescence" pathosystem										
	VDAG_03943	-	cyclopentanone 1,2-monooxygenase	556	n.t.	-2,48	0	-0,28	**-3,8**
	VDAG_01919	-	dienelactone hydrolase family protein	255	n.t.	-7,29	-2,26	-2,14	**-3,63**
	VDAG_02559	-	elongation factor 1-alpha	474	n.t.	**-8**	**-3,91**	**-3,92**	-3,43
	VDAG_00461	-	elongation factor 2	845	n.t.	-7,81	**-3,49**	**-4,12**	**-3,93**
	VDAG_02959	-	endoglucanase-4	338	SignalP3.1	-5,66	-1,49	**-3,2**	**-5,27**
	VDAG_06254	-	endoglucanase-5	324	SignalP3.1	**-8,76**	0	-0,02	-1,13
	VDAG_04977	-	endopolygalacturonase	371	n.t.	**-9,55**	-0,49	-1,39	-3,05
	VDAG_00499	-	endothiapepsin	410	n.t.	**-8,16**	0	-0,02	-0,38
	VDAG_02832	-	FAD binding domain-containing protein	535	n.t.	**-8,68**	-1,58	-2,15	-3,26
	VDAG_07622	-	fasciclin domain family	441	n.t.	-5,15	**-2,93**	-1,69	-2,07
	VDAG_06992	-	ferric reductase transmembrane component 4	727	n.t.	**-8,38**	0	-0,86	-0,78
	VDAG_02046	-	ferric reductase transmembrane component 5	654	n.t.	**-8,32**	-0,26	-1,02	-1,78
	VDAG_00973	-	fumarate reductase	622	n.t.	**-8,07**	**-2,85**	**-3,11**	**-3,66**
	VDAG_05550	-	general alpha-glucoside permease	539	n.t.	**-8,4**	-2,2	-1,6	-2,82
	VDAG_09510	-	glucan 1,3-beta-glucosidase	520	SignalP3.1	-6,5	**-4,05**	-2,9	-1,11
	VDAG_01467	-	glucose-repressible gene protein	72	n.t.	-2,84	**-2,89**	-1,77	**-4,23**
	VDAG_06784	-	glutamate synthase	1333	n.t.	**-7,86**	-2,38	-2,27	**-3,54**
	VDAG_08916	-	glyceraldehyde-3-phosphate dehydrogenase	339	n.t.	-7,72	**-3,06**	**-3,33**	**-4,48**
	VDAG_06037	-	GPR1/FUN34/yaaH family protein	306	n.t.	**-8,21**	-1	-1,15	-2,38
	VDAG_08683	-	GTP-binding protein EsdC	327	n.t.	**-8,02**	-0,85	-2,01	-3,02
	VDAG_05732	-	guanine nucleotide-binding protein subunit alpha	354	n.t.	-7,41	-2,37	**-3,29**	-3,13
	VDAG_09071	-	high-affinity glucose transporter RGT2	546	n.t.	-7,34	**-3,2**	**-3,04**	-2,9
	VDAG_01193	-	high-affinity nicotinic acid transporter	499	n.t.	**-8,94**	-0,49	-0,7	-0,95
	VDAG_09414	-	histone H2A	135	n.t.	**-8,23**	**-3,46**	**-3,7**	**-3,97**
	VDAG_06910	-	hsp70-like protein	652	n.t.	**-8,47**	**-3,04**	**-4,17**	-3,17
	VDAG_09109	-	hypothetical protein	32	No	**-7,87**	**-2,63**	-2,86	-3,4
	VDAG_02430	-	hypothetical protein	55	non-classically secreted	**-8,13**	-0,68	-0,02	-2,74
	VDAG_01802	-	hypothetical protein	64	non-classically secreted	-7,1	**-3,56**	**-3,91**	**-3,81**
CE8	VDAG_00454	-	hypothetical protein	65	non-classically secreted	-7,62	**-3,17**	**-3,59**	**-4,02**
	VDAG_02753	-	hypothetical protein	77	non-classically secreted	-0,09	-0,49	-0,69	**-3,91**
	VDAG_05961	-	hypothetical protein	89	SignalP3.1	**-9,76**	**-5,35**	**-5,86**	**-5,75**
CE9	VDAG_03129	-	hypothetical protein	107	non-classically secreted	-7,32	**-2,84**	-2,88	-2,6
	VDAG_02103	-	hypothetical protein	145	SignalP3.1	-0,3	**-5,6**	**-4,7**	**-5,5**
	VDAG_05180	-	hypothetical protein	146	SignalP3.1	-7,81	-1,38	-2,62	**-4,95**
	VDAG_08653	-	hypothetical protein	155	SignalP3.1	**-9,07**	-2	-2,59	**-4,78**

induced in the "wilting" pathosystem in comparison to "early senescence" pathosystem										
		VDAG_06439	-	hypothetical protein	306	No	-5,74	-2,49	**-3,7**	**-4,61**
		VDAG_10047	-	ice nucleation protein	406	n.t.	**-7,94**	-2,46	**-3,7**	**-4,1**
		VDAG_04122	-	inorganic pyrophosphatase	291	n.t.	**-8,24**	**-3,17**	**-3,55**	-2,85
		VDAG_05103	-	isochorismatase hydrolase	191	n.t.	**-8,67**	-1	-0,7	-1,43
	CEL	VDAG_06204	-	ligninase H8	353	SignalP3.1	-1,48	**-5,29**	**-4,67**	**-5,58**
		VDAG_01167	-	multidrug resistance protein CDR1	1518	n.t.	-0,48	**-3,2**	**-3,81**	**-4,67**
		VDAG_05703	-	NAD-specific glutamate dehydrogenase	1054	n.t.	-6,82	**-2,89**	-1,51	-3,18
		VDAG_09523	-	pectate lyase D	234	SignalP3.1	0,44	-1,14	**-3**	**-5,13**
		VDAG_07238	-	pectin lyase	377	SignalP3.1	**-9,55**	-0,26	-1,7	-3,29
		VDAG_07583	-	phosphate-repressible phosphate permease	622	n.t.	-7,69	-1,77	**-3,12**	**-4,94**
		VDAG_07142	-	polysaccharide deacetylase family protein	248	SignalP3.1	-6,87	-2,38	**-3,38**	**-4,36**
	CE3	VDAG_10515	-	predicted protein	128	SignalP3.1	-1,08	**-3,41**	-2,81	-2,99
		VDAG_02256	-	predicted protein	135	SignalP3.1	-4,9	**-2,81**	-1,94	-2,06
		VDAG_05817	-	predicted protein	155	non-classically secreted	**-7,86**	**-2,58**	**-3,54**	-3,21
		VDAG_02230	-	predicted protein	165	SignalP3.1	0,44	**-3,32**	-0,02	-3,27
		VDAG_06168	-	predicted protein	472	n.t.	-3,8	0	**-3**	-0,37
		VDAG_08100	-	serin endopeptidase	841	n.t.	**-10,09**	-1	-1,54	-1,41
		VDAG_00824	-	serine hydroxymethyltransferase	484	n.t.	-7,03	**-2,72**	-2,33	-3,24
		VDAG_04892	-	short chain dehydrogenase	237	n.t.	**-10,64**	**-4,52**	**-4,02**	**-4,92**
		VDAG_09805	-	siderophore iron transporter mirB	585	n.t.	**-9,22**	-0,26	-1,3	-1,27
		VDAG_09836	-	sodium transport ATPase	1073	n.t.	**-8,03**	**-3,1**	-2,97	**-4,46**
		VDAG_01137	-	STI35 protein	319	n.t.	-7,81	-2,49	**-3**	-2,88
		VDAG_03738	-	translationally-controlled tumor protein	171	n.t.	-7,72	**-2,96**	**-3,04**	**-3,42**
		VDAG_05595	-	ubiquitin	230	n.t.	**-8,19**	**-3**	**-3,73**	-2,81
		VDAG_06686	-	WD repeat-containing protein 5B	317	n.t.	**-8,22**	**-2,95**	**-3,26**	-3,23

Table S3: Normalized RNA-seq reads of the selected candidate effector genes in the different transcriptome samples for all analysed time points.

RNA-seq reads of the candidate effectors (CEs) were normalized by calculation of reads per million (RPM) for each sample of mock-treated or *V. dahliae* infected plants; *V. dahliae* isolates representing the "early senescence" interaction class are highlighted in **brown**; *V. dahliae* isolates representing the "wilting" interaction class are highlighted in **dark green**; the reference isolate w-VdJR2 is highlighted in **green**; early senescence inducing isolates are marked with the prefix s-; wilt inducing isolates are marked with the prefix w-; symbols indicate the intensity of disease symptom development: -/+ = mild symptoms, + = moderate symptoms, ++ = strong symptoms, +++ = very strong symptoms. d = cotton/olive defoliating, nd = cotton non-defoliating; RPM values were conditionally formatted via a graded color scale: RPM values coloured in green indicate low amount of RNA-seq reads, RPM values coloured in red indicate high amount of RNA-seq reads; RPM values of infected samples ≤ RPM values of mock-treated samples are marked in **bold** and indicate no RNA-seq reads.

CE	Gene ID	Time point	Mock	s-V76 (++; d)	s-T9 (++; d)	s-ST100 (+++; d)	s-V138I (++; d)	s-V781I (+++; d)	w-VdJR2 (+++)	w-VdLs.17 (+)	w-DVD-S29 (+++)	w-DVD31 (+++)	w-V192I (-/+; nd)
CEL	ST100.00022g00100	4 dpi	93	**33**	**27**	**35**	**14**	**31**	**11**	**5**	**6**	**35**	**23**
		8 dpi	110	2608	11453	132	8151	9129	3223	**94**	1507	2024	1894
		12 dpi	94	513	2170	173	3877	9450	1919	1266	361	1240	754
		16 dpi	95	**83**	131	598	**27**	2807	2308	1285	499	1097	808
CE1	ST100.00067g00160	4 dpi	109	3619	669	1279	1112	2871	1457	3119	**5**	**7**	**12**
		8 dpi	95	3702	419	882	1616	1621	305	**94**	**79**	**75**	**73**
		12 dpi	125	4158	2100	2156	2231	4582	402	226	**72**	**71**	**69**
		16 dpi	95	2635	555	3255	3642	5095	652	866	**83**	110	**73**
CE2	ST100.00358g00100	4 dpi	124	**33**	**27**	**35**	425	**22**	**90**	**57**	**31**	**32**	**88**
		8 dpi	95	322	419	573	184	211	10857	**94**	516	3899	6922
		12 dpi	125	1720	420	1635	475	2309	5415	949	613	3861	788
		16 dpi	110	22684	6337	3484	23266	6368	14026	4930	333	2963	2790
CE3	ST100.00508g00020	4 dpi	93	**13**	**18**	**35**	**14**	**18**	**11**	**3**	**2**	**18**	**41**
		8 dpi	95	869	761	**88**	3488	811	271	**94**	635	525	656
		12 dpi	94	128	280	**74**	622	984	248	**90**	216	602	240
		16 dpi	95	**64**	**65**	**53**	**8**	235	282	239	125	402	184
CE4	ST100.00552g00080	4 dpi	109	1018	840	753	970	1343	1406	1197	1033	1245	1133
		8 dpi	95	354	152	**88**	**73**	211	**68**	**94**	**79**	**75**	255
		12 dpi	110	462	140	**74**	**110**	215	**93**	**90**	216	**71**	137
		16 dpi	95	413	261	141	130	594	282	**90**	291	**73**	294
CE5	ST100.00260g00060	4 dpi	93	2640	3794	1875	1459	3391	**11**	**10**	**7**	**81**	**53**
		8 dpi	110	483	266	132	367	211	**68**	**94**	**79**	112	**73**
		12 dpi	94	231	210	372	183	394	**93**	**90**	**72**	**71**	**69**
		16 dpi	95	375	359	493	586	445	**53**	**60**	**83**	110	**73**
CE6	ST100.00212g00110	4 dpi	124	1563	3307	3241	2543	1678	1710	1627	1155	1781	1075
		8 dpi	110	451	761	309	661	670	746	**94**	317	300	474
		12 dpi	110	1283	840	1487	768	1808	928	136	397	461	685
		16 dpi	95	2889	1372	1443	2526	2350	987	329	291	549	441

CE7	ST100.00737g00020	4 dpi	47	775	669	456	460	832	6	2	1	4	6
		8 dpi	63	418	152	88	220	634	34	47	40	37	36
		12 dpi	47	719	105	372	256	1682	31	45	36	35	34
		16 dpi	47	1016	327	598	612	1805	18	30	42	37	37
CE8	ST100.00205g00130	4 dpi	140	1110	461	368	290	890	1159	882	595	1634	2390
		8 dpi	110	290	152	88	330	458	611	142	79	525	801
		12 dpi	125	308	210	99	146	626	805	136	180	567	514
		16 dpi	95	679	229	194	423	606	670	418	333	146	698
CE9	ST100.00088g00030	4 dpi	93	282	714	543	482	348	1271	1430	992	929	605
		8 dpi	110	290	342	132	110	423	611	94	555	225	291
		12 dpi	125	308	280	719	146	555	526	181	144	461	377
		16 dpi	95	876	327	545	1041	742	1322	448	416	695	294
CE10	ST100.00314g00060	4 dpi	109	322	298	210	652	207	298	235	89	77	117
		8 dpi	95	483	1522	353	881	775	1323	94	198	375	219
		12 dpi	110	539	455	644	695	1217	619	90	108	354	69
		16 dpi	95	1454	1307	774	737	890	599	359	125	293	184
CE11	ST100.00104g00140	4 dpi	47	276	262	228	212	418	11	2	1	4	6
		8 dpi	47	322	266	44	73	141	34	47	40	37	36
		12 dpi	47	385	245	248	110	268	31	45	36	35	34
		16 dpi	47	895	196	246	897	742	18	30	42	37	37
CE12	ST100.00992g00010	4 dpi	93	394	479	280	496	396	11	5	126	337	170
		8 dpi	95	386	152	88	73	247	68	94	119	375	109
		12 dpi	94	642	105	273	146	931	62	90	325	106	171
		16 dpi	95	826	163	545	831	767	35	60	83	110	147
CE13	ST100.01886g00010	4 dpi	93	33	27	53	135	18	11	5	2	7	12
		8 dpi	95	225	76	176	110	247	136	94	79	75	73
		12 dpi	94	308	105	50	219	501	248	90	72	71	69
		16 dpi	95	438	131	229	178	544	247	60	83	73	73

Table S4: Mapping of the reads derived from RNA-seq approaches to the genomes of early senescence and wilt inducing *V. dahliae* isolates of the core collection.
RNA-seq reads encoding the genes of CEL (ST100.00022g00100) and CE1 (ST100.00067g00160) were mapped to the genomes of the early senescence and the wilting interaction class; *V. dahliae* isolates representing the "early senescence" interaction class are highlighted in **brown**; *V. dahliae* isolates representing the "wilting" interaction class are highlighted in **dark green**; early senescence inducing isolates are marked with the prefix s-; wilt inducing isolates are marked with the prefix w-; symbols indicate the intensity of disease symptom development: -/+ = mild symptoms, ++ = strong symptoms, +++ = very strong symptoms; d = cotton/olive defoliating, nd = cotton non-defoliating; alignment lengths of ≥ 90 bp mapping to the candidate genes and are marked in **red**.

Gene ID	*V. dahliae* genome	Identity [%]	Alignment length	Mismatches	Gap openings	Query start	Query end	Sequence start	Sequence end	E-value	Score Bits
CEL											
ST100.00022g00100.1	s-V781I (+++, d)	100.00	970	0	0	1	970	10391736	10390767	0.0	1923
ST100.00022g00100.1	s-V781I (+++, d)	100.00	90	0	0	970	1059	10390696	10390607	4,00E-43	178
ST100.00022g00100.1	s-V781I (+++, d)	100.00	18	0	0	667	684	18579554	18579537	42066	36.2
ST100.00022g00100.1	s-V138I (++, d)	100.00	970	0	0	1	970	21567180	21566211	0.0	1923
ST100.00022g00100.1	s-V138I (++, d)	100.00	90	0	0	970	1059	21566140	21566051	4,00E-43	178
ST100.00022g00100.1	s-V138I (++, d)	100.00	18	0	0	667	684	20141635	20141618	42066	36.2
ST100.00022g00100.1	s-T9 (++, d)	100.00	970	0	0	1	970	19910966	19911935	0.0	1923
ST100.00022g00100.1	s-T9 (++, d)	100.00	90	0	0	970	1059	19912006	19912095	4,00E-43	178
ST100.00022g00100.1	s-T9 (++, d)	100.00	18	0	0	667	684	10517844	10517827	42066	36.2
ST100.00022g00100.1	s-V76 (++, d)	100.00	970	0	0	1	970	29828454	29829423	0.0	1923
ST100.00022g00100.1	s-V76 (++, d)	100.00	90	0	0	970	1059	29829494	29829583	4,00E-43	178
ST100.00022g00100.1	s-V76 (++, d)	100.00	18	0	0	667	684	26331123	26331140	42066	36.2
ST100.00022g00100.1	w-V192I (-/+, nd)	98.87	970	11	0	1	970	15395336	15394367	0.0	1836
ST100.00022g00100.1	w-V192I (-/+, nd)	100.00	90	0	0	970	1059	15394296	15394207	4,00E-43	178
ST100.00022g00100.1	w-V192I (-/+, nd)	100.00	18	0	0	667	684	14343508	14343491	42066	36.2
ST100.00022g00100.1	w-DVD-S29 (+++)	98.87	970	11	0	1	970	22581	21612	0.0	1836
ST100.00022g00100.1	w-DVD-S29 (+++)	100.00	90	0	0	970	1059	21541	21452	4,00E-43	178
ST100.00022g00100.1	w-DVD-S29 (+++)	100.00	18	0	0	667	684	11358	11375	42066	36.2
ST100.00022g00100.1	w-DVD31 (+++)	98.87	970	11	0	1	970	27788	26819	0.0	1836
ST100.00022g00100.1	w-DVD31 (+++)	100.00	90	0	0	970	1059	26748	26659	4,00E-43	178
ST100.00022g00100.1	w-DVD31 (+++)	100.00	18	0	0	667	684	17156	17139	42066	36.2
CE1											
ST100.00067g00160.1	s-V781I (+++, d)	98.63	1241	16	1	1308	2547	26594279	26595519	0.0	2317
ST100.00067g00160.1	s-V781I (+++, d)	99.21	1133	8	1	1	1132	11386294	11387426	0.0	2167
ST100.00067g00160.1	s-V781I (+++, d)	99.65	286	1	0	1077	1362	3403586	3403871	2E-157	559

ST100.00067g00160.1	s-V781I (+++, d)	97.54	285	7	0	1078	1362	32128803	32129087	2E-142	509
ST100.00067g00160.1	s-V781I (+++, d)	88.30	94	11	0	1847	1940	28205517	28205424	6E-19	99.6
ST100.00067g00160.1	s-V781I (+++, d)	86.67	90	12	0	1851	1940	28233365	28233276	4E-14	83.8
ST100.00067g00160.1	s-V781I (+++, d)	100.00	80	0	0	2493	2572	3453339	3453418	8E-37	159
ST100.00067g00160.1	s-V781I (+++, d)	98.75	80	1	0	2493	2572	26627829	26627908	2E-34	151
ST100.00067g00160.1	s-V781I (+++, d)	84.06	69	11	0	1150	1218	22386873	22386941	0,0005	50.1
ST100.00067g00160.1	s-V781I (+++, d)	87.18	39	5	0	2092	2130	27388955	27388993	2.0	38.2
ST100.00067g00160.1	s-V781I (+++, d)	96.77	31	1	0	2033	2063	28233183	28233153	0,00003	54.0
ST100.00067g00160.1	s-V781I (+++, d)	100.00	26	0	0	1	26	25118286	25118311	0,0001	52.0
ST100.00067g00160.1	s-V781I (+++, d)	95.45	22	1	0	1559	1580	31075920	31075899	42012	36.2
ST100.00067g00160.1	s-V781I (+++, d)	100.00	19	0	0	843	861	23152408	23152390	2.0	38.2
ST100.00067g00160.1	s-V781I (+++, d)	100.00	19	0	0	169	187	25719020	25719038	2.0	38.2
ST100.00067g00160.1	s-V138I (++, d)	98.47	1241	18	1	1308	2547	20624485	20625725	0.0	2302
ST100.00067g00160.1	s-V138I (++, d)	98.94	1132	12	0	1	1132	1383011	1384142	0.0	2149
ST100.00067g00160.1	s-V138I (++, d)	99.65	286	1	0	1077	1362	1380313	1380598	2E-157	559
ST100.00067g00160.1	s-V138I (++, d)	97.54	285	7	0	1078	1362	2943441	2943725	2E-142	509
ST100.00067g00160.1	s-V138I (++, d)	83.17	101	14	1	2033	2130	1098329	1098429	0,0000001	61.9
ST100.00067g00160.1	s-V138I (++, d)	88.30	94	11	0	1847	1940	2813998	2814091	6E-19	99.6
ST100.00067g00160.1	s-V138I (++, d)	86.67	90	12	0	1851	1940	1098147	1098236	4E-14	83.8
ST100.00067g00160.1	s-V138I (++, d)	100.00	80	0	0	2493	2572	26374876	26374955	8E-37	159
ST100.00067g00160.1	s-V138I (++, d)	98.78	82	1	0	2491	2572	25684351	25684270	1E-35	155
ST100.00067g00160.1	s-V138I (++, d)	84.06	69	11	0	1150	1218	2813297	2813365	0,0005	50.1
ST100.00067g00160.1	s-V138I (++, d)	100.00	26	0	0	1	26	26766611	26766636	0,0001	52.0
ST100.00067g00160.1	s-V138I (++, d)	95.45	22	1	0	1559	1580	1895213	1895192	42012	36.2
ST100.00067g00160.1	s-V138I (++, d)	100.00	19	0	0	169	187	21137894	21137876	2.0	38.2
ST100.00067g00160.1	s-V138I (++, d)	100.00	19	0	0	843	861	31628720	31628702	2.0	38.2
ST100.00067g00160.1	s-V138I (++, d)	100.00	18	0	0	2201	2218	27441118	27441135	42012	36.2
ST100.00067g00160.1	s-T9 (++, d)	98.07	1243	23	1	1308	2549	32305914	32304672	0.0	2266
ST100.00067g00160.1	s-T9 (++, d)	98.94	1133	12	0	1	1133	707591	708723	0.0	2151
ST100.00067g00160.1	s-T9 (++, d)	97.54	285	7	0	1078	1362	35933062	35933346	2E-142	509
ST100.00067g00160.1	s-T9 (++, d)	99.65	284	1	0	1078	1361	36780302	36780585	4E-156	555
ST100.00067g00160.1	s-T9 (++, d)	83.17	101	14	1	2033	2130	19684215	19684315	0,0000001	61.9

ST100.00067g00160.1	s-T9 (++, d)	88.30	94	11	0	1847	1940	21171325	21171418	6E-19	99.6
ST100.00067g00160.1	s-T9 (++, d)	86.67	90	12	0	1851	1940	19684033	19684122	4E-14	83.8
ST100.00067g00160.1	s-T9 (++, d)	100.00	80	0	0	2493	2572	35883837	35883916	8E-37	159
ST100.00067g00160.1	s-T9 (++, d)	98.75	80	1	0	2493	2572	23910427	23910506	2E-34	151
ST100.00067g00160.1	s-T9 (++, d)	84.06	69	11	0	1150	1218	21170624	21170692	0,0005	50.1
ST100.00067g00160.1	s-T9 (++, d)	100.00	26	0	0	1	26	19682162	19682187	0,0001	52.0
ST100.00067g00160.1	s-T9 (++, d)	95.45	22	1	0	1559	1580	21199951	21199930	42012	36.2
ST100.00067g00160.1	s-T9 (++, d)	100.00	19	0	0	169	187	7861660	7861642	2.0	38.2
ST100.00067g00160.1	s-T9 (++, d)	100.00	19	0	0	843	861	32087420	32087402	2.0	38.2
ST100.00067g00160.1	s-T9 (++, d)	100.00	18	0	0	2201	2218	23943407	23943390	42012	36.2
ST100.00067g00160.1	s-V76 (++, d)	97.90	1241	25	1	1308	2547	27604470	27603230	0.0	2246
ST100.00067g00160.1	s-V76 (++, d)	98.94	1132	12	0	1	1132	26439042	26440173	0.0	2149
ST100.00067g00160.1	s-V76 (++, d)	99.65	285	1	0	1078	1362	34202179	34202463	9E-157	557
ST100.00067g00160.1	s-V76 (++, d)	97.54	285	7	0	1078	1362	34896705	34896989	2E-142	509
ST100.00067g00160.1	s-V76 (++, d)	83.17	101	14	1	2033	2130	32021335	32021435	0,0000001	61.9
ST100.00067g00160.1	s-V76 (++, d)	88.30	94	11	0	1847	1940	4200797	4200890	6E-19	99.6
ST100.00067g00160.1	s-V76 (++, d)	86.67	90	12	0	1851	1940	32021153	32021242	4E-14	83.8
ST100.00067g00160.1	s-V76 (++, d)	100.00	80	0	0	2493	2572	11966647	11966726	8E-37	159
ST100.00067g00160.1	s-V76 (++, d)	98.75	80	1	0	2493	2572	31467890	31467969	2E-34	151
ST100.00067g00160.1	s-V76 (++, d)	84.06	69	11	0	1150	1218	4200096	4200164	0,0005	50.1
ST100.00067g00160.1	s-V76 (++, d)	100.00	26	0	0	1	26	32019282	32019307	0,0001	52.0
ST100.00067g00160.1	s-V76 (++, d)	95.45	22	1	0	1559	1580	4229423	4229402	42012	36.2
ST100.00067g00160.1	s-V76 (++, d)	100.00	19	0	0	169	187	2494697	2494679	2.0	38.2
ST100.00067g00160.1	s-V76 (++, d)	100.00	19	0	0	843	861	14186043	14186025	2.0	38.2
ST100.00067g00160.1	s-V76 (++, d)	100.00	18	0	0	2201	2218	5116712	5116729	42012	36.2
ST100.00067g00160.1	w-V192I (-/+, nd)	98.86	264	3	0	116	379	4577272	4577009	2E-139	500
ST100.00067g00160.1	w-V192I (-/+, nd)	83.17	101	14	1	2033	2130	30008487	30008387	0,0000001	61.9
ST100.00067g00160.1	w-V192I (-/+, nd)	95.65	23	1	0	1847	1869	3211087	3211065	2.0	38.2
ST100.00067g00160.1	w-V192I (-/+, nd)	100.00	19	0	0	843	861	2138607	2138589	2.0	38.2
ST100.00067g00160.1	w-V192I (-/+, nd)	100.00	19	0	0	169	187	7436414	7436396	2.0	38.2
ST100.00067g00160.1	w-V192I (-/+, nd)	100.00	18	0	0	2201	2218	4174144	4174127	42012	36.2
ST100.00067g00160.1	w-V192I (-/+, nd)	100.00	18	0	0	2201	2218	25475189	25475206	42012	36.2

ST100.00067g00160.1	w-V192I (-/+, nd)	100.00	18	0	0	2201	2218	26781386	26781369	42012	36.2
ST100.00067g00160.1	w-V192I (-/+, nd)	100.00	18	0	0	2201	2218	27144946	27144929	42012	36.2
ST100.00067g00160.1	w-DVD-S29 (+++)	95.65	23	1	0	1847	1869	6166	6144	2.0	38.2
ST100.00067g00160.1	w-DVD-S29 (+++)	100.00	19	0	0	843	861	22118	22136	2.0	38.2
ST100.00067g00160.1	w-DVD-S29 (+++)	100.00	19	0	0	169	187	30536	30554	2.0	38.2
ST100.00067g00160.1	w-DVD-S29 (+++)	100.00	18	0	0	2201	2218	49930	49913	42012	36.2
ST100.00067g00160.1	w-DVD-S29 (+++)	100.00	18	0	0	2201	2218	5385	5402	42012	36.2
ST100.00067g00160.1	w-DVD31 (+++)	95.65	23	1	0	1847	1869	6091	6069	2.0	38.2
ST100.00067g00160.1	w-DVD31 (+++)	100.00	19	0	0	169	187	11965	11947	2.0	38.2
ST100.00067g00160.1	w-DVD31 (+++)	100.00	19	0	0	843	861	21904	21922	2.0	38.2
ST100.00067g00160.1	w-DVD31 (+++)	100.00	18	0	0	2201	2218	309	292	42012	36.2
ST100.00067g00160.1	w-DVD31 (+++)	100.00	18	0	0	2201	2218	93	76	42012	36.2
ST100.00067g00160.1	w-DVD31 (+++)	100.00	18	0	0	2201	2218	400	417	42012	36.2
ST100.00067g00160.1	w-DVD31 (+++)	100.00	18	0	0	2201	2218	51197	51180	42012	36.2
ST100.00067g00160.1	w-DVD31 (+++)	100.00	18	0	0	2201	2218	7804	7821	42012	36.2

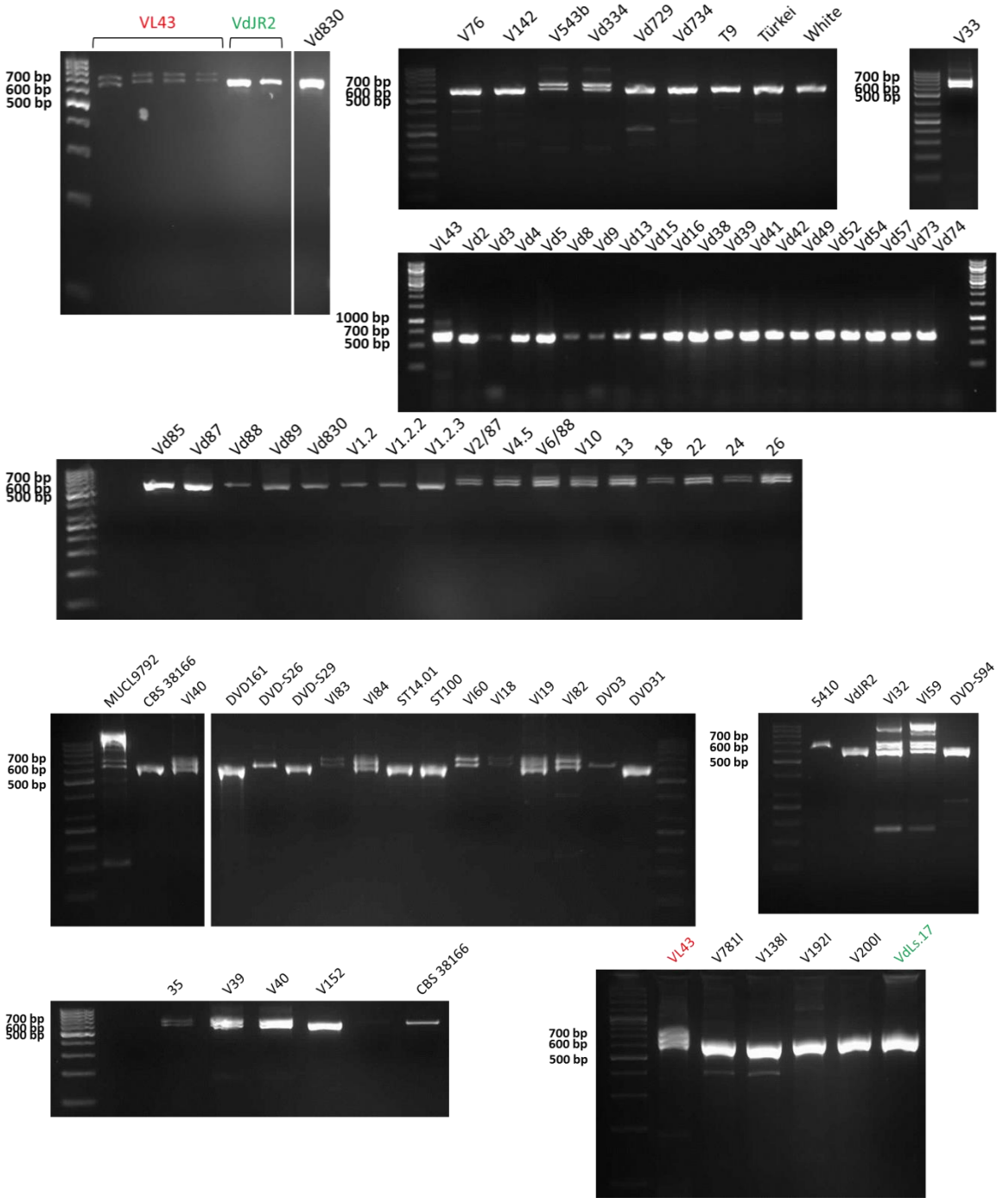

Figure S1: Amplification of the *Verticillium* transcription activator (VTA) 2 sequence from the various *Verticillium* isolates of the *Verticillium* strain collection to classifiy the strains as *V. longisporum* or *V. dahliae*. *VTA2* was amplified with the primers VTA2 forward and VTA2 revers (2.1.3). Note that *V. longisporum* isolates possess two different *VTA2* isogenes deriving from *V. dahliae* (620 bp) or *V. albo-atrum* (690 bp). *V. dahliae* isolates possess only one isogene variant (620 bp) (van Tran *et al.*, 2013). The reference *V. longisporum* isolate VL43 is highlighted in **red** and the reference *V. dahliae* isolate VdJR2 in **green**.

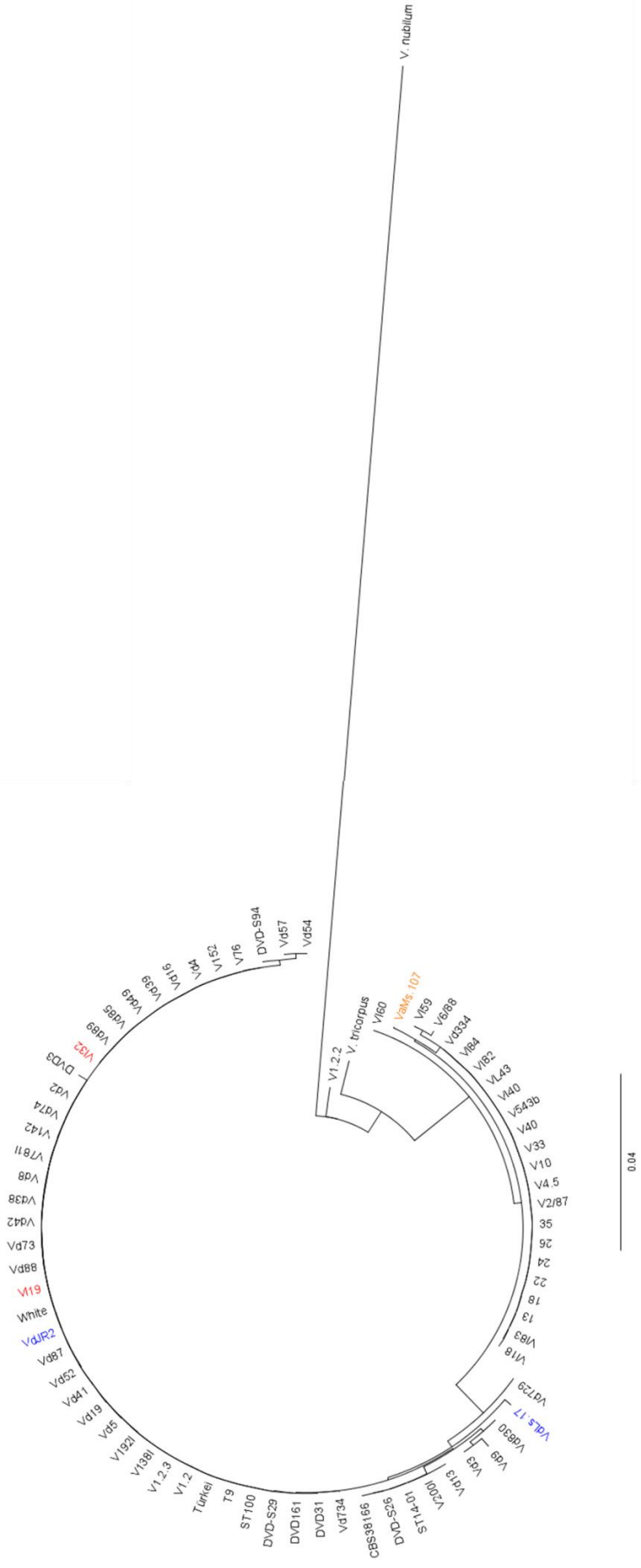

Figure S2: Phylogenetic tree of ribosomal internal transcribed spacer (ITS) sequences amplified from the various *Verticillium* isolates of the *Verticillium* strain collection. ITS sequences were amplified via PCR with the primers ITSRTl and ITSRTr (2.1.3). ITS sequences of *V. nubilum* and *V. tricorpus* were included in the phylogenetic tree. *V. albo-atrum* strain VaMs.102 (**orange**) as well as *V. dahliae* isolate VdJR2 and VdLs.17 (**blue**) served as reference ITS sequences. *V. longisporum* strains belonging to the lineage A1/D1 possess an ITS sequence like *V. albo-atrum* (Inderbitzin *et al.*, 2011; van Tran *et al.*, 2013). Note that *V. longisporum* isolates Vl19 and Vl32 taxonomically grouped with the isolates which were identified as *V. dahliae* isolates via VTA2 amplification. This identifies the two strains to belong to the lineage A1/D3 (Inderbitzin *et al.*, 2011; van Tran *et al.*, 2013). The unrooted phylogenetic tree was constructed using the software Geneious™ Pro v. 8.1.6; Biomatters Ltd., (Kearse *et al.*, 2012) employing the Tamura-Nei genetic distance model (Tamura and Nei, 1993) and neighbor-joining method (Saitou and Nei, 1987). The bar indicates genetic distance.

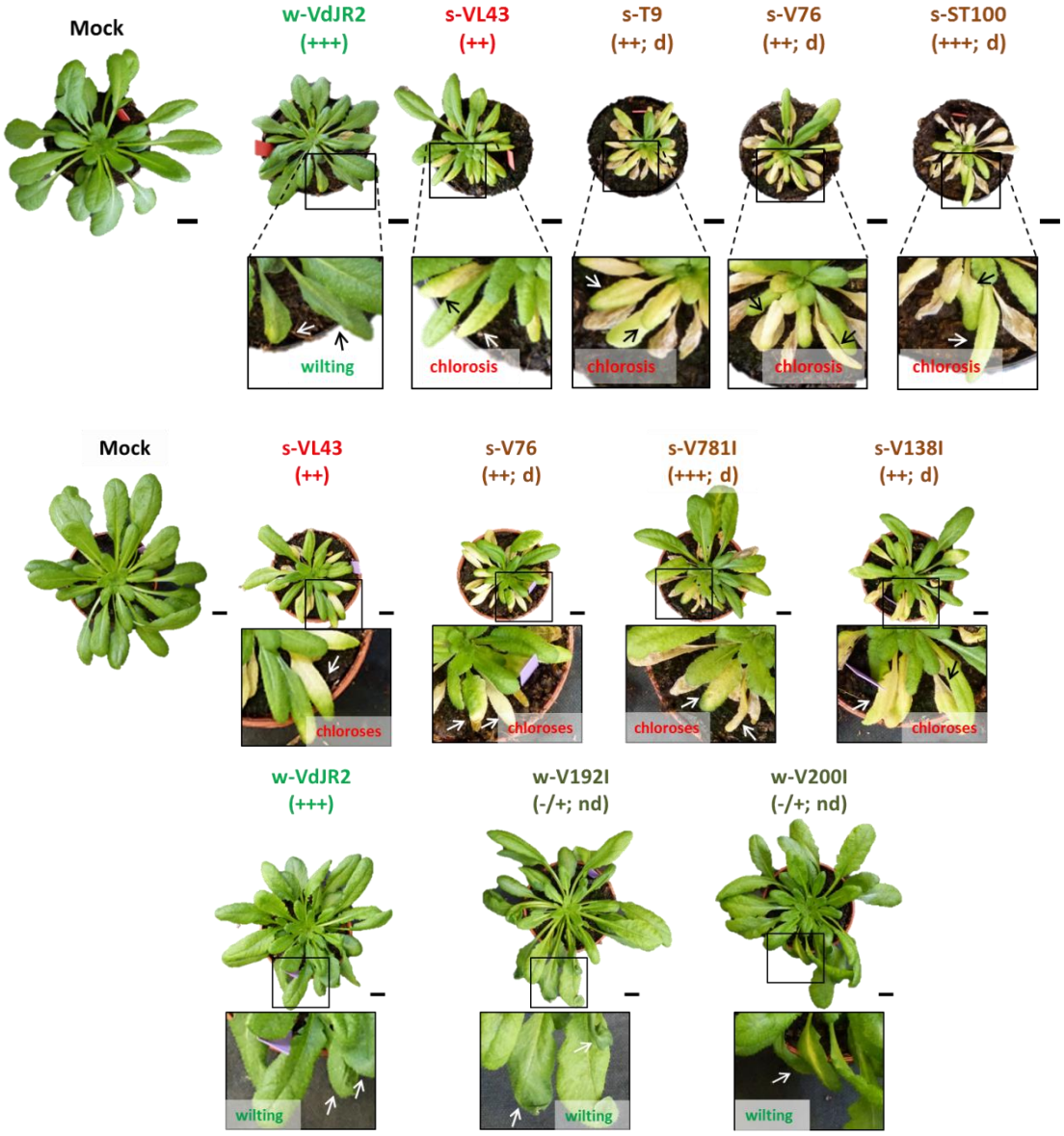

Figure S3: Disease symptom development of *A. thaliana* Col-0 infected with *V. dahliae* isolates s-T9, s-V76, s-ST100, s-V781I, s-V138I, w-V192I and w-V200I in comparison to s-VL43 and w-VdJR2 inoculated plants. *V. dahliae* isolates representing the "early senescence" interaction class are highlighted in **brown**. *V. dahliae* isolates representing the "wilting" interaction class are highlighted in **dark green**. The reference isolates s-VL43 and w-VdJR2 are highlighted in **red** and **green**, respectively. Early senescence inducing isolates are marked with the prefix s-. Wilt inducing isolates are marked with the prefix w-. Symbols indicate the intensity of disease symptom development: -/+ = mild symptoms, ++ = strong symptoms, +++ = very strong symptoms. d = cotton/olive defoliating, nd = cotton non-defoliating. Phenotype of *Verticillium* infected plants was recorded at 28 dpi. Boxes indicate magnifications of leaves with infection symptom development. Arrows indicate the declared symptoms. Scale bar = 1 cm. Experiments were repeated three times (upper panel) and once (lower panel) and representative data are shown.

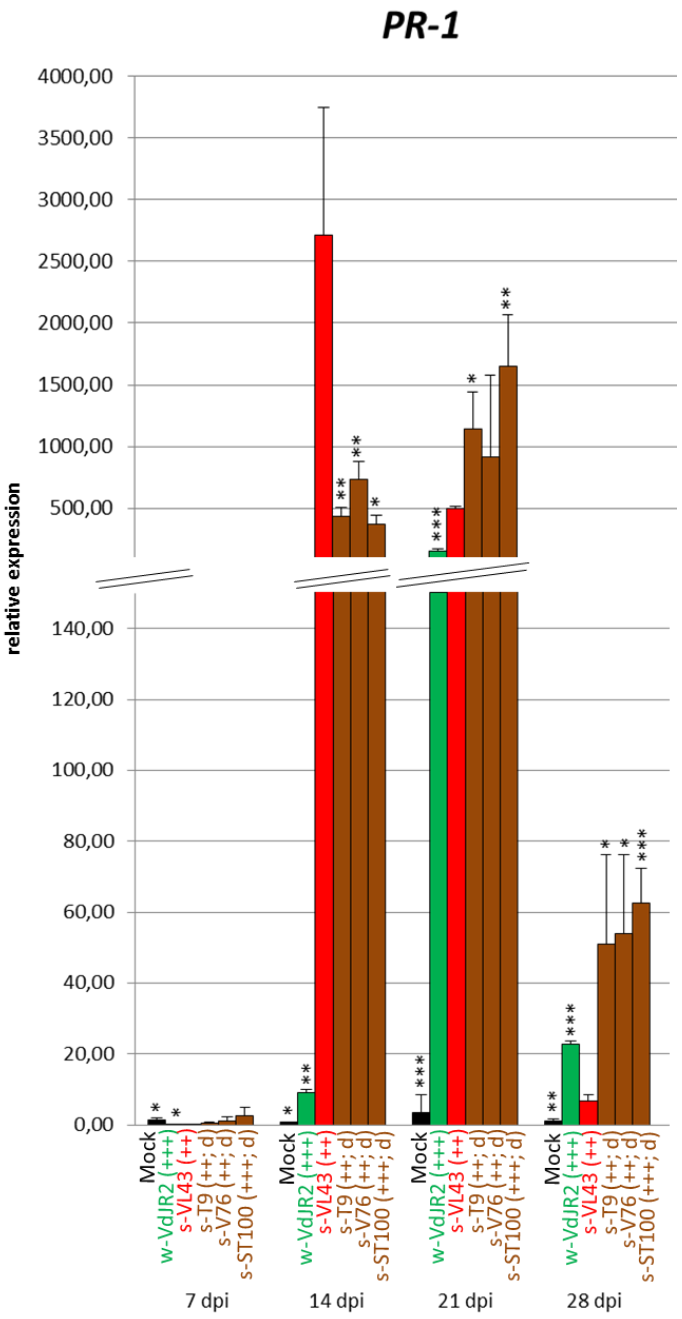

Figure S4: Expression analysis of *PR-1* in mock-treated and w-VdJR2, s-VL43, s-T9, s-V76 and s-ST100 infected plants. *V. dahliae* isolates representing the "early senescence" interaction class are highlighted in **brown**. The reference isolates s-VL43 and w-VdJR2 are highlighted in **red** and **green**, respectively. Early senescence inducing isolates are marked with the prefix s-. Wilt inducing isolates are marked with the prefix w-. Symbols indicate the intensity of disease symptom development: ++ = strong symptoms, +++ = very strong symptoms. d = cotton/olive defoliating. Relative expression of *PR-1* in mock-treated and *Verticillium* infected plants measured via qRT-PCR (n=4; pool of 4 plants). Error bars show standard deviation. Asterisks indicate statistical significance between *V. longisporum* s-VL43 infected and mock-treated or *V. dahliae* infected plants (t-test; * p≤0.05, ** p≤0.01, *** p≤0.001). Experiment was repeated three times.

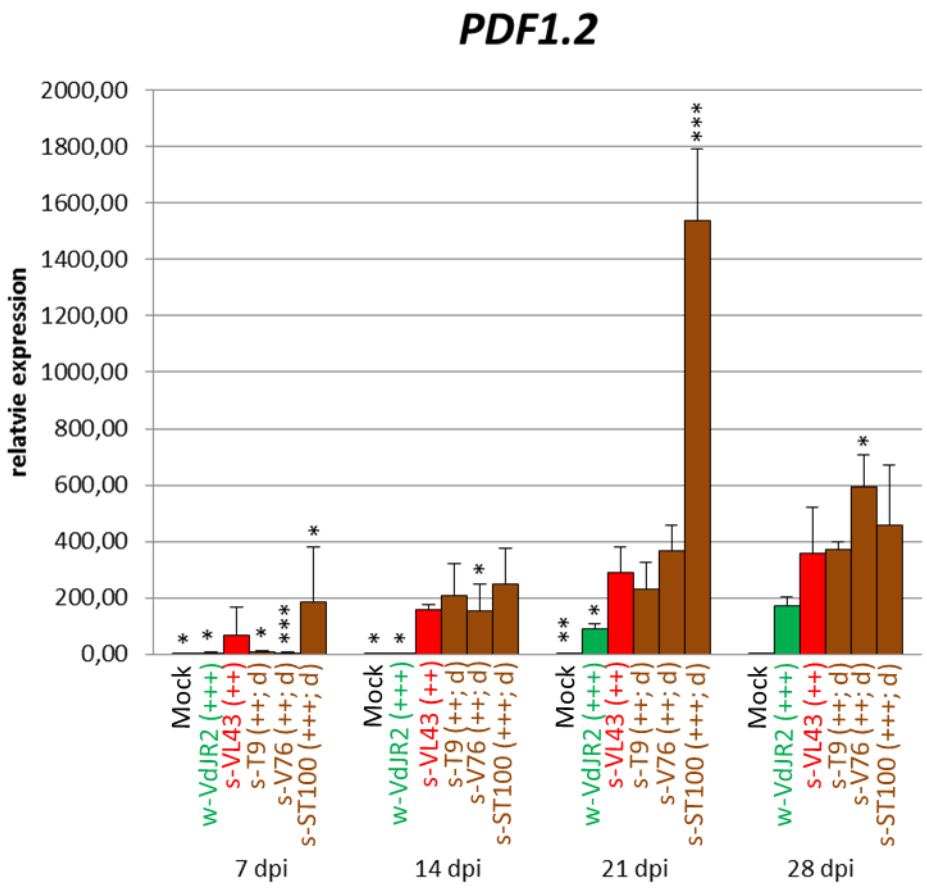

Figure S5: Expression analysis of *PDF1.2* in mock-treated and w-VdJR2, s-VL43, s-T9, s-V76 and s-ST100 infected plants. *V. dahliae* isolates representing the "early senescence" interaction class are highlighted in **brown**. The reference isolates s-VL43 and w-VdJR2 are highlighted in **red** and **green**, respectively. Early senescence inducing isolates are marked with the prefix s-. Wilt inducing isolates are marked with the prefix w-. Symbols indicate the intensity of disease symptom development: ++ = strong symptoms, +++ = very strong symptoms. d = cotton/olive defoliating. Relative expression of *PDF1.2* in mock-treated and *Verticillium* infected plants measured via qRT-PCR (n=4; pool of 4 plants). Error bars show standard deviation. Asterisks indicate statistical significance between *V. longisporum* s-VL43 infected and mock-treated or *V. dahliae* infected plants (t-test; * p≤0.05, ** p≤0.01, *** p≤0.001). Experiment was repeated three times.

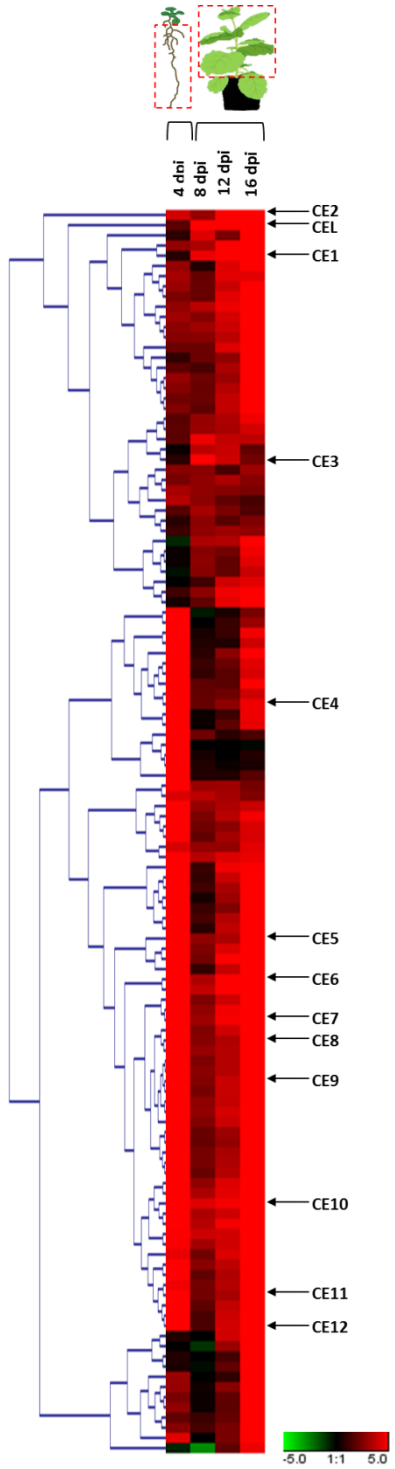

Figure S6: Hierarchical clustering of the Top50 *in planta* induced *V. dahliae* genes of the "early senescence" interaction class in comparison to the "wilting" interaction class. Hierarchical clustering (HCL) was performed via the expression data of *V. dahliae* genes in *A. thaliana* Col-0 roots (4 dpi) and in the aerial parts of *N. benthamiana* plants (8 dpi, 12 dpi and 16 dpi). Relative log2FC values of the 50 genes with the highest transcript abundance in the "early senescence" interaction class of every time point were used for HCL. Note that the incorporation of the Top50 genes for every time point results in a gene number larger than 50 genes (122 genes), since the Top50 genes are only partially congruent among the diverse time points. For coloration of HCL the upper maximum was set to log2FC = 5 and the lower maximum was set to log2FC = -5. The transcription profiles of candidate effector genes *CEL* and *CE1-CE12* are highlighted in the HCL. Note that *CE13* is not among the Top50 transcribed genes (3.4.2.1). Clustering was performed with the software Genesis v.1.7.7 (Sturn *et al.*, 2002).

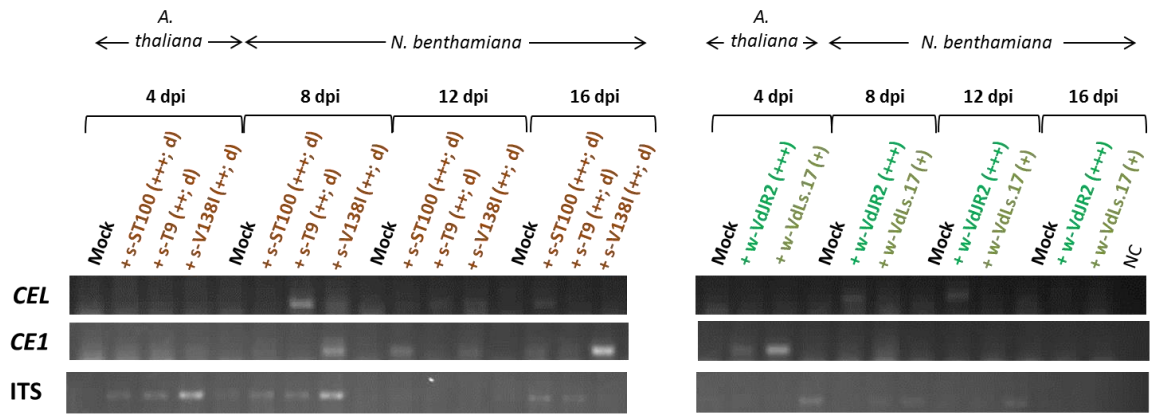

Figure S7: Agarose gels of semi qRT-PCRs for expression detection of *CEL* and *CE1* on cDNA. Semi-qRT-PCR for expression detection of *CEL* (first row) and *CE1* (second row) via cDNA derived from the same RNA samples which were used for RNA-sequencing. Primers were designed to bind sequences which are present in the transcripts of both s-ST100 and w-VdLs.17 homologues. 4 dpi samples derived from infected *A. thaliana* roots and 8 dpi, 12 dpi and 16 dpi derived from aerial tissues of infected *N. benthamiana* plants. Samples of plants infected with the early senescence inducing isolates s-ST100, s-T9 and s-V138I and with the wilt inducing isolates w-VdJR2 and w-VdLs.17 were used. Early senescence inducing isolates are marked with the prefix s-. Wilt inducing isolates are marked with the prefix w-. Symbols indicate the intensity of disease symptom development: + = moderate symptoms, ++ = strong symptoms, +++ = very strong symptoms. d = cotton/olive defoliating. Semi-qRT-PCR with samples of the additional isolates are shown in Figure 3.23. Amplification of ITS sequence was used as loading control (third row).

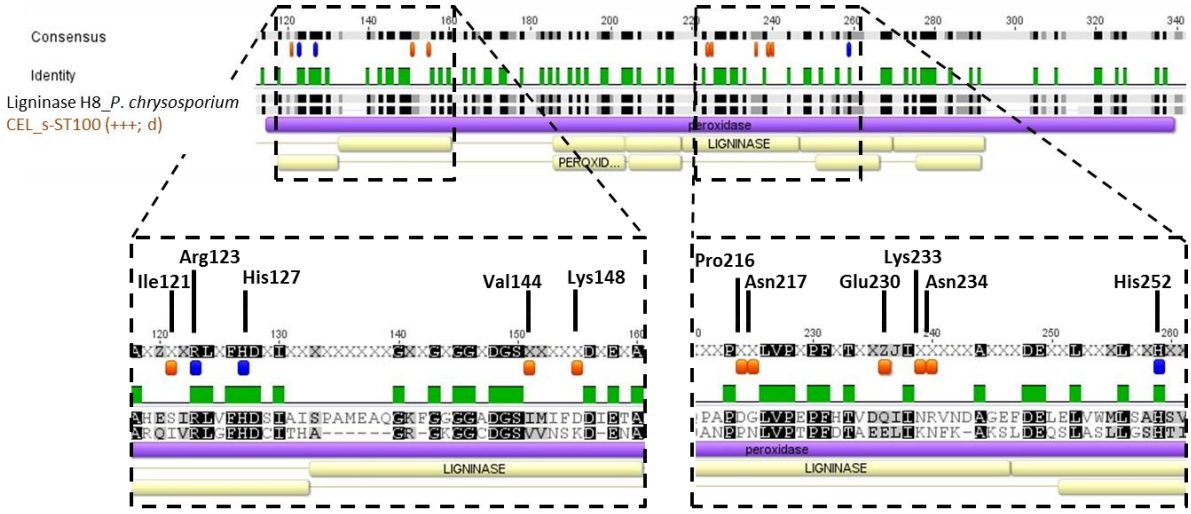

Figure S8: Amino acid sequence alignment of CEL encoded by *V. dahliae* isolates of the "early senescence" interaction class and the ligninase H8 of *Phanerochaete chrysosporium*. CEL of s-ST100 was chosen as representative CEL amino acid sequence of the "early senescence" interaction class and is highlighted in **brown** and marked with the prefix s-. Symbols indicate the intensity of disease symptom development: +++ = very strong symptoms. d = cotton/olive defoliating. **Orange** bars indicate amino acid substitution between isolates of the "early senescence" and "wilting" interaction class (Ile121, Val144, Lys148, Pro216, Asn217, Glu230, Lys233 and Asn234). **Blue** bars indicate the two histidine residues (His127 and His252) and the arginine residue (Arg123) essential for peroxidase activity which are present in the protein sequence of CEL of every tested *Verticillium* isolate. Sequence regions encircled with black dashed lines mark the magnification illustrated in the lower panel. Representative protein domains predicted consistently for all CEL proteins of the *Verticillium* isolates. Used databases: Lilac = Pfam, light yellow = Prints. Alignments were done via the software Geneious™ Pro v. 8.1.6; Biomatters Ltd., (Kearse *et al.*, 2012). Protein domain prediction was done via the InterProScan plugin in Geneious™ (Quevillon *et al.*, 2005).

Danksagung

Am Schluss meiner Arbeit möchte ich noch einigen Personen danken, die mich während meiner Doktorarbeit begleitet und unterstützt haben.

Zu allererst möchte ich mich bei Prof. Dr. Volker Lipka bedanken, der mir die Möglichkeit gab meine Doktorarbeit in seiner Abteilung anzufertigen. Seine konstruktive Kritik während regelmäßiger Meetings und Seminare hielten mich stets dazu an, meine Arbeit kritisch zu überdenken und „über den Tellerrand zu schauen“. Sein breitgefächertes Fachwissen und seine anregenden, fachlichen Diskussionen trugen maßgeblich zum Gelingen dieser Doktorarbeit bei. Zudem möchte ich mich für seine stets freundschaftliche Art bedanken mit der er mich motivierte, wenn zeitweise Schwierigkeiten in dem Projekt auftraten. Die regelmäßigen Abteilungsaktivitäten, die er bereitwillig förderte und unterstützte, trugen positiv zum Arbeitsklima und dem Gemeinschaftsgefühl unserer Abteilung bei. Ebenso möchte ich mich bei ihm für die Funktion als Erstprüfer und die Begutachtung meiner Arbeit bedanken.

Ein großer Dank geht vor allem an PD Dr. Thomas Teichmann: für seine Geduld und konstruktive Kritik beim Lesen meiner Arbeit und dafür, dass er immer eine offene Tür, sowie ein offenes Ohr für mich hatte.

Den zuvor genannten sowie Prof. Dr. Andrea Polle, Prof. Dr. Christiane Gatz, Prof. Dr. Ivo Feußner und Prof. Dr. Gerhard Braus danke ich für die Bereitschaft meine Prüfungskommission zu bilden.

Des Weiteren möchte ich Dr. Michael Reusche dafür danken, dass er mich am Anfang meiner Doktorarbeit unterstützt hat und mir bei fachlichen Fragen und Problemen immer mit Rat und Tat zur Seite stand.

Ein weiterer Dank geht an Dr. Hassan Ghareeb, der mir während der Auswertung der bioinformatischen Daten eine große Hilfe war. Zudem bedanke ich mich bei Dr. Corinna Thurow für die Unterstützung bei der Verwendung der *R*obi*NA* Software.

Ebenso möchte ich mich bei Prof. Dr. Andreas von Tiedemann, Prof. Dr. Gerhard Braus und Prof. Dr. Rafael M. Jiménez-Díaz danken, dass sie mir die diversen *Verticillium* Stämme zur Verfügung gestellt haben. Zudem bedanke ich mich herzlich bei unseren Kollaboratoren Prof. Dr. Rolf Daniel, Dr. Andrea Thürmer und Dr. Sascha Dietrich von der Universität Göttingen, sowie Prof. Dr. Bart Thomma, Dr. Luigi Faino und Xiaoqian Shi-Kunne von der Universität Wageningen für die große Unterstützung bei der

Sequenzierung und den bioinformatischen Analysen und der Bereitstellung der *V. dahliae* Genome.

Ich danke Michaela, Dimitri, Sabine, Hassan und Gaby für die erheiternde und entspannte Arbeitsatmosphäre im Labor. Zudem möchte ich mich bei Inga bedanken, die mich während meiner Doktorarbeit im Zuge ihrer Masterarbeit tatkräftig unterstützt hat.

Zudem möchte ich mich bei unseren Gärtner/innen, Feli, Susanne und Herrn Wedemeyer, für das Stopfen zahlreicher Erdtöpfe bedanken und für ihre Bereitschaft immer ein spontanes Tray dazwischen zu schieben.

Ein weiterer Dank geht an alle aktuellen und ehemaligen Mitglieder der gesamten Abteilung: für die überaus freundliche und angenehme Arbeitsatmosphäre, sowie die vielen, unterhaltsamen Abteilungsauflüge und Mittagspausen, die wir miteinander verbracht haben und die ein unverwechselbares Miteinander in der Abteilung schafften.

Ein ganz besonderer Dank geht an meine Freunde, die mich während meiner Doktorarbeit begleitet und unterstützt haben. Danke Yvonne, Charlotte, Alexandra, Michaela und Johanna für die gute Zeit, die wir gemeinsam hatten. Ohne euch wäre es nur halb so schön gewesen und ich werde unsere gemeinsamen Labortage und –abende sehr vermissen. Charlotte danke ich zudem für das Korrekturlesen meiner Doktorarbeit. An dieser Stelle möchte ich mich auch bei meinen Garreler Freundinnen Kirsten, Sarah, Monika, Katharina und vor allem Claudia bedanken. Ihr habt euch jederzeit meine Probleme angehört und mir am Wochenende die nötige Abwechslung zum Laboralltag geboten. Ich bin froh und stolz, dass unsere Freundschaft über so viele Jahre hinweg besteht und hoffe euch für immer in meinem Leben zu wissen.

Ein weiterer Dank geht an Justus, Peter und Bob, die es trotz meines ständigen Gedankenkarussells während der Schreibphase schafften mich in den Schlaf zu reden.

Ein riesen großes Dankeschön geht an meine Eltern, die mir das Studium ermöglichten, mich immer unterstützt haben und mir in stressigen Zeiten seelischen Beistand leisteten. Danke, dass ihr immer für mich da seid und hinter mir steht. Ohne euch wäre meine Doktorarbeit nicht möglich gewesen. Auch möchte ich mich bei meiner Schwester Sonja bedanken: du hast immer die richtigen Worte gefunden und konntest mich stets motivieren, wenn es mal schwierig wurde. Ich bin froh, dass es dich gibt.

Zu guter Letzt danke ich vor allem meinem Freund Stephan: du verstehst es immer mich aufzubauen, wenn mir alles über den Kopf wächst. Danke, dass du zu jeder Tages- und Nachtzeit für mich da bist, mich unterstützt und bei allem was ich tue hinter mir stehst.